On the reactivity of strained seven- and eight-membered rings in click chemistry

J.A.M. Damen

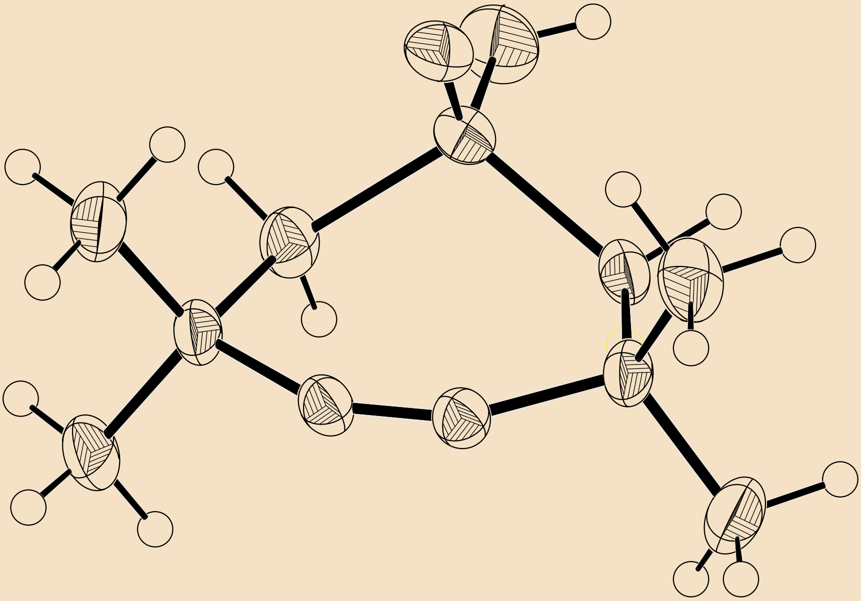

Propositions

1. Secondary orbital interactions are a negligible factor in the rates of SPOCQ cycloadditions.
   (this thesis)

2. Conclusions about the reactivity of click reagents can only be drawn from standardized kinetics studies.
   (this thesis)

3. The excessive use of abbreviations in scientific research complicates rather than simplifies matters.

4. Transfer of experimental skills requires urgent attention in order to prevent further loss of the craft.

5. Circumventing a paywall to access literature is morally acceptable.

6. The 24 hour-society is ideal.

7. Gossiping is the best method of knowledge transfer in ways of both speed and efficacy.

Propositions belonging to the thesis, entitled
On the reactivity of strained seven- and eight-membered rings in click chemistry

Johannes Antonius Maria Damen
Wageningen, 28 October 2024

On the reactivity of strained seven- and eight-membered rings in click chemistry

Johannes Antonius Maria Damen

Thesis committee

Promotors
Prof. Dr F.L. van Delft
Special chair, Bioconjugate Chemistry
Wageningen University & Research

Prof. Dr H. Zuilhof
Professor of Organic Chemistry
Wageningen University & Research

Co-promotor
Dr B. Albada
Associate professor, Laboratory of Organic Chemistry
Wageningen University & Research

Other members
Prof. Dr F.A.M. Leermakers, Wageningen University & Research
Prof. Dr E. Ruijter, Vrije Universiteit Amsterdam
Prof. Dr I. Dijkgraaf, Maastricht University
Prof. Dr S.I. van Kasteren, Leiden University

This research was conducted under the auspices of VLAG Graduate School (Biobased, Biomolecular, Chemical, Food and Nutrition Sciences)

On the reactivity of strained seven- and eight-membered rings in click chemistry

Johannes Antonius Maria Damen

Thesis
submitted in fulfilment of the requirements for the degree of doctor
at Wageningen University
by the authority of the Rector Magnificus,
Prof. Dr C. Kroeze,
in the presence of the
Thesis Committee appointed by the Academic Board
to be defended in public
on Monday 28 October 2024
at 1 p.m. in the Omnia Auditorium.

Johannes Antonius Maria Damen
On the reactivity of strained seven- and eight-membered rings in click chemistry, 164 pages.

PhD thesis, Wageningen University, Wageningen, the Netherlands (2024)
With references, with summaries in English and in Dutch

ISBN 978-94-6473-605-2
DOI https://doi.org/10.18174/673988

Table of contents

Chapter 1 General Introduction – Reaction Rates in Click Chemistry **7**

Chapter 2 Synthetic efforts towards oxa- and azacyclooctynes **29**

Chapter 3 Synthesis of a novel thiacycloheptyne probe for bioconjugations **47**

Chapter 4 High Rates of Quinone-Alkyne Cycloaddition Reactions are Dictated by Entropic Factors **77**

Chapter 5 Temperature-Dependent Reaction Rates of Quinone-Alkene Cycloaddition Reveal that Only Entropy Determines the Rate of SPOCQ Reactions **95**

Chapter 6 Synthesis of novel click-declick probes for cell surface chemokine release **111**

Chapter 7 General Discussion **133**

Summary **147**
Samenvatting **150**

Acknowledgements **153**

About the author **159**
Curriculum vitae **161**
List of publications **162**
Overview of completed training activities **163**

Chapter 1

General Introduction – Reaction Rates in Click Chemistry

J.A.M. Damen

1. Introduction

1.1 Click Chemistry

The term “click chemistry” was coined in the seminal publication of Sharpless *et. al.* in 2001, in which the authors pose a number of rules as requirements for a chemical reaction to be ideal.[1] The reaction must be modular, wide in scope, give very high yields, generate only inoffensive byproducts (removable by nonchromatographic methods) and must be stereospecific (not per se enantioselective).[1] The synthesis process should involve readily available reagents and starting materials, include simple reaction conditions. Solvents should either be benign, or easily removable, or not be used at all (neat). The process should ideally also be compatible with water and oxygen. Furthermore, product isolation should be simple and, if required, purification should be done by easy methods such as crystallization or distillation (no chromatography). Finally, the product should be stable under physiological conditions.[1] As such, in contrast to conventional synthetic organic chemistry that comprises a plethora of available reactions, only a few reactions meet these criteria. Currently, only a handful of “spring-loaded” reactions are considered click reactions. Click reactions that are covered in this dissertation are 1,3-dipolar cycloadditions[2-4] and inverse electron-demand Diels-Alder reactions.[5]

1.2 Bioconjugation

Since its inception over two decades ago, click chemistry has amongst other methods become popular as a tool for bio-orthogonal protein modification. It allows for the probing or altering of protein functionality, extending to *in vitro* or even *in vivo* applications.

Biomolecules can be chemically altered with desired functionalities, preferably using highly controlled chemical reactions[6] (in combination with genetic encoding[7]), without loss of native function of the protein.[8-11] Protein modification therefore allows for decorating these biomolecules with a vast array of functional groups or payloads such as: (i) chemical mimics of post-translational modifications (*e.g.* glycosylation,[12] ubiquitination,[13] lipidation[14]); (ii) attachment of affinity tags or functionalities that increase water solubility (respectively for example biotinylation[15] or PEGylation[16]); (iii) fluorescent labelling for probing of native function;[17] (iv) attachment of cytotoxic payloads or other drugs for targeted delivery.[18-21] Such bioconjugation strategies have been used to investigate the function of post-translational modifications on proteins,[22] for super-resolution imaging of biomolecules[17] or to achieve control over biomolecules *in vivo*.[23]

Forging covalent chemical bonds on complex biomolecules such as proteins in an *in vitro* or *in vivo* setting poses additional stringent requirements on bio-orthogonal click reactions. Specifically, such reaction has to proceed at physiological pH in aqueous solution, which renders most organic reactions incompatible. Also, such reaction should be selective for a specific functionality and should not display cross reactivity with other functional groups present on a protein or within the complex biological environment of a cell or organism. Of similar importance is that reactivity should be high, within the range of room temperature to physiological temperature, in order to ensure sufficient reaction rate under high dilution (often substantially below millimolar concentrations), ideally accompanied by high coupling efficiency.[6,7,24] Logically, few bio-orthogonal click reactions meet all of these requirements, *i.e.,* each has its own limitations when applied in a biological environment.

As such, prior to use in a in biological context, proper analysis has to be made in order to select the most applicable click method. For example, the necessity of toxic copper(I) in Cu(I)-catalyzed (3+2) azide–alkyne cycloadditions (CuAAC) complicates application *in vivo*.[25,26] The development of the strain-promoted (3+2) azide–alkyne cycloaddition (SPAAC) reaction avoids the use of copper and can be used for labelling of a metabolically azide-enriched glycocalyx of tumor cells *in vivo*.[27] However, cross reactivity emerged as an issue as some cyclooctyne reagents tend to undergo radical thiol-yne coupling with cysteine thiol residues.[28,29] Fortunately, inverse electron-demand Diels–Alder (IEDDA) reactions, such as the [4+2] cycloaddition of tetrazines with dienophiles, are less prone to cross reactivity and display a high reaction rate,[24] but a tetrazine tag is much less easily incorporated in biological structures than an azide. The strain-promoted oxidation-controlled *ortho*-quinone (SPOCQ) [4+2] cycloaddition with an alkyne or alkene, developed in our group, also exhibits a high reactivity while an *ortho*-quinone can be readily generated enzymatically on surface-exposed tyrosine residues of proteins. The drawback of this approach occurs from proximal nucleophilic residues that can also attack the *ortho*-quinone by Michael addition, which after rearomatization leads to a covalent linkage to an unreactive substituted 1,2-catechol.

These examples show that some click reactions are compatible with biomolecules in aqueous solution, whilst being selective and fast, but none meets all of the requirements in a cellular setting. Development of new methodologies in this young research field is challenging, but has high upside potential due to unique applications in chemical biology.

In this Chapter the reader will be guided through a selection of well-established metal-free click chemistries with an emphasis on their chemical reactivity and reaction rate, focusing on cycloadditions. Other click methodologies such as the sulfur(VI) fluoride exchange (SuFEx) reaction[30-34] or CuAAC[35-38] are covered elsewhere and are beyond the scope of this Chapter.

2. SPAAC

In order to circumvent the use of toxic Cu(I) catalysts, the strain-promoted (3+2) azide-alkyne cycloaddition (SPAAC) was developed. The reactivity in SPAAC is driven by a highly strained cycloalkyne, by virtue of the deviation from the optimal 180° bond angle of the C-C≡C-C moiety, see **Scheme 1**. The intrinsic reactivity of strained alkynes with azide was first shown in 1953 by Blomquist *et al.* who reported that the reaction of phenyl azide with cyclooctyne is highly exothermic,[39] but was not applied in the context of bio-orthogonal chemistry until Bertozzi *et al.* reported in 2004 the successful labelling of metabolically azide-enriched tumor cells with cyclooctyne-based probes.[27] This discovery has had an enormous impact on the field of chemical biology (and beyond), and therefore Bertozzi was awarded with the 2022 Nobel prize in Chemistry for the development of bio-orthogonal chemistry, together with Sharpless and Meldal for click chemistry.

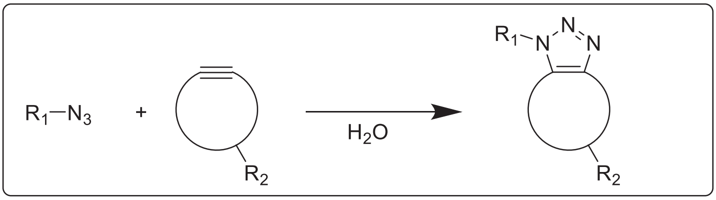

Scheme 1: The general reaction scheme of SPAAC.

As mentioned above, a cycloalkyne may be intrinsically reactive due to the strain imposed on the C≡C triple bond, which increases with decreasing ring size. However, strain may also be accompanied by spontaneous degradation. The eight-membered cyclooctyne is generally the smallest isolable carbon-based cycloalkyne with a ring strain of 18 kcal/mol (versus 12.1 kcal/mol for cyclooctane),[40-42] although exceptions are known of smaller ring sizes bearing heteroatoms (such as THS as discussed in **Chapter 3**). An all-carbon ring size smaller than seven is unstable and can only be made *in situ*.[43,44]

Even though SPAAC is orders of magnitude slower than CuAAC,[27] developments of novel strained reagents to increase this reactivity have been ongoing ever since.[40] As such, the rate difference between both methodologies is dependent on the specific ring size of the reagent (SPAAC) and the reaction conditions (CuAAC). The typically slower reaction kinetics of SPAAC, as compared to CuAAC, has resulted in drawbacks to applications in biological labeling studies as it often necessitates long incubation times and the use of vast excesses of reagents to produce sufficient amounts of desired product. Therefore, the development of more reactive, yet stable strained click reagents has been an important topic of research since the initial discovery of SPAAC biolabeling with the 1st generation cyclooctyne (OCT) used for bio-orthogonal labeling.

The first reported increase of cyclooctyne reactivity was achieved by installation of a fluoro group or a *gem*-difluoro group onto the propargylic position in MOFO and DIFO, respectively, see **Scheme 2**. This led to a minor increase in SPAAC reaction rate of 1.8 times for monofluorinated OCT, but to a major increase of 32 times in the case of difluorinated OCT when compared to the first developed reagent OCT (k_2 = 0.0024 $M^{-1}s^{-1}$).[45,46] This enhancement in reactivity is attributed to a LUMO lowering effect of propargylic fluorination, resulting in a faster cycloaddition.[45]

Another means of increasing reactivity of cyclooctynes for SPAAC is to further increase the strain of the reagent. A commonly employed method of increasing strain on a cyclooctyne is by installing sp^2-hybridized atoms in the ring chain, *e.g.*, by benzoannulation. Where the installation of a pyrrole in PYRROC[47] only minimally increases reactivity by 2.5-fold as compared to OCT, a much more pronounced effect of 98-fold reactivity increase occurs in the case of benzoannulation in COMBO.[48] Apparently, positioning of the annulated benzene ring onto the cyclooctyne is key, because the reaction rate enhancement of MOBO is only 4 times versus OCT.[45] By combining both propargylic difluorination and benzoannulation, a combined reactivity increase of 92-fold occurs in DIFBO. However, DIFBO is unstable and homotrimerizes spontaneously.[45] Further reactivity enhancement by increasing the number of sp^2-hybridized ring atoms can be achieved by dibenzoannulation, which was first done in the case of DIBO,[49] which has a reactivity increase of 50 times compared to OCT. Therefore, dibenzoannulation works synergistically over monobenzoannulation when comparing to MOBO. Further reactivity increments can be achieved by installing extra sp^2 character on an endocyclic nitrogen atom using an exocyclic amide bond as was done in DBCO. DBCO was first published by Van Delft *et al.*[50] followed by similar reports by Popik *et al.* and Feringa *et al.*[51,52] DBCO (originally dubbed DIBAC by Van Delft) has become the most commonly employed probe for SPAAC, likely due to the fact that it is readily synthetically accessible, while it combined a 129-fold reactivity enhancement versus OCT with high stability. Installation of an endocyclic amide bond as in BARAC further enhanced reactivity, but also made the compound unstable.[53,54] A major downside of (di)benzoannulation is the enhanced steric encumbrance and the substantially increased lipophilicity. The latter may lead to solubility issues in bioassays, which may in some instances be mitigated by the use of cosolvents such as DMSO, but the amount of cosolvent may not always be compatible with the biological setting.

To address the issue of aqueous solubility, several other cyclooctynes were developed that built in more heteroatoms for increased hydrogen bonding and thus solubility. An example of this is the water-soluble DIMAC, but this compound bears a similarly low reactivity as OCT.[55] BCN, as reported by van Delft *et al.*,[56] omits the lipophilic aromatic rings and imposes strain by installation of a cyclopropane ring, forming the bicyclo[6.1.0]non-4-yne structure. BCN displays a rate enhancement of 58 times over that of OCT and has become next to DBCO one of the most commonly employed SPAAC reagents. Apart from eight-membered cyclic alkynes, seven-membered rings have also been explored. For example, the seven-membered ring system TMTH was reported to be the most reactive in SPAAC,[40,57] but is a notoriously unstable compound due to its high ring strain.[58] Another notable example is the sulfoximine analogue of TMTH, named TMTH-SI or THS, which is a highly reactive stable compound. Its exceptional reactivity in various click methodologies is one of the topics of this dissertation and is covered in more detail in **Chapters 3 and 4**.

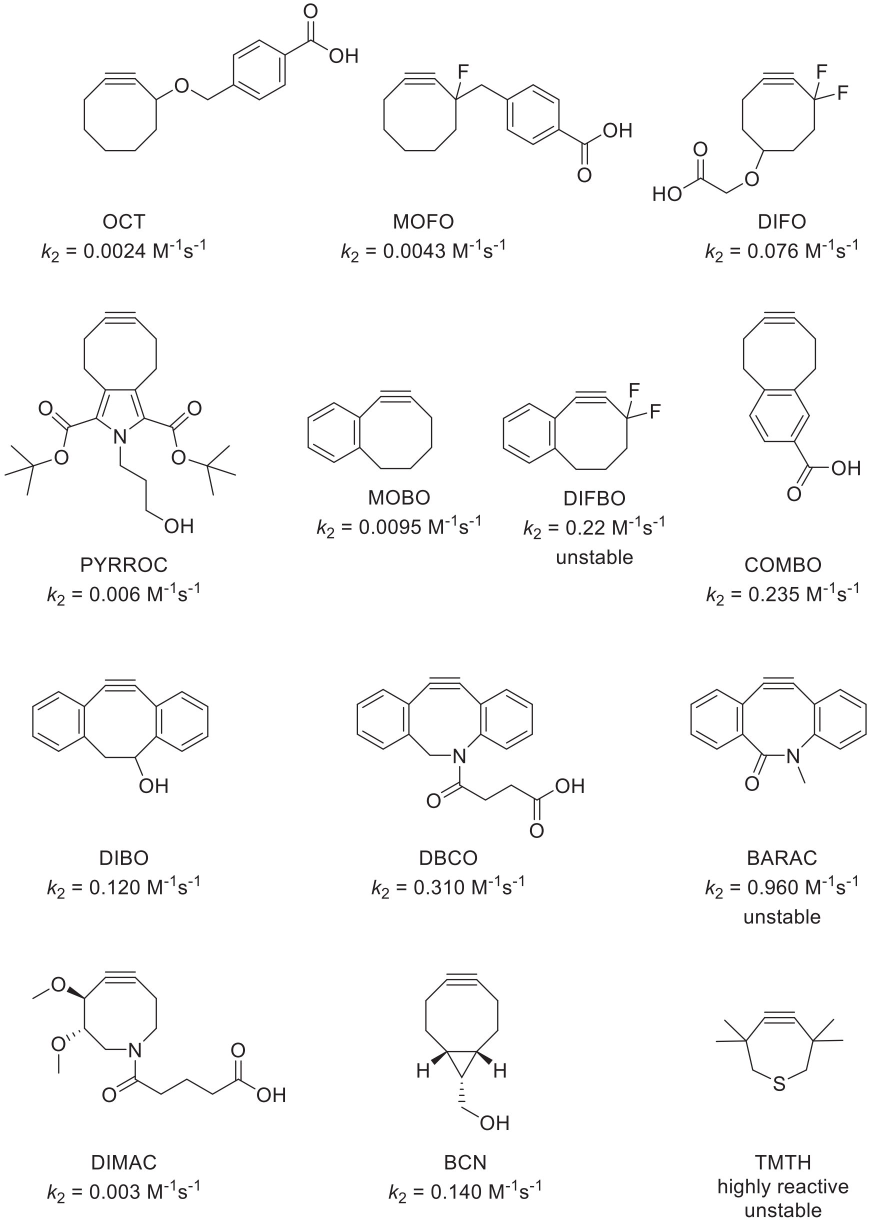
OCT
$k_2 = 0.0024\ M^{-1}s^{-1}$
MOFO
$k_2 = 0.0043\ M^{-1}s^{-1}$
DIFO
$k_2 = 0.076\ M^{-1}s^{-1}$
PYRROC
$k_2 = 0.006\ M^{-1}s^{-1}$
MOBO
$k_2 = 0.0095\ M^{-1}s^{-1}$
DIFBO
$k_2 = 0.22\ M^{-1}s^{-1}$
unstable
COMBO
$k_2 = 0.235\ M^{-1}s^{-1}$
DIBO
$k_2 = 0.120\ M^{-1}s^{-1}$
DBCO
$k_2 = 0.310\ M^{-1}s^{-1}$
BARAC
$k_2 = 0.960\ M^{-1}s^{-1}$
unstable
DIMAC
$k_2 = 0.003\ M^{-1}s^{-1}$
BCN
$k_2 = 0.140\ M^{-1}s^{-1}$
TMTH
highly reactive
unstable

Scheme 2: Various cycloalkynes with their second-order rate constants in reaction with aliphatic organic azides. The higher the numerical value for a second-order reaction rate constant in $M^{-1}s^{-1}$, the faster a bimolecular reaction. The abbreviation for each reagent is the same as in the original publications. For references, see the main text.

3. SPOCQ

Strain-promoted oxidation-controlled *ortho*-quinone (SPOCQ) cycloaddition emerged as an alternative methodology for labeling of biomolecules with generally a 2-3 orders of magnitude higher reaction rates than SPAAC.**[59-64]** SPOCQ involves the [4+2] inverse electron-demand Diels–Alder cycloaddition of an *ortho*-quinone with either a highly strained cycloalkyne or a highly strained (*trans*-)cycloalkene, see **Scheme 3**.

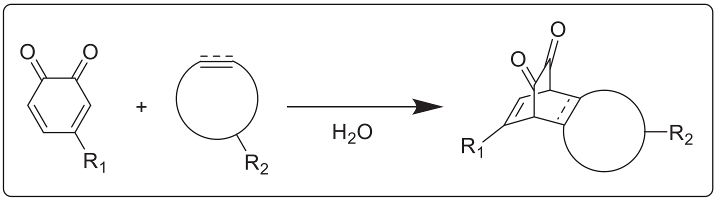

Scheme 3: The general reaction scheme of SPOCQ.

3.1 Generation of ortho-quinones

An *ortho*-quinone can be easily obtained by the oxidation of catechol (1,2-dihydroxybenzene) with $NaIO_4$.**[65]** As catechol functionalities do not occur on proteins, a more biocompatible approach is by the enzymatic oxidative generation of *ortho*-quinones from phenolic functionalities. This makes the canonical amino acid tyrosine the preferred substrate for generating the *ortho*-quinone click handle. The sole condition to such a click approach to protein conjugation is the presence of a sufficiently exposed tyrosine residue (which may already be present on the target protein or can be incorporated by recombinant DNA technology). As such, it offers a beneficial pathway over the use of a non-natural amino acid click tag that requires incorporation by genetic recoding. Oxidation of a phenol group to an *ortho*-quinone can be induced enzymatically by copper-metalloenzymes, most notably mushroom tyrosinase (mTyr). The enzymatic approach was shown early on to be applicable to peptides and small proteins and later even to antibodies: SPOCQ induced by mTyr allowed for the clean and homogeneous formation of antibody-drug conjugates (ADCs),**[66-69]** potentially after enzymatic deglycosylation of a conserved glycan chain that covered a conserved tyrosine residue that could be subjected to conjugation by means of SPOCQ.**[70]** The toxicity of the copper-containing tyrosinase metalloenzyme is not expected to be as concerning as that of free Cu(I) ions in the case of CuAAC click chemistry, as the resting state of the enzyme is comprised of two coordinated Cu(II) metal centers, and potentially toxic Cu(I) states are only generated transiently in the catalytic cycle.**[75-82]** However, tyrosinase-based click chemistry has not been applied *in vivo* yet. Another option for generating an *ortho*-quinone from a phenol group is by chemical oxidation with hypervalent iodine(V) reagents, such as IBX, in the case of small molecule substrates.**[71-74]** The details of both mTyr and IBX oxidations are described in the **Appendix**.

3.2 Kinetics of SPOCQ

Early kinetic investigations revealed that *ortho*-quinones are reactive in [4+2] cycloadditions to various strained cycloalkynes and cycloalkenes:**[61,63,64,67]** Whereas cyclopropenes display a relatively low reactivity in the range of 10^0 $M^{-1}s^{-1}$, *trans*-cyclooctene is more reactive (~10^1 $M^{-1}s^{-1}$), while cyclooctyne BCN showed an estimated reactivity of 10^3 $M^{-1}s^{-1}$. Surprisingly poor reactivity was found for cycloalkyne DBCO. Notably, only qualitative estimation of the magnitude of the kinetics values can be provided at best, as most kinetic studies were performed poorly with regards to assay design, equipment setup and supporting mathematics.

Nevertheless, the high reaction rate constants for SPOCQ reactions led to a computational study by Houk *et al.*, who attributed the orders of magnitude reactivity difference between BCN cycloalkyne and TCO cycloalkene SPOCQ to a constructive Secondary Orbital Interaction (SOI), resulting from additional orbital overlaps in the Transition State (TS) of cycloalkyne SPOCQ,[83,84] see **Scheme 4**. This constructive SOI results in the lowering of the TS barrier, resulting in enhanced reaction rates of cycloalkyne SPOCQ.

Further investigations into the reaction kinetics of SPOCQ and into the underlying physico-chemical phenomena are covered in this dissertation.

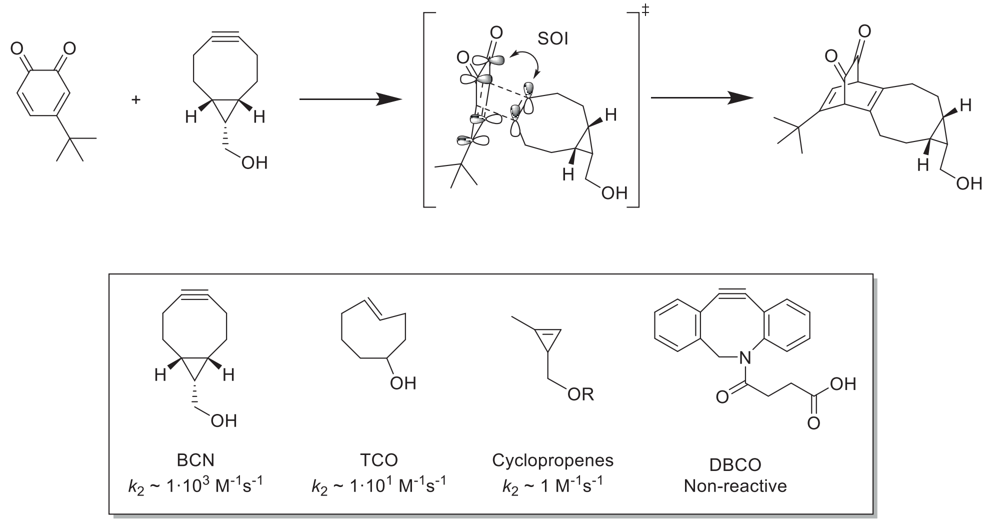
O
O
+
H
H
OH
‡
O
O
SOI
H
H
OH
O
O
H
H
OH
H
H
OH
OH
OR
N
O
OH
O
BCN
k_2 ~ 1·10^3 M^{-1}s^{-1}
TCO
k_2 ~ 1·10^1 M^{-1}s^{-1}
Cyclopropenes
k_2 ~ 1 M^{-1}s^{-1}
DBCO
Non-reactive

Scheme 4: (Top) Model SPOCQ experiments for which the involvement of SOIs is proposed. (Bottom) Reported reactivities of several strained reagents in SPOCQ click chemistry, in orders of magnitude.

4. Tetrazine IEDDA

Lastly, the inverse electron-demand Diels–Alder (IEDDA) reaction of tetrazines with various strained dienophiles is a click chemistry methodology in the highest reactivity range (10^1 – 10^6 $M^{-1}s^{-1}$).**[24]** IEDDA involves the [4+2] cycloaddition of an electron-poor 1,2,4,5-tetrazine with an electron-rich dienophile, see **Scheme 5**. Typically, a strained cycloalkene is used for this reaction, the most prototypical being *trans*-cyclooctenol (TCO-OH). A highly strained bicyclic intermediate is formed after the cycloaddition as a transient intermediate species, which immediately undergoes retro-Diels–Alder (rDA) reaction with the evolution of nitrogen gas. The initially formed 4,5-dihydropyridazine cycloadduct isomerizes to the 1,4-isomer typically followed by air oxidation to an aromatic pyridazine as a the final, stable product.**[24]**

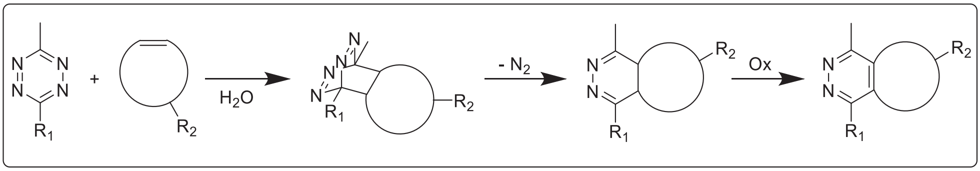

Scheme 5: The general reaction scheme of tetrazine IEDDA.

The reaction rate of IEDDA depends on a number of factors. First, the disubstitution pattern on tetrazine dictates its reactivity, as studies with TCO revealed that electron-donating substituents induce slower kinetics (10^2 – 10^3 $M^{-1}s^{-1}$) while electron-withdrawing groups such as pyridine or pyrimidine result in much more reactive tetrazines (10^3 – 10^4 $M^{-1}s^{-1}$).**[85-90]** While also in this case induction of reactivity is accompanied by lowering of stability, mono-methyl, mono-aryl substituted tetrazines are typically the preferred compromise.

A large variety of strained cycloalkenes and -alkynes can be used as dienophiles in IEDDA reaction with tetrazines, see **Scheme 6**. The most typical reagent for this reaction is TCO, due to its high reactivity in IEDDA and orthogonality towards azides in SPAAC. The TCO reagent was introduced by Fox *et al.*, who reported excellent reactivity with tetrazines of 1140 $M^{-1}s^{-1}$ in pure MeOH; 2000 $M^{-1}s^{-1}$ in 9:1 MeOH/H_2O and 22,600 $M^{-1}s^{-1}$ and 80,200 $M^{-1}s^{-1}$ for the respective equatorial and axial isomer in pure water.**[91,92]** Fox later reported that sTCO (or cpTCO) is even more reactive due to its half-chair conformation that mimics the transition state of the IEDDA reaction. The reactivity of sTCO is unprecedented with 22,000 $M^{-1}s^{-1}$ in pure MeOH and 3,300,000 $M^{-1}s^{-1}$ in pure water.**[92,93]** However, TCO-derivatives bear some problems though when in use: (i) they are photoisomerizeable and thus photosensitive; (ii) they isomerize in the presence of high thiol concentrations ($t_{1/2}$ = 3.26 hours in serum**[94]**) and in presence of metals, such as copper; (iii) the more reactive sTCO compounds are intrinsically unstable.

Another suitable class of dienophile reagents that suffers less from these limitations are the methylcyclopropenes. These reagents react with tetrazines much slower, typical second-order rate constant of 2.3 $M^{-1}s^{-1}$ in 50% aqueous solution,**[95-97]** however, with the advantage of enhanced stability and suffering less from steric encumbrance. The small cyclopropene ring size also enables metabolic incorporation (*e.g.*, metabolic take up and incorporation of methylcyclopropene-modified monosaccharides into tumor glycocalyx).

Lastly, tetrazines are also reactive towards some cycloalkynes. The best-known example is BCN, which possesses an intermediate reactivity towards tetrazines of 45 $M^{-1}s^{-1}$ in pure MeOH and 1245 $M^{-1}s^{-1}$ in 55% MeOH/H_2O.[98,99] In contrast, cycloalkyne DBCO does not show any reactivity with tetrazines, presumably due to sterics.

The differences in reaction rates per probe in different solvents are evident and it is known that these type of organic reactions occur faster in water.[100] Therefore, this should be taken into account when comparing reactivities of different probes. Typically kinetic analyses of small molecules should be performed in 50% water/organic solvent (such as methanol or acetonitrile) to ensure solubility of the compounds in the assay. Kinetic analyses of proteinaceous probes should be performed in water or buffer.[24]

In conclusion, tetrazine-based IEDDA reactions with *trans*-cyclooctenes are the fastest amongst the click reactions and the main advantage is the orthogonality of tetrazine IEDDA reagents with SPAAC reagents, *i.e.,* orthogonal bio-orthogonality, allowing for dual labelling in biological systems using both approaches. Another advantage of tetrazine IEDDA's fast kinetics is that it allows probes to be used at biologically relevant concentrations, whilst maintaining optimal labelling efficacies on a short time scale. This allows for the probing of fast biological processes, where other click methodologies would be too slow at those relevant concentrations.

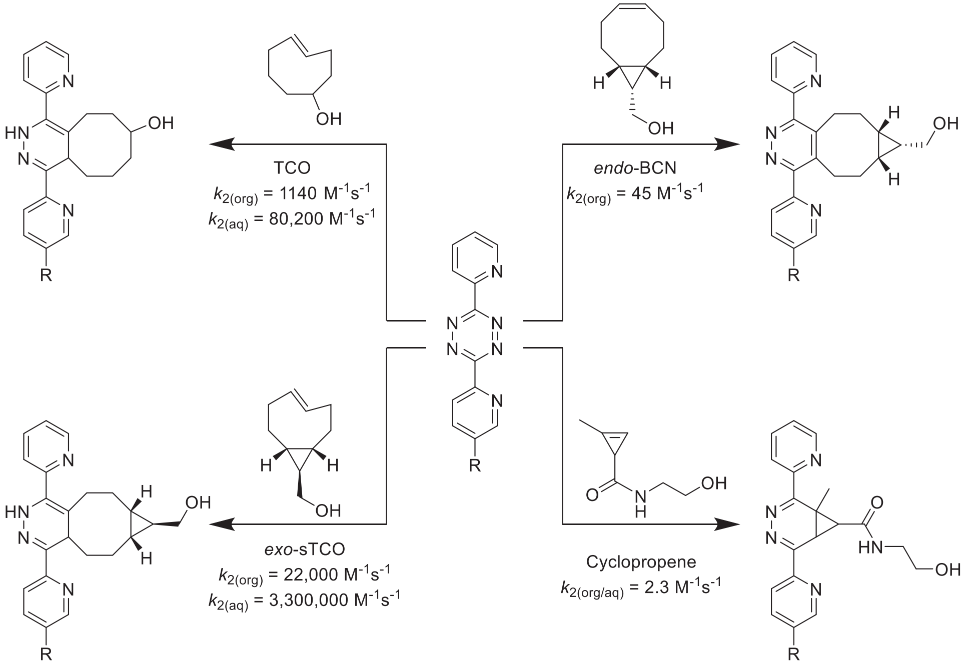
TCO
$k_{2(org)}$ = 1140 $M^{-1}s^{-1}$
$k_{2(aq)}$ = 80,200 $M^{-1}s^{-1}$
endo-BCN
$k_{2(org)}$ = 45 $M^{-1}s^{-1}$
exo-sTCO
$k_{2(org)}$ = 22,000 $M^{-1}s^{-1}$
$k_{2(aq)}$ = 3,300,000 $M^{-1}s^{-1}$
Cyclopropene
$k_{2(org/aq)}$ = 2.3 $M^{-1}s^{-1}$
OH
H
N
HN
R
O

Scheme 6: Reactivity matrix of several strained reagents with dipyridyl tetrazines (R = -$NHCOCH_2NH$-PEG_{14}-NHBoc). Representative second order rate constants in organic solvents; aqueous systems; or mixed systems are shown.

5. Reaction rates in bioconjugations

In order to place the aforementioned second-order rate constants of the various click reactions into context, the relevant concentration for a given experiment is a key consideration. Biological processes typically proceed at high dilution (typically µM), thereby necessitating both a high coupling efficiency and high reaction rate. A simulation of the reaction time for a bimolecular equimolar reaction (second-order kinetics) between 100 µM of two reactants as depicted in **Figure 1**[24] clearly shows the well-known time-dependency on the second-order rate constants (in $M^{-1}s^{-1}$). Importantly, conjugations in a biological environment proceed at substantially higher dilution than those in **Figure 1**, leading to excessively long reaction times to reach complete conversion. For example: bioconjugations on monoclonal antibodies (mAbs) to produce antibody-drug conjugates (ADCs) are typically performed on 5–25 µM mAb concentration and cellular labeling in the 10–50 µM concentration range, see **Chapter 3**. In these cases, the dilution factor as compared to the 100 µM used in **Figure 1**, is reflected in the elongation of the reaction time: *e.g.* working at 20-fold dilution at 5 µM results in a 20-fold longer reaction time for reaching full conversion. In order to circumvent long reaction times, one of the reagents is employed in excess (pseudo first-order kinetics). This excess linearly relates to shortening the reaction time. For example, a 1000-fold stoichiometric excess of one reagent, leads to a 1000-fold reduction in reaction time. So both concentration and stoichiometry can be employed as variables for modulating the reaction time. As such, an understanding of the quantitative kinetic values of a click reaction is important for its applicability. When using these rules, **Figure 1** can be used to estimate the reaction time when employing a reaction that has a known second-order rate constant at a particular concentration and stoichiometry.

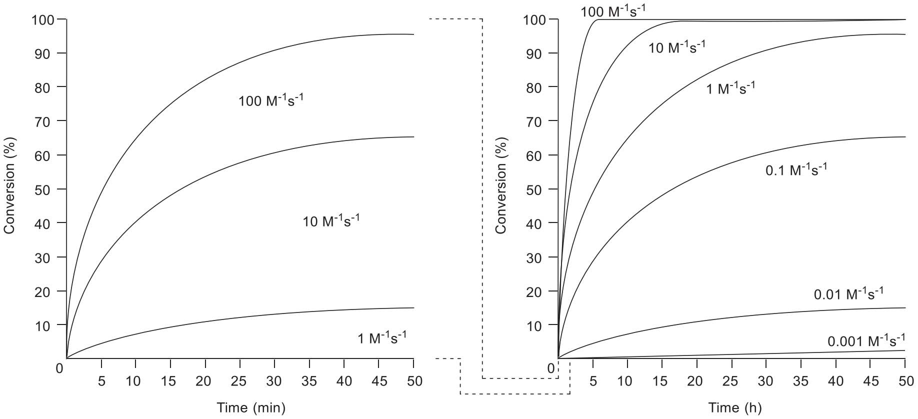

Figure 1: Simulation of second-order reactions between two reactants, both at 100 µM concentration, adapted from Bernardes *et al.*[24]

6. Thermodynamics of bimolecular reactions

With the development of transition state theory (or activated complex theory) and the development of the Eyring equation, the height of a reaction barrier can also be expressed in terms of Gibbs energy of activation ($\Delta G^{\ddagger}$), see **Figure 2**.[101-104] This value is experimentally acquired from Eyring plots by measuring the second-order rate constant at varying temperatures. It subsequently allows for the abstraction of the enthalpy of activation ($\Delta H^{\ddagger}$) and entropy of activation ($\Delta S^{\ddagger}$), giving insights into the relative contributions of the individual physical components when acquiring a Transition State (TS). $\Delta H^{\ddagger}$ reflects the sum of energies in bond breakings and bond formations when going into the TS, whereas $\Delta S^{\ddagger}$ describes the increase or decrease in order (or disorder) that is associated with acquiring the TS, along with whether a reaction is associative or dissociative. Of note, the value of $\Delta G^{\ddagger}$ should be derived from adequate kinetic analyses (experimentally determined values are expressed in italics). Experimental kinetic analyses can at maximum determine the kinetic value of the rate-determining step. As such, kinetic data of a complex multistep reaction should be handled with care as it may lead to the wrong $\Delta G^{\ddagger}$ values attributed to the wrong (intermediate) species. Therefore, Eyring analyses should only be performed on one-way, one-step reactions (as transmission coefficient κ is set to 1), unless proper justifications are provided. An example would be the case in which only the first step of a longer cascade reaction is rate-determining and therefore observed and this is verified. Eyring analyses should also not be employed to equilibria reactions.

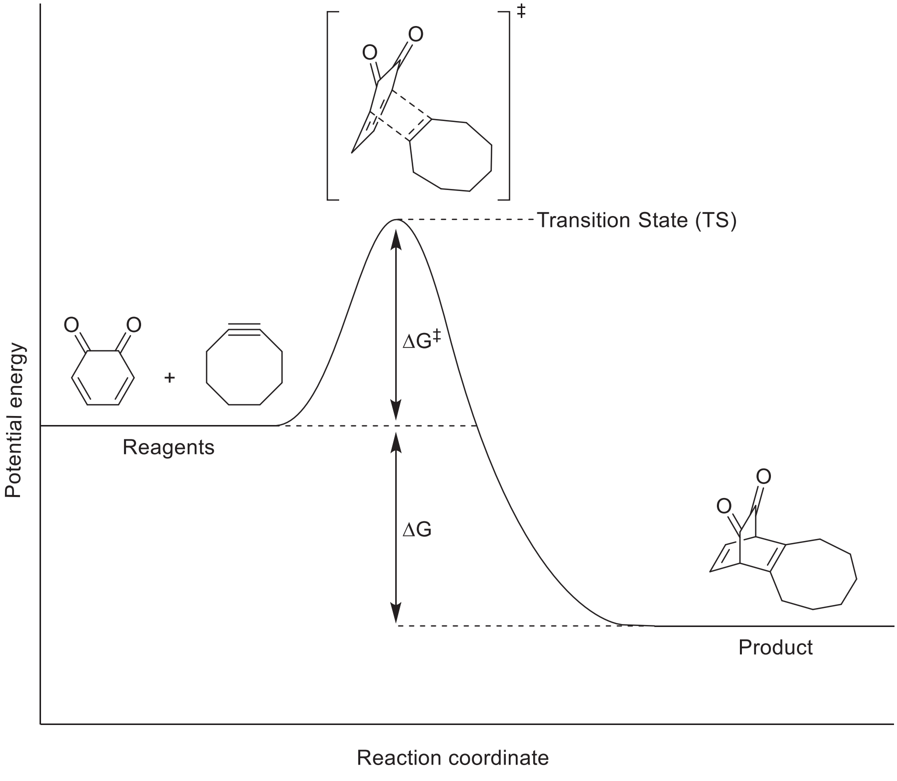

Figure 2: A reaction profile diagram for a one-step exothermic associative reaction.

7. Outline of this dissertation

The research described in this dissertation embodies the development of new click reagents, the development of new click and declick methodologies for application in bioconjugations and a detailed study of their kinetics. The new click methodologies allow for the attachment of payloads onto antibodies or tumor cell surfaces, whereas the declick methodologies allow for induced release of that payload. The fundamental chemical investigations towards such functional molecules are performed by means of rational design and acquired by means of synthetic organic chemistry. Another main topic is the analysis of the driving forces behind certain types of click chemistries (*i.e.*, SPOCQ and SPAAC). This dissertation therefore comprises an interplay between synthetic and physical organic chemistry in unveiling the role of strained bonds in click chemistry.

Chapter 2 describes approaches for the development of faster cycloalkyne click reagents for SPAAC reactions, based on the rationale and synthetic efforts towards *O*- and *N*-based monobenzoannulated cyclooctynes, accompanied by a mechanistic explanation why these species were not isolable.

In continuation of the search for faster SPAAC reagents, **Chapter 3** describes the successful development of the *S*-based cycloheptyne THS. THS is most strained stable cycloalkyne to date according to XRD. Derivatization of THS afforded new fluorescent probes that gave optimal results in SPAAC on cell surfaces and were also used successfully in SPOCQ labelling on antibodies.

Chapter 4 dives into the reactivity of THS in SPOCQ. Kinetic analyses on a matrix of various strained reagents were performed by means of stopped-flow UV-Vis spectroscopy. Based on subsequent Eyring analyses we concluded that cycloalkyne SPOCQ is controlled by entropic factors.

Further kinetic studies as elaborated in **Chapter 5** demonstrate that cycloalkene SPOCQ is also dictated by entropic factors, disproving the involvement of SOIs. Various structural effects of cycloalkyne/cycloalkene reagents in SPOCQ and SPAAC are investigated, including the XRDs of BCN and DBCO.

Chapter 6 describes the design and synthetic efforts towards a non-fluorescent bifunctional declickable linker system for fluorescent labeling of a target protein and/or a tumor cell and concomitant declicking of a functional probe.

Chapter 7 provides a general discussion regarding the research.

The supporting information and appendices are made available via the QR-code below.

8.References

(1) Kolb, H. C.; Finn M. G.; Sharpless, K. B. Click Chemistry: Diverse Chemical Function from a Few Good Reactions. *Angew. Chem. Int. Ed.* **2001**, *40*, 2004–2021.
(2) Huisgen, R. 1,3-Dipolar Cycloadditions. Past and Future. *Angew. Chem. Int. Ed. Engl.* **1963**, *2*, 565–598.
(3) Huisgen, R. 1.3-Dipolare Cycloadditionen Rückschau und Ausblick. *Angew. Chem.* **1963**, *75*, 604–637.
(4) Breugst, M.; Reissig, H.-U. The Huisgen Reaction: Milestones of the 1,3-Dipolar Cycloaddition. *Angew. Chem. Int. Ed.* **2020**, *59*, 12293–12307.
(5) Carey, F. A.; Sundberg, R. J. Advanced Organic Chemistry. Part A: Structure and Mechanisms. Fourth Edition. New York, New York, United States of America: Kluwer Academic / Plenum Publishers; **2000**. Chapter 11.3. Cycloaddition Reactions, specifically p. 642–643.
(6) Boutureira, O.; Bernardes, G. J. L. Advances in Chemical Protein Modification. *Chem. Rev.*, **2015**, *115*, 2174–2195.
(7) Lang, K.; Chin, J. W. Cellular Incorporation of Unnatural Amino Acids and Bioorthogonal Labeling of Proteins. *Chem. Rev.*, **2014**, *114*, 4764–4806.
(8) Li, J.; Chen, P. R. Development and application of bond cleavage reactions in bioorthogonal chemistry. *Nat. Chem. Biol.*, **2016**, *12*, 129–137.
(9) Spicer, C. D.; Davis, B. G. Selective chemical protein modification. *Nat. Commun.*, **2014**, *5*, 4740.
(10) Xue, L.; Karpenko, I. A.; Hiblot, J.; Johnsson, K. Imaging and manipulating proteins in live cells through covalent labeling. *Nat. Chem. Biol.*, **2015**, *11*, 917–923.
(11) Krall, N.; da Cruz, F. P.; Boutureira, O.; Bernardes, G. J. L. Site-selective protein-modification chemistry for basic biology and drug development. *Nat. Chem.*, **2016**, *8*, 103–113.
(12) Robinson, P. V.; Tsai, C. T.; De Groot, A. E.; McKechnie, J. L.; Bertozzi, C. R. Glyco-seek: Ultrasensitive Detection of Protein-Specific Glycosylation by Proximity Ligation Polymerase Chain Reaction. *J. Am. Chem. Soc.*, **2016**, *138*, 10722–10725.
(13) Rösner, D.; Schneider, T.; Schneider, D.; Scheffner, M.; Marx, A. Click chemistry for targeted protein ubiquitylation and ubiquitin chain formation. *Nat. Protoc.*, **2015**, *10*, 1594–1611.
(14) Wright, M. H.; Clough, B.; Rackham, M. D.; Rangachari, K.; Brannigan, J. A.; Grainger, M.; Moss, D. K.; Bottrill, A. R.; Heal, W. P.; Broncel, M.; Serwa, R. A.; Brady, D.; Mann, D. J.; Leatherbarrow, R. J.; Tewari, R.; Wilkinson, A. J.; Holder, A. A.; Tate, E. W. Validation of N-

myristoyltransferase as an antimalarial drug target using an integrated chemical biology approach. *Nat. Chem.*, **2014**, *6*, 112–121.
(15) Trippier, P. C. Synthetic Strategies for the Biotinylation of Bioactive Small Molecules. *ChemMedChem*, **2013**, *8*, 190–203.
(16) Stefan, N.; Zimmermann, M.; Simon, M.; Zangemeister-Wittke, U.; Pluckthun, A. Novel Prodrug-Like Fusion Toxin with Protease-Sensitive Bioorthogonal PEGylation for Tumor Targeting. *Bioconjugate Chem.*, **2014**, *25*, 2144–2156.
(17) Nikic, I.; Plass, T.; Schraidt, O.; Szymanski, J.; Briggs, J. A.; Schultz, C.; Lemke, E. A. Minimal Tags for Rapid Dual-Color Live-Cell Labeling and Super-Resolution Microscopy. *Angew. Chem. Int. Ed.*, **2014**, *53*, 2245–2249.
(18) Rossin, R.; Van Duijnhoven, S. M.; Ten Hoeve, W.; Janssen, H. M.; Kleijn, L. H.; Hoeben, F. J.; Versteegen, R. M.; Robillard, M. S. Triggered Drug Release from an Antibody–Drug Conjugate Using Fast "Click-to-Release" Chemistry in Mice. *Bioconjugate Chem.*, **2016**, *27*, 1697–1706.
(19) De Bever, L.; Popal, S.; Van Schaik, J.; Rubahamya, B.; Van Delft, F. L.; Thurber, G. M.; Van Berkel, S. S. Generation of DAR1 Antibody-Drug Conjugates for Ultrapotent Payloads Using Tailored GlycoConnect Technology. *Bioconjugate Chem.*, **2023**, *34*, 538–548.
(20) Wijdeven, M. A.; Van Geel, R.; Hoogenboom, J. H.; Verkade, J. M. M.; Janssen, B. M. G.; Hurkmans, I.; De Bever, L.; Van Berkel, S. S.; Van Delft, F. L. Enzymatic glycan remodeling–metal free click (GlycoConnect™) provides homogenous antibody-drug conjugates with improved stability and therapeutic index without sequence engineering. *mAbs*, **2022**, *14*, article number 2078466.
(21) Khera, E.; Dong, S.; Huang, H.; De Bever, L.; Van Delft, F. L.; Thurber, G. M. Cellular-Resolution Imaging of Bystander Payload Tissue Penetration from Antibody-Drug Conjugates. *Mol. Cancer Ther.*, **2022**, *21*, 310–321.
(22) Wright, T. H.; Bower, B. J.; Chalker, J. M.; Bernardes, G. J. L.; Wiewiora, R.; Ng, W. L.; Raj, R.; Faulkner, S.; Vallee, M. R.; Phanumartwiwath, A.; Coleman, O. D.; Thezenas, M. L.; Khan, M.; Galan, S. R.; Lercher, L.; Schombs, M. W.; Gerstberger, S.; Palm - Espling, M. E.; Baldwin, A. J.; Kessler, B. M.; Claridge, T. D.; Mohammed, S.; Davis, B. G. Posttranslational mutagenesis: A chemical strategy for exploring protein side-chain diversity. *Science*, **2016**, *354*, 597.
(23) Walker, O. S.; Elsässer, S. J.; Mahesh, M.; Bachman, M.; Balasubramanian, S.; Chin, J. W. Photoactivation of Mutant Isocitrate Dehydrogenase 2 Reveals Rapid Cancer-Associated Metabolic and Epigenetic Changes. *J. Am. Chem. Soc.*, **2016**, *138*, 718–721.
(24) Oliveira B. L.; Guo, Z.; Bernardes, G. J. L. Inverse electron demand Diels-Alder reactions in chemical biology. *Chem. Soc. Rev.*, **2017**, *46*, 4895–4950.
(25) Tornøe, C. W.; Christensen, C.; Meldal, M. Peptidotriazoles on Solid Phase: [1,2,3]-Triazoles by Regiospecific Copper(I)-Catalyzed 1,3-Dipolar Cycloadditions of Terminal Alkynes to Azides. *J. Org. Chem.*, **2002**, *67*, 3057–3064.
(26) Rostovtsev, V. V.; Green, L. G.; Fokin, V. V.; Sharpless, K. B. A Stepwise Huisgen Cycloaddition Process: Copper(I)-Catalyzed Regioselective "Ligation" of Azides and Terminal Alkynes. *Angew. Chem. Int. Ed.*, **2002**, *41*, 2596–2599.
(27) Agard, N. J.; Prescher, J. A.; Bertozzi, C. R. A Strain-Promoted [3 + 2] Azide−Alkyne Cycloaddition for Covalent Modification of Biomolecules in Living Systems. *J. Am. Chem. Soc.*, **2004**, *126*, 15046–15047.

(28) Amgarten, B.; Rajan, R.; Martínez-Sáez, N.; Oliveira, B. L.; Albuquerque, I. S.; Brooks, R. A.; Reid, D. G.; Duer, M. J.; Bernardes, G. J. L. Collagen labelling with an azide-proline chemical reporter in live cells. *Chem. Commun.*, **2015**, *51*, 5250–5252.
(29) Beatty, K. E.; Fisk, J. D.; Smart, B. P.; Lu, Y. Y.; Szychowski, J.; Hangauer, M. J.; Baskin, J. M.; Bertozzi, C. R.; Tirrell, D. A. Live-Cell Imaging of Cellular Proteins by a Strain-Promoted Azide–Alkyne Cycloaddition. *ChemBioChem*, **2010**, *11*, 2092–2095.
(30) Dong, J.; Krasnova, L.; Finn, M. G.; Sharpless, K. B. Sulfur(VI) fluoride exchange (SuFEx): Another good reaction for click chemistry. *Angew. Chem. Int. Ed.* **2014**, *53*, 9430–9448.
(31) Barrow A. S.; Smedley C. J.; Zheng Q.; Li S.; Dong J.; Moses J. E. The growing applications of SuFEx click chemistry. *Chem. Soc. Rev.* **2019**, *48*, 4731–4758.
(32) Liu, F.; Wang, H.; Li, S.; Bare, G. A. L.; Chen, X.; Wang, C.; Moses, J. E.; Wu, P.; Sharpless, K. B. Biocompatible SuFEx Click Chemistry: Thionyl Tetrafluoride (SOF_4)-Derived Connective Hubs for Bioconjugation to DNA and Proteins. *Angew. Chem. Int. Ed.* **2019**, *58*, 8029–8033.
(33) Liang, D.-D.; Pujari, S. P.; Subramaniam, M.; Besten, M.; Zuilhof, H. Configurationally Chiral SuFEx-Based Polymers. *Angew. Chem. Int. Ed.* **2022**, *61*, e202116158.
(34) Liang, D.-D.; Streefkerk, D. E.; Jordaan, D.; Wagemakers, J.; Baggerman, J.; Zuilhof, H. Silicon-Free SuFEx Reactions of Sulfonimidoyl Fluorides: Scope, Enantioselectivity, and Mechanism. *Angew. Chem. Int. Ed.* **2020**, *59*, 7494–7500.
(35) Worrell B. T.; Malik J. A.; Fokin, V. V. Direct evidence of a dinuclear copper intermediate in Cu(I)-catalyzed azide-alkyne cycloadditions. *Science*, **2013**, *340*, 457–460.
(36) Liang, L.; Astruc, D. The copper(I)-catalyzed alkyne-azide cycloaddition (CuAAC) "click" reaction and its applications. An overview. *Coord. Chem. Rev.*, **2011**, *255*, 2933–2945.
(37) Presolski, S. I.; Hong, V.; Cho, S.-H.; Finn, M. G. Tailored Ligand Acceleration of the Cu-Catalyzed Azide−Alkyne Cycloaddition Reaction: Practical and Mechanistic Implications. *J. Am. Chem. Soc.*, **2010**, *132*, 14570–14576.
(38) Soriano Del Amo, D.; Wang, W.; Jiang, H.; Besanceney, C.; Yan, A. C.; Levy, M.; Liu, Y.; Marlow, F. L.; Wu, P. Biocompatible Copper(I) Catalysts for in Vivo Imaging of Glycans. *J. Am. Chem. Soc.*, **2010**, *132*, 16893–16899.
(39) Blomquist, A. T.; Liu, L. H. Many-membered carbon rings. VII. Cyclooctyne. *J. Am. Chem. Soc.*, **1953**, *75*, 2153–2154.
(40) Dommerholt, J.; Rutjes, F. P. J. T.; Van Delft, F. L. Strain-Promoted 1,3-Dipolar Cycloaddition of Cycloalkynes and Organic Azides. *Top. Curr. Chem. (Z)*. **2016**, *374*, 16.
(41) Bach, R. D. Ring strain energy in the cyclooctyl system. The effect of strain energy on [3 + 2] cycloaddition reactions with azides. *J. Am. Chem. Soc.*, **2009**, *131*, 5233–5243.
(42) Turner, R. B.; Jarrett, A. D.; Goebel, P.; Mallon, B. J. Heats of hydrogenation. IX. Cyclic acetylenes and some miscellaneous olefins. *J. Am. Chem. Soc.*, **1973**, *95*, 790–792.
(43) Wittig, G.; Krebs, A. On the existence of small-membered cycloalkynes, I. *Chem. Ber.*, **1961**, *94*, 3260–3275.
(44) Krebs, A.; Wilke, J. Angle strained cycloalkynes. *Top. Curr. Chem.*, **1983**, *109*, 189–233.
(45) Sletten, E. M.; Nakamura, H.; Jewett, J. C.; Bertozzi, C. R. Difluorobenzocyclooctyne: Synthesis, Reactivity, and Stabilization by β-Cyclodextrin. *J. Am. Chem. Soc.*, **2010**, *132*, 11799–11805.
(46) Baskin, J. M.; Prescher, J. A.; Laughlin, S. T.; Agard, N. J.; Chang,P. V.; Miller, I. A.; Lo, A.; Codelli, J. A.; Bertozzi, C. R. Copper-free click chemistry for dynamic *in vivo* imaging. *Proc. Natl. Acad. Sci. U.S.A.*, **2007**, *104*, 16793–16797.
(47) Gröst, C.; Berg, T. PYRROC: the first functionalized cycloalkyne that facilitates isomer-free generation of organic molecules by SPAAC. *Org. Biomol. Chem.*, **2015**, *13*, 3866–3870.

(48) Varga, B. R.; Kállay, M.; Hegyi, K.; Béni, S.; Kele, P. A non-fluorinated monobenzocyclooctyne for rapid Copper-free click reactions. *Chem. Eur. J.*, **2012**, *18*, 822–828.
(49) Ning, X.; Guo, J.; Wolfert, M. A.; Boons, G. J. Visualizing metabolically labeled glycoconjugates of living cells by copper-free and fast Huisgen cycloadditions. *Angew. Chem. Int. Ed.*, **2008**, *47*, 2253–2255.
(50) Debets, M. F.; Van Der Doelen, C. W. J.; Rutjes, F. P. J. T.; Van Delft, F. L. Azide: a unique dipole for metal-free bioorthogonal ligations. *ChemBioChem*, **2010**, *11*, 1168–1184.
(51) Kuzmin, A.; Poloukhtine, A.; Wolfert, M. A.; Popik, V. V. Surface functionalization using catalyst-free azide-alkyne cycloaddition. *Bioconjugate Chem.*, **2010**, *21*, 2076–2085.
(52) Campbell-Verduijn, L. S.; Mirfeizi, L.; Schoonen, A. K.; Dierckx, R. A.; Elsinga, P. H.; Feringa, B. L. Strain-Promoted Copper-Free “Click” Chemistry for ^{18}F Radiolabeling of Bombesin. *Angew. Chem. Int. Ed.*, **2011**, *123*, 11313–11316.
(53) Jewett, J. C.; Sletten, E. M.; Bertozzi, C. R. Rapid Cu-free click chemistry with readily synthesized biarylazacyclooctynones. *J. Am. Chem. Soc.*, **2010**, *132*, 3688–3690.
(54) Gordon, C. G.; MacKey, J. L.; Jewett, J. C.; Sletten, E. M.; Houk K. N.; Bertozzi, C. R. Reactivity of biarylazacyclooctynones in copper-free click chemistry. *J. Am. Chem. Soc*. **2012**, *134*, 9199−9208.
(55) Sletten, E. M.; Bertozzi, C. R. A hydrophilic azacyclooctyne for Cu-free click Chemistry. *Org. Lett.*, **2008**, *10*, 3097–3099.
(56) Dommerholt, J.; Schmidt, S.; Temming, R.; Hendriks, L. J. A.; Rutjes, F. P. J. T.; Van Hest, J. C. M.; Lefeber, D. J.; Friedl, P.; Van Delft, F. L. Readily accessible bicyclononynes for bioorthogonal labeling and three-dimensional imaging of living cells. *Angew. Chem. Int. Ed*. **2010**, *49*, 9422–9425.
(57) De Almeida, G.; Sletten, E. M.; Nakamura, H.; Palaniappan, K. K.; Bertozzi, C. R. Thiacycloalkynes for copper-free click chemistry. *Angew. Chem. Int. Ed.* **2012**, *51*, 2443–2447.
(58) Krebs, A.; Kimling, H. 3.3.6.6-tetramethyl-1-thiacyclopheptin ein isolierbares siebenringacetylen. *Tetrahedron Lett.* **1970**, *11*, 761–764.
(59) Albada, B.; Keijzer, J. F.; Zuilhof, H.; van Delft, F. Oxidation-Induced “One-Pot” Click Chemistry. *Chem. Rev.* **2021**, *121*, 7032–7058.
(60) Bruins, J. J.; Albada, B.; Van Delft, F. *ortho*-Quinones and Analogues Thereof: Highly Reactive Intermediates for Fast and Selective Biofunctionalization. *Chem. Eur. J.* **2018**, *24*, 4749–4756.
(61) Escorihuela, J.; Das, A.; Looijen, W. J. E.; Van Delft, F. L.; Aquino, A. J. A.; Lischka, H.; Zuilhof, H. Kinetics of the Strain-Promoted Oxidation-Controlled Cycloalkyne-1,2-quinone Cycloaddition: Experimental and Theoretical Studies. *J. Org. Chem*. **2018**, *83*, 244−252.
(62) Escorihuela, J.; Looijen, W. J. E.; Wang, X.; Aquino, A. J. A.; Lischka, H.; Zuilhof, H. Cycloaddition of Strained Cyclic Alkenes and Ortho-Quinones: A Distortion/Interaction Analysis. *J. Org. Chem*. **2020**, *85*, 13557−13566.
(63) Sen, R.; Escorihuela, J.; van Delft, F.; Zuilhof, H. Rapid and Complete Surface Modification with Strain-Promoted Oxidation-Controlled Cyclooctyne-1,2-Quinone Cycloaddition (SPOCQ). *Angew. Chem. Int. Ed*. **2017**, *56*, 3299–3303.
(64) Gahtory, D.; Sen, R.; Kuzmyn, A. R.; Escorihuela, J.; Zuilhof, H. Strain-Promoted Cycloaddition of Cyclopropenes with o-Quinones: A Rapid Click Reaction. *Angew. Chem. Int. Ed*. **2018**, *57*, 10118–10122.
(65) Borrmann, A.; Fatunsin, O.; Dommerholt, J.; Jonker, A. M.; Löwik, D. W. P. M.; Van Hest, J. C. M.; Van Delft, F. L. Strain-promoted oxidation-controlled cyclooctyne-1,2-quinone

cycloaddition (SPOCQ) for fast and activatable protein conjugation. *Bioconjugate Chem*. **2015**, *26*, 257–261.
(66) Bruins, J. J.; Westphal, A. H.; Albada, B.; Wagner, K.; Bartels, L.; Spits, H.; Van Berkel, W. J. H.; Van Delft, F. L. Inducible, Site-Specific Protein Labeling by Tyrosine Oxidation-Strain-Promoted (4 + 2) Cycloaddition. *Bioconjugate Chem.* **2017**, *28*, 1189−1193.
(67) Bruins, J. J.; Blanco-Ania, D.; Van Der Doef, V.; Van Delft, F. L.; Albada, B. Orthogonal, dual protein labelling by tandem cycloaddition of strained alkenes and alkynes to: *Ortho*-quinones and azides. *Chem. Commun.*, **2018**, *54*, 7338–7341.
(68) Bruins, J. J.; Van de Wouw, C.; Keijzer, J. F.; Albada, B.; van Delft, F. L. Inducible, Selective Labeling of Proteins via Enzymatic Oxidation of Tyrosine. In *Enzyme-Mediated Ligation Methods*, Nuijens, T.; Schmidt, M., Eds.; Springer New York: New York, NY, **2019**; p. 357–368.
(69) Bruins, J. J.; Van de Wouw, C.; Wagner, K.; Bartels, L.; Albada B.; Van Delft, F. L. Highly Efficient Mono-Functionalization of Knob-in-Hole Antibodies with Strain-Promoted Click Chemistry. *ACS Omega*. **2019**, *4*, 11801−11807.
(70) Bruins, J. J.; Damen, J. A. M.; Wijdeven, M. A.; Lelieveldt, L. P. W. M.; Van Delft, F. L.; Albada, B. Non-Genetic Generation of Antibody Conjugates Based on Chemoenzymatic Tyrosine Click Chemistry. *Bioconjugate Chem*. **2021**, *32*, 2167−2172.
(71) Zhdankin, V. V. Organoiodine(V) Reagents in Organic Synthesis. *J. Org. Chem.*, **2011**, *76*, 1185–1197.
(72) Magdziak, D.; Rodriguez, A. A.; Van De Water, R. W.; Pettus, T. R. R. Regioselective oxidation of phenols to *o*-quinones with *o*-iodoxybenzoic acid (IBX). *Org. Lett.*, **2002**, *4*, 285–288.
(73) Kuboki, A.; Yamamoto, T.; Ohira, S. Total Synthesis of (±)-Aiphanol, a Novel Cyclooxygenase-inhibitory Stilbenolignan. *Chem. Lett.*, **2003**, *32*, 420–421.
(74) Huang, Y.; Zhang, J.; Pettus, T. R. R. Synthesis of (±)-Brazilin Using IBX. *Org. Lett.*, **2005**, *7*, 5841–5844.
(75) Ito, S.; Sugumaran, M.; Wakamatsu, K. Chemical reactivities of *ortho*-quinones produced in living organisms: Fate of quinonoid products formed by tyrosinase and phenoloxidase action on phenols and catechols. *Int. J. Mol. Sci.*, **2020**, *21*, 1–36.
(76) Ramsden, C. A.; Riley, P. A. Tyrosinase: The four oxidation states of the active site and their relevance to enzymatic activation, oxidation and inactivation. *Bioorg. Med. Chem.*, **2014**, *22*, 2388–2395.
(77) Ismaya, W. T.; Rozeboom, H. J.; Weijn, A.; Mes, J. J.; Fusetti, F.; Wichers, H. J.; Dijkstra, B. W. Crystal structure of Agaricus bisporus mushroom tyrosinase: Identity of the tetramer subunits and interaction with tropolone. *Biochemistry*, **2011**, *50*, 5477–5486.
(78) Land, E. J.; Ramsden, C. A.; Riley, P. A. Tyrosinase autoactivation and the chemistry of *ortho*-quinone amines. *Acc. Chem. Res.*, **2003**, *36*, 300–308.
(79) Solomon, E. I.; Heppner, D. E.; Johnston, E. M.; Ginsbach, J. W.; Cirera, J.; Qayyum, M.; Kieber-Emmons, M. T.; Kjaergaard, C. H.; Hadt, R. G.; Tian, L. Copper active sites in biology. *Chem. Rev.*, **2014**, *114*, 3659–3853.
(80) Land, E. J.; Ramsden, C. A.; Riley, P. A. The mechanism of suicide-inactivation of tyrosinase: A substrate structure investigation. *Tohoku J. Exp. Med.*, **2007**, *212*, 341–348.
(81) Land, E. J.; Ramsden, C. A.; Riley, P. A.; Stratford, M. R. L. Evidence consistent with the requirement of cresolase activity for suicide inactivation of tyrosinase. *Tohoku J. Exp. Med.*, **2008**, *216*, 231–238.
(82) Stratford, M. R. L.; Ramsden, C. A.; Riley, R. A. Mechanistic studies on the inactivation of tyrosinase by resorcinol. *Bioorg. Med. Chem.*, **2013**, *21*, 1166–1173.

(83) Levandowski, B. J.; Svatunek, D.; Sohr, B.; Mikula, H.; Houk K. N. Secondary Orbital Interactions Enhance the Reactivity of Alkynes in Diels-Alder Cycloadditions. *J. Am. Chem. Soc*. **2019**, *141*, 2224–2227.
(84) Levandowski, B. J.; Svatunek, D.; Sohr, B.; Mikula, H.; Houk K. N. Correction to "Secondary Orbital Interactions Enhance the Reactivity of Alkynes in Diels–Alder Cycloadditions". *J. Am. Chem. Soc*. **2019**, *141*, 18641.
(85) Karver, M. R.; Weissleder, R.; Hilderbrand, S. A. Synthesis and evaluation of a series of 1,2,4,5-tetrazines for bioorthogonal conjugation. *Bioconjugate Chem.*, **2011**, *22*, 2263–2270.
(86) Li, C.; Ge, H.; Yin, B.; She, M.; Liu, P.; Li, X.; Li, J. Novel 3,6-unsymmetrically disubstituted-1,2,4,5-tetrazines: S-induced one-pot synthesis, properties and theoretical study. *RSC Adv.*, **2015**, *5*, 12277–12286.
(87) Boger, D. L.; Schaum, R. P.; Garbaccio, R. M. Regioselective Inverse Electron Demand Diels-Alder Reactions of N-Acyl 6-Amino-3-(methylthio)-1,2,4,5-tetrazines. *J. Org. Chem.*, **1998**, *63*, 6329–6337.
(88) Wang, D.; Chen, W.; Zheng, Y.; Dai, C.; Wang, K.; Ke, B.; Wang, B. 3,6-Substituted-1,2,4,5-tetrazines: tuning reaction rates for staged labeling applications. *Org. Biomol. Chem.*, **2014**, *12*, 3950–3955.
(89) Hamasaki, A.; Ducray, R.; Boger, D. L. Two novel 1,2,4,5-tetrazines that participate in inverse electron demand Diels-Alder reactions with an unexpected regioselectivity. *J. Org. Chem.*, **2006**, *71*, 185–193.
(90) Jain, S.; Neumann, K.; Zhang, Y.; Geng, J.; Bradley, M. Tetrazine-Mediated Postpolymerization Modification. *Macromolecules*, **2016**, *49*, 5438–5443.
(91) Blackman, M. L.; Royzen, M.; Fox, J. M. Tetrazine ligation: fast bioconjugation based on inverse-electron-demand Diels-Alder reactivity. *J. Am. Chem. Soc.*, **2008**, *130*, 13518–13519.
(92) Darko, A.; Wallace, S.; Dmitrenko, O.; Machovina, M. M.; Mehl, R. A.; Chin, J. W.; Fox, J. M. Conformationally strained *trans*-cyclooctene with improved stability and excellent reactivity in tetrazine ligation. *Chem. Sci.*, **2014**, *5*, 3770–3776.
(93) Taylor, M. T.; Blackman, M. L.; Dmitrenko, O.; Fox, J. M. Design and synthesis of highly reactive dienophiles for the tetrazine-*trans*-cyclooctene ligation. *J. Am. Chem. Soc.*, **2011**, *133*, 9646–9649.
(94) Rossin, R.; van den Bosch, S. M.; Ten Hoeve, W.; Carvelli, M.; Versteegen, R. M.; Lub, J.; Robillard, M. S. Highly reactive *trans*-cyclooctene tags with improved stability for Diels-Alder chemistry in living systems. *Bioconjugate Chem.*, **2013**, *24*, 1210–1217.
(95) Yang, J.; Liang, Y.; Seckute, J.; Houk, K. N.; Devaraj, N. K. Synthesis and reactivity comparisons of 1-methyl-3-substituted cyclopropene mini-tags for tetrazine bioorthogonal reactions. *Chem. Eur. J.*, **2014**, *20*, 3365–3375.
(96) Yang, J.; Seckute, J.; Cole, C. M.; Devaraj, N. K. Live-cell imaging of cyclopropene tags with fluorogenic tetrazine cycloadditions. *Angew. Chem. Int. Ed.*, **2012**, *51*, 7476–7479.
(97) Patterson, D. M.; Nazarova, L. A.; Xie, B.; Kamber, D. N.; Prescher, J. A. Functionalized cyclopropenes as bioorthogonal chemical reporters. *J. Am. Chem. Soc.*, **2012**, *134*, 18638–18643.
(98) Chen, W.; Wang, D.; Dai, C.; Hamelberg, D.; Wang, B. Clicking 1,2,4,5-tetrazine and cyclooctynes with tunable reaction rates. *Chem. Commun.*, **2012**, *48*, 1736–1738.
(99) Lang, K.; Davis, L.; Wallace, S.; Mahesh, M.; Cox, D. J.; Blackman, M. L.; Fox, J. M.; Chin, J. W. Genetic Encoding of bicyclononynes and trans-cyclooctenes for site-specific protein labeling in vitro and in live mammalian cells via rapid fluorogenic Diels-Alder reactions. *J. Am. Chem. Soc.*, **2012**, *134*, 10317–10320.

(100) Meijer, A.; Otto, S.; Engberts, J. B. F. N. Effects of the Hydrophobicity of the Reactants on Diels−Alder Reactions in Water. *J. Org. Chem.*, **1998**, *63*, 8989–8994.
(101) Laidler, K. J.; King, M. C. The development of transition-state theory. *J. Phys. Chem*. **1983**, *87*, 2657–2664.
(102) Eyring, H. The activated complex in chemical reactions. *J. Chem. Phys*. **1935**, *3*, 107–115.
(103) Evans, M. G.; Polanyi, M. Some applications of the transition state method to the calculation of reaction velocities, especially in solution. *Trans. Faraday Soc*. **1935**, *31*, 875–894.
(104) Wynne-Jones, W. F. K.; Eyring, H. The Absolute Rate of Reactions in Condensed Phases. *J. Chem. Phys*. **1935**, *3*, 492–502.

Chapter 2

Synthetic efforts towards oxa- and azacyclooctynes

J.A.M. Damen, Dr. B. Albada, Prof. Dr. F.L. van Delft

Abstract
A need for highly reactive and polar cycloalkyne reagents for strain-promoted azide-alkyne cycloaddition (SPAAC) click chemistry was born from unsuccessful DBCO-SPAAC click labelling of azide-enriched tumor cell glycocalyx. To this end, various monobenzoannulated oxa and azacyclooctynes were designed, and synthetic routes explored to acquire these structures. A competing decomposition pathway that is postulated to mechanistically occur via a 1,4-*tele*-elimination prevented isolation or trapping of the desired molecules.

1. Introduction

The cellular glycocalyx comprises the polysaccharide exterior of cells and is a dominant factor in cell-cell interactions, cell-virus interactions and various other biological processes. In our current research we are interested in visualizing how the thickness and dynamics of the glycocalyx affect cellular interactions with lymphocytes. For example, does the glycocalyx move away when interacting with immune cells, resulting in notable differences in thickness at the contact points when compared to unaffected regions? Does it relocalize in these events? Hypertrophic tumor cells often exhibit a thicker than normal glycocalyx layer, due to enhanced metabolism. As the glycocalyx becomes thicker, it poses a larger physical barrier, thereby suppressing cell-cell interactions. This phenomenon may result in successful tumor cell evasion, as such hypertrophic tumor cells may go undetected for innate immune responses by virtue of their thicker glycan "fur-coat". At the same time, we reasoned that the hypertrophic nature of these tumor cells could be employed as their Achilles' heel in a two-stage strategy: (a) exposure of tumors to artificially tagged monosaccharides that are processed by the biosynthetic machinery and incorporated in the glycocalyx structure,[1] followed by (b) bio-orthogonal labeling of the tagged tumors for visualization or enhanced T cell engagement. When unnatural monosaccharides bearing orthogonal click tags such as azides are used, the extracellular glycocalyx is enriched with an azide tag that can function as a handle for the covalent tethering of any payload to the cell surface by means of ligation methods such as copper-free click chemistry. Such payloads may comprise (i) fluorophores for visualizing the glycocalyx with confocal microscopy, or (ii) interleukins to recruit and/or re-activate of immune cells towards these tumor cells. We will focus on the first approach in this **Chapter** and in **Chapter 3**, and on the second approach in **Chapter 6**.

Peracetylated *N*-α-azidoacetyl-D-mannosamine (Ac_4ManNAz) was chosen as unnatural monosaccharide source. The more lipophilic peracetylated version of ManNAz has been shown to freely diffuse through membranes of mammalian cells, while the azido group is a stable label on cell surfaces that allows for bio-orthogonal ligation.[2-4] After uptake, *O*-deacetylation to ManNAz is affected intracellularly by cytosolic or ER esterases.[1,5] The main advantage of peracetylated non-natural sugars is that they can be used at substantially lower concentration (*e.g.,*~200-fold), as compared to the non-acetylated sugars, to achieve similar levels of surface expression.[1,6] Once ManNAz is intracellularly present, it enters the well-known sialic acid biosynthetic pathway resulting in terminal sialylation of N-glycans with azidoacetylneuraminic acid (SiaNAz) by various sialyltranferases.

The main advantage of sialic acid residues is that they are positioned at the non-reducing end of cell surface N-glycans and play a privileged role in cellular, viral and proteinaceous interactions.[7] Fluorescent labelling can therefore be used to reveal overall glycocalyx thickness in super resolution microscopy, schematically depicted in **Figure 1A**. This is not achieved when GalNAz or GlcNAz are used, as this places the azide at substantially shorter *O*- or *N*-linked glycan chains (with possible different distributions within or around the cells), which will perturb the fluorescent read-out after the click reaction in assessing glycocalyx thickness. Furthermore, sialic acids are a known component of carbohydrate antigens that are highly abundant on tumor cells due to overexpressed sialyltransferase.[8] Combining this feature with a general enhanced level of metabolism suggests disproportionally high incorporation of sialic acids into the glycocalyx.[9]

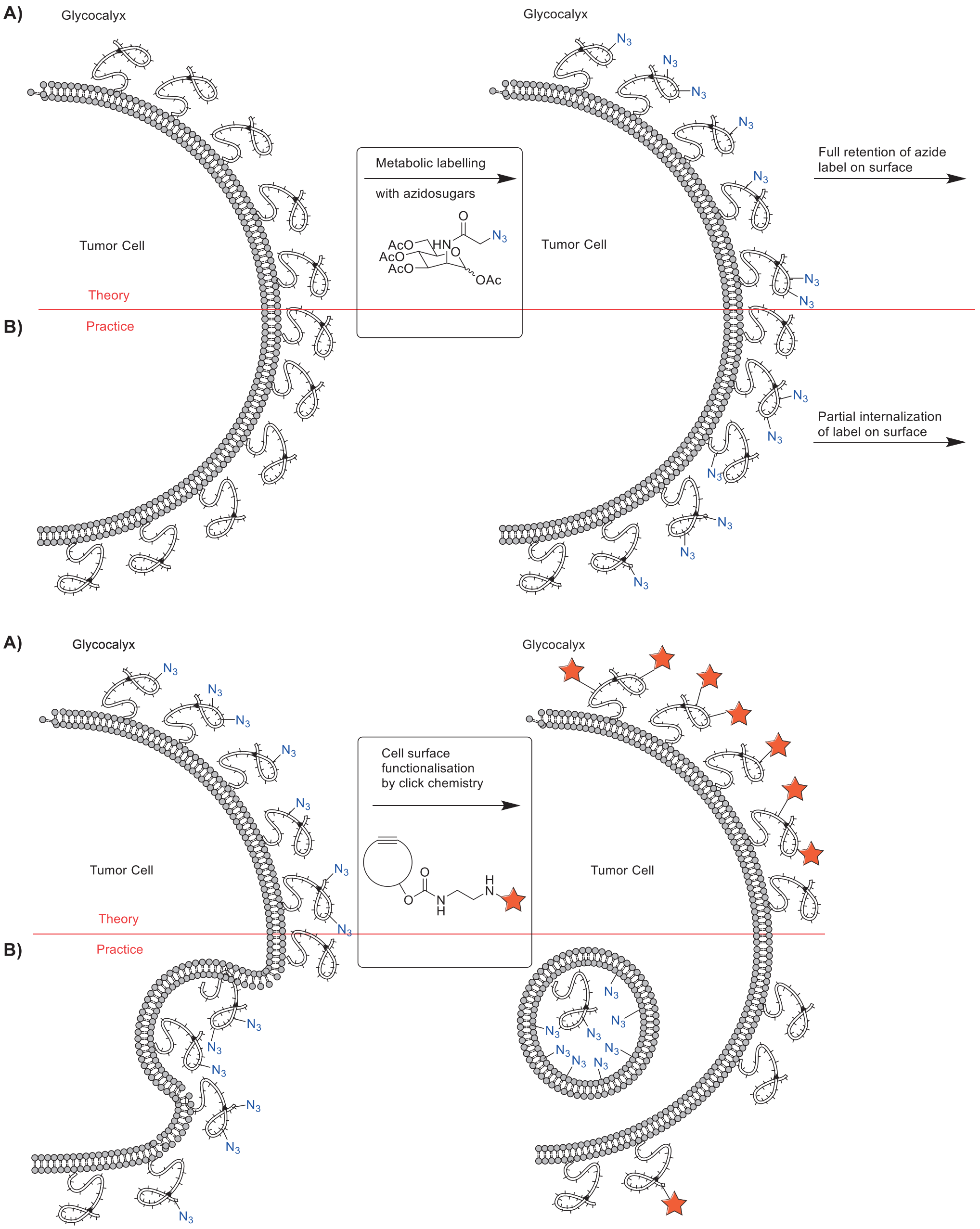
A)
Glycocalyx
Glycocalyx
Metabolic labelling
with azidosugars
AcO
AcO
AcO
HN
O
O
OAc
N3
Tumor Cell
Tumor Cell
Full retention of azide label on surface
Theory
Practice
B)
Partial internalization of label on surface
N3
A)
Glycocalyx
Glycocalyx
Cell surface functionalisation by click chemistry
O
O
N
H
H
N
Tumor Cell
Tumor Cell
Theory
Practice
B)
N3

Figure 1: **A)** Top panels: Idealized sequence of metabolic labelling with $Ac_4ManNAz$, and subsequent fluorescent labelling with SPAAC (shown in second part of this figure on the next page). **B)** Bottom panels: A more realistic depiction of metabolic labelling that includes internalization of azide-labelled glycocalyx, which leads to (strongly) reduced fluorescent labelling.

In a preliminary study, B16F10/OVA cell lines were incubated with $Ac_4ManNAz$ at physiological temperature, after which labelling was performed using commercially available DBCO-Cy5 by means of strain-promoted azide-alkyne cycloaddition (SPAAC) click chemistry.[10] Unfortunately, only minimal fluorescent labelling of the cells was observed, thus preventing unraveling of glycocalyx dynamics in tumor cell evasion. It was attributed to known membrane internalization and recycling by endocytosis,[11,12] occurring on the same timescale as the labelling should take place, leading to only minimal labelling of the glycocalyx with the dye. This process is schematically depicted in **Figure 1B**. Alteration of the azide to other handles (*e.g.* aryl azides, tetrazines and *ortho*-quinones) is not possible due to the size constraints of the sialic acid biosynthetic pathway.[1] These considerations therefore require the development of faster SPAAC cycloalkyne probes, *i.e.* with increased second-order rate constant k_2.

2. Design of oxa- and azacyclooctynes

For the development of a more reactive cycloalkyne for SPAAC we envisioned designing a COMBO-type cyclooctyne and further decorating it with heteroatoms at the propargylic positions in the ring, see **Figure 2**. COMBO **1** was reported to be a stable yet highly reactive cyclooctyne in SPAAC (k_2 = 0.235 $M^{-1}s^{-1}$) with a similar reactivity to BCN and DBCO.[13,14] As we anticipated that the lipophilicity of the structure would hamper application in aqueous solutions, it was chosen to incorporate oxygen or nitrogen groups in the ring backbone to function as hydrogen bond acceptors or donors, to enhance water solubility of the click handles. Moreover, incorporation of heteroatoms at these positions would also lead to even higher reactivity, according to computational investigations by Alabugin.[15] This results in the basic structures of oxacyclooctyne **2** and azacyclooctyne **3**, see **Figure 2**. Fluorescent groups then have to be attached either directly onto the aromatic ring or in case of **3** to the nitrogen atom. However, reactivity of the oxa- and azacyclooctynes needs to be assessed prior to functionalization.

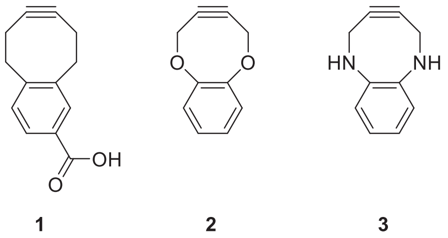

Figure 2: Structures of COMBO **1** and the newly designed oxacyclooctyne **2** and azacyclooctyne **3**.

3. Results and Discussion

3.1 Syntheses towards oxacyclooctyne

We therefore designed a synthesis pathway to oxacyclooctyne **2** via its protected analogue **6**, see **Scheme 1**. It was envisaged that an alkyne precursor could be installed as part of the 8-membered cyclic system by dialkylation of catechol with a dicobalt hexacarbonyl-alkyne complex, similar to a Nicholas reaction.[16] Such a complex was formed by reacting 1,4-dichloro-2-butyne **4** with dicobalt octacarbonyl in hexane, followed by the rapid evolution of carbon monoxide gas and subsequent purification by crystallization, affording complex **5**.[17] The use of complex has three main advantages: (i) it serves as a protecting group; (ii) it breaks the linearity of the alkyne; (iii) it activates the chloride atoms as leaving groups. The alkylation of catechol with complex **5** was then performed under a variety of mild basic conditions, see **Scheme 1**. Unfortunately, none of these conditions afforded the target product. Instead, the starting material complex **5** decomposed upon addition of base in the presence of catechol, indicative of a redox reaction between deprotonated catechol[18] and dicobalt(II) hexacarbonyl-alkyne complex **5**, leading to the formation of Co(I) or Co(0) species and decomposition of the complex. A control reaction of complex **5** with non-redox reactive propylene glycol in the presence of AgOTf and NaH in THF, successfully afforded cyclization to **7** without decomposition of the complex, supporting the redox theory. Structure **7** is not of interest as similar compounds were already reported.[16]

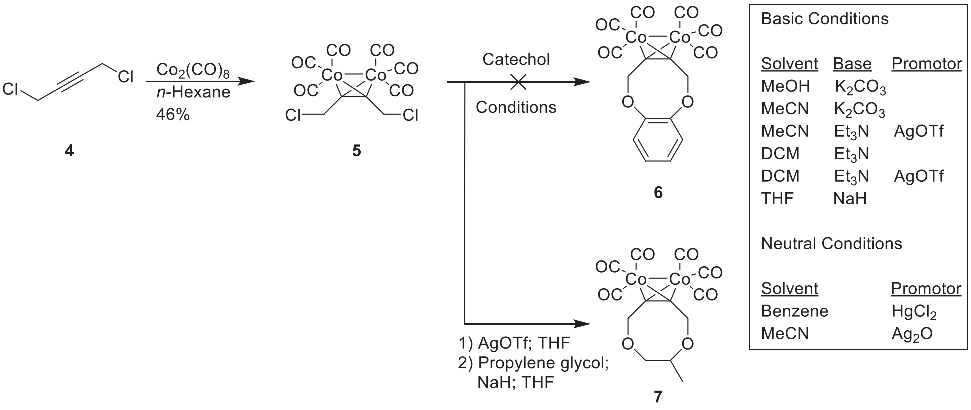

Basic Conditions

Solvent	Base	Promotor
MeOH	K_2CO_3	
MeCN	K_2CO_3	
MeCN	Et_3N	AgOTf
DCM	Et_3N	
DCM	Et_3N	AgOTf
THF	NaH	

Neutral Conditions

Solvent	Promotor
Benzene	$HgCl_2$
MeCN	Ag_2O

Scheme 1: Synthesis efforts towards protected oxacyclooctynes **6** and **7** .

Various silyl ether-based protecting groups (PGs) were screened for monoprotection of catechol **8** in order to suppress redox reactivity, see **Scheme 2**. The triethylsilyl (TES) PG was the optimal candidate and was installed on catechol by treatment with TES-Cl and triethylamine in DCM in quantitative yield. *tert*-Butyldimethylsilyl (TBDMS) ether monoprotected catechol was afforded in a similar way. Subsequent alkylation with complex **5** worked for mono-TES-catechol **10**, but did not work for mono-TBDMS-catechol **11** presumably due to steric reasons. Deprotection of the TES group with TBAF resulted in immediate decomposition of the complex of compound **12**, presumably due to nucleophilic attack of F⁻ onto the Co(II) centers. Other deprotection conditions were also evaluated, see **Scheme 2**, however all led to either decomposition or no reaction.

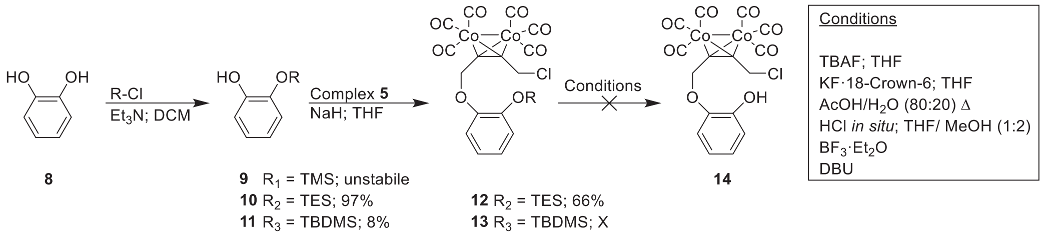
HO
OH
R-Cl
Et3N; DCM
HO
OR
Complex 5
NaH; THF
OC
CO
CO
Co
Co
CO
Cl
O
OR
Conditions
OH
8
9 R1 = TMS; unstabile
10 R2 = TES; 97%
11 R3 = TBDMS; 8%
12 R2 = TES; 66%
13 R3 = TBDMS; X
14
Conditions
TBAF; THF
KF·18-Crown-6; THF
AcOH/H2O (80:20) Δ
HCl in situ; THF/ MeOH (1:2)
BF3·Et2O
DBU

Scheme 2: Synthesis attempts towards protected oxacyclooctyne precursor **14**.

In a final attempt to acquire the target cyclooctyne, direct alkylation of the (mono-protected) catechol was attempted in order to remove the protecting group prior to metal complex installation and cyclisation. Alkylation with 1,4-dichloro-2-butyne only occurred upon refluxing, however after isolation the product spontaneously polymerized, see **Scheme 3**. Upon heating, the alkylated product concomitantly potentially formed a cumulene as an elimination product, which is highly prone to polymerization.[19,20] In order to perform the alkylation at room temperature 1,4-diiodo-2-butyne was used, which was easily furnished from 1,4-dichloro-2-butyne precursor by means of a Finkelstein reaction with NaI in acetone in 51% yield. However, using 1,4-diiodo-2-butyne for alkylation at room temperature also led to polymerization, by either the same mechanism or potentially by means of formation of 1-iodo-butatriene.

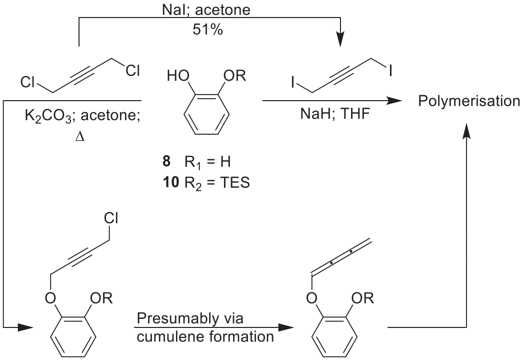
NaI; acetone
51%
Cl
Cl
HO
OR
I
I
K2CO3; acetone;
Δ
NaH; THF
Polymerisation
8 R1 = H
10 R2 = TES
Cl
O
OR
Presumably via
cumulene formation
O
OR

Scheme 3: Synthesis attempts towards unprotected oxacyclooctyne precursors.

3.2 Syntheses towards azacyclooctyne

As the oxacyclooctynes were synthetically unfeasible, it was decided to switch to azacyclooctyne derivative compound **18**. First, *ortho*-phenylenediamine **15** was tosylated forming non-redox reactive bis-*N,N′*-tosyl-*ortho*-phenylenediamide **16**, see **Scheme 4**. The installation of tosyl as a protecting group was anticipated to facilitate monoalkylation in the next step, and to prevent polymerization and cross-linking. Bis-*N,N′*-tosyl-*ortho*-phenylenediamide **16** was then reacted with dicobalt hexacarbonyl-alkyne complex **5** in acetone with K_2CO_3 to afford the eight membered ring structure **17** in 5% yield after purification by flash chromatography. This reaction was accompanied by the formation of 2:1 and 1:2 trimer structures, as was confirmed by high resolution mass spectrometry (HRMS). With the target protected cycloalkyne compound **17** in hand, deprotection of the dicobalt hexacarbonyl complex was performed with trimethylamine *N*-oxide (TMANO) in MeCN, resulting in an instantaneous reaction with full consumption of compound **17**. To our surprise target cyclooctyne **18** was not detected, nor isolated from the reaction mixture. In order to determine whether the desired species had been formed transiently, several trapping experiments of the cyclooctyne were performed by generating it *in situ* in the presence of an excess of benzyl azide, phenyl azide or 4-*tert*-butyl-*ortho*-quinone. Subsequent liquid chromatography–high resolution mass spectrometry (LC-HRMS) measurements did not identify any azacyclooctyne species, nor trapped click products or derivatives thereof. This implies that the formed cycloalkyne species, if at all formed, is extremely short-lived and thus would be highly unstable. Albeit of academic interest, such an unstable probe would have no applicability in dilute biological systems, as it would decompose prior to performing click reactions.

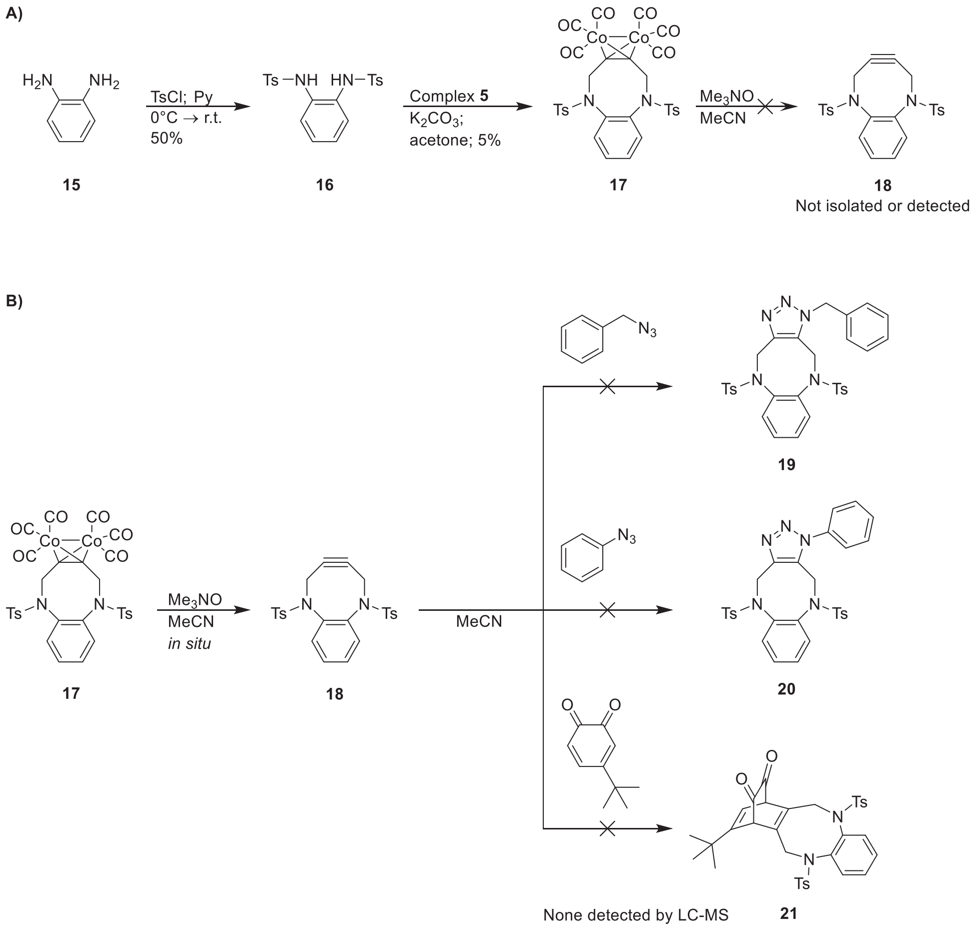
A)
H2N
NH2
TsCl; Py
0°C → r.t.
50%
Ts–NH
HN–Ts
Complex 5
K2CO3;
acetone; 5%
OC
CO
CO
Co
Co
CO
OC
CO
Ts
N
N
Ts
Me3NO
MeCN
18
Not isolated or detected
15
16
17
B)
N3
N
N
N
Me3NO
MeCN
in situ
MeCN
19
20
21
O
O
None detected by LC-MS
17
18

Scheme 4: **A)** Synthesis attempts to azacyclooctyne **18**. **B)** Trapping experiments to detect azacyclooctyne **18** following *in situ* formation.

4. Conclusions

Approximately a year after terminating this research project, a research paper was published in which highly structurally similar cycloalkynes were investigated as compared to the compounds we pursued,[21] describing benzoannulated eight to ten membered cyloalkynes, bearing an oxygen or nitrogen heteroatom attached to the propargylic carbon, see **Scheme 5**. The main conclusion was that eight-membered, and even some of nine-membered rings, were also highly unstable. These finding are in line with earlier reports describing a monobenzoannulated cyclooctyne system bearing sulfur heteroatoms tethered to the propargylic position compound **25**, that upon cobalt complex deprotection also were too unstable for isolation, where this was not the case for their saturated analogues.[16]

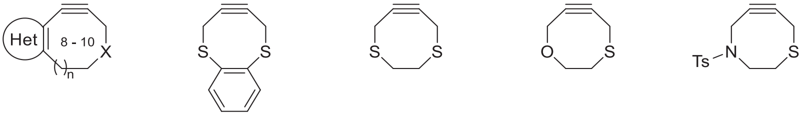

22-24
n=1 unstable
n=2-3 stable

25
unstable

26
stable

27
stable

28
stable
$k_2 = 8.5 \cdot 10^{-3}\ M^{-1}s^{-1}$

Scheme 5: Several related stable or unstable compounds. Balova's systems (left); Bräse's systems (middle); and system by Ni *et al.* (right).[16,21,25]

Based on these and our findings, it is clear that formation of benzoannulated oxa- or azacyclooctynes under non-basic conditions is futile. Besides, even formation of the cyclooctyne species after cobalt complex deprotection is highly challenging, given it is very short-lived. It presumably decomposes in a 1,4-*tele*-elimination, see **Scheme 6**. This mechanism under basic conditions was already described for the reaction of linear *N*,*N*-dialkyl-4-alkoxy-2-butyn-1-amines $R_2NCH_2C{\equiv}CCH_2OR$ **29** with KO*t*Bu in THF, forming *N*,*N*-dialkyl-3-buten-yn-1-amines $R_2NC{\equiv}C{-}CH{=}CH_2$ **32**.[22-24] Apparently, in our more strained compounds, any species in solution, as well as the solvent, could serve as a base in such an elimination.

That we pushed our designed system too far in the amount of strain employed by benzoannulation is proven by the fact that compounds **26–28** are stable compounds, see **Scheme 5**. However, the k_2 value of compound **28** in SPAAC is $8.5 \cdot 10^{-3}\ M^{-1}s^{-1}$ and as such 36 times slower than DBCO ($k_2 = 0.31\ M^{-1}s^{-1}$).[14,25] Thus these stable analogues are not useful for cell labelling.

Fortunately, during these studies, a paper appeared that described a more reactive probe in SPAAC click chemistry. In **Chapter 3** we describe how this probe was prepared, functionalized with dyes, and implemented in glycocalyx studies.

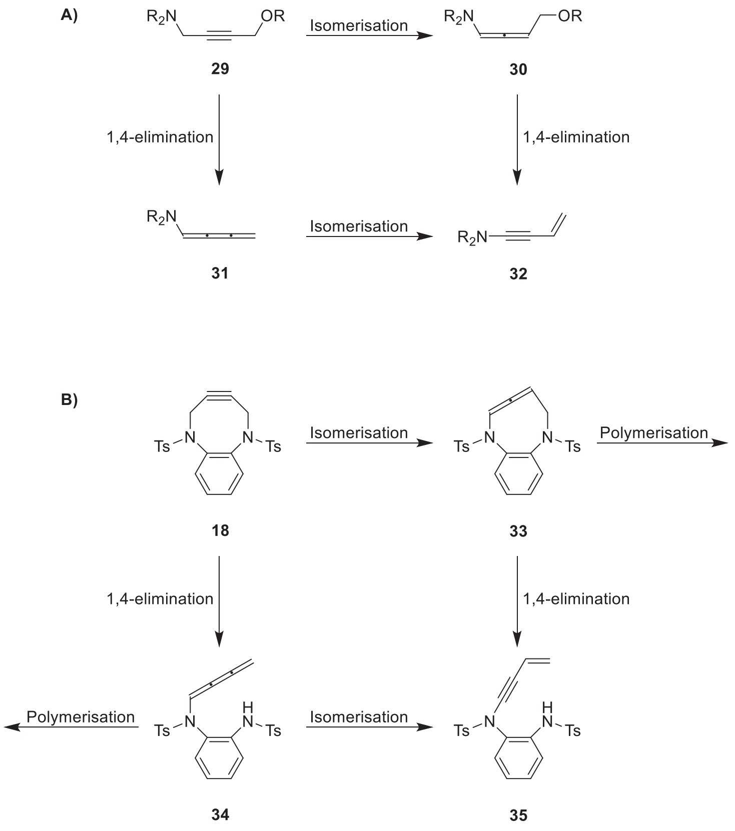
A)
R2N
OR
29
Isomerisation
30
1,4-elimination
1,4-elimination
31
Isomerisation
32
B)
Ts
N
N
Ts
18
Isomerisation
33
Polymerisation
1,4-elimination
1,4-elimination
34
Polymerisation
Isomerisation
H
35

Scheme 6: **A)** 1,4-*tele*-elimination mechanism, as proven by the works of Brandsma. **B)** 1,4-*tele*-elimination as a proposed decomposition pathway of compound **18**.

5. Experimental

5.1. General information

5.1.1 Instruments

^{1}H-NMR (400 MHz) and ^{13}C-NMR spectra (101 MHz) were recorded on a Bruker 400 MHz AV400 NMR spectrometer. Chemical shifts were reported in ppm referenced against the residual solvent peaks of the NMR solvent. ESI-HRMS spectra or DART-HRMS spectra were recorded on an Exactive Mass Spectrometer (Thermo Scientific) with a DART setup from Ion Sense. Mass values were calculated with enviPat Web.[26]

5.1.2 NMR spectroscopy of cobalt complexes

Signal broadening due to formation of paramagnetic decomposition rests of cobalt, originating over a short period of time (hours) from diamagnetic dicobalt hexacarbonyl – alkyne complexes, is well known and described by Garçon.[27] Acquisition time and relaxation delay were adjusted to 100 ms and an increased number of scans were recorded in case of paramagnetic ^{1}H-NMR measurements, providing them as fingerprint spectra.

5.1.3 General chemicals:

Dicobalt octacarbonyl (stabilized with 1-5% hexane) and 1,2-diaminobenzene were purchased from TCI Europe. *p*-Toluenesulfonyl chloride, catechol and potassium carbonate were purchased from Alfa Aesar. Chlorotriethylsilane, hydrochloric acid (37%), benzyl azide (0.5 M in dichloromethane) and sodium hydride (60 % dispersion in mineral oil) were purchased from Sigma-Aldrich Merck. 1,4-Dichloro-2-butyne, triethylamine; sodium sulfate were all purchased from Thermo Scientific™ / Fisher Scientific. Pyridine was purchased from Acros Organics. Ethyl acetate (GPR Rectapur) was purchased from VWR Chemicals. *n*-Hexane, acetone and dichloromethane (Puriss. p.a.) were purchased from Honeywell Riedel-de Haën™. THF (unstabilized; HPLC) was purchased from Biosolve. All of these chemicals were used as purchased unless otherwise stated. *n*-Hexane was dried over 4 Å MS (flame dried) and degassed by sparging with argon for 30 minutes, prior to use. Acetone was also degassed by sparging with argon for 30 minutes, prior to use.

5.1.4 Chromatography:

Flash chromatography was performed on SiliaFlash® P60 40–63µm (230–400 mesh) 60 Å Irregular Silica Gel (R12030B) (SiliCycle, Quebec City (Quebec), Canada). Thin Layer Chromatography was performed on TLC Silica gel 60 F_{254} on aluminium sheets (Merck, Darmstadt, Germany). After development, TLC plates were dip stained and heated with a heat gun for visualization of spots. $KMnO_4$ stain was used as a general stain and was prepared by dissolving 1.5 g $KMnO_4$, 10 g K_2CO_3 and 1.25 mL 10% NaOH in 200 mL water. Cerium ammonium molybdate stain was used as a general stain and was prepared by dissolving 12 g of ammonium molybdate, 0.5 g of ceric ammonium sulfate and 15 mL of sulfuric acid in 235 mL water.

5.2. Chemical syntheses

Phenylazide was synthesized according to literature procedure of Kwok.[28] 4-*tert*-butyl-*ortho*-quinone was synthesized by the method of Borrmann.[29]

5.2.1 Synthesis of dicobalt hexacarbonyl-μ,η^2,η^2-1,4-dichloro-2-butyne 5

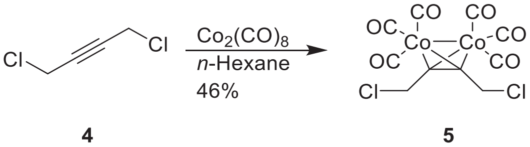

A 25 mL flame-dried round-bottom flask was charged with dicobalt octacarbonyl (1.026 g; 3 mmol; 1 eq) and a magnetic stirring bar. The flask was fitted with a septum and was placed under Ar. The solids were then dissolved in 12 mL *n*-hexane to give a dark red homogeneous solution. 1,4-Dichloro-2-butyne **4** (286 µL; 2.9 mmol; 1 eq) was added via syringe and the septum was fitted with a bleed needle. CO gas evolved immediately from the reaction mixture, which was left to stir for 21 hours at room temperature. The deep dark red reaction mixture was filtered over a sintered glass filter and the powder bed was washed with 50 mL *n*-hexane. The filtrate was collected and solvent was removed *in vacuo* to yield a dark red solid crude product. The crude product was recrystallized three times from *n*-hexane to afford 0.5443 g of dicobalt hexacarbonyl-*μ*,η^2,η^2-1,4-dichloro-2-butyne **5** as red platelet crystals. Yield 46%.

^{1}H NMR (400 MHz, $CDCl_3$) δ 4.87 (b s, 4H). ^{13}C NMR (101 MHz, $CDCl_3$) δ 46.71. HRMS (DART) calc. for $C_{10}H_4ClCo_2O_6$ $[M-Cl]^+$ 372.8355; found 372.8358.

5.2.3 Synthesis of triethyl (2-hydroxy-phenoxy)silane 10

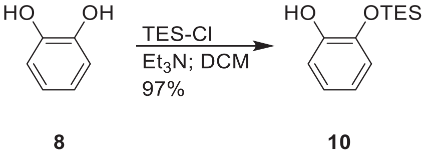

A 100 mL round-bottom flask was charged with catechol **8** (1.09 g; 9.9 mmol; 1 eq) and was dispersed in 50 mL DCM under magnetic stirring. Et_3N (1.4 mL; 10 mmol; 1 eq) was added to reaction mixture, which was stirred to give a homogeneous solution. The neck of the flask was fitted with a septum and flask cooled in an ice-water bath. Chlorotriethylsilane (1.7 mL; 10.1 mmol; 1 eq) was added dropwise via syringe over the course of 2 minutes. The reaction mixture was left to stir in an ice/water bath at 0 °C for 30 minutes and another 15 minutes at room temperature, after which the formation of target compound **10** was complete according to TLC (R_f = 0.63 in 10% EtOAc/PE. R_f = 0.13 for catechol). The reaction mixture was then transferred to a 250 mL separatory funnel and was washed with 50 mL demineralized water. The aqueous phase was reextracted twice with 50 mL DCM. The combined organic phases were dried over Na_2SO_4; filtered; and solvent removed *in vacuo* to afford 2.16 g of triethyl (2-hydroxy-phenoxy)silane **10** as an oil. Yield 97%.

^{1}H NMR (400 MHz, $CDCl_3$) δ 6.93 (dd, *J* = 7.9, 1.7 Hz, 1H), 6.87 (dd, *J* = 7.3, 1.6 Hz, 1H), 6.85 – 6.80 (m, 1H), 6.74 (ddd, *J* = 8.0, 7.2, 1.7 Hz, 1H), 5.55 (s, 1H), 1.01 (t, *J* = 7.9 Hz, 9H), 0.81 (q, *J* = 7.8 Hz, 6H). ^{13}C NMR (101 MHz, $CDCl_3$) δ 147.3, 142.6, 122.2, 120.1, 117.6, 114.9, 6.7, 5.2.

5.2.4 Synthesis of dicobalt hexacarbonyl-μ,η²,η²-1-chloro-4-(2-triethylsilyloxy-phenyoxy)-2-butyne 12

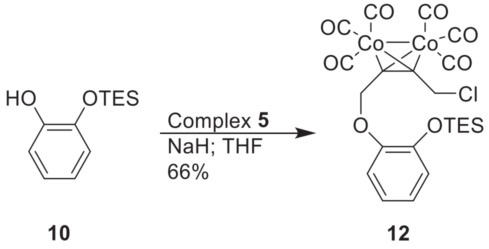

A 25 mL round-bottom flask was charged with dicobalt hexacarbonyl-*μ*,*η*^{2},*η*^{2}-1,4-dichloro-2-butyne **5** (61.1 mg; 149 µmol; 1 eq) and triethyl (2-hydroxy-phenoxy)silane **10** (37.9 mg; 169 µmol; 1.1 eq), which were dissolved in 12 mL THF under magnetic stirring to form a deep dark red homogeneous solution. The flask was cooled in an ice-water bath and sodium hydride (60 % dispersion in mineral oil; 10 mg; 250 µmol; 1.7 eq) was added to the mixture. The reaction mixture was left to stir in an ice/water bath at 0 °C for 30 minutes and another 45 minutes at room temperature, after which TLC indicated clean formation of target compound **12** (R_f = 0.70 in 10% EtOAc/PE. Red spot and UV active). The mixture was quenched by addition of 10 mL of brine, also affording phase separation. The biphasic mixture was extracted and the aqueous phase was reextracted with 10 mL THF. The combined organic phases were dried over Na_2SO_4; filtered; and solvent removed *in vacuo*. TLC indicated that only product **12** was present after workup. This affords 58.8 mg of dicobalt hexacarbonyl-*μ*,*η*^{2},*η*^{2}-1-chloro-4-(2-triethylsilyloxy-phenyoxy)-2-butyne **12** as a dark red solid. Yield 66%.

^{1}H NMR (400 MHz, $CDCl_3$) δ 6.87 (b s, 2H), 4.86 (b s, 2H), 1.87 – 0.58 (b m, 13H), 0.00 (b s, 6H). ^{13}C NMR (101 MHz, $CDCl_3$) unable to record any resonances due to paramagnetism.

5.2.5 Synthesis of 1,2-bis-(tosylamido)-benzene 16

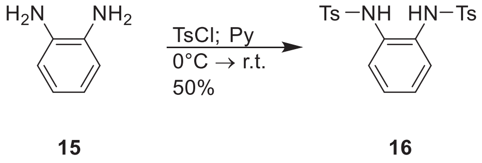

A 50 mL round-bottom flask was charged with 1,2-diaminobenzene **15** (1.59 g; 14.7 mmol; 1 eq) and was dissolved in 20 mL pyridine under magnetic stirring. The flask was cooled in an ice-water bath and *p*-toluenesulfonyl chloride (5.77 g; 30.3 mmol; 2.1 eq) was added to the mixture. The reaction mixture was left to warm up to room temperature and stir for 96 hours. The solvent was concentrated *in vacuo* and the residue was taken up in 70 mL DCM, which was washed with 25 mL 1M HCl and 5 times with 50 mL demineralized water. The organic phase was dried over Na_2SO_4; filtered; and solvent removed *in vacuo* to afford 3.09 g of 1,2-bis-(tosylamido)-benzene **16** as an orange powder. Yield 50%.

^1H NMR (400 MHz, $CDCl_3$) δ 7.57 (d, *J* = 8.4 Hz, 4H), 7.22 (d, *J* = 8.1 Hz, 4H), 7.07 – 7.01 (m, 2H), 6.99 – 6.93 (m, 2H), 6.84 (s, 2H), 2.39 (s, 6H). ^{13}C NMR (101 MHz, $CDCl_3$) δ 144.4, 135.6, 131.0, 129.8, 127.7, 127.5, 126.4, 21.7.

5.2.6 Synthesis of dicobalt hexacarbonyl-μ,η²,η²-(N,N-ditosyl)-azacyclooctyne 17

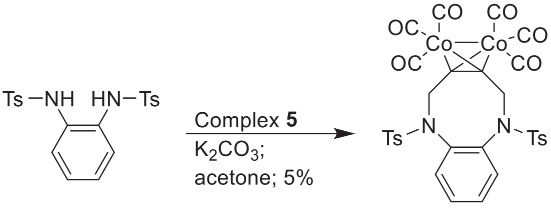

16

17

A 50 mL round-bottom flask was charged with dicobalt hexacarbonyl-*μ*,*η*²,*η*²-1,4-dichloro-2-butyne **5** (354 mg; 0.87 mmol; 1 eq) and 1,2-bis-(tosylamido)-benzene **16** (360.5 mg; 0.87 mmol; 1 eq), which were dissolved in 20 mL degassed acetone under magnetic stirring to give a deep dark red homogeneous reaction mixture. K_2CO_3 (620 mg; 4.49 mmol; 5.2 eq) was added and the mixture was stirred for 5 days, following the formation of target compound **17** (R_f = 0.54 in 30% EtOAc/PE. Red spot and UV active). The dispersion was left to settle and the deep dark red supernatant was decanted and collected. The solvent was removed *in vacuo* and the residue was dry packed on silica with DCM. Target product **17** was purified by Flash Chromatography (eluent: 0% → 40% EtOAc/*n*-hexane) and relevant fractions were identified by TLC and HRMS. This afforded 29.8 mg of dicobalt hexacarbonyl-*μ*,*η*²,*η*²-(*N*,*N*- ditosyl)-azacyclooctyne **17** as a red solid glass. Yield 5%.

Paramagnetic ^1H NMR (400 MHz, $CDCl_3$) δ 7.92, 7.29, 6.83, 6.46, 5.20, 4.73, 4.58, 4.12, 2.43, 2.05, 1.26, 0.88. HRMS (ESI) calc. for $C_{30}H_{23}Co_2N_2O_{10}S_2$ $[M+H]^+$ 752.9453; found 752.9436.

The supporting information and appendices are made available via the QR-code below.

6. References

(1) Jacobs C. L.; Goon S.; Yarema K. J.; Hinderlich S.; Hang H. C.; Chai D. H.; Bertozzi C. R. Substrate specificity of the sialic acid biosynthetic pathway. *Biochemistry* **2001**, *40*, 12864–12874.
(2) Saxon, E.; Bertozzi, C. R. Cell surface engineering by a modified Staudinger reaction. *Science.* **2000**, *287*, 2007–2010.
(3) Saxon, E.; Luchansky, S. J.; Hang, H. C.; Yu, C.; Lee, S. C.; Bertozzi, C. R. Investigating cellular metabolism of synthetic azidosugars with the Staudinger ligation. *J. Am. Chem. Soc.* **2002**, *124*, 14893–14902.
(4) Bertozzi C. R.; Kiessling L. L. Chemical glycobiology. *Science* **2001**, *291*, 2357–2364.
(5) Sarkar, A. K.; Fritz, T. A.; Taylor, W. H.; Esko, J. D. Disaccharide uptake and priming in animal cells: Inhibition of sialyl Lewis X by acetylated Galβ1→4GlcNAcβ-O-naphthalenemethanol. *Proc. Natl. Acad. Sci. USA* **1995**, *92*, 3323–3327.
(6) Jacobs, C. L.; Yarema, K. J.; Mahal, L. K.; Nauman, D. A.; Charters, N. W.; Bertozzi, C. R. Metabolic labeling of glycoproteins with chemical tags through unnatural sialic acid biosynthesis. *Methods in Enzymology* **2000**, *327*, 260–275.
(7) Dube, D. H.; Bertozzi, C. R. Metabolic oligosaccharide engineering as a tool for glycobiology. *Curr. Opin. Chem. Biol.* **2003**, *7*, 616−625.
(8) Kelm, S.; Schauer, R. Sialic acids in molecular and cellular interactions. *Int. Rev. Cytol.* **1997**, *175*, 137–240.
(9) Mahal, L. K.; Yarema, K. J.; Lemieux, G. A.; Bertozzi, C. R. Chemical approaches to glycobiology: Engineering cell surface sialic acids for tumor targeting. In: Inoue Y.; Lee Y. C.; Troy F. A., editors. *Sialobiology and Other Novel Forms of Glycosylation*. Osaka, Japan: Gakushin Publishing Company; **1999**, p. 273–280.
(10) Personal communication with our collaborators Daan Smits and Prof. dr. Peter Friedl.
(11) Watanabe, S.; Boucrot, E. Fast and ultrafast endocytosis. *Curr. Opin. Cell Biol.* **2017**, *47*, 64–71.
(12) Grant, B. D.; Donaldson, J. G. Pathways and mechanisms of endocytic recycling. *Nat. Rev. Mol. Cell Biol.* **2009**, *10*, 597–608.
(13) Varga, B. R.; Kállay, M.; Hegyi, K.; Béni, S.; Kele, P. A non-fluorinated monobenzocyclooctyne for rapid copper-free click reactions. *Chem. Eur. J.* **2012**, *18*, 822–828.
(14) Dommerholt, J.; Rutjes, F. P. J. T.; van Delft, F. L. Strain-Promoted 1,3-Dipolar Cycloaddition of Cycloalkynes and Organic Azides. *Top. Curr. Chem. (Z)*. **2016**, *374*, 16.
(15) Gold, B.; Dudley, G. B.; Alabugin, I. V. Moderating strain without sacrificing reactivity: Design of fast and tunable noncatalyzed alkyne-azide cycloadditions via stereoelectronically controlled transition state stabilization. *J. Am. Chem. Soc.* **2013**, *135*, 1558−1569.
(16) Hagendorn, T.; Bräse, S. A new route to dithia- and thiaoxacyclooctynes via Nicholas reaction. *RSC Adv.*, **2014**, *4*, 15493–15495.
(17) Cetini G.; Gambino O.; Rossetti R.; Sappa E. Acetylenic derivatives of metal carbonyls I. Substitution reactions of $Co_2(CO)_6C_2RR'$ complexes. *J. Organometal. Chem.* **1967**, *8*, 149–154.
(18) Yang, J.; Cohen Stuart, M. A.; Kamperman, M. Jack of all trades: Versatile catechol crosslinking mechanisms. *Chem. Soc. Rev.* **2014**, *43*, 8271–8298.
(19) Brandsma, L. Studies in Organic Chemistry 34: Preparative Acetylenic Chemistry. Second edition. Amsterdam, The Netherlands: Elsevier Science Publishers B.V.; **1988**. Chapter IX: 2.14 Diacetylene from 1,4-Dichloro-2-butyne, p. 179–181.

(20) Verkruijsse H. D.; Brandsma L. A Detailed Procedure for the Preparation of Butadiyne. *Synth. Commun.* **1991**, *21*, 657–659.
(21) Danilkina, N. A.; Govdi, A. I.; Khlebnikov, A. F.; Tikhomirov, A. O.; Sharoyko, V. V.; Shtyrov, A. A.; Ryazantsev, M. N.; Bräse, S.; Balova, I. A. Heterocycloalkynes Fused to a Heterocyclic Core: Searching for an Island with Optimal Stability-Reactivity Balance. *J. Am. Chem. Soc.* **2021**, *143*, 16519–16537.
(22) Verboom, W.; Everhardus, R. H.; Bos, H. J. T.; Brandsma, L. A simple synthesis of *N,N*-dialkyl-3-alken-1-yn-1-amines. *Recl. Trav. Chim., Pays-Bas* **1979**, *98*, 508–511.
(23) Brandsma, L. Synthesis of Acetylenes, Allenes and Cumulenes: Methods and Techniques. First edition. Oxford, UK: Elsevier Ltd.; **2004**. Chapter: 10 Acetylenes, Allenes and Cumulenes by Elimination Reactions, p. 203–228. *Specifically: 10.1.5 Tele-elimination of alcohol or thiol from acetylenic, allenic or cumulenic derivatives, p. 205.*
(24) Brandsma, L. Studies in Organic Chemistry 34: Preparative Acetylenic Chemistry. Second edition. Amsterdam, The Netherlands: Elsevier Science Publishers B.V.; **1988**. Chapter XI Base-Promoted Interconversions of Acetylenes, p. 231–246.
(25) Ni, R.; Mitsuda, N.; Kashiwagi, T.; Igawa, K.; Tomooka, K. Heteroatom-embedded medium-sized cycloalkynes: Concise synthesis, structural analysis, and reactions. *Angew. Chem. Int. Ed.* **2015**, *54*, 1190–1194.
(26) Loos, M.; Gerber, C.; Corona, F.; Hollender, J.; Singer, H. Accelerated isotope fine structure calculation using pruned transition trees, *Anal. Chem.* **2015**, *87*, 5738–5744.
(27) Garçon, M.; Cabré, A.; Verdaguer, X.; Riera, A. Synthesis, Coordination Study, and Catalytic Pauson-Khand Reactions of QuinoxP*$(CO)_4$-μ-Alkyne Dicobalt Complexes. *Organometallics* **2017**, *36*, 1056–1065.
(28) Kwok, S. W.; Fotsing, J. R.; Fraser, R. J.; Rodionov, V. O.; Fokin, V. V. Transition-metal-free catalytic synthesis of 1,5-diaryl-1,2,3-triazoles. *Org. Lett.* **2010**, *12*, 4217–4219.
(29) Borrmann, A.; Fatunsin, O.; Dommerholt, J.; Jonker, A. M.; Löwik, D. W. P. M.; Van Hest, J. C. M.; Van Delft, F. L. Strain-promoted oxidation-controlled cyclooctyne-1,2-quinone cycloaddition (SPOCQ) for fast and activatable protein conjugation. *Bioconj. Chem*. **2015**, *26*, 257–261.

Chapter 3

Synthesis of a novel thiacycloheptyne probe for bioconjugations

J.A.M. Damen, D. Smits, Dr. B. Albada, Prof. Dr. P. Friedl, Prof. Dr. F.L. van Delft

Abstract
The synthesis of novel cycloheptyne 3,3,6,6-tetramethyl-1-thiacycloheptyne-sulfoximine (THS) and fluorescent probes THS-AF488 and THS-SulfoCy5 is described. Bioconjugation of antibodies and cell surface labeling experiments reveal that the THS reagents are highly reactive in both SPOCQ and SPAAC click chemistry. The XRD structure of THS reveals that both C−C≡C bonds of the alkyne are bent at 151°, deviating 29° from normal alkyne geometry. THS is therefore the current recordholder in alkyne bending, whilst maintaining to be a stable reagent.

Parts of this work were published in *Chem. Eur. J.* **2023**
Parts of this work are under review at *Nat. Chem. Biol.* **2024**

1. Introduction

The metabolic incorporation of azido-sugars into the glycocalyx of hypertrophic tumor cells allows for subsequent covalent attachment of fluorescent probes by means of strain-promoted azide-alkyne cycloaddition (SPAAC). This strategy allows for probing of glycocalyx thickness and its subsequent effects on cell-cell interactions by means of confocal microscopy. Main objective of the research described in this **Chapter** is to answer the question whether a SPAAC probe with sufficiently high reaction kinetics with azide would be able to outcompete glycocalyx internalization.

1.1 Thiacycloheptyne

3,3,6,6-Tetramethyl-1-thiacycloheptyne (TMTH) is a probe developed in 1970 by Krebs and Kimling. Later it became known for its unsurpassed reactivity in SPAAC.[1,2] Unfortunately, TMTH suffers from high instability due to its seven-membered ring size, see **Figure 1 (top)**, despite the presence of the four methyl groups for anticipated kinetic stabilization and prevention of dimerization or polymerisation.[3,4] In 2020 Liskamp *et al.* published a paper in which TMTH was functionalized with a sulfoximine functionality, naming it TMTH-SI.[5] For clarity and ease of pronunciation, we refer to this molecule as THS, see **Figure 1 (top)**. This cycloheptyne is deemed indefinitely bench stable at room temperature, whilst displaying unprecedented high reactivity with azides. Another apparent advantage of THS over other commonly employed cycloalkynes (*e.g.*, DBCO, BCN) is the diminished lipophilicity of the probe, which translates to higher aqueous solubility and reduced tendency to accumulate in lipophilic cellular environment (*e.g.*, membranes and hydrophobic interior of proteins).[5] These improved properties of THS urged us to explore this reagent in metabolic cell labelling studies and thus prompted us to develop the required fluorescent probes based on THS chemistry, see **Figure 1 (middle and bottom)**.

1.2 Outline of this Chapter

The syntheses of TMTH precursor compounds **2–6**, along with synthetic improvements, are described in this **Chapter 3**.The synthesis steps generally give just one product with greatly simplified purification processes (*e.g.*, silica plugs rather than extensive flash chromatography on 10–100 gram scale; crystallizations; or just a simple extraction). Afterwards, an improved synthesis method for THS **7** is described, along with the functionalization of this click handle to afford fluorescent probes **9–10**, see **Scheme 1**. The effectiveness of these fluorescent probes in bioconjugations on monoclonal antibody and on cellular surface level are then shown.

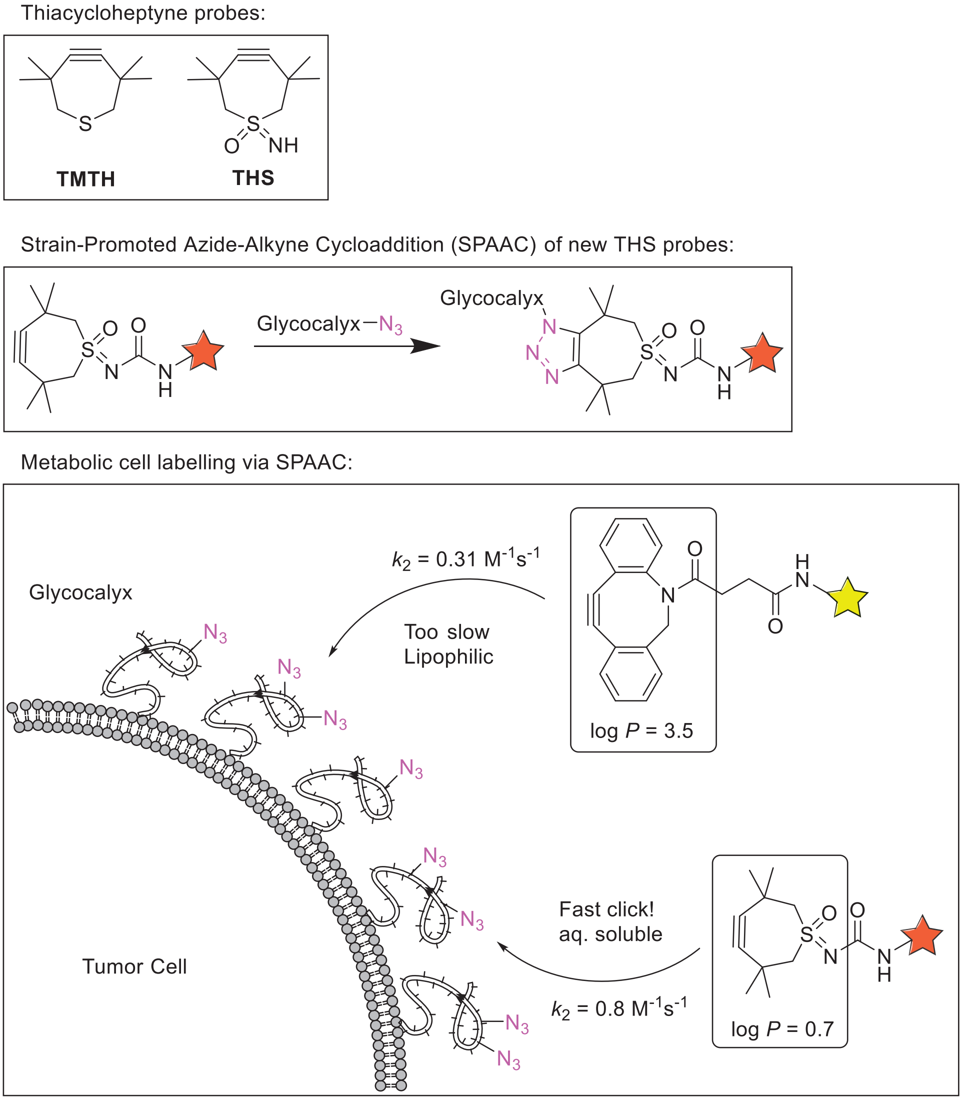
Thiacycloheptyne probes:
TMTH
THS
Strain-Promoted Azide-Alkyne Cycloaddition (SPAAC) of new THS probes:
Glycocalyx–N3
Glycocalyx
Metabolic cell labelling via SPAAC:
k2 = 0.31 M-1s-1
Too slow
Lipophilic
log P = 3.5
Glycocalyx
Tumor Cell
Fast click!
aq. soluble
k2 = 0.8 M-1s-1
log P = 0.7

Figure 1: **Top:** Structures of TMTH and THS. **Middle:** Strain-promoted azide-alkyne cycloaddition (SPAAC) of functionalized THS with azide-enriched glycocalyx. **Bottom:** Envisioned SPAAC of THS-fluorophores outcompeting conventional DBCO-based reagents.

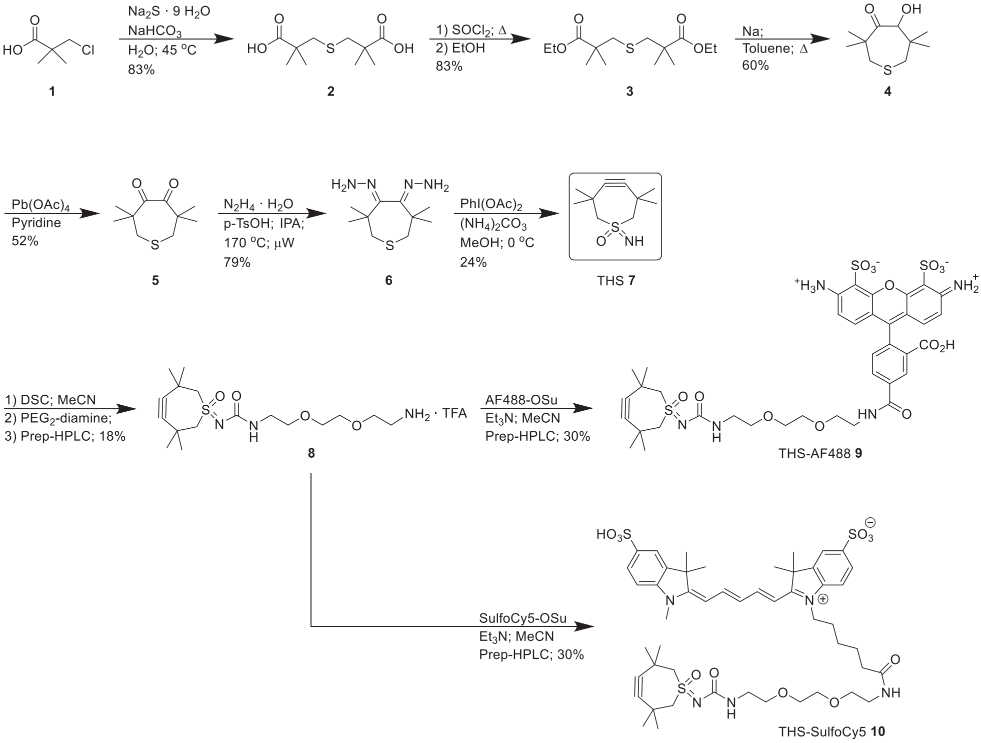

Scheme 1: General synthesis route to THS 7 and functionalized probes THS-AF488 9 and THS-SulfoCy5 10.

2. Results and Discussion

2.1 Syntheses

We performed the first synthesis step as a direct scale-up of the modified protocol of Feeder *et al.*, based on the classic protocol of De Groot and Wijnberg.[6,7] Thus, sodium sulfide nonahydrate was dialkylated with (deprotonated) chloropivalic acid **1** in an aqueous solution containing sodium bicarbonate as base, whilst being stirred overnight at 45 °C. The crude diacid 3,3'-thiobis(2,2-dimethylpropanoic acid) **2** precipitated after acidification and was recrystallized from THF/water, then dried in a desiccator to yield pure compound **2** in 83% yield. Subsequently, the diacid was refluxed in excess thionyl chloride to form the crude bis-acid chloride, which was quenched by pouring the reaction mixture in well-stirred ethanol, forming the ethyl diester **3**. Work-up afforded pure diethyl 3,3'-thiobis(2,2-dimethylpropanoate) **3** in 83% yield. We also performed the esterification step by Fischer esterification with ethanol in toluene with a catalytic amount of sulfuric acid in a set-up equipped with a Dean-Stark trap. On a smaller scale this gave a lower yield (55%) and necessitated column chromatography to separate the diester from the monoester side-product. Therefore, the former procedure is preferred.

With pure diester **3** in hand, cyclisation was performed by means of an acyloin condensation, a well-known approach to medium-to-large ring-size molecules (6 to 34-membered rings).[8-10] Specifically, the acyloin condensation is performed on molten sodium (m.p. 97.8 °C) in refluxing toluene (b.p. 111 °C). Thus, a solution of diester **3** in toluene is added dropwise to a refluxing dispersion of liquid sodium in toluene, under vigorous stirring to maximize sodium droplet formation and surface area. Upon quenching of the reaction mixture with aqueous sulfuric acid the dihydroxyalkene is provided, which undergoes keto-enol tautomerization to form the hydroxy-ketone. Also this reaction gives merely one product after workup, providing 5-hydroxy-3,3,6,6-tetramethylthiepan-4-one **4** in 60% yield.

Hydroxyketone **4** was then oxidized to the target diketone with lead(IV) acetate in pyridine at room temperature. This method cleanly affords the diketone **5** as only product, without sulfur oxidation. The lead(II) by-product can easily be removed by treating the reaction mixture with two equivalents of aqueous HCl to precipitate $PbCl_2$. Filtration and distillation of pyridine *in vacuo* forms a crude product that is extracted and passed over a short silica pad to yield the diketone 3,3,6,6-tetramethylthiepane-4,5-dione **5** in 52% yield. Although the reaction can also be performed by means of Swern oxidation, the associated procedure requires temperature control and time management.[5] As chromatographic purification is simplified to a short silica plug in our method, the lead-based oxidation method has our preference.

In the original procedure by Krebs and Kimling bishydrazone **6** was formed by heating a mixture of diketone **5** with hydrazine monohydrate and hydrazine monohydrochloride in ethylene glycol to 180 °C for 13 hours.[1] We found however that reaction time could be reduced to 4 hours by reacting a mixture of diketone **5**, hydrazine monohydrate and *p*-toluenesulfonic acid monohydrate in 2-propanol in a pressurized microwave reactor at 170 °C. When shorter reaction times (*i.e.*, two hours) were applied, some monohydrazone was still present, whereas heating for 4 hours led to clean formation of bishydrazone **6**. The solvent is then removed *in vacuo* and the sample is purified either on a pad of silica or by flash chromatography to afford pure bishydrazone **6** as needle crystals. Direct crystallization from the reaction mixture is not recommended, as the hydrazinium tosylate salts that tend to co-crystallize with the product substantially hamper the subsequent reaction. Unfortunately, due to the nature of microwave chemistry, this reaction is not scalable: the current reaction mixture volume limit of microwave reactions is 30 mL.[11]

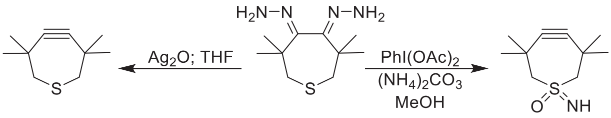

TMTH **6** **THS 7**

Scheme 2: Synthesis of TMTH or THS from bishydrazone **6**.

With bishydrazone **6** in hand, the cycloheptyne TMTH could be accessed under oxidative conditions using silver(I)oxide in THF, see **Scheme 2**.[1] Liskamp envisioned that installation of the sulfoximine moiety would provide a symmetrical handle for further functionalization and that both reactions can be performed concomitantly to yield the more stable THS. The originally published reaction conditions consisted of the addition of a suspension of phenyliodine(III) diacetate (PIDA) in DCM to a cooled mixture of ammonium acetate and bishydrazone **6** in methanol/water (15:1).[5] However, in our own lab multiple attempts to synthesize THS according to these conditions failed. This led us to develop an improved synthesis protocol of THS by combining TMTH synthesis with sulfoximidation protocols[1,2,12-15] in a new one-pot procedure, see **Scheme 2**. This new protocol consists of the reaction of bishydrazone **6** with PIDA and ammonium carbonate in stringently cooled methanol.

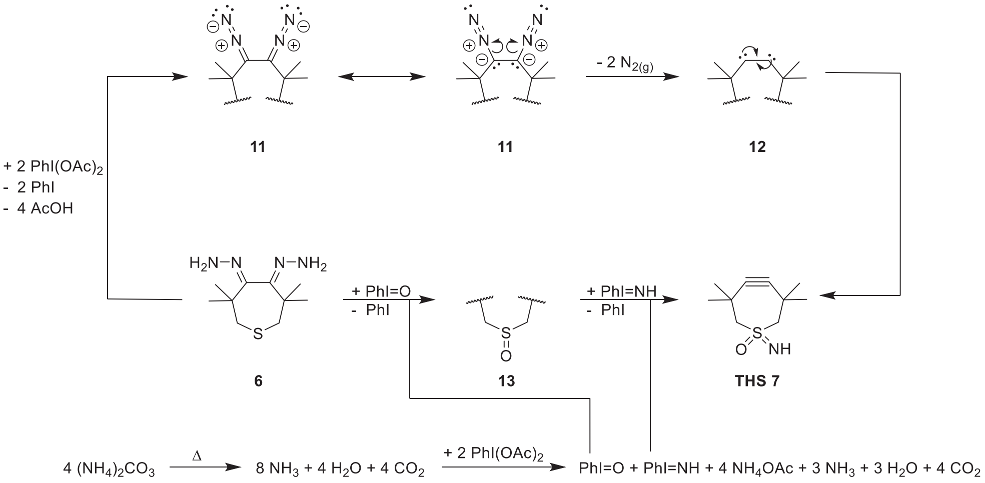
11
11
- 2 $N_{2(g)}$
12
+ 2 $PhI(OAc)_2$
- 2 PhI
- 4 AcOH
H_2N-N
$N-NH_2$
S
6
+ PhI=O
- PhI
S
O
13
+ PhI=NH
- PhI
S
O
NH
THS 7
$4\ (NH_4)_2CO_3 \xrightarrow{\Delta} 8\ NH_3 + 4\ H_2O + 4\ CO_2 \xrightarrow{+ 2\ PhI(OAc)_2} PhI{=}O + PhI{=}NH + 4\ NH_4OAc + 3\ NH_3 + 3\ H_2O + 4\ CO_2$

Scheme 3: Simplified reaction mechanism for the formation of THS **7** from bishydrazone **6**.

Formation of the final THS compound **7** consists of two concomitant reactions in a one-pot procedure. First, the strained alkyne is formed by means of oxidation of both hydrazone moieties with PIDA to the double diazo species **11**. This double diazo intermediate **11** then eliminates two equivalents of N_2 to form the strained alkyne: in the experiment the immediate formation and subsequent decay of this intermediate can be evaluated visually, by the transient formation of a yellow solution resulting from the diazo compounds. As the color decays withing 5 minutes gas bubbles (N_2) form within the reaction mixture. The reaction logically will proceed by stepwise oxidation reactions, after which the double diazo intermediate eliminates in either a stepwise fashion via a diazoalkene, or in a concerted single-step fashion. The latter is depicted for clarity in **Scheme 3** top panel. After the elimination of nitrogen gas, the resulting electron-deficient vicinal dicarbene will collapse into a triple bond. Not only do the four methyl groups force the formation of the alkyne, rather than a 1,3-diene system, they also stabilize the strained cycloalkyne. An alternative reaction sequence of oxidation, elimination, oxidation, elimination steps is unlikely because it requires the formed carbene intermediates to be longer-lived, which would be accompanied by a lot of cross reactivity (*e.g.*, trapping with protic solvent molecules) and this was not observed.

The second reaction in forming THS consists of exothermic sulfoximide formation. The divalent thioether is oxidatively transformed into a hexavalent sulfoximine by means of hypervalent iodine reagents in a stepwise manner, see **Scheme 3** bottom panel for the oxidation-imidation sequence (although the reagents can also react in the opposite order). The reagents iodosylbenzene ($PhI^{(III)}$=O) and phenyliodonium imine ($PhI^{(III)}$=NH) are formed *in situ* from the reaction of PIDA with water or ammonia, respectively. Ammonium carbonate serves as the source for ammonia and water as it thermally decomposes into ammonia, water and carbon dioxide. The *in situ* formation of iodosylbenzene is beneficial for the reaction, as it is solvated and thus more reactive than normal iodosylbenzene, which is an organic polymer that only reacts sluggishly at the reagent surface.[16] Similarly, *in situ* formed phenyliodonium imine is more reactive than otherwise used reagents, such as PhI=NTs, which normally requires Cu or Fe catalysis for oxidative transfer.[17-20]

The most important prerequisite for this synthesis to succeed is to control the temperature: sulfoximine installation is a highly exothermic reaction and the (formation of the) cycloalkyne is thermosensitive. Poor temperature control (*e.g.*, no cooling) leads to immediate decomposition of the product or intermediates due to the exothermic reaction. Cooling the reaction mixture too extensively (*e.g.*, to the range of −10 °C to −78 °C) will only lead to TMTH formation, which then decomposes in the methanolic solution.[21] The sulfoximidation reaction does not occur (fast enough) at those low temperatures. We found that cooling the flask containing all the pre-mixed solid reagents to 0 °C and subsequent addition of cold methanol (precooled at 0 °C) affects facile and reproducible formation of THS. Formed THS could then be purified by flash chromatography to yield a highly crystalline product.

Notably, the above protocol does not yield any inseparable THS-alkene side product and solvent-derived formaldehyde, as in the previous procedures,[22,23] a known side-reaction from concerted hydrogen transfer reaction between the alkyne TMTH with methanol.[21] The fact that this also occurs in the case of the less strained THS (see section ***2.2 XRD of THS***) is not surprising, but should be slower or should occur at higher temperatures (as is the case for eight-membered rings[24]). Therefore, the absence of THS-alkene impurities in our newly developed improved protocol is ascribed to the temperature control during the reaction.

With THS in hand we decided to tether it to a small polyethylene glycol (PEG) linker according to a known methodology.[5] For this, THS was reacted with disuccinimidyl carbonate (DSC) in MeCN to give the THS-OSu-carbamate intermediate, which was then quenched with PEG_2-diamine to form the urea bond and provide the product THS-PEG_2-amine **8**. This compound was completely water-soluble due to the (i) small ring size and low lipophilicity of THS, (ii) the polar urea bond, and (iii) the polar PEG linker. After preparative HPLC, THS-PEG_2-amine **8** was isolated as a TFA salt in 18% yield. This compound **8** was then reacted with commercially available activated OSu-esters of isomerically pure 5-AF488 or SulfoCy5 in MeCN with Et_3N as a base. The reaction mixtures were directly purified by preparative HPLC to yield THS-AF488 **9** and THS-SulfoCy5 **10**, both in 30% yield. The use of very polar, large, and multiply charged fluorophores resulted in THS-AF488 **9** and THS-SulfoCy5 **10** being completely water-soluble (this was also reflected in the very polar eluent conditions when performing preparative HPLC).

2.2 XRD of THS

Single crystals of THS **7** suitable for X-ray crystallography were grown from chloroform/pentane via the vapor diffusion method, resulting in the crystal structure shown in **Figure 2**. The structure revealed that the single bonds to the alkyne triple bond are bent at 150.99° and 151.37° angles respectively in a coplanar symmetrical fashion (torsion angle of only 0.2°). The C≡C bond length is 1.191 Å, and the alkyne is slightly bent out of plane at a 12° angle versus the backbone carbon atoms formed by the four sp^3 hybridized carbon atoms between the alkyne and sulfoximine. The propargylic C−C≡C bonds are both 1.48 Å long and are thereby considerably shorter than the other C−C bonds in the molecule ranging from 1.53–1.55 Å. The C−S bonds are elongated to 1.81 Å and the sulfur atom lies at a 76° torsion angle above the plane of the ring. Lastly, the oxygen atom is positioned as the axial substituent (S=O 1.466 Å) and the imine as the equatorial substituent (S=NH 1.516 Å) in all THS molecules present in the unit cell. The sulfoximine functionality as such enforces the strain on the formed six carbon atom plane, whilst itself hinging out of that plane and maintaining normal geometry (C−S−C bond angle of 109.3°). The strain of the plane is also perturbing the angular distortions of the other sp^3 carbon atoms, reflecting in 102.5–102.7° C−C−C bond angles for the propargylic carbon atoms and 118.5–118.9° C−C−S bond angles for the carbon atoms tethered to the sulfoximine. It also creates a 2.95 Å interatomic distance between C1 and C10 (the begin and the end of the six-carbon atom chain). The sharp resonances in the ^{1}H-NMR spectrum at room temperature indicates that only one conformational structure is present in solution. There is therefore no evidence for potential ring flipping of the structure, which would place the imine in the axial position and the oxide in the equatorial position. We therefore assume that the structure of THS in the solid state is representative for the structure in solution.

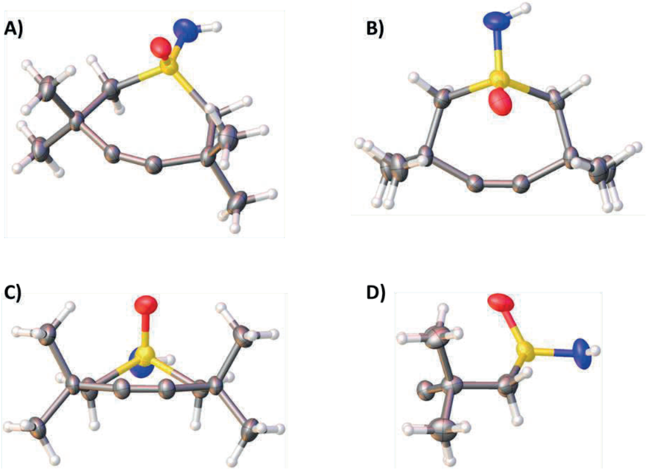

Figure 2: Molecular structure of THS **7** according to X-ray structure determination. ORTEP depicted with thermal ellipsoids drawn at 50 % probability level. The figure was generated with Olex2.**[25]** The structure can be retrieved from the Cambridge Crystallographic Data Centre (CDCC deposition number 2249007).

2.3 Bioconjugations

2.3.1 mAb labeling with SPOCQ

With the THS-dye constructs in hands, we tested their usefulness in *ortho*-quinone-based bioconjugation (SPOCQ). For this, we selected trastuzumab (anti-HER2 antibody) expressed with a G_4Y-tag on both C-termini of the light chains (abbreviated as: Tras[LC]G_4Y), see **Figure 3**. These G_4Y-tags ensure the presence of two surface-exposed tyrosine residues, each of which can be oxidatively transformed into an *ortho*-quinone by the enzyme mushroom tyrosinase (mTyr), suitable for conjugation with a strained alkyne in an one-pot procedure, as shown for BCN.[26] Indeed, we were happy to find that THS-AF488 **9** was able to exclusively react with the light chains of this antibody under the applied reaction conditions. After DTT-treatment to reduce interchain disulfide bonds, LC-HRMS analysis showed that the fluorescent tag was only present on the light chain, see **Figure 4**. This was confirmed by the 488 nm channel in the chromatogram that shows only a signal for the light chain. Also, the deconvoluted mass spectrum of the HPLC peak of the light chain corresponded to the SPOCQ click product (m/z = mass native light chain + 14 + mass THS-AF488), when compared to the native light chain, see **Figure 5**.

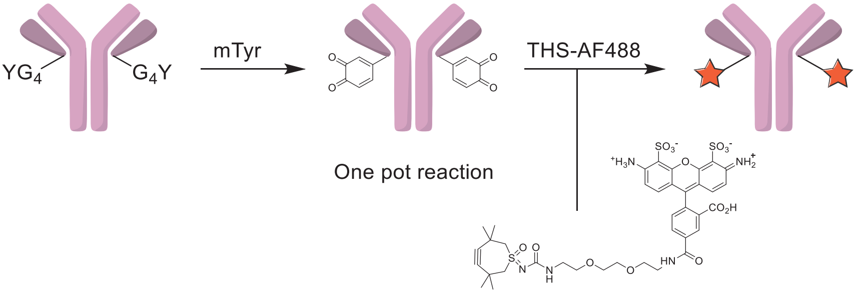

Figure 3: Bioconjugation of Tras[LC]G_4Y antibodies with THS-AF488 via SPOCQ.

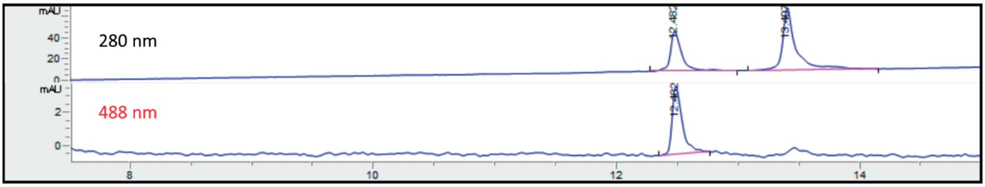

Figure 4: HPLC-MS traces at both 280 nm and 488 nm of Tras[LC]G_4Y-THS-AF488 antibody conjugate after DTT reduction confirms that fluorescent labeling only occurs on the light chain (elutes first), and not on the heavy chain (elutes second).

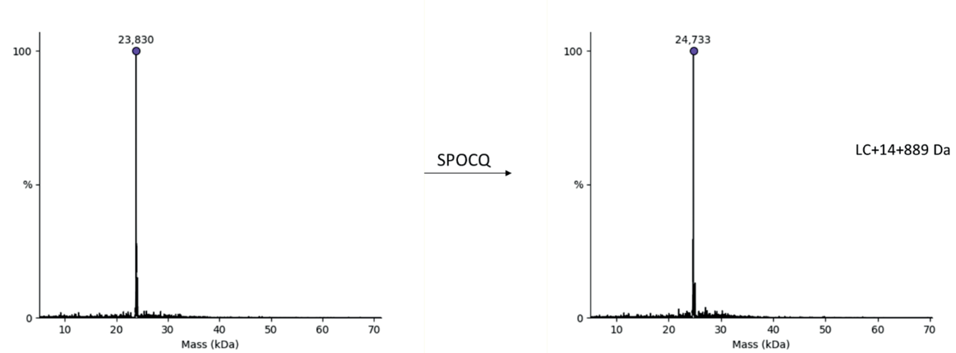

Figure 5: HPLC-MS analysis shows complete labelling of the light chain, when comparing the deconvoluted mass spectra of the light chain before (left) and after the SPOCQ reaction (right).

2.3.2 Metabolic cell labelling with SPAAC

THS-AF488 **9** was also used for metabolic labelling studies, in a direct comparison to DBCO-AF488. The results are shown in **Figure 6**. The SPAAC reaction was performed in live cell culture in 2D to detect sialic acid-containing surface glycans. Mouse B16F10 cells were cultured with 50 µM Ac$_4$ManNAz for metabolic labeling for 5 days. The cells were then washed (3x, PBS, 10 min), incubated with DBCO-Alexa Fluor 488, or THS-Alexa Fluor 488 **9** (all 50 µM, 60 min, unless otherwise indicated, 4 °C), washed 3x (PBS, 10 min) and subjected to flow cytometry or fixed. In the latter case, high-resolution fixed imaging (Airyscan mode) was performed.

The increase in fluorescence indeed is steeper per time unit after THS-labelling compared to DBCO-labelling (**Figure 6A**), possibly allowing glycocalyx labelling with minimal membrane internalization. We further aimed to determine whether THS-labelling resulted in increased conjugation efficiency on single-cell and subcellular levels. Compared to DBCO-AF488, THS-AF488 **9** labeling increased the average whole-cell fluorescence as detected using flow cytometry 1.7-fold (**Figure 6B**) With this increased efficiency, >5-fold more cells with particularly high glycocalyx could be detected when using THS-AF488 **9**-based labelling compared to DBCO-AF488 (**Figure 6B**, right panel). High-resolution Airyscan-based microscopy similarly shows higher single-cell fluorescence after labelling with THS-AF488 **9** compared to DBCO-AF488 (**Figure 6C**). Since fluorescent intensity and signal-to-background level positively correlate (**Figure 6D**), increased labelling efficiency of THS-AF488 **9** allows imaging with higher signal-to-background level compared to DBCO-AF488. These results show that THS-based labeling outperforms DBCO-based click chemistry by improving the mean fluorescence intensity and detecting a high-uptake cell subset with improved fluorescence intensity and signal-to-noise ratio, enabling establishment of yet-unnoticed biological phenomena.

The other probe, THS-SulfoCy5 **10** was used for stochastic optical reconstruction microscopy (STORM) super resolution microscopy. These results are still pending.

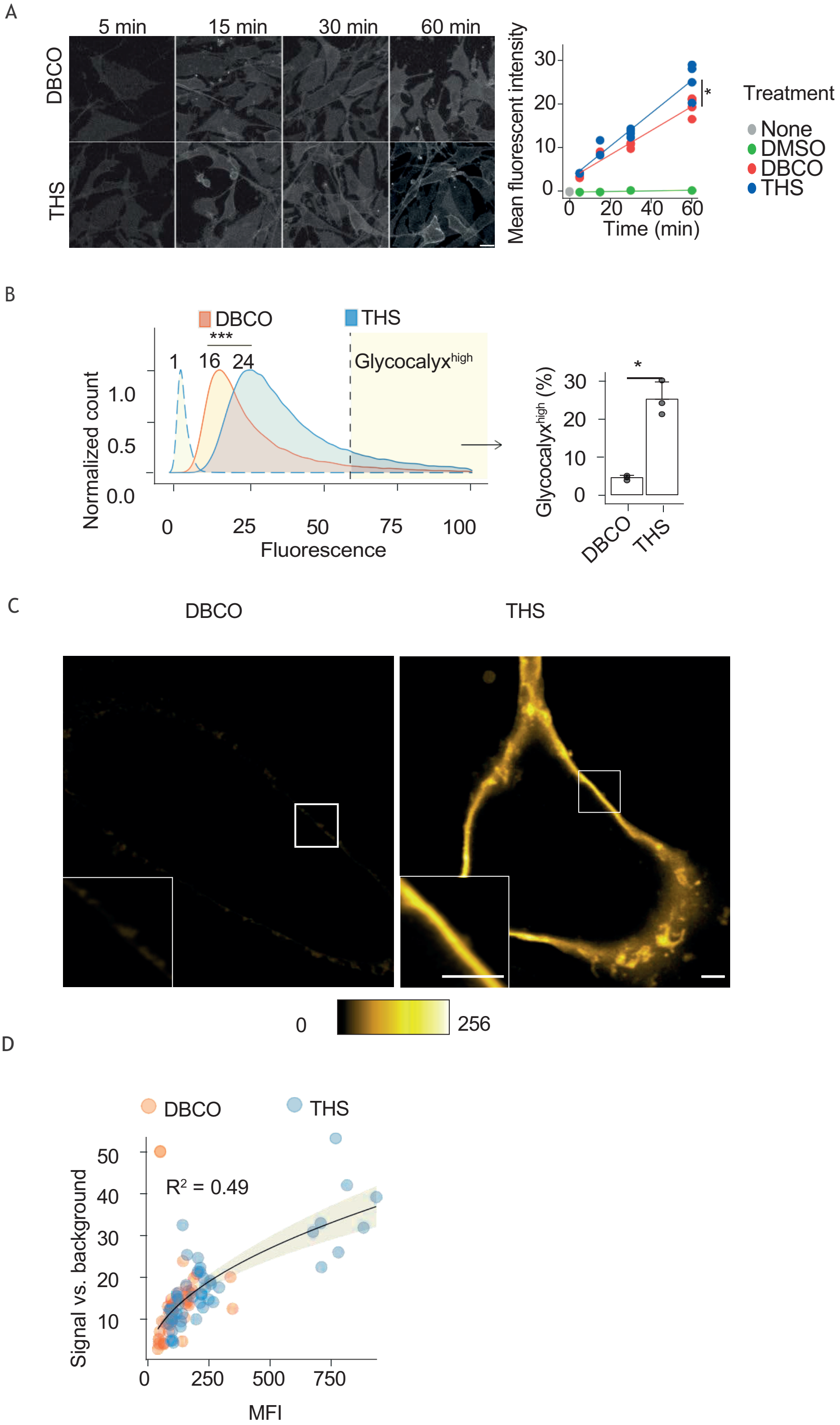
A
5 min
15 min
30 min
60 min
DBCO
THS
Mean fluorescent intensity
30
20
10
0
0
20
40
60
Time (min)
*
Treatment
None
DMSO
DBCO
THS
B
DBCO
THS
***
1
16
24
Glycocalyx^{high}
Normalized count
1.0
0.5
0.0
0
25
50
75
100
Fluorescence
Glycocalyx^{high} (%)
30
20
10
0
*
DBCO
THS
C
DBCO
THS
0
256
D
DBCO
THS
$R^2 = 0.49$
Signal vs. background
50
40
30
20
10
0
250
500
750
MFI

Figure 6: **A)** Representative micrographs showing fluorescent signal at different SPAAC times (left) and quantification (right). Scale bar, 5 µm. Datapoints present mean fluorescent intensity of all pixels above background. **B)** Fluorescence intensity achieved by DBCO-AF488 and THS-AF488 **9**-based SPAAC reaction measured by flow cytometry. Density plots present the normalized count of cells that corresponds to the presented fluorescence. Right, the percentage of total cells that is glycocalyx^{high}, where datapoints present means of individual experiments. Dashed line, density plot without $Ac_4ManNAz$ labelling; Solid line, density plot with $Ac_4ManNAz$ metabolic labelling. **C)** Single-channel micrographs displaying representative cells with the highest fluorescence from DBCO-AF488 and THS-AF488 **9** of high-resolution imaging. Yellow ho LUT. Scale bars, 2 µm **D)** quantification showing relationship between intensity and signal vs. background, based on line profiles recorded perpendicularly to the membrane in high-resolution images.

3. Discussion / Conclusion

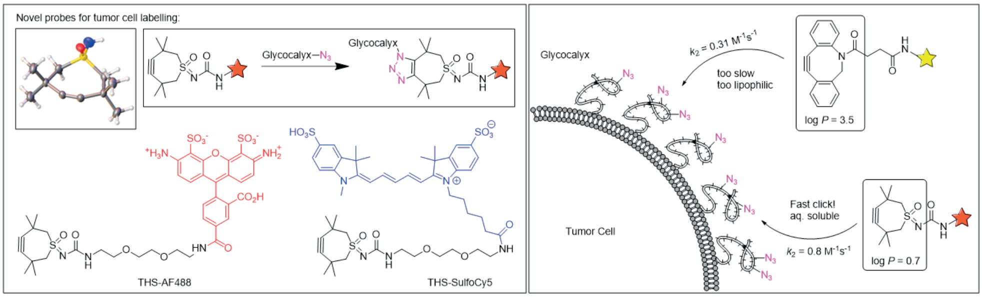

Figure 7: 3,3,6,6-tetramethyl-1-thiacyclo-heptyne sulfoximine (**THS**) is a novel cycloalkyne that exhibits high reactivity towards strain-promoted azide–alkyne cycloaddition (SPAAC) reactions.[5] THS is a superior reagent regarding reactivity in SPAAC, whilst combining improved water solubility due to its small ring size (k_2 = 0.8 $M^{-1}s^{-1}$; log P = 0.7), as compared to BCN (k_2 = 0.14 $M^{-1}s^{-1}$; log P = 2.0) or DBCO (k_2 = 0.31 $M^{-1}s^{-1}$; log P = 3.5).[5,27-29]

It was already earlier established that thiacycloheptyne-type reagents are substantially more reactive in SPAAC than other commonly applied and commercially available reagents, such as BCN or DBCO.[1,2,15,30] However, thiacycloheptynes, including the tetramethylated analogue, suffer from instability and therefore are seldomly used.[2,15,21,24] THS, however, possesses greatly enhanced stability, resulting in THS and its derivatives being bench-stable for extended periods (>1 year).[5]

In our current research, X-ray crystallographic structure determination of the THS warhead revealed that the C–C≡C bonds are bent at 150.99° and 151.37° angles on each side of the alkyne in a coplanar symmetrical fashion, see **Figure 7** (left panel). The angular deviation from the normal alkyne geometry of 180° thereby explains the high reactivity of THS. According to Bertozzi, smaller alkyne bond angles in cycloalkynes do correspond to higher reactivity in SPAAC.[31] The crystallographic determination of the structure of DBCO therefore allowed for a direct comparison of bond angles and thus reactivity. DBCO possesses unsymmetrical alkyne bond angles of both 154.16° and 152.26° (for XRD description see **Chapter 5**). This substantial difference in bond angles supports the observed reactivity trend between THS and DBCO. THS is the current record-holder of alkyne bond strain, whilst remaining a stable reagent (angular strains of other cycloalkynes are described in literature[31]). For comparison, the highly unstable parent thioether compound TMTH possesses a bond angle of 145.8° as determined by electron diffraction in the gas phase or of 147.0–147.6° as determined by XRD of the copper(I) chloride adduct.[32,33] TMTH, however, readily decomposes in solution.[21,24] This means that with the current development and improvements of THS, we are working at the edge of combining reactivity with probe stability.

In addition to enhanced ring strain, the small ring size also affects the aqueous solubility of THS and allows for improved reactivity with polar substrates, such as the glycocalyx. This also suppresses the so-called “observer effect” in which apolar interactions can affect a biological response or can afford a different cellular distribution/pharmacokinetics.[5,34] In the design of the novel fluorescent probes THS-AF488 and THS-SulfoCy5, improved aqueous solubility was achieved by incorporating a polar urea bond to a short polyethylene glycol (PEG) linker. Subsequent attachment to multiply charged fluorophores isomerically pure 5-AF-488 and sulfo-Cyanine5 afforded the novel, water-soluble bioconjugation probes THS-AF488 and THS-SulfoCy5. The fluorescent probes derived from THS were shown to be functional in SPOCQ and SPAAC bioconjugations on antibody level and on metabolically labelled cellular surfaces, respectively.

4. Acknowledgements

We thank Gabriele Kociok-Köhn (University of Bath, UK) for her work on obtaining and processing of the single crystal X-ray structure. Dr. Jordi Keijzer and Irene Shajan (Wageningen University & Research, The Netherlands) are acknowledged for their help with bioconjugations and analytical LC-MS. Jorren Steenbergen is acknowledged for his assistance in the development of the synthesis of bishydrazone **6**.

5. Experimental

5.1. General information

5.1.1 Instruments

^{1}H-NMR (700 MHz) and ^{13}C-NMR spectra (176 MHz) were recorded on a Bruker 700 MHz Avance NMR spectrometer. ^{1}H-NMR (400 MHz) and ^{13}C-NMR spectra (101 MHz) were recorded on a Bruker 400 MHz AV400 NMR spectrometer. Chemical shifts were reported in ppm referenced against the residual solvent peaks of the NMR solvent. ESI-HRMS spectra were recorded on an Exactive Mass Spectrometer (Thermo Scientific) and mass values were calculated with enviPat Web.[35] Semi-preparative reverse phase high-performance liquid chromatography (RP-HPLC) was performed on a Agilent 1260 Preparative HPLC system equipped with a DAD G7115A and MSD. Analytical RP-HPLC was performed on Agilent 1290 Infinity UHPLC system with DAD or on a Agilent 1220 HPLC Infinity system with DAD. Deionized water was produced with a Milli-Q Integral 3 system (Millipore, Molsheim/France). Microwave syntheses were performed in an Anton Paar Monowave 400 Microwave Synthesis Reactor equipped with a Ruby Thermometer for internal temperature measurements. Chemical compound crystallinity was assessed optically using an Olympus BH-2 light microscope equipped with polarizing filters.

5.1.2 General chemicals:

3-Chloropivalic acid was purchased from TCI Europe. Hydrochloric acid (37%); sodium metal; hydrazine monohydrate (98%); 2,2'-(ethylenedioxy)bis(ethylamine) (98%); and ammonium acetate (≥98%) were purchased from Sigma-Aldrich Merck. Iodobenzene diacetate; N,N'-disuccinimidyl carbonate (85%); 4-*tert*-butylcatechol; triethylamine; ammonium carbonate (extra pure); sodium sulfate and sodium periodate were all purchased from Thermo Scientific™ / Fisher Scientific. Sodium sulfide nonahydrate; thionyl chloride (99.5+%); pyridine; and *p*-toluenesulfonic acid monohydrate were purchased from Acros Organics. Lead(IV) acetate, 96% (dry wt.), stab. with 5–10% glacial acetic acid was purchased from Alfa Aesar. Sulfuric acid (96%) was purchased from Carl Roth GmbH. Sodium carbonate was purchased from VWR. AF488 NHS ester and sulfo-Cyanine5 NHS ester were both purchased at Lumiprobe GmbH. Methanol (absolute AR grade); toluene (HPLC) and trifluoroacetic acid (HPLC) were purchased from Biosolve. Ethyl acetate (GPR Rectapur) was purchased from VWR Chemicals. Dichloromethane (Puriss. p.a.) and acetonitrile (CHROMASOLV™, for HPLC) were purchased from Honeywell Riedel-de Haën™. 2-Propanol (HPLC-Isocratic Grade) was purchased from Carlo Erba Reagents GmbH. All of these chemicals were used as purchased unless otherwise stated. MilliQ deionized water was produced with a Milli-Q Integral 3 system (Millipore, Molsheim/France). Acetonitrile (HiPerSolv CHROMANORM® HPLC-LC-MS grade, VWR), including 0.1% Formic acid (ULC/MS grade, Biosolve), was specifically used for mass spectrometry measurements.

5.1.3 Antibodies and enzymes:

Trastuzumab with GGGGY on the light chains (Tras[LC]G$_4$Y) was ordered from Evitria AG (Zürich, Switzerland) and purified according to the method published by Bruins *et al.*[26] Mushroom tyrosinase (mTyr) was obtained from Sigma-Aldrich.

5.1.4 Chromatography:

Flash chromatography was performed on SiliaFlash® P60 40–63µm (230–400 mesh) 60 Å Irregular Silica Gel (R12030B) (SiliCycle, Quebec City (Quebec), Canada). Thin Layer Chromatography was performed on TLC Silica gel 60 F_{254} on aluminium sheets (Merck, Darmstadt, Germany). After development, TLC plates were dip stained and heated with a heat gun for visualization of spots. $KMnO_4$ stain was used as a general stain and was prepared by dissolving 1.5 g $KMnO_4$, 10 g K_2CO_3 and 1.25 mL 10% NaOH in 200 mL water. tBuOQ stain was specifically used for the identification of strained cycloalkynes. It was prepared by dissolving 50 mg 4-*tert*-butyl-*ortho*-quinone in 10 mL 1-butanol. After dipping and prolonged heating of the TLC plate, strained cycloalkynes form light beige spots against a darker red background. The stain does have limited shelf-life.

Semi-preparative RP-HPLC was performed on a semi-preparative Zorbax Eclipse XDB-C18, 5-Micron, 9.4 x 250 mm column at a flow rate of 10 mL/min. Eluent systems are specified per procedure. Analytical RP-HPLC was performed on a Dr. Maisch ReproSil Gold 120 C18, 3 µm, 250 x 3 mm column using a linear gradient of 20 minutes from 5–95% MeCN in MilliQ deionized water containing 0.1% formic acid at a flowrate of 0.1 mL/min.

Analytical RP-HPLC-MS analysis of bioconjugates was performed on a MAbPac™ RP 3.0 × 100 mm 4 µm (Thermo Scientific) column with a column temperature of 80 °C. A linear gradient was applied in 15 minutes from 25% to 40% acetonitrile in MilliQ deionized water containing 0.1% formic acid at a flowrate of 0.6 mL/min (Mobile phase A: MQ+0.1% formic acid; Mobile phase B: MeCN+0.1% formic acid). The mass spectrometer was operated with a spray voltage of 3.9 kV. Acquisitions were performed on the m/z range 500-3000.

5.2. Chemical syntheses

The 4-*tert*-butyl-*ortho*-quinone reagent for staining was synthesized by the method of Borrmann.[36]

5.2.1 Synthesis of 3,3'-thiobis(2,2-dimethylpropanoic acid) 2

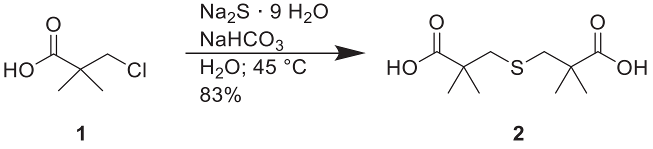

A 1L pear shaped round-bottom flask was charged with finely ground 3-chloropivalic acid **1** (150.14 g; 1.099 mol; 2 eq) and a large magnetic stirring bar. The solid was suspended in 100 mL deionized water and was vigorously stirred. Na_2CO_3 (59.18 g; 0.558 mol; 1 eq) was added portion wise to the vigorously stirred reaction mixture over the course of 30 minutes. After completion of addition and ceasing of gas formation, a thick white slurry was obtained. A solution of $Na_2S \cdot 9\ H_2O$ (131.89 g; 0.549 mol; 1 eq) in 120 mL deionized water was added portion wise over the course of 7 minutes to the reaction mixture, which turned into an even harder to stir slurry. The reaction mixture was heated to 45 °C under magnetic stirring in an oil bath and upon heating turned into a fully homogeneous solution. The reaction mixture was left to stir for 19 hours at 45 °C. The heating was stopped and the flask was fitted with a 250 mL addition funnel, which was charged with 150 mL 50% aqueous H_2SO_4 solution. The 50% aqueous H_2SO_4 solution was added dropwise over the course of 1.5 hours to the vigorously stirred reaction mixture until a turbid dispersion was formed. The reaction mixture was filtered over a sintered glass filter and the powder bed was washed four times with 150 mL portions of a 1% v/v H_2SO_4 solution in deionized water (pH 1). This yielded 131.95 g of wet white solid crude product. The crude product was recrystallized from 5L THF / 1% v/v H_2SO_4 solution in deionized water (pH 1) in a 5L Erlenmeyer flask overnight. The mother liquor gave two crops of very fluffy white needle crystals **(note 1)**, which were filtered off on a large glass filter. The white solid filter cake was washed four times with aqueous 1.3% HCl solution (pH 1; total volume 700 mL) to remove remnants of sulfuric acid; and was then sucked dry on the filter. This resulted in 177.22 g of wet product, which was dried for a prolonged time (1.5 month) in a desiccator under high vacuum. This afforded 106.62 g of very pure 3,3'-thiobis(2,2-dimethylpropanoic acid) **2** as a dry white crystalline powder. Yield 83%. The compound structure was confirmed by ^{1}H-NMR. All analytical data agrees with values presented in the literature.**[7]**

^{1}H NMR (400 MHz, CD_3OD) δ 2.80 (s, 4H), 1.23 (s, 12H).

Notes:
1) Crystallinity was assessed by visual inspection of samples on a Olympus BH-2 light microscope equipped with polarizing filters.

5.2.2 Synthesis of diethyl 3,3'-thiobis(2,2-dimethylpropanoate) 3

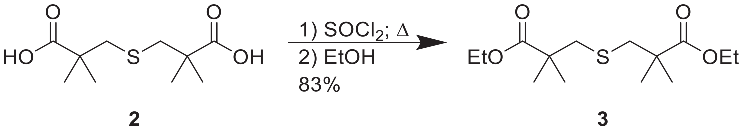

A 500 mL three neck round-bottom flask was charged with solid 3,3'-thiobis(2,2-dimethylpropanoic acid) **2** (106.62 g; 0.455 mol; 1 eq) and a large stirring bar. The flask was fitted with a reflux condenser. One side arm was fitted with a 250 mL addition funnel, which was charged with 200 mL thionyl chloride (2.74 mol; 6 eq), and the other arm was stoppered. Thionyl chloride was added over the course of 20 minutes, followed by a violent exotherm and considerable frothing. After completion of addition, the reaction mixture was refluxed for 2.5 hours. The mixture was then poured out in 2L Erlenmeyer flask containing 1.25 L absolute ethanol and was stirred for 1 hour until TLC indicated full formation of product **3** (R_f = 0.70 in EtOAc/PE 1:6). Solvent was removed *in vacuo*. The crude oil was taken up in 1L DCM and was washed sequentially with 750 mL deionized water and with 1L saturated $NaHCO_3$ solution. Combined organic phases were dried over Na_2SO_4; filtered; and the solvent was removed *in vacuo* to afford 109.24 g of diethyl 3,3'-thiobis(2,2-dimethylpropanoate) **3** as an oil. Yield 83%. The compound structure was confirmed by ^{1}H-NMR. All analytical data agrees with values presented in the literature.[2,7]

^{1}H NMR (400 MHz, CDCl$_3$) δ 4.14 (q, J = 7.1 Hz, 4H), 2.77 (s, 4H), 1.26 (t, J = 7.2 Hz, 6H), 1.23 (s, 12H).

5.2.3 Synthesis of 5-hydroxy-3,3,6,6-tetramethylthiepan-4-one 4

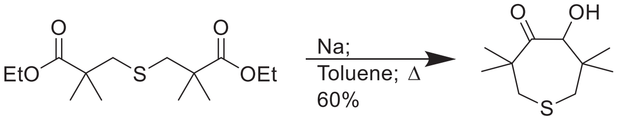

3 **4**

A 2L three neck round-bottom flask was charged with 800 mL toluene; freshy cut sodium metal (38.88 g; 1.69 mol; 4.5 eq) and a large magnetic stirring bar. The flask was fitted with a reflux condenser. One side arm was stoppered and the other side arm was fitted with a 500 mL addition funnel. The setup was heated to reflux and the reaction mixture was vigorously stirred until all sodium formed a fine dispersion of molten metal droplets (to maximize surface area). The addition funnel was charged with a solution of diethyl 3,3'-thiobis(2,2-dimethylpropanoate) **3** (109.24 g; 0.376 mol; 1 eq) in 320 mL toluene, which was added dropwise to the refluxing reaction mixture over the course of 40 minutes, resulting in a violent exotherm. The reaction mixture was then refluxed for another 3 hours until TLC indicated full formation of product **4** (R_f = 0.46 in EtOAc/PE 1:6). The hot reaction mixture was then poured out in a 5L Erlenmeyer flask that contained 2 L 1M aqueous H_2SO_4 solution, which was precooled in an ice/water bath, and the mixture was vigorously stirred **(note 2)**. Additional aliquots of 96% H_2SO_4 were added to promote the quenching of sodium metal. The biphasic mixture was then transferred to a 4L separatory funnel and was extracted. The aqueous phase was reextracted with 300 mL toluene. The combined organic phases were then washed with 1 L saturated $NaHCO_3$ solution, after which the aqueous phase was reextracted again with 300 mL toluene **(note 3)**. The combined organic phases were dried over Na_2SO_4; filtered; and solvent removed *in vacuo* to afford 45.47 g of 5-hydroxy-3,3,6,6-tetramethylthiepan-4-one **4** as a foul smelling oil. Yield 60%. The compound structure was confirmed by ^{1}H-NMR. All analytical data agrees with values presented in the literature.[7]

^{1}H NMR (400 MHz, $CDCl_3$) δ 4.19 (d, *J* = 7.7 Hz, 1H), 3.41 (d, *J* = 7.8 Hz, 1H), 2.79 (d, *J* = 14.7 Hz, 1H), 2.70 (d, *J* = 15.2 Hz, 1H), 2.64 (d, *J* = 15.3 Hz, 1H), 2.48 (d, *J* = 14.6 Hz, 1H), 1.30 (s, 3H), 1.16 (s, 3H), 1.13 (s, 3H), 0.80 (s, 3H).

Notes:

2) This mixture generally autoignites due to the large accumulation of hydrogen gas. Take appropriate safety measures.

3) TLC indicated that only compound **4** was present after workup.

5.2.4 Synthesis of 3,3,6,6-tetramethylthiepane-4,5-dione 5

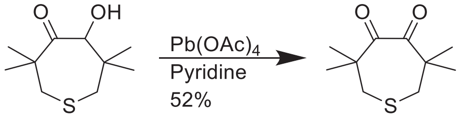

4 **5**

5-hydroxy-3,3,6,6-tetramethylthiepan-4-one **4** (45.47 g; 0.224 mol; 1 eq) was dissolved into 910 mL pyridine in a 2L round-bottom flask. $Pb(OAc)_4$ (122.59 g; 0.276 eq; 1.23 eq) was added and the homogenous solution was stirred for 7 days. 48 mL 37% HCl (2.46 eq) was added to the reaction mixture and resulted into the immediate formation of a $PbCl_2$ precipitate, which was filtered over Celite. The Celite pad was then washed two times with 200 mL Et_2O, and resulted in a clear red filtrate. Solvent was removed *in vacuo* at 60 °C on a high vacuum setup. The resulting oil was then taken up in 500 mL DCM and was washed sequentially with 500 mL 1M HCl and with 500 mL saturated $NaHCO_3$ solution. Re-extractions were performed with 100 mL DCM between each respective wash. The combined organic phases were dried over Na_2SO_4. This solution was then passed over a silica pad (2.5 cm height x 10 cm diameter) on a sintered glass filter and the pad was eluted with more DCM until the filtrate became colorless. TLC indicated only the presence of product **5** (R_f = 0.65 in EtOAc/PE 1:6). Solvent was removed *in vacuo* to afford 23.47 g of 3,3,6,6-tetramethylthiepane-4,5-dione **5** as an orange oil. Yield 52%. The compound structure was confirmed by ^{1}H-NMR. All analytical data agrees with values presented in the literature.[2]

^{1}H NMR (400 MHz, $CDCl_3$) δ 2.59 (s, 4H), 1.28 (s, 12H).

5.2.5 Synthesis of (3,3,6,6-Tetramethylthiepane-4,5-diylidene)bis(hydrazine) 6

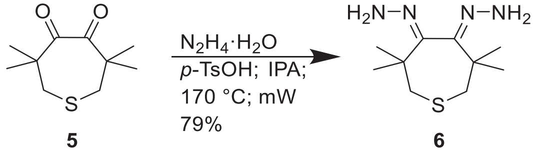

A G30 Anton Paar microwave tube was charged with 3,3,6,6-tetramethylthiepane-4,5-dione **5** (1.25 g; 6.24 mmol; 1 eq) and was dissolved in 9.5 mL 2-propanol under magnetic stirring. Then *p*-toluenesulfonic acid monohydrate (2.41 g; 12.67 mmol; 2 eq) and hydrazine monohydrate (4 mL; 82.46 mmol; 13.2 eq) were added to reaction mixture, which was stirred to give a homogeneous solution. The tube was sealed off and was placed in a Anton Paar Monowave 400 Microwave Synthesis Reactor and was heated to 170 °C for 4 hours under 900 rpm stirring, after which TLC indicated clean formation of bishydrazone product **6** (R_f = 0.46 in EtOAc/PE 1:1). The tube was left to cool down **(note 4)** and solvent was removed *in vacuo*. The crude product was taken up in 50 mL EtOAc and was washed two times with 50 mL deionized water. The combined aqueous phases were reextracted two times with 30 mL EtOAc. The combined organic phases were dried over Na_2SO_4 and this solution was then directly passed over a pad of silica, which was eluted with more EtOAc **(note 5)**. Solvent was removed *in vacuo* to afford 1.12 g of (3,3,6,6-Tetramethylthiepane-4,5-diylidene)bis(hydrazine) **6** as a white crystalline solid. Yield 79%. The compound structure was confirmed by ^{1}H-NMR. All analytical data agrees with values presented in the literature.[2]

^{1}H NMR (400 MHz, $CDCl_3$) δ 5.24 (s, 4H), 2.54 (d, *J* = 14.3 Hz, 2H), 2.48 (d, *J* = 14.4 Hz, 2H), 1.34 (s, 6H), 1.21 (s, 6H).

Notes:

4) At this stage often crystallization occurs: The formed cubical crystals consist of target compound **6** co-crystallized with hydrazinium tosylate salts. One can not use this material for the subsequent synthesis step, as it hampers the formation of THS **7**. It is advisable to redissolve the crystals under heating with a heat gun and to continue the workup.

5) If diketone **5** or monohydrazone contaminants are still present in the crude product according to TLC, one should purify this by Flash Chromatography rather than a silica plug.

5.2.6 Synthesis of THS 7

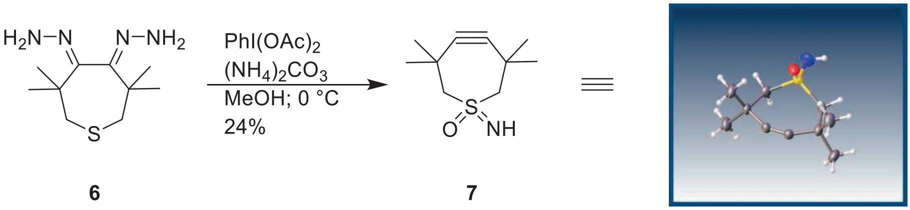

A 250 mL round-bottom flask was charged with (3,3,6,6-tetramethylthiepane-4,5-diylidene)bis(hydrazine) **6** (878.1 mg; 3.84 mmol; 1 eq), ammonium carbonate (1.55 g; 16.1 mmol; 4.2 eq), iodobenzene diacetate (5.09 g; 15.8 mmol; 4.1 eq) and a magnetic stirring bar. The solid reagents were dry mixed in the flask affording a homogeneous powder mixture. The flask was then precooled in an ice-water bath for 15 minutes. Upon stirring, 45 mL precooled methanol (at 0 °C) was added to the flask at once. The reaction mixture immediately turned yellow and gasses evolved **(note 6)**. The neck of the flask was fitted with a septum including a bleed needle. The yellow color disappears within ten minutes. The reaction mixture was left to stir in an ice/water bath at 0 °C for 3.5 hours and formation of the target compound could be monitored with TLC (R_f = 0.18 in EtOAc) **(notes 7 & 8)**. The solvent was then removed *in vacuo*. The residue was taken up in 100 mL DCM and was washed twice with 50 mL demineralized water. The target compound was re-extracted twice from the combined aqueous phases using 50 mL DCM. The combined organic phases were dried over Na_2SO_4 and filtered over a folding filter into a 250 mL round-bottom flask. Solvent was removed *in vacuo*. Target product was purified by flash chromatography (dry packed on silica with DCM; eluent: isocratic EtOAc). This afforded 184 mg of THS **7** as colorless needle crystals. Yield 24%.

Single crystals of THS **7** suitable for x-ray crystallography were grown from chloroform/pentane via the vapor diffusion method.

^{1}H NMR (700 MHz, $CDCl_3$) δ 3.24 (d, *J* = 14.1 Hz, 2H), 3.15 (d, *J* = 14.1 Hz, 2H), 1.43 (s, 6H), 1.27 (s, 6H). ^{13}C NMR (176 MHz, $CDCl_3$) δ 101.6, 71.2, 34.8, 27.7, 26.7. HRMS (ESI) calc. for $C_{10}H_{18}NOS$ $[M+H]^+$ 200.1104; found 200.1105.

Notes:

6) The yellow color is indicative of the formation of a double diazo species upon oxidation, which then forms the strained triple bond under elimination of 2 equivalents of N_2.

7) Temperature control is essential for this reaction to succeed, as this protocol has proven very reproducible. The reaction is intrinsically exothermic, so the use of insufficiently cooled solvent will afford decomposition of the cycloalkyne. We found that the use of even lower temperatures to cool the reaction hampers formation of the sulfoximine.

8) Target compound THS **7** is the only compound that stains positive for $KMnO_4$ stain and tBuOQ stain and is stable on silica checked for by 2D-TLC (it is the only species that remains on the diagonal of the 2D-TLC plate). After several hours under these conditions, the parent thioether compound TMTH will either get converted to THS **7** or will decompose.**[21,24]** This will then simplify the identification of THS **7** by TLC according to the methods mentioned above.

5.2.7 Synthesis of THS-PEG$_2$-amine·TFA 8

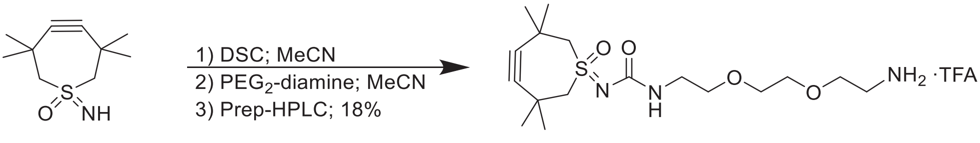

7 **8**

A 4 mL scintillation vial was charged with THS **7** (54.6 mg; 0.274 mmol; 1 eq) and was dissolved in 1.5 mL MeCN under magnetic stirring to form a homogeneous solution. 85% *N*,*N'*-disuccinimidyl carbonate (91 mg; 0.302 mmol; 1.2 eq) was added to the reaction mixture and dissolved immediately. The formation of the THS-OSu-carbamate intermediate was complete after 30 minutes according to TLC (R_f = 0.72 in EtOAc). 2,2'-(Ethylenedioxy) bis(ethylamine) (200 µL; 1.37 mmol; 5 eq) was added to the reaction mixture and was stirred for 1 hour. TLC indicated complete consumption of the THS-OSu-carbamate intermediate and formation of THS-PEG$_2$-amine **8** (R_f = baseline in EtOAc). The reaction mixture was filtered and immediately purified with semi-preparative RP-HPLC (Zorbax Eclipse XDB-C18 column; 5–95% MeCN in MilliQ deionised water, 0.1% (v/v) TFA, linear gradient for 25 min @ 10 mL/min). Product fractions were collected according to confirmation by MS. These fractions were combined and lyophilized to afford 24.5 mg of THS-PEG$_2$-amine·TFA **8** as a crystalline solid. Yield 18%.The compound structure was confirmed by MS. All analytical data agrees with values presented in the literature.[5]

5.2.8 Synthesis of THS-AF488 9

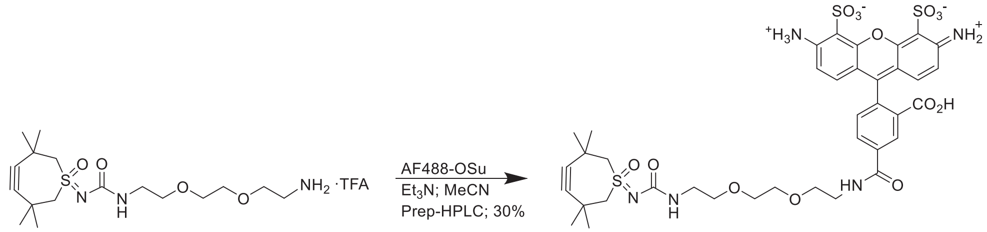

8 THS-AF488 **9**

A 4 mL scintillation vial was charged with AF488-NHS-ester (24 mg; 33 µmol; 1 eq) and under magnetic stirring a solution of THS-PEG$_2$-amine·TFA **8** (15.9 mg; 33 µmol; 1 eq) in 1.3 mL MeCN was added. The reaction was started by addition of Et$_3$N (10 µL; 72 µmol; 2.2 eq) and was left to stir for 75 minutes. The reaction volume was reduced to 0.5 mL in a flow of argon and was then diluted with 0.25 mL MilliQ deionized water. The reaction mixture was then purified with semi-preparative RP-HPLC (Zorbax Eclipse XDB-C18 column; 5–95% MeCN in MilliQ deionised water, 0.1% (v/v) TFA, linear gradient for 25 min @ 10 mL/min). The product fractions eluted at t_R = 13.5–14.0 min as confirmed by MS. The product fractions were combined and lyophilized to afford 8.8 mg of THS-AF488 **9** as an orange / red solid, which is completely water soluble. Yield 30%.

Analytical HPLC: t_R = 14.3 min. HRMS (ESI) calc. for $C_{38}H_{42}N_5O_{14}S_3$ $[M-H]^-$ 888.1896; found 888.1901.

5.2.9 Synthesis of THS-SulfoCy5 10

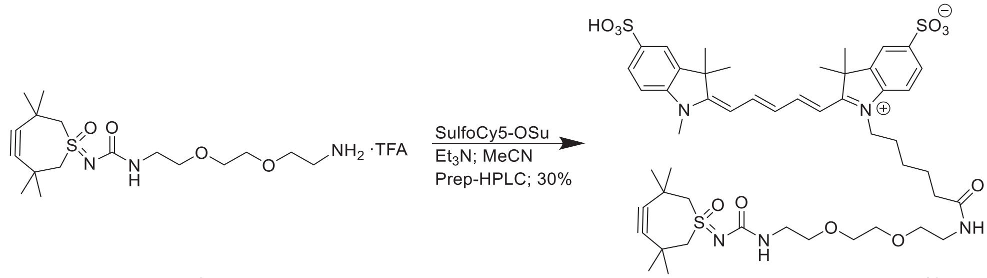

8

THS-SulfoCy5 **10**

A 4 mL scintillation vial was charged with SulfoCyanine5-NHS-ester (15.6 mg; 20 µmol; 1.1 eq) and under magnetic stirring a solution of THS-PEG$_2$-amine·TFA **8** (8.9 mg; 18 µmol; 1 eq) in 1 mL MeCN was added. The reaction was started by addition of Et$_3$N (15 µL; 108 µmol; 6 eq) yielding a deep dark blue solution. The reaction mixture was left to stir for 45 minutes, after which it was quenched by addition of 2 mL MilliQ deionized water. The reaction mixture was then purified by semi-preparative RP-HPLC (Zorbax Eclipse XDB-C18 column; 67.5% buffer A / 32.5% buffer B, isocratic for 25 minutes @ 10 mL/min. Buffer A: 5% MeCN in MilliQ deionized water, 10 mM NH$_4$OAc. Buffer B: 60% MeCN in MilliQ deionized water, 10 mM NH$_4$OAc). The product fractions eluted at t_R = 12–16 min as confirmed by MS. The product fractions were combined according to analytical HPLC runs and lyophilized to afford 5.4 mg of THS-SulfoCy5 **10** as a dark blue solid / powder, which is completely water soluble. Yield 30%.

Analytical HPLC: t_R = 15.4 min. HRMS (ESI) calc. for $C_{49}H_{68}N_5O_{11}S_3$ $[M+H]^+$ 998.4072; found 998.4084.

5.3. Bioconjugations

5.3.1 Bioconjugation of Tras[LC]G$_4$Y with THS-AF488

Tras[LC]G$_4$Y (10 µg, 0.63 µL, 15.8 mg/mL, PBS buffer pH 7.4) was diluted with 8.5 µL PBS buffer pH 5.5 and incubated with THS-AF488 **9** (1.2 µg, 1.2 µL, 1 mg/mL in DMSO, 10 equiv.) and mushroom tyrosinase (mTyr) (1.72 µL, 10 mg/mL in phosphate buffer pH 6, 1 equiv.) at 4 °C for 16 h. After overnight incubation, the product was filtered through Amicon spin filter with 50 kD MWCO to PBS buffer pH 5.5.

5.3.2 General procedure for analytical RP-HPLC-MS

Prior to RP-HPLC analysis, 40 µL of 12.5 mM DTT in 100 mM Tris·HCl pH 8 was added to IgG (10 µL, 1 mg/mL in PBS pH 7.4) and incubated for 15 minutes at 37 °C. Prior to injection, the reaction was quenched by adding 49% acetonitrile, 49% water, 2% formic acid (FA) (50 µL). The mass spectrometer was operated with a spray voltage of 3.9 kV. Acquisitions were performed on the m/z range 500-3000. RP-HPLC analysis was performed on an Agilent 1290 series instrument. The sample (20 µL) was injected with 0.6 mL/min onto MAbPac™ RP 3.0 × 100 mm 4 µm (Thermo Scientific) with a column temperature of 80 °C. A linear gradient was applied in 15 minutes from 25% to 40% acetonitrile in 0.1% FA and water. Mobile phase: A-MQ+0.1% FA, B- ACN+0.1% FA.

5.4. Metabolic cell labelling

Mouse B16F10 cells that express the ovalbumin-derived CTL epitope SIINFEKL (B16F10-OVA) were obtained, generated maintained as previously described.[37] Cells were cultured in RPMI 1640 medium (GIBCO, 21875-034) supplemented with 10% FCS (SIGMA, F7524), 1% sodium pyruvate (GIBCO, 13360-039) and 1% penicillin and streptomycin (PAA, P11-010). For metabolic labeling, 50 µM 1,3,4,6-tetra-*O*-acetyl-*N*-azidoacetylmannosamine ($Ac_4ManNAz$; Carbosynth, MA46004) was added to the culture medium for 5 days (refreshed each 3 days). To detect the intensity of glycocalyx labeling for method optimization and along cell-cell contact in 2D culture, cells were seeded in an 8 or 18-well microscopy plate prior to the day of fixation (Ibidi, Cat# 80826 and Cat# 81816). To detect sialic acid-containing surface glycans, strain-promoted-azide-alkyne cycloaddition (SPAAC) reaction was performed in live cell culture in 2D. B16F10-OVA cells were washed (3x, PBS, 10 min), incubated with DBCO-Alexa Fluor 488 (Click Chemistry Tools, Cat# 1278-1), or THS-Alexa Fluor 488 **9** (all 50 µM, 60 min, unless otherwise indicated, 4 °C), washed 3x (PBS, 10 min) and subjected to flow cytometry or fixed. In the latter case, cells were fixed (2% PBS-buffered PFA, 30 min, 20 °C) and washed 3x (PBS, 10 min). Fixed cells were stored in 0.05% NaN_3 in PBS at 4 °C. High-resolution fixed imaging was performed using a Zeiss LSM880, Airyscan mode, Plan-Apochromat 63x oil objective, voxel size 0.042x0.042x0.17 µm. For pixel-based large-field analysis, cells were imaged in Airyscan mode (Plan-Apochromat 20x/0.8 NA objective, 8-bit, voxel size, 0.21x0.21x1.5 µm). To measure glycocalyx signal vs. background, single slices with perpendicularly-oriented membrane sections were selected and 1-pixel line ROIs perpendicular to the membrane and intracellular ROIs were drawn. To ensure measurement of glycocalyx signal of the entire membrane, the mean signal of the modal signal and the flanking 1.68 µm for high-resolution, or 1.44 µm for low-resolution, were measured. Signal vs. background was subsequently calculated using **Formula 1**.

Formula 1: Signal vs. background calculation.

$$Signal\ vs.background = \frac{mean(Membrane) - mean(Intracellular)}{sd(Intracellular)}$$

The supporting information and appendices are made available via the QR-code below.

6. References

(1) Krebs, A.; Kimling, H. 3.3.6.6-tetramethyl-1-thiacyclopheptin ein isolierbares siebenringacetylen. *Tetrahedron Lett.* **1970**, *11*, 761–764.
(2) De Almeida, G.; Sletten, E. M.; Nakamura, H.; Palaniappan, K. K.; Bertozzi, C. R. Thiacycloalkynes for copper-free click chemistry. *Angew. Chem. Int. Ed.* **2012**, *51*, 2443–2447.
(3) Krebs, A.; Kimling, H. 3,3,7,7-Tetramethylcycloheptyne, an Isolable Seven-Membered Carbocyclic Alkyne. *Angew. Chem. internat. Edit.* **1971**, *10*, 509–510.
(4) Krebs, A.; Kimling, H. 3,3,7,7-Tetramethylcycloheptin, ein isolierbares carbocyclisches Siebenring-Alkin. *Angew. Chem.* **1971**, *83*, 540–541.
(5) Weterings, J.; Rijcken, C. J. F.; Veldhuis, H.; Meulemans, T.; Hadavi, D.; Timmers, M.; Honing, M.; Ippel, H.; Liskamp, R. M. J. TMTHSI, a superior 7-membered ring alkyne containing reagent for strain-promoted azide–alkyne cycloaddition reactions. *Chem. Sci*. **2020**, *11*, 9011–9016.
(6) de Groot, Ae; Wynberg, H. The Synthesis of o-Di-t-butyl Heteroaromatic Compounds. *J. Org. Chem*. **1966**, *31*, 3954–3958.
(7) Feeder, N.; Ginnelly, M. J.; Jones, R. V. H.; O'Sullivan, S.; Warren, S.; Wyatt, P. The X-ray crystal structure, conformation and preparation of anti-3,3,6,6-tetramethylthiepane-4,5-diol: Stereochemistry of reduction of a heterocyclic α-hydroxy ketone. *J. Chem. Soc., Perkin Trans. 1*. **1997**, *22*, 3479–3484.
(8) Scheidt K. A.; O'Bryan E. A. Acyloin Coupling Reactions. In: Knochel P.; Molander G. A., editors. Comprehensive Organic Synthesis. Second Edition. Amsterdam, Netherlands: Elsevier; **2014**. p. 621–655.
(9) Finley, K. T. The acyloin condensation as a cyclization method. *Chem. Rev.* **1964**, *64*, 573–589.
(10) Smith, M. B.; March, J. March's Advanced Organic Chemistry: Reactions, Mechanisms, and Structure. Sixth Edition. Hoboken, New Jersey, United States of America: John Wiley & Sons, Inc.; **2007**. Chapter 19 Oxidations and reductions: E. Reductive coupling, p. 1860–1862.
(11) de la Hoz, A.; Loupy, A. Microwaves in Organic Synthesis. Third Edition. Weinheim, Germany: Wiley-VCH Verlag & Co.; **2012**.
(12) Andresini, M.; Tota, A.; Degennaro, L.; Bull, J. A.; Luisi, R. Synthesis and Transformations of NH-Sulfoximines. *Chem. Eur. J.* **2021**, *27*, 17293–17321.
(13) Verbelen, B.; Siemes, E.; Ehnbom, A.; Räuber, C.; Rissanen, K.; Wöll, D.; Bolm, C. From One-Pot NH-Sulfoximidations of Thiophene Derivatives to Dithienylethene-Type Photoswitches. *Org. Lett*. **2019**, *21*, 4293–4297.
(14) Lohier, J.-F.; Glachet, T.; Marzag, H.; Gaumont, A.-C.; Reboul, V. Mechanistic investigation of the NH-sulfoximination of sulfide. Evidence for λ^6-sulfanenitrile intermediates. *Chem. Commun*. **2017**, *53*, 2064–2067.
(15) King, M.; Baati, R.; Wagner, A. New tetramethylthiepinium (TMTI) for copper-free click chemistry. *Chem. Commun*. **2012**, *48*, 9308–9309.
(16) Wegeberg, C.; Frankær, C. G.; McKenzie, C. J. Reduction of hypervalent iodine by coordination to iron(III) and the crystal structures of PhIO and $PhIO_2$. *Dalton Trans.* **2016**, *45*, 17714–17722.
(17) Okamura, H.; Bolm, C. Sulfoximines: Synthesis and catalytic applications. *Chem. Lett.* **2004**, *33*, 482–487.
(18) Nakayama, J.; Sano, Y.; Sugihara, Y.; Ishii, A. Thiophene sulfoximides: 2,4- and 3,4-di-*tert*-butyl-1-imino-1,1- dihydrothiophene 1-oxides. *Tetrahedron Lett.* **1999**, *40*, 3785–3788.

(19) Nakayama, J.; Otani, T.; Sugihara, Y.; Sano, Y.; Ishii, A.; Sakamoto, A. Syntheses and structures of sulfilimine, sulfone diimine, and sulfoximine derivatives of a monocyclic thiophene, 3,4-di-tert-butylthiophene. *Heteroat. Chem.* **2001**, *12*, 333–348.
(20) Cren, S.; Kinahan, T. C.; Skinner, C. L.; Tye, H. A study of the functional group compatibility of sulfoximination methods. *Tetrahedron Lett.* **2002**, *43*, 2749–2751.
(21) Krebs, A., Colberg, H. Untersuchungen über gespannte cyclische Acetylene, VIII. Hydrierung winkelgespannter Siebenring-Acetylene mit Alkoholen. *Chem. Ber.* **1980**, *113*, 2007–2014.
(22) Timmers, M.; Kipper, A.; Frey, R.; Notermans, S.; Voievudskyi, M.; Wilson, C.; Hentzen, N.; Ringle, M.; Bovino, C.; Stump, B.; Rijcken, C. J. F.; Vermonden, T.; Dijkgraaf, I.; Liskamp, R. Exploring the Chemical Properties and Medicinal Applications of Tetramethylthiocycloheptyne Sulfoximine Used in Strain-Promoted Azide–Alkyne Cycloaddition Reactions. *Pharmaceuticals*, **2023**, *16*, 1155.
(23) Timmers, M.; Peeters, W.; Hauwert, N. J.; Rijcken, C. J. F.; Vermonden, T.; Dijkgraaf, I.; Liskamp, R. M. J. Specific N-terminal attachment of TMTHSI linkers to native peptides and proteins for strain-promoted azide alkyne cycloaddition. *Chem. Commun.* **2023**, *59*, 11397–11400.
(24) Spang, W.; Hanack, M. Notizen. Hydrierung von Achtringacetylenen mit Alkoholen. *Chem. Ber.* **1980**, *113*, 2025–2027.
(25) Dolomanov, O. V.; Bourhis, L. J.; Gildea, R. J.; Howard, J. A. K.; Puschmann, H. OLEX2: A complete structure solution, refinement and analysis program. *J. Appl. Cryst.* **2009**, *42*, 339–341.
(26) Bruins, J. J.; Westphal, A. H.; Albada, B.; Wagner, K.; Bartels, L.; Spits, H.; Van Berkel, W. J. H.; Van Delft, F. L. Inducible, Site-Specific Protein Labeling by Tyrosine Oxidation-Strain-Promoted (4 + 2) Cycloaddition. *Bioconjugate Chem.* **2017**, *28*, 1189−1193.
(27) Debets, M. F.; van Berkel, S. S.; Schoffelen, S., Rutjes, F. P. J. T.; van Hest, J. C. M.; van Delft, F. L. *Chem. Commun.* **2010**, *46*, 97–99.
(28) Dommerholt, J.; Van Rooijen, O.; Borrmann, A.; Guerra, C. F.; Bickelhaupt, F. M.; Van Delft, F. L. Highly accelerated inverse electron-demand cycloaddition of electron-deficient azides with aliphatic cyclooctynes. *Nat. Commun.* **2014**, *5*, 5378.
(29) Dommerholt, J.; Rutjes, F. P. J. T.; van Delft, F. L. Strain-Promoted 1,3-Dipolar Cycloaddition of Cycloalkynes and Organic Azides. *Top. Curr. Chem. (Z)*. **2016**, *374*, 16.
(30) Debets, M. F.; Van Hest, J. C. M.; Rutjes, F. P. J. T. Bioorthogonal labelling of biomolecules: New functional handles and ligation methods. *Org. Biomol. Chem.* **2013**, *11*, 6439–6455.
(31) Gordon, C. G.; MacKey, J. L.; Jewett, J. C.; Sletten, E. M.; Houk K.N.; Bertozzi, C. R. Reactivity of biarylazacyclooctynones in copper-free click chemistry. *J. Am. Chem. Soc*. **2012**, *134*, 9199−9208.
(32) Haase, J.; Krebs, A. Die Molekülstruktur des 3.3.6.6-Tetramethyl-1-thiacycloheptins ($C_{10}H_{16}S$). *Z. Naturforsch. A*. **1972**, *27*, 624–627.
(33) Schulte, P.; Schmidt, G.; Kramer, C.-P.; Krebs, A.; Behrens, U. Metallorganische Verbindungen des Kupfers XIII . Kupfer(I)-chlorid-Komplexe winkelgespannter Cycloheptine Synthesen und Röntgenstrukturanalysen. *J. Organomet. Chem.* **1997**, *530*, 95–100.
(34) Engelsma, S. B.; Willems, L. I.; Van Paaschen, C. E.; Van Kasteren, S. I.; Van Der Marel, G. A.; Overkleeft, H. S.; Filippov, D. V. Acylazetine as a dienophile in bioorthogonal inverse electron-demand Diels-Alder ligation. *Org. Lett.* **2014**, *16*, 2744–2747.

(35) Loos, M.; Gerber, C.; Corona, F.; Hollender, J.; Singer, H. Accelerated isotope fine structure calculation using pruned transition trees, *Anal. Chem.* **2015**, *87*, 5738–5744.
(36) Borrmann, A.; Fatunsin, O.; Dommerholt, J.; Jonker, A. M.; Löwik, D. W. P. M.; Van Hest, J. C. M.; Van Delft, F. L. Strain-promoted oxidation-controlled cyclooctyne-1,2-quinone cycloaddition (SPOCQ) for fast and activatable protein conjugation. *Bioconjugate Chem*. **2015**, *26*, 257–261.
(37) Slaats, J.; Wagena, E.; Smits, D.; Berends, A. A.; Peters, E.; Bakker, G.-J.; van Erp, M.; Weigelin, B.; Adema, G. J.; Friedl, P. Adenosine A2a Receptor Antagonism Restores Additive Cytotoxicity by Cytotoxic T Cells in Metabolically Perturbed Tumors. *Cancer Immunol. Res.* **2022**, *10*, 1462–1474.

Chapter 4

High Rates of Quinone-Alkyne Cycloaddition Reactions are Dictated by Entropic Factors

J.A.M. Damen, Dr. J. Escorihuela, Prof. Dr. H. Zuilhof, Prof. Dr. F. L. van Delft, Dr. Bauke Albada

Abstract
The second order rate constants for the SPOCQ click reaction between an *ortho*-quinone and various strained systems are accurately determined. Thermodynamic activation parameters of the click reaction with two strained alkynes THS and *endo*-BCN-OH were determined using Eyring plots, and show that the reaction is controlled by entropic factors.

This work was published in *Chem. Eur. J.* **2023**

1. Introduction

The strain-promoted oxidation-controlled *ortho*-quinone (SPOCQ) cycloaddition is an oxidation-inducible [4+2] cycloaddition of a 1,2-quinone with a strained cyclic alkyne or alkene that follows an inverse electron demand Diels–Alder (IEDDA) reaction mechanism.[1,2] Due to its high rates and efficiency, SPOCQ chemistry has been successfully employed for the chemical modification of surfaces and for the preparation of bioconjugates.[3–6] In comparison to the widely applied strain-promoted azide-alkyne cycloaddition (SPAAC), SPOCQ benefits from reaction rates that are orders of magnitude higher and provides the option of spatiotemporal control by *in situ* generation of the *o*-quinone from phenols, including biogenic versions utilizing exposed tyrosine residues on proteins.[7–11] Whereas details of the mechanism and rate constants of SPAAC are well-established,[12,13] in-depth investigations into SPOCQ are scarce and mostly limited to computational studies.[14] In the current paper, the experimental determination of second-order rate constants and a detailed computational analysis of SPOCQ between a model *o*-quinone and various strained alkenes and alkynes is described. We determined thermodynamic activation parameters of the reaction with strained alkynes, and correlation to high-level computational analysis provided quantitative insight in the dominant forces driving the conversion, which surprisingly contradict earlier deduced explanations.[15,16] We also quantified the effect of derivatization of two of the most commonly employed strained unsaturated systems, BCN (*endo*-bicyclo[6.1.0]non-4-yne) and TCO (*trans*-cyclooctene), on the associated second-order rate constants to translate our findings to derivatives used in conjugation chemistry. Lastly, we report the unexplored SPOCQ reactivity of the newly reported cycloheptyne THS (compound **2** in **Scheme 1**; 3,3,6,6-tetramethyl-1-thiacyclo-heptyne sulfoximine, see **Chapter 3**).

2. Results and Discussion

The model SPOCQ reaction we investigated is depicted in **Scheme 1a**. Specifically, we employed the relatively stable 4-*tert*-butyl-*ortho*-quinone **1**, which has a distinct optical absorption maximum at 395 nm that allows an easy spectroscopic analysis of the reaction rates. Our matrix of unsaturated carbon-carbon bond-containing compounds **2–7** covers a range of ring sizes, associated strain and relevant derivatization (**Scheme 1b**).

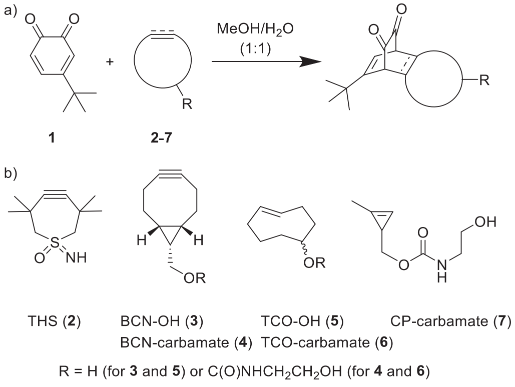

Scheme 1: (a) Generalized scheme for the SPOCQ reaction. (b) Matrix of strained unsaturated carbon-carbon bond containing reagents that were studied.

Firstly, we compared the recently published THS **2** –a highly strained 7-membered alkyne with unprecedented reaction rate constants in SPAAC reactions with azides[17,18]– with BCN-OH **3**, an 8-membered alkyne that is currently one of the benchmark reagents for metal-free click chemistry applications.[19] [Of note: DBCO, by far the most frequently employed cyclooctyne for SPAAC reactions, was found not to display significant reactivity in SPOCQ and was therefore omitted from the matrix.[1]] In addition, we applied two strained alkenes that are commonly used in tetrazine ligations,[20,21] *i.e.* 8-membered diastereomeric TCO-OH **5** (and its carbamate **6**) as well as a derivative of the 3-membered cyclopropene (CP) carbamate **7**; this compound was used in functionalized form due to instability of the parent alcohol.[22-24] Importantly, as all of these strained unsaturated systems are usually not applied as such, but incorporated into a functionalized construct, we also determined the effect of alcohol carbamoylation on the rate constants of BCN and TCO (with compounds **4** and **6**), respectively.

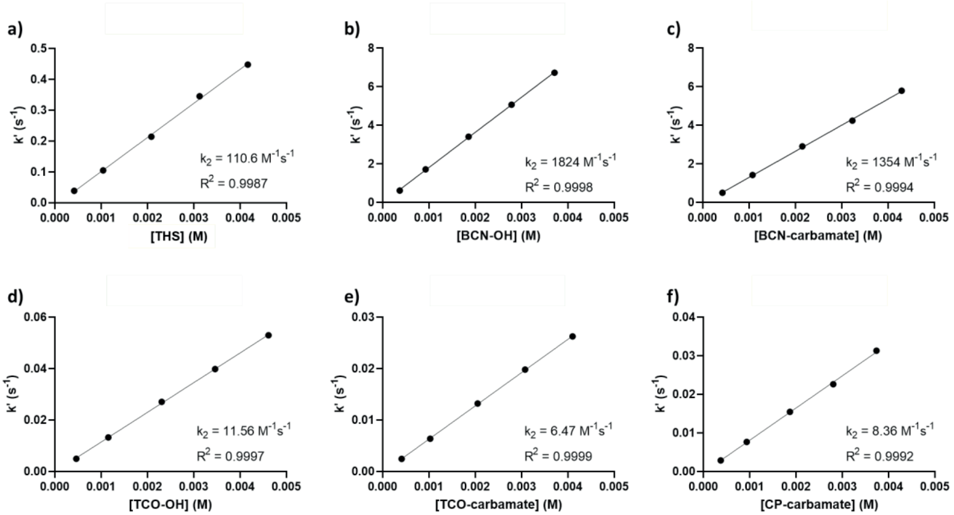

Figure 1: k_2–plots for the SPOCQ reactions of **2–7** determined at 25 °C in MeOH/H_2O (1:1) for: (a) THS **2**, (b) BCN-OH **3**, (c) BCN-carbamate **4**, (d) TCO-OH **5**, (e) TCO-carbamate **6**, (f) cyclopropene (CP) carbamate **7**.

Accurate determination of the reaction rates and second-order rate constants of the SPOCQ reaction was performed by stopped-flow UV-Vis spectroscopic analysis at 25 °C in a methanol-water (1:1) mixture (for set-up see **Section 6.4**).[25] Pseudo-first-order reaction conditions in which 10–100-fold excess of the strained systems **2–7** with respect to *o*-quinone **1** were used. The concentration-independent second-order rate constant k_2 was derived from the slope of the k' (or k_{obs}) versus $[B]_0$-plot (with $[B]_0$ equaling the starting concentration of the excess reagent, **Figure 1**). Notably, the SPOCQ rate constant for BCN-OH **3** of 1824 (± 16) $M^{-1}s^{-1}$ is substantially higher than previously reported values (496–1112 $M^{-1}s^{-1}$),[1,7] which may be rationalized by the fact that sub-optimal conditions were employed previously (*e.g.*, close to equimolar ratios, suboptimal mixing, inability to measure conversion within seconds after mixing). Secondly, we surprisingly found that the k_2 value for THS **2** of 110.6 (± 2.3) $M^{-1}s^{-1}$ is approximately 16 times lower than that of BCN-OH **3**, which is in striking contrast with the reported observation that THS **2** reacts at least 5 times faster than BCN-OH **3** in cycloaddition with azide (*i.e.*, SPAAC). In line with our earlier observations, strained alkenes undergo slower cycloaddition with *o*-quinone than strained alkynes. Specifically, TCO-OH **5** with a k_2 value of 11.56 (± 0.11) $M^{-1}s^{-1}$ is 10-fold less reactive than THS **2** and 160-fold compared to BCN-OH **3**. With respect to the influence of the chemical derivatization, conversion of the hydroxyl group of the well-established probes BCN and TCO into a carbamate lowered the rate slightly (26–44%), *i.e.*, to 1354 (± 19) $M^{-1}s^{-1}$ for BCN-carbamate **4**, and to 6.47 (± 0.04) $M^{-1}s^{-1}$ for TCO-carbamate **6**. Surprisingly, the k_2 value of 8.36 (± 0.14) $M^{-1}s^{-1}$ for cyclopropene-derived probe **7** is somewhat higher than that of TCO-carbamate **6**, suggesting that cyclopropene derivatives are potentially a preferred class of strained alkenes for application in SPOCQ chemistry, specifically when a small ring size is preferred, such as in crowded environments.[4]

The unexpected rate difference between THS **2** and BCN-OH **3** was rationalized by thermodynamic activation parameters obtained from the linearized Eyring equation (**Equation 2.4**, see **Section 6.3**).[26–29] To this end, the k_2 values were determined at 5 °C, 13 °C, 21 °C, 29 °C and 37 °C, respectively (**Figure 2**). This range was chosen as the lower temperatures represents values used for the preparation of protein conjugates such as ADCs, while the highest temperature is relevant for potential *in vivo* applications. As a result, the reaction of *o*-quinone **1** with THS **2** is associated with a $\Delta H^‡$ of 0.80 kcal/mol, $\Delta S^‡ = -46.8$ cal/K·mol, and $\Delta G^‡ = 14.8$ kcal/mol (at 25 °C). Similarly, for reaction of **1** with BCN-OH **3**, $\Delta H^‡ = 2.25$ kcal/mol, $\Delta S^‡ = -36.3$ cal/K·mol, and $\Delta G^‡ = 13.1$ kcal/mol (at 25 °C).

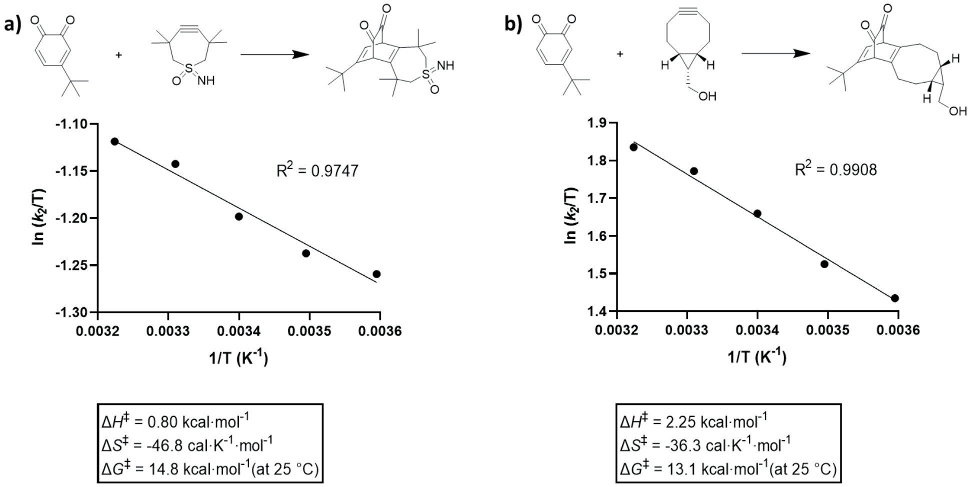

Figure 2: Eyring plots of the reaction of quinone **1** with (a) THS **2** or (b) BCN-OH **3**.

Clearly, the enthalpy required to form the TS for the reaction between **1** and either BCN-OH **3** or THS **2** is only minimal. Considering that the kinetic energy kT at room temperature translates to 0.6 kcal/mol, we found thermodynamic parameters that will aid in the interpretation of the contributions of any secondary orbital interactions that were recently proposed for the SPOCQ reaction between BCN-OH **3** and *o*-quinone **1**.[15,16] The investigated SPOCQ reactions are by and large entropy-controlled reactions. Specifically, the large negative $\Delta S^\ddagger$ values prove that both reactions are associative in nature and require precise positioning of the reagents to form the transition states. In addition, more order needs to be imposed on the reaction of THS **2** than on that of BCN-OH **3** (in other words, BCN **3** is intrinsically more preorganized towards the TS than THS **2**), which we tentatively explain by considering that the TS formed during approach of THS **2** to the plane of **1** has to accommodate the steric bulk of the four methyl groups next to the alkyne. This difference in entropy at 25 °C between **2** and **3** (difference in $T\Delta S^\ddagger$ = 3.2 kcal/mol) apparently outcompetes the difference in enthalpic factors (–1.5 kcal/mol) to yield an overall difference in Gibbs energy of activation at 25 °C of 1.7 kcal/mol in the advantage of BCN-OH **3** SPOCQ over THS **2** SPOCQ.

To further support our empirical findings, computational investigations on the TS were performed using the M06-2X functional with the 6-311+G(d,p) basis set and including the implicit solvent model SMD.[30] To this end, the free energy barriers for the cycloaddition of the minimal reactive warheads of TCO, *endo*-BCN, THS, and CP were calculated for the reaction in water and in MeOH. The transition state structures and the calculated activation free energies ($\Delta G^\ddagger$) and reaction free energies (ΔG_{RXN}) are displayed in **Figure 3**. As observed, the activation free energies for these SPOCQ reactions range from 15 to 20 kcal/mol, in reasonable agreement with experiment, given the non-explicit nature of our solvent model. In all cases, the reaction proceeds via a non-synchronous transition state with C···C distances ranging from 2.11 Å to 2.46 Å. In agreement with experimental results, the computed rate constants predict that BCN will react appreciably faster with *o*-quinone **1** than THS and TCO, with a factor 4 and 50 times, respectively.

3. Conclusions

Stopped-flow UV-Vis spectroscopic analysis of the cycloaddition of 4-*tert*-butyl-*ortho*-quinone **1** first of all revealed that the novel strained alkyne THS **2** reacts 16 times slower than BCN-OH **3** in SPOCQ. Also, we find that derivatization of the strained warhead reduces this rate slightly. Most importantly, experimentally quantified thermodynamic activation parameters showed that the reaction of THS **2** and BCN-OH **3** with *o*-quinone **1** is essentially an entropy-controlled reaction.

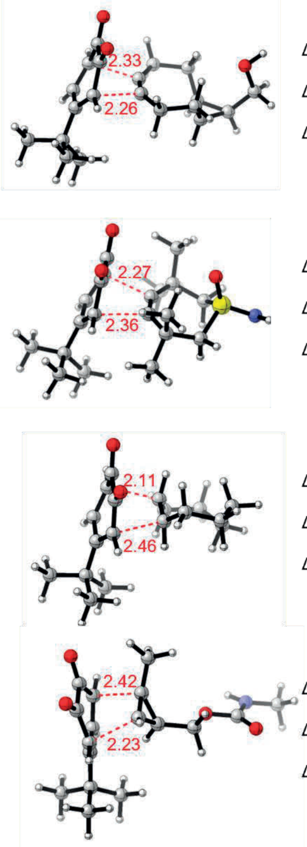

ΔG_{RXN} = –33.8 (H_2O)
–32.6 (MeOH)
$\Delta G^{\ddagger}$ = 14.7 (H_2O)
16.1 (MeOH)
$\Delta H^{\ddagger}$ = 1.1 (H_2O)
2.3 (MeOH)

ΔG_{RXN} = –34.4 (H_2O)
–32.6 (MeOH)
$\Delta G^{\ddagger}$ = 15.9 (H_2O)
17.3 (MeOH)
$\Delta H^{\ddagger}$ = 0.5 (H_2O)
2.7 (MeOH)

ΔG_{RXN} = –25.7 (H_2O)
–24.2 (MeOH)
$\Delta G^{\ddagger}$ = 16.9 (H_2O)
18.4 (MeOH)
$\Delta H^{\ddagger}$ = 2.7 (H_2O)
4.3 (MeOH)

ΔG_{RXN} = –37.5 (H_2O)
–36.2 (MeOH)
$\Delta G^{\ddagger}$ = 18.9 (H_2O)
20.5 (MeOH)
$\Delta H^{\ddagger}$ = 4.1 (H_2O)
5.6 (MeOH)

Figure 3: Transition state structures with associated Gibbs free energies of reaction, Gibbs activation free energies, and enthalpy of activation for the SPOCQ of BCN, THS, TCO and CP (top to bottom), with quinone **1** in the two solvents that were used in the experiment. Bond lengths are shown in red in Å and energies and enthalpies are given in kcal/mol.

4. Experimental Section

4.1. General information

4.1.1 Instruments

^1H (700 MHz) and ^{13}C NMR spectra (176 MHz) were recorded on a Bruker 700 MHz Avance NMR spectrometer and chemical shifts were reported in ppm referenced against the residual solvent peaks of the NMR solvent. ESI-HRMS spectra were recorded on an Exactive Mass Spectrometer (Thermo Scientific) and mass values were calculated with enviPat Web.[31] Stopped-flow UV-Vis spectra were recorded on a Cary 60 UV-Vis spectrophotometer (Agilent) equipped with a RX2000 Rapid Kinetics Spectrometer Accessory (Applied Photophysics), which was attached to a Lauda RCS 6-D thermostatic water bath. During UV-Vis experiments, the temperature was measured internally in in RX2000 Accessory, as well as externally in the water bath by the thermostat, along with an external third independent thermometer. Deionized water was produced with a Milli-Q Integral 3 system (Millipore, Molsheim/France).

4.1.2 General chemicals:

Ethanolamine was purchased from Sigma-Aldrich Merck. N,N'-disuccinimidyl carbonate; 4-*tert*-butylcatechol; triethylamine; sodium sulfate and sodium periodate were all purchased from Thermo Scientific™ / Fisher Scientific. Ethyl acetate (GPR Rectapur) was purchased from VWR Chemicals. Hexane and acetonitrile (CHROMASOLV™, for HPLC for UV) were purchased from Honeywell Riedel-de Haën™. All of these chemicals were used as purchased unless otherwise stated. Methanol (CHROMASOLV™) HPLC grade, Riedel-de Haën™ and MilliQ deionized water were specifically used for UV-Vis experiments. Acetonitrile (HiPerSolv CHROMANORM® HPLC-LC-MS grade, VWR), including 0.1% Formic acid (ULC/MS grade, Biosolve), was specifically used for mass spectrometry measurements.

4.1.3 Chromatography:

Flash chromatography was performed on SiliaFlash® P60 40–63 µm (230–400 mesh) 60 Å Irregular Silica Gel (R12030B) (SiliCycle, Quebec City (Quebec), Canada). Thin Layer Chromatography was performed on TLC Silica gel 60 F_{254} on aluminium sheets (Merck, Darmstadt, Germany). After development, TLC plates were dip stained and heated with a heat gun for visualization of spots. $KMnO_4$ stain was used as a general stain and was prepared by dissolving 1.5 g $KMnO_4$, 10 g K_2CO_3 and 1.25 mL 10% NaOH in 200 mL water. *t*BuOQ stain was specifically used for the identification of strained cycloalkynes. It was prepared by dissolving 50 mg 4-*tert*-butyl-*ortho*-quinone in 10 mL 1-butanol. After dipping and prolonged heating of the TLC plate, strained cycloalkynes form light beige spots against a darker red background. The stain does have limited shelf life.

4.2 Chemical syntheses

THS **2** was synthesized according to procedure described in **Chapter 3**. 4-*tert*-butyl-*ortho*-quinone **1** was synthesized by the method of Borrmann.[5] Methylcyclopropene-ethanolamine-carbamate (CP-carb) **7** was synthesized according to literature procedures.[32–34,23] *Trans*-cyclooct-4-enol (TCO-OH) **5** was purchased as a mixture of diastereomers from BroadPharm® (San Diego, CA, United States). *Endo*-bicyclo[6.1.0]non-4-yn-9-ol (BCN-OH) **3** was kindly donated by Synaffix (Oss, The Netherlands).

4.2.1 Synthesis of BCN-carbamate 4

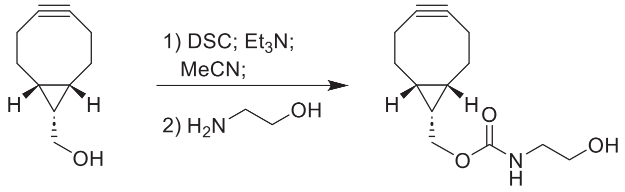

BCN-OH **3**

BCN-carbamate **4**

A scintillation vial was charged with *endo*-BCN-OH **3** (100.2 mg; 0.67 mmol; 1 eq), a magnetic stirring bar and the contents were then dissolved in 3 mL MeCN. N,N'-disuccinimidyl carbonate (264.5 mg; 1 mmol; 1.5 eq) and triethylamine (276 µL; 2 mmol; 3 eq) were added to the reaction mixture under magnetic stirring. The homogenous reaction mixture was stirred for 1.5 hour, after which TLC indicated complete formation of BCN succinimidyl carbonate (R_f = 0.6 in EtOAc/PE 1:1. R_f = 0.44 for *endo*-BCN-OH).Then, ethanolamine (200 µL; 3.3 mmol; 5 eq) was added to the reaction mixture, which turned into a very turbid dispersion. According to TLC the reaction was complete within 15 minutes (R_f = 0.17 in EtOAc/PE 1:1). The reaction mixture was taken up in 10 mL demineralized water and 20 mL EtOAc, which was subsequently extracted. The aqueous phase was reextracted with 10 mL EtOAc. The combined organic phases were washed with 10 mL demineralized water, dried over Na_2SO_4, filtered, and solvent was removed *in vacuo*. The crude product was then purified by flash chromatography, eluent: 50% EtOAc/hexane (isocratic). This afforded 123.9 mg of target compound *endo*-BCN-carb **4** as a clear viscous oil. Yield 78%.

^{1}H NMR (700 MHz, $CDCl_3$) δ 5.17 (s, 1H), 4.14 (d, *J* = 8.1 Hz, 2H), 3.71 (t, *J* = 5.1 Hz, 2H), 3.34 (q, *J* = 5.4 Hz, 2H), 2.51 (bs, 1H), 2.33–2.15 (m, 6H), 1.61–1.52 (m, 2H), 1.39–1.30 (m, 1H), 1.24 (s, 1H), 0.98–0.89 (m, 2H).
^{13}C NMR (176 MHz, $CDCl_3$) δ 157.7, 98.9, 63.2, 62.5, 43.5, 29.1, 21.5, 20.2, 17.8.
HRMS (ESI) calc. for $C_{13}H_{19}NO_3Na$ $[M+Na]^+$ 260.1257; found 260.1258.

4.2.2 Synthesis of TCO-carbamate 6

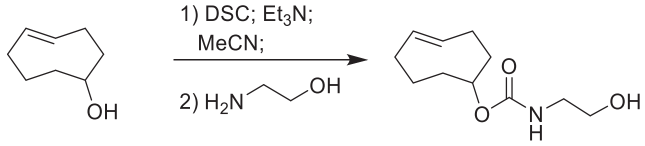

TCO-OH **5** TCO-carbamate **6**

A scintillation vial was charged with TCO-OH **5** (100 mg; 0.79 mmol; 1 eq) and was suspended in 5.5 mL MeCN under magnetic stirring. N,N'-disuccinimidyl carbonate (302.2 mg; 1.18 mmol; 1.5 eq) and triethylamine (332 µL; 2.38 mmol; 3 eq) were added. The reaction mixture was left to stir for 18 hours at room temperature in the dark, after which it formed a much less turbid dispersion. TLC indicated the complete formation of TCO succinimidyl carbonate (R_f = 0.73 in EtOAc/PE 1:1. R_f = 0.62 for TCO-OH). Ethanolamine (240 µL; 3.98 mmol; 5 eq) was added to the reaction mixture, which turned into a white turbid dispersion. According to TLC the reaction was complete within 15 minutes (R_f = 0.22 in EtOAc/PE 1:1). The reaction mixture was taken up in 20 mL EtOAc and was washed twice with 20 mL demineralized water. The combined aqueous phases were reextracted twice with 10 mL EtOAc. The combined organic phases were dried over Na_2SO_4, filtered, and solvent removed *in vacuo*. The crude product was purified by flash chromatography. Eluent: isocratic 50% EtOAc/hexane. This afforded 138.4 mg of target compound TCO-carb **6** as a clear oil. Yield 82%.

^{1}H NMR (700 MHz, $CDCl_3$) δ 5.58–5.53 (m, 1H), 5.50–5.46 (m, 1H), 5.09 (s, 1H), 4.32 (dd, *J* = 11.1, 6.0 Hz, 1H), 3.68 (s, 2H), 3.30 (t, *J* = 5.4 Hz, 2H), 2.68 (bs, 1H), 2.38–2.28 (m, 3H), 2.03–1.97 (m, 1H), 1.96–1.86 (m, 3H), 1.77–1.66 (m, 2H), 1.57–1.49 (m, 1H), 1.28–1.24 (m, 1H). ^{13}C NMR (176 MHz, $CDCl_3$) δ 157.2, 135.0, 133.1, 81.0, 62.6, 43.5, 41.2, 38.7, 34.4, 32.6, 31.1. HRMS (ESI) calc. for $C_{11}H_{20}NO_3$ $[M+H]^+$ 214.1438; found 214.1436.

All analytical data agrees with values presented in the literature.[35]

4.3 Mathematical equations

4.3.1 Correlation between pseudo-first-order and second order rate constants

Equation 1.1: Integrated rate equation when $[A]_0 \neq [B]_0$

$$k_2\mathrm{t} = \frac{1}{[\mathrm{B}]_0 - [\mathrm{A}]_0} \ln \frac{[\mathrm{B}][\mathrm{A}]_0}{[\mathrm{B}]_0[\mathrm{A}]}$$

Equation 1.2: When:

$$[\mathrm{B}]_0 \gg [\mathrm{A}]_0$$

Equation 1.3: Then:

$$[\mathrm{B}]_0 \approx [\mathrm{B}]$$

Equation 1.4: Plugging **equation 1.3** into **equation 1.1** gives:

$$k_2\mathrm{t} = \frac{1}{[\mathrm{B}]_0} \ln \frac{[\mathrm{A}]_0}{[\mathrm{A}]}$$

Equation 1.5: Rearranging **equation 1.4** into the exponential form, gives a similar form as a first order rate law:

$$[\mathrm{A}] = [\mathrm{A}]_0 \mathrm{e}^{-[\mathrm{B}]_0 k_2 \mathrm{t}} \equiv [\mathrm{A}] = [\mathrm{A}]_0 \mathrm{e}^{-k_1 \mathrm{t}}$$

Equation 1.6: Formally describing the k_1 rate constant as a pseudo-first-order rate constant k', allows for:

$$[\mathrm{B}]_0 \cdot k_2 = k'$$

Equation 1.7: Thus:

$$k_2 = \frac{k'}{[\mathrm{B}]_0}$$

4.3.2 Linearized Eyring equation

Equation 2.1: Eyring equation

$$k_2 = \frac{\kappa k_B \mathrm{T}}{h} \mathrm{e}^{-\frac{\Delta G^{\ddagger}}{\mathrm{RT}}}$$

Equation 2.2: Gibbs energy of activation

$$\Delta G^{\ddagger} = \Delta H^{\ddagger} - \mathrm{T}\Delta S^{\ddagger}$$

Equation 2.3: Merging Eq 2.1 and Eq. 2.2

$$k_2 = \frac{\kappa k_B \mathrm{T}}{h} \mathrm{e}^{\frac{\Delta S^{\ddagger}}{\mathrm{R}}} \mathrm{e}^{-\frac{\Delta H^{\ddagger}}{\mathrm{RT}}}$$

Equation 2.4: Linearization of Eq 2.3

$$\ln \frac{k_2}{\mathrm{T}} = \frac{-\Delta H^{\ddagger}}{\mathrm{R}} \cdot \frac{1}{\mathrm{T}} + \ln \frac{\kappa k_B}{h} + \frac{\Delta S^{\ddagger}}{\mathrm{R}}$$

Where:
k_2 = second order rate constant
$\Delta G^{\ddagger}$ = Gibbs energy of activation
$\Delta H^{\ddagger}$ = enthalpy of activation
$\Delta S^{\ddagger}$ = entropy of activation
κ = transmission coefficient (equals to one)
k_B = Boltzmann constant
h = Planck's constant
R = gas constant
T = temperature in Kelvin

4.4 Stopped flow experiments

4.4.1 Schematic of stopped-flow setup

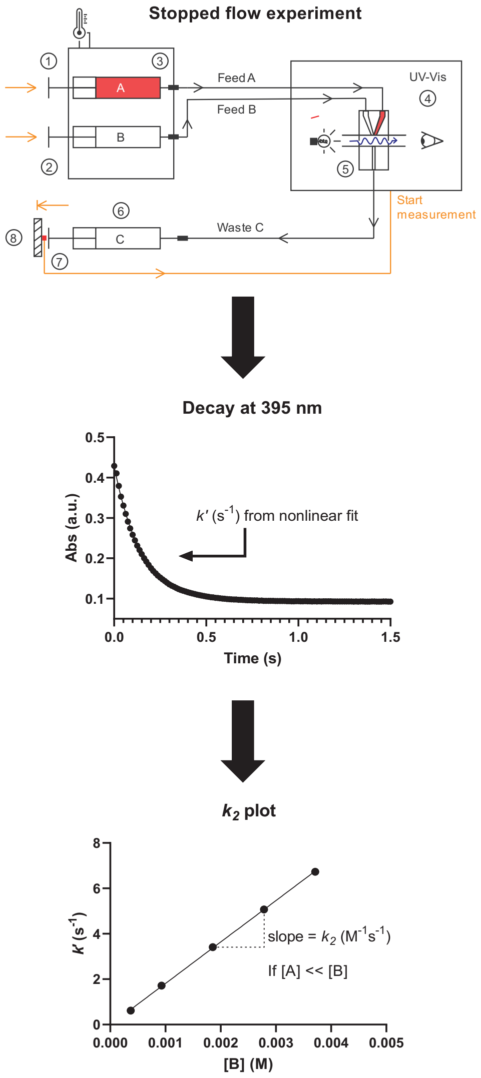
Stopped flow experiment
①
②
③
④
⑤
⑥
⑦
⑧
A
B
C
Feed A
Feed B
UV-Vis
Waste C
Start measurement
Decay at 395 nm
Abs (a.u.)
0.5
0.4
0.3
0.2
0.1
0.0
0.5
1.0
1.5
Time (s)
k′ (s⁻¹) from nonlinear fit
k₂ plot
k′ (s⁻¹)
8
6
4
2
0
0.000
0.001
0.002
0.003
0.004
0.005
[B] (M)
slope = k₂ (M⁻¹s⁻¹)
If [A] << [B]

Top panel: Schematic of the stopped-flow setup, indicating: (1) Syringe containing quinone 1 A; (2) Syringe containing click reagent B; (3) Thermostatic water bath for temperature control; (4) UV-Vis spectrophotometer; (5) mixing chamber and cuvette; (6) Waste syringe; (7) Microswitch button which, when pressed, starts the measurement; (8) Physical barrier that stops the piston of (6) and stops the flow. **Middle panel**: sub-second measurements allow for the recording of kinetic profiles by UV-Vis. *k′* is determined from exponential nonlinear fit of the decay signal of quinone **1**, depending on experimental conditions. **Bottom panel**: k_2 can then be derived from the slope of plotting *k′* versus the concentration of excess click reagent B.

4.4.2 General procedure for stopped-flow analysis

The reaction of 4-*tert*-butyl-*ortho*-quinone **1** with probes **2–7** was measured under pseudo-first order conditions in 1:1 MeOH/MilliQ water following the decay of the specific absorption band at 395 nm for *o*-quinone **1**. Two respective equivolume solutions of *o*-quinone **1** and the probe of interest were loaded into the two separate driver syringes of the RX2000 Rapid Kinetics Spectrometer Accessory (Applied Photophysics). The accessory is attached to a thermostat bath and to a Cary 60 UV-Vis spectrophotometer. The solutions in the driver syringes were thermostatted for at least 15 minutes prior to measurement. Upon measurement, the contents of the two driver syringes were flown simultaneously though the cuvette and measurement starts upon abruptly stopping the flow. Single wavelength measurements were then recorded every 12.5 ms at 395 nm. The measurements were performed in quadruplicate until the signal stabilizes. This setup utilizes equal volumes of the reagents, thereby halving each respective concentration in the cuvette.

The experiments were conducted with 40 µM solutions of *o*-quinone **1** (1 eq) and with 400 µM to 4 mM solutions of probe (10–100 eq) to allow for acquisition of sufficient data points for analysis. k_2-plots were determined at 25 °C with varying stoichiometry of the target probes, ranging from 10 to 100 equivalent. Eyring plots were determined at a set stoichiometry of 1:10 at varying temperatures of 5, 13, 21, 29, 37 °C. Data analysis was then performed in GraphPad Prism 9 Version 9.3.1 (471) by exponential one phase decay fitting using nonlinear regression until a plateau of constant value is reached, which determined an observed pseudo-first-order rate constant k'.

4.5 Computational details

All DFT calculations were performed using Gaussian16 Rev.B01.[30] The Minnesota functional M06-2X[36] with the 6-31G(d) basis was used for geometry optimization of minima and transition states. A frequency analysis was performed using the same level of theory to confirm the presence of a minima with no imaginary frequency or a transition state with a single imaginary frequency. Next, single point energy calculations were performed at the M06-2X with the augmented 6-311++G(d,p) basis set including the solvent with a polarizable continuum model (PCM)[37] using the M06-2X/6-31G(d) optimized geometries. Gibbs free energies were calculated by applying thermal corrections of the M06-2X/6-31G(d) frequency analysis to M06-2X/6-311++G(d,p)//M06-2X/6-31G(d) electronic energies. Intrinsic reaction coordinate (IRC) calculations were performed to verify the expected connections of the first-order saddle points with the local minima found on the potential energy surface.[38]

The supporting information and appendices are made available via the QR-code below.

5. References

(1) Escorihuela, J.; Das, A.; Looijen, W. J. E.; Van Delft, F. L.; Aquino, A. J. A.; Lischka, H.; Zuilhof, H. Kinetics of the Strain-Promoted Oxidation-Controlled Cycloalkyne-1,2-quinone Cycloaddition: Experimental and Theoretical Studies. *J. Org. Chem*. **2018**, *83*, 244−252.
(2) Albada, B.; Keijzer, J. F.; Zuilhof, H.; van Delft, F. Oxidation-Induced "One-Pot" Click Chemistry. *Chem. Rev.* **2021**, *121*, 7032–7058.
(3) Sen, R.; Escorihuela, J.; van Delft, F.; Zuilhof, H. Rapid and Complete Surface Modification with Strain-Promoted Oxidation-Controlled Cyclooctyne-1,2-Quinone Cycloaddition (SPOCQ). *Angew. Chem. Int. Ed*. **2017**, *56*, 3299–3303.
(4) Gahtory, D.; Sen, R.; Kuzmyn, A. R.; Escorihuela, J.; Zuilhof, H. Strain-Promoted Cycloaddition of Cyclopropenes with o-Quinones: A Rapid Click Reaction. *Angew. Chem. Int. Ed*. **2018**, *57*, 10118–10122.
(5) Borrmann, A.; Fatunsin, O.; Dommerholt, J.; Jonker, A. M.; Löwik, D. W. P. M.; Van Hest, J. C. M.; Van Delft, F. L. Strain-promoted oxidation-controlled cyclooctyne-1,2-quinone cycloaddition (SPOCQ) for fast and activatable protein conjugation. *Bioconjugate Chem*. **2015**, *26*, 257–261.
(6) Bruins, J. J.; Albada, B.; Van Delft, F. *ortho*-Quinones and Analogues Thereof: Highly Reactive Intermediates for Fast and Selective Biofunctionalization. *Chem. Eur. J.* **2018**, *24*, 4749–4756.
(7) Bruins, J. J.; Blanco-Ania, D.; Van Der Doef, V.; Van Delft, F. L.; Albada, B. Orthogonal, dual protein labelling by tandem cycloaddition of strained alkenes and alkynes to: *Ortho*-quinones and azides. *Chem. Commun.*, **2018**, *54*, 7338–7341.
(8) Bruins, J. J.; Westphal, A. H.; Albada, B.; Wagner, K.; Bartels, L.; Spits, H.; Van Berkel, W. J. H.; Van Delft, F. L. Inducible, Site-Specific Protein Labeling by Tyrosine Oxidation-Strain-Promoted (4 + 2) Cycloaddition. *Bioconjugate Chem.* **2017**, *28*, 1189−1193.
(9) Bruins, J. J.; Van de Wouw, C.; Keijzer, J. F.; Albada, B.; van Delft, F. L. Inducible, Selective Labeling of Proteins via Enzymatic Oxidation of Tyrosine. In *Enzyme-Mediated Ligation Methods*, Nuijens, T.; Schmidt, M., Eds.; Springer New York: New York, NY, **2019**; pp 357–368.
(10) Bruins, J. J.; Van de Wouw, C.; Wagner, K.; Bartels, L.; Albada B.; Van Delft, F. L. Highly Efficient Mono-Functionalization of Knob-in-Hole Antibodies with Strain-Promoted Click Chemistry. *ACS Omega*. **2019**, *4*, 11801−11807.
(11) Bruins, J. J.; Damen, J. A. M.; Wijdeven, M. A.; Lelieveldt, L. P. W. M.; Van Delft, F. L.; Albada, B. Non-Genetic Generation of Antibody Conjugates Based on Chemoenzymatic Tyrosine Click Chemistry. *Bioconjugate Chem*. **2021**, *32*, 2167−2172.
(12) Dommerholt, J.; Van Rooijen, O.; Borrmann, A.; Guerra, C. F.; Bickelhaupt, F. M.; Van Delft, F. L. Highly accelerated inverse electron-demand cycloaddition of electron-deficient azides with aliphatic cyclooctynes. *Nat. Commun.* **2014**, *5*, 5378.
(13) Scinto, S. L.; Bilodeau, D. A.; Hincapie, R.; Lee, W.; Nguyen, S. S.; Xu, M.; am Ende, C. W.; Finn M.G.; Lang, K.; Lin, Q.; Pezacki, J. P.; Prescher, J. A. Bioorthogonal chemistry. *Nat. Rev. Methods Primers*, **2021**, *1*, 30.
(14) Escorihuela, J.; Looijen, W. J. E.; Wang, X.; Aquino, A. J. A.; Lischka, H.; Zuilhof, H. Cycloaddition of Strained Cyclic Alkenes and Ortho-Quinones: A Distortion/Interaction Analysis. *J. Org. Chem*. **2020**, *85*, 13557−13566.
(15) Levandowski, B. J.; Svatunek, D.; Sohr, B.; Mikula, H.; Houk K. N. Secondary Orbital Interactions Enhance the Reactivity of Alkynes in Diels-Alder Cycloadditions. *J. Am. Chem. Soc*. **2019**, *141*, 2224−2227.

(16) Levandowski, B. J.; Svatunek, D.; Sohr, B.; Mikula, H.; Houk K. N. Correction to "Secondary Orbital Interactions Enhance the Reactivity of Alkynes in Diels–Alder Cycloadditions". *J. Am. Chem. Soc*. **2019**, *141*, 18641.
(17) Weterings, J.; Rijcken, C. J. F.; Veldhuis, H.; Meulemans, T.; Hadavi, D.; Timmers, M.; Honing, M.; Ippel, H.; Liskamp, R. M. J. TMTHSI, a superior 7-membered ring alkyne containing reagent for strain-promoted azide–alkyne cycloaddition reactions. *Chem. Sci*. **2020**, *11*, 9011–9016.
(18) Hebels, E. R.; Bindt, F.; Walther, J.; Van Geijn, M.; Weterings, J.; Hu, Q.; Colombo, C.; Liskamp, R.; Rijcken, C.; Hennink, W. E.; Vermonden, T. Orthogonal Covalent Entrapment of Cargo into Biodegradable Polymeric Micelles via Native Chemical Ligation. *Biomacromolecules*. **2023**, *24*, 4385–4396.
(19) Dommerholt, J.; Schmidt, S.; Temming, R.; Hendriks, L. J. A.; Rutjes, F. P. J. T.; Van Hest, J. C. M.; Lefeber, D. J.; Friedl, P.; Van Delft, F. L. Readily accessible bicyclononynes for bioorthogonal labeling and three-dimensional imaging of living cells. *Angew. Chem. Int. Ed*. **2010**, *49*, 9422–9425.
(20) Oliveira B. L.; Guo Z.; Bernardes G. J. L. Inverse electron demand Diels-Alder reactions in chemical biology. *Chem. Soc. Rev*. **2017**, *46*, 4895–4950.
(21) Baalmann, M.; Neises, L.; Bitsch, S.; Schneider, H.; Deweid, L.; Werther, P.; Ilkenhans, N.; Wolfring, M.; Ziegler, M. J.; Wilhelm, J.; Kolmar, H.; Wombacher, R. A Bioorthogonal Click Chemistry Toolbox for Targeted Synthesis of Branched and Well-Defined Protein–Protein Conjugates. *Angew. Chem. Int. Ed*. **2020**, *59*, 12885–12893.
(22) Patterson, D. M.; Nazarova, L. A.; Xie, B.; Kamber, D. N.; Prescher, J. A. Functionalized cyclopropenes as bioorthogonal chemical reporters. *J. Am. Chem. Soc*. **2012**, *134*, 18638–18643.
(23) Yang, J.; Šečkute, J.; Cole, C. M.; Devaraj, N. K. Live-cell imaging of cyclopropene tags with fluorogenic tetrazine cycloadditions. *Angew. Chem. Int. Ed*. **2012**, *51*, 7476–7479.
(24) Carter, F. L.; Frampton, V. L. Review of the chemistry of cyclopropene compounds. *Chem. Rev*. **1964**, *64*, 497–525.
(25) Wang, M.; Svatunek, D.; Rohlfing, K.; Liu, Y.; Wang, H.; Giglio, B.; Yuan, H.; Wu, Z.; Li, Z.; Fox, J. Conformationally strained trans-cyclooctene (sTCO) enables the rapid construction of 18F-PET probes via tetrazine ligation. *Theranostics*. **2016**, *6*, 887–895.
(26) Laidler, K. J.; King, M. C. The development of transition-state theory. *J. Phys. Chem*. **1983**, *87*, 2657–2664.
(27) Eyring, H. The activated complex in chemical reactions. *J. Chem. Phys*. **1935**, *3*, 107–115.
(28) Evans M. G.; Polanyi M. Some applications of the transition state method to the calculation of reaction velocities, especially in solution. *Trans. Faraday Soc*. **1935**, *31*, 875–894.
(29) Wynne-Jones W. F. K.; Eyring, H. The Absolute Rate of Reactions in Condensed Phases. *J. Chem. Phys*. **1935**, *3*, 492–502.
(30) Frisch, M. J.; Trucks, G. W.; Schlegel, H. B.; Scuseria, G. E.; Robb, M. A.; Cheeseman, J. R.; Scalmani, G.; Barone, V.; Petersson, G. A.; Nakatsuji, H.; Li, X.; Caricato, M.; Marenich, A. V.; Bloino, J.; Janesko, B. G.; Gomperts, R.; Mennucci, B.; Hratchian, H. P.; Ortiz, J. V.; Izmaylov, A. F.; Sonnenberg, J. L.; Williams-Young, D.; Ding, F.; Lipparini, F.; Egidi, F.; Goings, J.; Peng, B.; Petrone, A.; Henderson, T.; Ranasinghe, D.; Zakrzewski, V. G.; Gao, J.; Rega, N.; Zheng, G.; Liang, W.; Hada, M.; Ehara, M.; Toyota, K.; Fukuda, R.; Hasegawa, J.; Ishida, M.; Nakajima, T.; Honda, Y.; Kitao, O.; Nakai, H.; Vreven, T.; Throssell, K.; Montgomery, J. A., Jr.; Peralta, J. E.; Ogliaro, F.; Bearpark, M. J.; Heyd, J. J.; Brothers, E. N.; Kudin, K. N.; Staroverov, V. N.; Keith, T.

A.; Kobayashi, R.; Normand, J.; Raghavachari, K.; Rendell, A. P.; Burant, J. C.; Iyengar, S. S.; Tomasi, J.; Cossi, M.; Millam, J. M.; Klene, M.; Adamo, C.; Cammi, R.; Ochterski, J. W.; Martin, R. L.; Morokuma, K.; Farkas, O.; Foresman, J. B.; Fox, D. J. *Gaussian 16*, Revision B.01, Gaussian, Inc., Wallingford CT, **2016**.
(31) Loos, M., Gerber, C., Corona, F., Hollender, J., Singer, H. Accelerated isotope fine structure calculation using pruned transition trees, *Anal. Chem.* **2015**, *87*, 5738–5744.
(32) Liao, L.-A.; Zhang, F.; Yan, N.; Golen, J. A.; Fox, J. M. An efficient and general method for resolving cyclopropene carboxylic acids. *Tetrahedron*. **2004**, *60*, 1803–1816.
(33) Pallerla, M. K.; Fox, J. M. Diastereoselective intermolecular Pauson-Khand reactions of chiral cyclopropenes. *Org. Lett*. **2005**, *7*, 3593–3595.
(34) Yang, J.; Liang, Y.; Šečkute, J.; Houk K.N.; Devaraj, N. K. Synthesis and reactivity comparisons of 1-methyl-3-substituted cyclopropene mini-tags for tetrazine bioorthogonal reactions. *Chem. Eur. J*. **2014**, *20*, 3365–3375.
(35) D. Liang, K. Wu, R. Tei, T.W. Bumpus, J. Ye, J.M. Baskin, *Proc. Natl. Acad. Sci. USA*, **2019**, *116*, 15453–15462.
(36) Zhao Y.; Truhlar D.G. The M06 suite of density functionals for main group thermochemistry, thermochemical kinetics, noncovalent interactions, excited states, and transition elements: Two new functionals and systematic testing of four M06-class functionals and 12 other functionals. *Theor. Chem. Acc*. **2006**, *120*, 215–241
(37) Miertuš, S.; Scrocco, E.; Tomasi, J. Electrostatic interaction of a solute with a continuum. A direct utilization of AB initio molecular potentials for the prevision of solvent effects. *Chem. Phys*. **1981**, *55*, 117–129.
(38) Fukui, K. The path of chemical-reactions – The IRC approach. *Acc. Chem. Res*. **1981**, *14*, 363–368.

Chapter 5

Temperature-Dependent Reaction Rates of Quinone-Alkene Cycloaddition Reveal that Only Entropy Determines the Rate of SPOCQ Reactions

J.A.M. Damen, Prof. Dr. H. Zuilhof, Dr. B. Albada

Abstract

The second-order rate constants for the SPOCQ click reaction of an expanded array of strained *trans*-cyclooctene and cyclooctyne reagents were determined at various temperatures, providing detailed kinetic insights via the thermodynamic activation parameters. Great reaction rate enhancements were found in the sTCO class of reagents as compared to TCO. It was demonstrated that *ortho*-quinone-cycloalkene cycloadditions are fully entropy-controlled reactions, which does not support a previously hypothesized involvement of secondary orbital interactions as rate-enhancing factor. The *endo/exo* differences of BCN in SPOCQ and SPAAC were also (re)evaluated. Finally, full crystallographic descriptions of *endo*-BCN-OH and DBCO are provided, allowing for angular comparisons.

This work is under review at *Chem. Sci.* **2024**

1. Introduction

Strain-promoted oxidation-controlled *ortho*-quinone (SPOCQ) alkene/alkyne cycloadditions are a family of click reactions that involve the [4+2] inverse electron-demand Diels-Alder (IEDDA) cycloaddition between the electron-poor diene of the quinone and the strained unsaturated carbon-carbon bond of the strained cycloalkene or cycloalkyne. Highly attractive features of this click reaction are the high reaction rates, compatibility with biological settings and the on-demand oxidative generation of the *ortho*-quinone from catechols.[1,2] When the oxidation involves the phenol functionality of an exposed tyrosine residue, the resulting biogenic SPOCQ cycloaddition can be used to attach foreign properly functionalized moieties to the protein of interest.[3,4] As such, toxic payloads as well as biological entities have been covalently tethered to monoclonal antibodies (mAbs) by means of SPOCQ reactions.[5-9] The SPOCQ reaction has also been employed as an efficient tool for rapid and efficient surface modification.[10,11] Despite this wide applicability and rapidly increasing use, understanding the chemoselectivity and orthogonality of various strained reagents in SPOCQ has mainly been limited to computational studies.[12-15] Specifically, theoretical studies into the mechanism postulated the involvement of secondary orbital interactions (SOIs) to rationalize the higher reactivity of strained alkynes ($1\cdot10^{3}$ $M^{-1}s^{-1}$) over that of strained alkenes ($1\cdot10^{1}$ $M^{-1}s^{-1}$).[14,15] A recent mechanistic study by our group provided accurate experimental data that revealed that the SPOCQ reactions with alkynes are entropy-controlled, and only minimal enthalpies are involved.[16]

In this current study we extensively map the kinetics and thermodynamic driving forces in SPOCQ click chemistry in order to reveal the origin of the unusually high reaction rates of this reaction. Our previous work showed that the alkyne-SPOCQ reaction with *endo*-BCN-OH and THS occurs via a transition state (TS) characterized by activation enthalpies of typically just a few kcal/mol, pointing to entropic differences as central factor in the rate determination. In this paper we address the more fundamental question regarding the involvement of secondary orbital interactions (SOIs) by expanding our matrix to *trans*-cyclooctenol (TCO-OH) and the structurally related cyclopropanated strained-*trans*-cyclooctene (sTCO; sometimes also referred to as cyclopropanated TCO, cpTCO) derivatives.[17] Temperature-dependent stopped-flow kinetics were used to acquire the second-order rate constants k_2 and – from Eyring analyses – the thermodynamic activation parameters $\Delta H^{\ddagger}$ and $\Delta S^{\ddagger}$. In this extended matrix (**Scheme 1B**), the following structural features are addressed: (i) effects of chirality of exocyclic tethering points (*exo* versus *endo*); (ii) effects of different functional groups (alcohol versus ester); and (iii) effects of the annulation of *cis*-cyclopropane rings onto the cyclic backbone.[17,18]

Scheme 1 A) Generalized scheme for the SPOCQ reaction showing diene **1** and dienophiles **2–10**. **B)** Matrix of strained dienophiles.

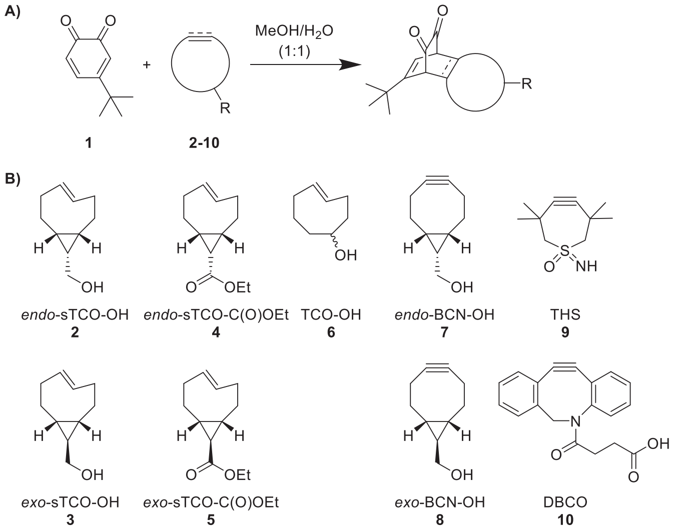

2. Results and Discussion

2.1 Kinetic studies

The second-order rate constants were determined under pseudo-first order conditions by means of stopped-flow UV-Vis spectroscopy in a 1:1 (v/v) MeOH/H_2O system at 25 °C using 4-*tert*-butyl-1,2-*ortho*-quinone **1** as the electron-poor diene. Eyring analyses were performed under similar conditions while maintaining temperatures at 8-centigrade intervals between 5–37 °C. The obtained kinetic and thermodynamic data are shown in **Table 1**. The relationship between the magnitude of k_2 values and the height of the $\Delta G^‡$ barrier are similar to experimentally determined values for other click reactions, such as the IEDDA between sTCO and tetrazine.[17] The large negative $\Delta S^‡$ values in all cases show that SPOCQ is an associative reaction. Although the k_2 value for TCO-OH **6** of 11.6 $M^{-1}s^{-1}$ was already reported by us, the currently determined associated Eyring analysis shows that the energy barrier for TCO-OH **6** SPOCQ consist of an extremely small enthalpic contribution ($\Delta H^‡$ = 0.5 (± 0.1) kcal/mol) as compared to the entropic contributions ($\Delta S^‡$ = -51.9 (± 0.4) cal/K·mol; $T\Delta S^‡$ = -15.4 kcal/mol at 25 °C), resulting in an overall Gibbs free energy of activation ($\Delta G^‡$) of 16.0 kcal/mol at 25 °C. Installation of an annulated *cis*-cyclopropane ring onto a TCO structure enhances its SPOCQ reactivity >300 fold, resulting in *exo*-sTCO-OH **3** as the most reactive reagent in the entire set. This compound displays a k_2 value of 3525 $M^{-1}s^{-1}$ and thus reacts twice as fast its *exo*-BCN-OH **8** counterpart, while being one order of magnitude slower than its reaction with a diphenyltetrazine.[19] Interestingly, the enthalpies of activation are near-identical for TCO-OH **6** and *exo*-sTCO-OH **3** ($\Delta\Delta H^‡$ = 0.1 kcal/mol, which is within the standard deviation of both values). It is the difference in the entropic component of the barrier (the value for $\Delta(T\Delta S^‡)$ for TCO-OH **6** is 3.6 kcal/mol larger than that for *exo*-sTCO-OH **3**), which accounts for the difference in free energy of activation ($\Delta\Delta G^‡$ = -3.4 kcal/mol). From this we conclude that in the reactant complex *exo*-sTCO-OH **3** is already more preorganized towards the TS compared to TCO-OH **6**. A similar trend is observed when TCO-OH **6** is compared to *endo*-sTCO-OH **2**. Our results support an earlier conclusion that a *cis*-fused cyclopropane on TCO, as in sTCO, results in a “half-chair”- conformation that is higher in energy than the typical TCO crown conformation (**Figure 1**),**[17]** but also more preorganized towards the TS of the reaction, resulting in a lower entropic barrier. As all our tested sTCO derivatives exhibit a substantially lower entropic barrier than TCO-OH **6** (ranging from 3.1 – 3.6 kcal/mol), whilst maintaining only minimal enthalpic barriers (ranging from 0.7 – 1.1 kcal/mol), this preorganization is the dominant origin for the enhanced rates of these dienophiles in this SPOCQ reaction. As DBCO **10** is often applied in SPAAC conjugations and is sometimes used for SPOCQ-based bioconjugation,**[20-22]** we decided to also determine its rate constant in SPOCQ as well. For this, pseudo-first order conditions with a 10-fold excess of DBCO-acid **10** (as potassium salt) were applied, resulting in a k_2 value of 0.166 $M^{-1}s^{-1}$. This slower rate, and the more stringent demands for long-term temperature control precluded us, unfortunately, to derive thermodynamic parameters from an Eyring plot for DBCO-acid **10**.

Table 1: Thermodynamic activation parameters and second order rate constants for the inverse electron-demand Diels-Alder SPOCQ cycloadditions between 4-*tert*-butyl-1,2-*ortho*-quinone **1** and different strained dienophiles **2–9**. Standard deviations are given between the brackets.

	Eyring plot					**k_2 plot**	
probe name	**R^2**	**$\Delta H^\ddagger$ (kcal/mol)**	**$\Delta S^\ddagger$ (cal/K·mol)**	**$T\Delta S^\ddagger$ (kcal/mol)**	**$\Delta G^\ddagger$ (kcal/mol)[b]**	**R^2**	**k_2 ($M^{-1}s^{-1}$)**
exo-sTCO-OH **3**	0.9924	**0.7** (±0.1)	-39.8 (±0.4)	**-11.9**	**12.5**	0.9996	**3525** (±52)
endo-sTCO-OH **2**	0.9610	**0.8** (±0.2)	-40.0 (±0.7)	**-11.9**	**12.7**	0.9995	**3354** (±52)
exo-sTCO-COOEt **5**	0.9976	**1.1** (±0.1)	-41.7 (±0.2)	**-12.4**	**13.6**	0.9979	**818** (±22)
endo-sTCO-COOEt **4**	0.9844	**1.1** (±0.2)	-39.9 (±0.6)	**-11.9**	**13.0**	0.9945	**1868** (±80)
exo-BCN-OH **8**	0.9603	**1.7** (±0.4)	-38.3 (±1.5)	**-11.4**	**13.2**	0.9999	**1684** (±11)
endo-BCN-OH **7**[a]	0.9908	**2.3** (±0.3)	-36.3 (±0.9)	**-10.8**	**13.1**	0.9998	**1824** (±16)
THS **9**[a]	0.9747	**0.8** (±0.2)	-46.9 (±0.6)	**-14.0**	**14.8**	0.9987	**110.6** (±2.3)
TCO-OH **6**[a]	0.9774	**0.5** (±0.1)	-51.9 (±0.4)	**-15.4**	**16.0**	0.9997	**11.6** (±0.1)

Notes: [a] these values were already reported previously**[16]**. [b] calculated at 25 °C.

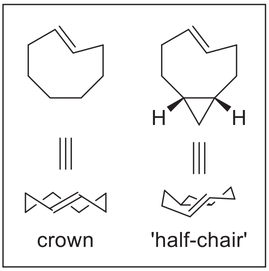

Figure 1: TCO crown conformation (left) versus *cis*–fused sTCO ‘half chair’ conformation (right).**[17]**

The ester analogues of sTCO, *exo*-sTCO-C(O)OEt **5** and *endo*-sTCO-C(O)OEt **4**, also show a high reactivity in SPOCQ reactions, albeit lower than their alcohol counterparts. Interestingly, we observed a two-fold difference in reactivity between *endo*-sTCO-C(O)OEt **4** (1868 $M^{-1}s^{-1}$) and *exo*-sTCO-C(O)OEt **5** (818 $M^{-1}s^{-1}$), resulting in a $k_{rel,\ exo/endo}$ = 0.44. Examining the thermodynamic activation parameters by Eyring analyses revealed that both esters exhibit a slightly higher enthalpy of activation ($\Delta H^\ddagger_{endo}$ = 1.1 (± 0.2) kcal/mol; $\Delta H^\ddagger_{exo}$ = 1.1 (± 0.1) kcal/mol) as compared to those of TCO and the sTCO alcohols. Naturally, the difference in $\Delta H^‡$ is reflected in the overall $\Delta G^‡$ value for *endo*-sTCO-C(O)OEt **4**, which has the same $\Delta S^‡$ value as both sTCO-OH molecules. For *exo*-sTCO-C(O)OEt **5** an additional increase in entropy of activation is found, although the enthalpy of activation is the same as for the *endo* counterpart. This higher entropic barrier ($\Delta(T\Delta S^‡)$ = 0.5 kcal/mol) is reflected in the overall reaction barrier ($\Delta\Delta G^‡$ = 0.6 kcal/mol), resulting in the observed ca. 2.3-fold difference in reactivity.[23] This rather unexpected observation is currently not well understood and needs to be further investigated by means of high-level computational studies. The difference in entropy is presumably explained by that the positioning of the larger C(O)OEt group on the cyclopropane ring forces the entire appending eight membered ring in a slightly different conformation, resulting in slightly less preorganization towards the TS.

We observed that the *exo* and *endo* isomers of sTCO-OH did not display a significant difference in their reactivity towards ortho-quinone **1** nor in the underlying activation parameters between its isomers ($k_{rel,\ exo/endo}$ = 1.05), as previously been observed for their reactivity towards tetrazines.[19] Therefore, we also evaluated the kinetics of the *exo* and *endo* isomers of the eight-membered cycloalkyne BCN-OH. First, we determined the SPOCQ kinetics of *exo*-BCN-OH **8** with *ortho*-quinone **1**, and compare this with our previously reported values for *endo*-BCN-OH **7**.[16] We found that *exo*-BCN-OH **8** exhibits a second-order rate constant k_2 of 1684 $M^{-1}s^{-1}$, which is of the same order of magnitude as we determined for *endo*-BCN-OH **7** (k_2 of 1824 $M^{-1}s^{-1}$, yielding $k_{rel,\ endo/exo}$ = 1.08), and our studies were not able to detect a notable difference in the thermodynamic activation parameters of both isomers.

This seemed to be at variance with an earlier claim regarding the *exo/endo* difference of BCN-OH in SPAAC reactions.[18] To properly understand whether there was indeed a significant difference between the reactivity of these two stereoisomers in SPAAC, we aimed to study the reactivity of both BCN isomers with aliphatic azides in our stopped-flow UV-Vis equipment. However, these attempts were unsuccessful, as overlap of the absorption bands of both the azide and the formed triazole product at 213 nm prevented UV-vis measurements of this transformation. Fortunately, switching to fluorescence spectroscopy using the known fluorogenic substrate 3-azido-7-hydroxycoumarin **11** enabled successful determination of the SPAAC kinetics of both *exo*-BCN-OH **8** and *endo*-BCN-OH **7**. Specifically, the non-fluorescent 3-azido-7-hydroxycoumarin **11** was reacted with *exo*-BCN-OH **8** or *endo*-BCN-OH **7** under pseudo-first order conditions in (1:1) MeOH/H_2O to form the fluorescent triazole product (**Figure 2**).[24] We found that *exo*-BCN-OH **8** reacts with a k_2 value of 0.88 (± 0.06) $M^{-1}s^{-1}$ and *endo*-BCN-OH **7** with a k_2 value of 0.90 (± 0.08) $M^{-1}s^{-1}$, resulting in a $k_{rel,\ exo/endo}$ of 0.98. Again, no statistically significant different was observed. Therefore, we were not able to confirm the reported difference between *exo* and *endo*-BCN-OH in SPAAC click chemistry. As this matches our observation on the SPOCQ reaction, we conclude that it is likely that the reported difference originated from a sub-optimal experimental setup, and not from intrinsic differences in reactivities of the two isomers. The fact that aromatic azides are more reactive than aliphatic azides was already established and the magnitude of the k_2 values is in accordance with literature.[25]

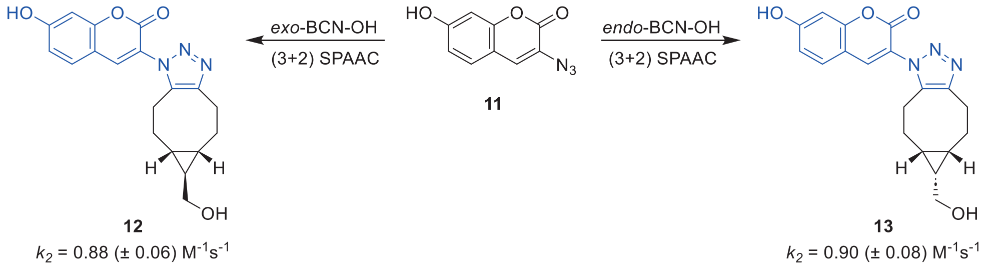
exo-BCN-OH
(3+2) SPAAC
endo-BCN-OH
(3+2) SPAAC
HO
O
O
N_3
11
N
N
N
H
H
OH
12
k_2 = 0.88 (± 0.06) $M^{-1}s^{-1}$
13
k_2 = 0.90 (± 0.08) $M^{-1}s^{-1}$

Figure 2: The kinetics of *exo*-BCN-OH **8** and *endo*-BCN-OH **7** SPAAC were determined by reaction with non-fluorescent 3-azido-7-hydroxycoumarin **11**, following the formation of the fluorescent triazole product. No *exo/endo* difference was found. k_2 values are depicted under each respective probe.

2.2 Single crystal X-ray structure analysis of endo-BCN-OH 7 and DBCO-acid 10

To provide structural insights into the conformation of the BCN and DBCO skeleton, single crystals suitable for X-ray diffraction (XRD) analysis were grown. For BCN suitable crystals were grown from a concentrated hot Et_2O solution, for DBCO this was from a hot THF solution. The resulting crystal structures of *endo*-BCN-OH and DBCO-acid are depicted in **Figure 3**.

Regarding the structure of BCN, the cyclopropane bond length in the XRD of *endo*-BCN-OH **7** is 1.52 Å, which is a typical bond length between sp^3-sp^3 hybridized carbon atoms. As such, we show that ring pinching is actually afforded by means of reducing the interatomic distance between the two methylene groups attached to the cyclopropane ring to 3.277 Å or 3.294 Å respectively (C14–C19 and C4–C9, see **Supporting Information**), forming a more strained plane within the molecule that forces BCN into a conformation in which the alkyne is oriented in a coplanar fashion (only 1.2° torsional angles). This results in bond angles of 154.2°–154.5° between the sp and sp^3 hybridized carbon atoms, which are markedly lower that the value of 158.5° that was reported for the parent compound cyclooctyne.[26] The positioning of both alkyne and cyclopropane planes bend the interconnecting methylene groups of the propargylic position inwards to 105.2°–105.5° and of those next to the cyclopropane ring outwards to 112.0°–112.8°. As such, they deviate substantially from the idealized 109.3° bond angles expected for sp^3 carbon atoms.[27] Therefore, the enhanced reactivity of BCN in click chemistry over that of cyclooctyne is caused by an increase of angular strain of the alkyne and by a reduction of conformational degrees of freedom of the alkane backbone.[18,28]

We were also able to grow crystals of DBCO-acid **10** (**Figure 3**). The two individually planar aromatic rings are tethered together by a heavily distorted alkyne functionality, which is unsymmetrically bent at 152.3° and 154.2°. The alkyne also possesses dihedral distortion by means of a 17.0° torsional angle. This is also reflected in the antiparallel positioning of the aromatic planes relative to each other. Another bridge between the two rings is formed by a nitrogen atom and a methylene group with a dihedral angle of 121.6°. The methylene group has a bond angle of 115.6°, thus deviating largely from normal sp^3 geometry. The nitrogen atom has a bond angle of 120.2° with the ring system, which could be expected for sp^2

hybridization as it is part of an amide. The sp^2 geometry of this nitrogen atom is indeed confirmed by its planarity and the sum of all its bond angles of 359.6°. This confirms that there is no angular perturbation onto the nitrogen atom, *i.e.*, the 120.2° angle originates from a normal sp^2 geometry and not from distorted sp^3 geometry. Interestingly, the linker attached to the amide protrudes in an axial fashion from the DBCO ring system.

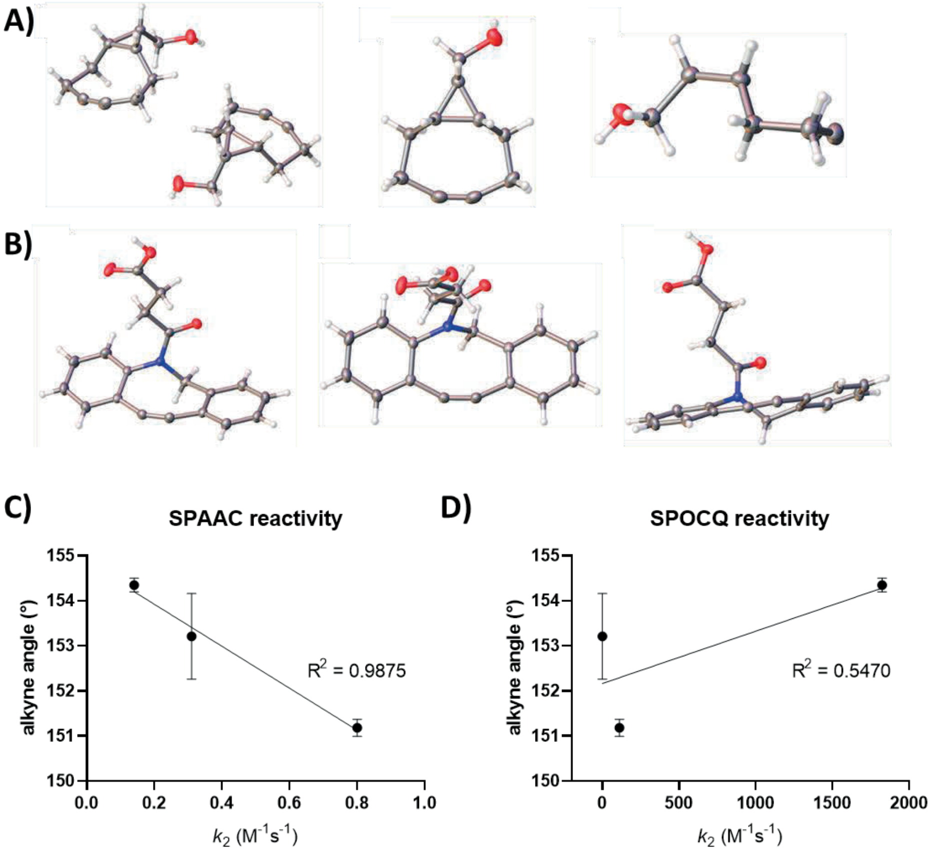

Figure 3: A) The molecular structure of *endo*-BCN-OH **7** according to X-ray structure determination. ORTEP depicted with thermal ellipsoids drawn at 50% probability level. The panel shows the presence of two molecules in the unit cell (*left*), and top and side view of isolated BCN molecules (*middle* and *right*). **B)** The molecular structure of DBCO-acid **10** according to X-ray structure determination. ORTEP depicted with thermal ellipsoids drawn at 50% probability level. The panel shows DBCO from the side, top and front (*left-to-right*). **C)** Chart showing a correlation between the strained alkyne bond angles, and the second-order rate constant for the SPAAC reaction. **D)** Chart showing the absence of a correlation between the strained alkyne bond angles, and the second-order rate constant for the SPOCQ reaction. The average bond length is depicted as a dot with the caps on the bars corresponding to the upper and lower bond angle values as derived from the X-ray structures.

2.3 Structural comparison and reactivity

The XRD structures of *endo*-BCN-OH and DBCO acquired for this paper **(Figure 3 A,B)** allows direct comparison with THS for a detailed assessment of the importance of bond angles in click reactions.[16] THS possesses symmetrical alkyne bond angles of 151.0°–151.4° and is therefore the most strained stable cycloalkyne to date. However, even though it is one of the fastest click reagents for SPAAC, it only displays intermediate reactivity in SPOCQ chemistry. Our previously published data indicate that this is due to higher entropic barriers, which were ascribed to its substantial steric bulk originating from the methyl groups neighboring the alkyne functionality.[16] Even though alkyne bond angles in cycloalkynes directly relate to reactivity in (3+2) SPAAC cycloadditions **(Figure 3C)**,[29] this is not the case for the [4+2] SPOCQ reactions **(Figure 3D)**. The planar TS of (3+2) SPAAC fundamentally differs from the three-dimensionally demanding TS of [4+2] SPOCQ. The current data and previous discussions show that the main height of the TS barrier in SPOCQ is dictated by entropy and that reagent bulkiness has to be taken into account.[16] If any trends in reactivity were to exist regarding differences in bond angles of these transition state mimics, then they would be reflected in *(differences in)* enthalpies of activation. The structures of the TSs often resemble the molecular structures of the reagents in the case of an early TS exergonic reaction, according to Hammond's Postulate. This means that the net bond breaking plus bond formation energy barrier ($\Delta H^{\ddagger}$) would be lower for more strained systems. This phenomenon is observed in our dataset when comparing THS and *endo*-BCN-OH ($\Delta\Delta H^{\ddagger}$ = 1.4 kcal/mol).

Nonetheless this means that we are working at the frontline of alkyne bending, in balancing stability with reactivity. The ability to bend alkynes to bond angles that reside in between ideal geometries of sp–sp (180°) bonds and of sp^2–sp^2 (120°) bonds is astonishing. A similar, but distinct phenomenon is observed for *trans*-cyclooctenes. The crown-like conformation of the molecule enforces dihedral bending of the sp^2–sp^2 bond plane of the alkene to an extend of 133.0°, as was shown crystallographically by Fox *et al*.[30] This 47° geometrical distortion of alkene planarity likely attributes to the extremely low $\Delta H^{\ddagger}$ contributions found in cycloalkene SPOCQ, described here. Lastly, we observed that the $\Delta H^{\ddagger}$ for sTCO-OH are significantly lower than those for the BCN-OH counterpart, with 0.6–1.0 kcal/mol versus 1.3–2.5 kcal/mol (standard deviations are included in these values), respectively. As such, we can conclude that our data does not support the involvement of secondary orbital interactions (SOIs) in this cycloaddition; if these would play a role, the enthalpy of activation of BCN-OH would be lower than that of sTCO-OH.

3. Conclusion

Our current kinetic and mechanistic studies by means of stopped-flow UV-Vis spectroscopy has provided detailed insights into *o*-quinone–cycloalkene click chemistry. We found that the $\Delta H^{\ddagger}$ values amongst the TCO class only minimally differ and are extremely small, and that mainly the entropy factor $\Delta S^{\ddagger}$ dictates the height of the $\Delta G^{\ddagger}$ barrier. Introduction of a cyclopropane ring enforces reactivity and suppresses the $\Delta S^{\ddagger}$ value in SPOCQ reactions. These findings support the proposed theorem that sTCO adapts a half chair conformation which is higher in energy when compared to TCO, but is more preorganized towards the TS, leading to higher reactivity. As such, the sTCO class provides the new benchmark reagents in SPOCQ chemistry, reaching k_2 values of 3525 $M^{-1}s^{-1}$. Our data excludes notable involvement of secondary orbital interactions in SPOCQ chemistry. No reactivity differences were found between *exo* and *endo* diastereomers of the probes in SPOCQ, unless bulkier substituents were involved. The long claimed difference in *exo* and *endo* BCN SPAAC chemistry, was also found not to be true. The XRD analysis of both BCN and DBCO allowed us to conclude that the higher angular tension of DBCO does not affect its reactivity in SPOCQ, as BCN is 11,000 times more reactive.

Acknowledgements

We thank dr. Gabriele Kociok-Köhn (University of Bath, UK) for her work on obtaining and processing of the single crystal X-ray structures, and Barend van Lagen for his assistance with fluorescence spectroscopy.

Funding sources

This work is funded by the NWO Gravity Program Institute for Chemical Immunology (ICI), project number ICI00027.

4. Experimental Section

4.1 General information

4.1.1 Instruments

Stopped-flow UV-Vis spectra were recorded on a Cary 60 UV-Vis spectrophotometer (Agilent) equipped with a RX2000 Rapid Kinetics Spectrometer Accessory (Applied Photophysics), which was attached to a Lauda RCS 6-D thermostatic water bath. During UV-Vis experiments, the temperature was measured internally in in RX2000 Accessory, as well as externally in the water bath by the thermostat, along with an external third independent thermometer. Fluorescence measurements were performed on a Edinburgh Instruments FLS900 fluorescence spectrometer equipped with a 450 W xenon lamp and PMT detector. Deionised water was produced with a Milli-Q Integral 3 system (Millipore, Molsheim/France).

4.1.2 General chemicals

4-*tert*-butyl-*ortho*-quinone **1** was synthesized by the method described by Borrmann.[1] 3-Azido-7-hydroxycoumarin **11** was purchased at TCI. ((1R,8S,9s,E)-bicyclo[6.1.0]non-4-en-9-yl)methanol (*endo*-sTCO-OH) **2** ; ((1R,8S,9r,E)-bicyclo[6.1.0]non-4-en-9-yl)methanol (*exo*-sTCO-OH) **3** ; ethyl (1R,8S,9s,E)-bicyclo[6.1.0]non-4-ene-9-carboxylate (*endo*-sTCO-COOEt) **4** and ethyl (1R,8S,9r,E)-bicyclo[6.1.0]non-4-ene-9-carboxylate (*exo*-sTCO-COOEt) **5** were purchased from Synvenio (Nijmegen, The Netherlands). *Trans*-cyclooct-4-enol (TCO-OH) **6** was purchased as a mixture of diastereomers from BroadPharm (San Diego, CA, United States). DBCO-acid **10** was also purchased from BroadPharm (San Diego, CA, United States). *Exo*-bicyclo[6.1.0]non-4-yn-9-ol (*exo*-BCN-OH) **8** was purchased from Sirius Fine Chemicals SiChem (Bremen, Germany). *Endo*-bicyclo[6.1.0]non-4-yn-9-ol (*endo*-BCN-OH) **7** was kindly donated by Synaffix (Oss, The Netherlands). Methanol (CHROMASOLV™) HPLC grade, Riedel-de Haën™ and MilliQ deionised water were specifically used for UV-Vis spectroscopy experiments and for fluorescence spectroscopy experiments.

4.2 Single crystals for XRD analysis

Single crystals of *endo*-BCN-OH suitable for X-ray crystallography analysis were grown from a hot Et_2O solution. Single crystals of DBCO-acid suitable for X-ray crystallography analysis were grown from a hot THF solution. The structures can be retrieved from the Cambridge Crystallographic Data Centre (CDCC deposition numbers 2378937 and 2378938). Figures for publication were generated with Olex2.[31]

4.3 Stopped-flow UV-Vis kinetic studies

The reaction of 4-*tert*-butyl-*ortho*-quinone **1** with probes **2–10** was measured under pseudo-first order conditions in 1 : 1 MeOH/MilliQ water following the decay of the specific absorption band at 395 nm for *o*-quinone **1**. Two respective equivolume solutions of *o*-quinone **1** and the probe of interest were loaded into the two separate driver syringes of the RX2000 Rapid Kinetics Spectrometer Accessory (Applied Photophysics). The accessory is attached to a thermostat bath and to a Cary 60 UV-Vis spectrophotometer. The solutions in the driver syringes were thermostatted for at least 15 min prior to measurement. Upon measurement, the contents of the two driver syringes were flown simultaneously though the cuvette and measurement starts upon abruptly stopping the flow. Single wavelength measurements were then recorded every 12.5 ms at 395 nm. The measurements were performed in quadruplicate until the signal stabilizes. This setup utilizes equal volumes of the reagents, thereby halving each respective concentration in the cuvette. Concentrations are hereby referred to as final concentrations in the reaction mixture.

The experiments were conducted using 40 µM solutions of *o*-quinone **1** (1 eq) and 0.4–4 mM solutions of probe (*i.e.*, 10–100 eq) to allow for acquisition of sufficient data points for analysis. From these, k_2 plots were determined at 25 °C with the varying stoichiometry of the target probes. Eyring plots were determined at a set stoichiometry of 1:10 at varying temperatures of 5, 13, 21, 29, 37 °C. Measurements for DBCO-acid (as potassium salt) were performed at a higher concentration of 4 mM DBCO with 0.4 mM *o*-quinone **1** at a set stoichiometry of 1:10 equivalents. Data analysis was then performed in GraphPad Prism 9 Version 9.3.1 (471) by exponential one phase decay fitting using nonlinear regression until a plateau of constant value is reached, leading to an observed pseudo-first-order rate constant *k′* (see Supporting Information for additional details). The k_2 values were then determined from the slope of the linear *k′* versus [probe] plot. The thermodynamic activation parameters $\Delta H^{\ddagger}$ and $\Delta S^{\ddagger}$ were determined via the classic method of Eyring utilizing the following linearized equation, with transmission coefficient κ (equals one); Boltzmann constant k_B; Planck's constant *h*; gas constant R; temperature T (in K).**[32-35]**

$$\ln\frac{k_2}{\mathrm{T}} = \frac{-\Delta H^{\ddagger}}{\mathrm{R}}\cdot\frac{1}{\mathrm{T}} + \ln\frac{\kappa k_B}{h} + \frac{\Delta S^{\ddagger}}{\mathrm{R}}$$

4.4 Fluorescence spectroscopy kinetic studies

Fluorescence measurements were performed on a Edinburgh Instruments FLS900 Fluorescence spectrometer at 20 °C under pseudo-first order conditions in 1:1 MeOH/MilliQ water (v/v). Two equivolume solutions of 10 µM 3-azido-7-hydroxycoumarin **11** and 10 mM *endo*-BCN-OH **7** or *exo*-BCN-OH **8** were mixed in a quartz cuvette at a set stoichiometry of 1:1000 equivalents. Concentrations are referred to as final concentrations as in the reaction mixture. Formation of the fluorescent triazole click product was followed over time (λ_{ex} = 395 nm; λ_{em} = 472 nm). Emission spectra were recorded every 9 seconds for 15 minutes at 472 nm, at which point the increase of signal reached a plateau. Data analysis was then performed in GraphPad Prism 9 Version 9.3.1 (471) by exponential plateau fitting using nonlinear regression, leading to an observed pseudo-first-order rate constant *k′*, from which the k_2 values were then obtained by dividing *k′* by [BCN]. The measurements were performed in triplicate for each compound.

The supporting information and appendices are made available via the QR-code below.

5. References:

(1) Borrmann, A.; Fatunsin, O.; Dommerholt, J.; Jonker, A. M.; Löwik, D. W. P. M.; Van Hest, J. C. M.; Van Delft, F. L. Strain-promoted oxidation-controlled cyclooctyne-1,2-quinone cycloaddition (SPOCQ) for fast and activatable protein conjugation. *Bioconjugate Chem*. **2015**, *26*, 257–261.
(2) Albada, B.; Keijzer, J. F.; Zuilhof, H.; Van Delft, F. Oxidation-Induced “One-Pot” Click Chemistry. *Chem. Rev.* **2021**, *121*, 7032–7058.
(3) Bruins, J. J.; Westphal, A. H.; Albada, B.; Wagner, K.; Bartels, L.; Spits, H.; Van Berkel, W. J. H.; Van Delft, F. L. Inducible, Site-Specific Protein Labeling by Tyrosine Oxidation-Strain-Promoted (4 + 2) Cycloaddition. *Bioconjugate Chem.* **2017**, *28*, 1189−1193.
(4) Bruins, J. J.; Albada, B.; Van Delft, F. *ortho*-Quinones and Analogues Thereof: Highly Reactive Intermediates for Fast and Selective Biofunctionalization. *Chem. Eur. J.* **2018**, *24*, 4749–4756.
(5) Bruins, J. J.; Blanco-Ania, D.; Van Der Doef, V.; Van Delft, F. L.; Albada, B. Orthogonal, dual protein labelling by tandem cycloaddition of strained alkenes and alkynes to: *Ortho*-quinones and azides. *Chem. Commun.* **2018**, *54*, 7338–7341.
(6) Bruins, J. J.; Van de Wouw, C.; Keijzer, J. F.; Albada, B.; Van Delft, F. L. Inducible, Selective Labeling of Proteins via Enzymatic Oxidation of Tyrosine. In *Enzyme-Mediated Ligation Methods*, Nuijens, T.; Schmidt, M., Eds.; Springer New York: New York, NY, **2019**; pp 357–368.
(7) Bruins, J. J.; Van de Wouw, C.; Wagner, K.; Bartels, L.; Albada, B.; Van Delft, F. L. Highly Efficient Mono-Functionalization of Knob-in-Hole Antibodies with Strain-Promoted Click Chemistry. *ACS Omega*. **2019**, *4*, 11801−11807.
(8) Bruins, J. J.; Damen, J. A. M.; Wijdeven, M. A.; Lelieveldt, L. P. W. M.; Van Delft, F. L.; Albada, B. Non-Genetic Generation of Antibody Conjugates Based on Chemoenzymatic Tyrosine Click Chemistry. *Bioconjugate Chem*. **2021**, *32*, 2167−2172.
(9) Shajan I.; Rochet L. N. C.; Tracey S. R.; Jackowska B.; Benazza R.; Hernandez-Alba O.; Cianférani S.; Scott C. J.; Van Delft F. L.; Chudasama V.; Albada B. Rapid Access to Potent Bispecific T Cell Engagers Using Biogenic Tyrosine Click Chemistry. *Bioconjugate Chem.* **2023**, *34*, 2215–2220.
(10) Sen, R.; Escorihuela, J.; van Delft, F.; Zuilhof, H. Rapid and Complete Surface Modification with Strain-Promoted Oxidation-Controlled Cyclooctyne-1,2-Quinone Cycloaddition (SPOCQ). *Angew. Chem. Int. Ed*. **2017**, *56*, 3299–3303.

(11) Gahtory, D.; Sen, R.; Kuzmyn, A. R.; Escorihuela, J.; Zuilhof, H. Strain-Promoted Cycloaddition of Cyclopropenes with o-Quinones: A Rapid Click Reaction. *Angew. Chem. Int. Ed*. **2018**, *57*, 10118–10122.
(12) Escorihuela, J.; Das, A.; Looijen, W. J. E.; Van Delft, F. L.; Aquino, A. J. A.; Lischka, H.; Zuilhof, H. Kinetics of the Strain-Promoted Oxidation-Controlled Cycloalkyne-1,2-quinone Cycloaddition: Experimental and Theoretical Studies. *J. Org. Chem*. **2018**, *83*, 244−252.
(13) Escorihuela, J.; Looijen, W. J. E.; Wang, X.; Aquino, A. J. A.; Lischka, H.; Zuilhof, H. Cycloaddition of Strained Cyclic Alkenes and Ortho-Quinones: A Distortion/Interaction Analysis. *J. Org. Chem*. **2020**, *85*, 13557−13566.
(14) Levandowski, B. J.; Svatunek, D.; Sohr, B.; Mikula, H.; Houk, K. N. Secondary Orbital Interactions Enhance the Reactivity of Alkynes in Diels-Alder Cycloadditions. *J. Am. Chem. Soc*. **2019**, *141*, 2224−2227.
(15) Levandowski, B. J.; Svatunek, D.; Sohr, B.; Mikula, H.; Houk K. N. Correction to "Secondary Orbital Interactions Enhance the Reactivity of Alkynes in Diels–Alder Cycloadditions". *J. Am. Chem. Soc*. **2019**, *141*, 18641.
(16) Damen, J. A. M.; Escorihuela, J.; Zuilhof, H.; Van Delft, F. L.; Albada, B. High Rates of Quinone-Alkyne Cycloaddition Reactions are Dictated by Entropic Factors. *Chem. Eur. J.* **2023**, *29*, e202300231.
(17)Taylor, M. T.; Blackman, M. L.; Dmitrenko, O.; Fox, J. M. Design and synthesis of highly reactive dienophiles for the tetrazine-*trans*-cyclooctene ligation. *J. Am. Chem. Soc.* **2011**, *133*, 9646–9649.
(18) Dommerholt, J.; Schmidt, S.; Temming, R.; Hendriks, L. J. A.; Rutjes, F. P. J. T.; Van Hest, J. C. M.; Lefeber, D. J.; Friedl, P.; Van Delft, F. L. Readily accessible bicyclononynes for bioorthogonal labeling and three-dimensional imaging of living cells. *Angew. Chem. Int. Ed*. **2010**, *49*, 9422–9425.
(19) Wang, M.; Svatunek, D.; Rohlfing, K.; Liu, Y.; Wang, H.; Giglio, B.; Yuan, H.; Wu, Z.; Li, Z.; Fox, J. Conformationally strained trans-cyclooctene (sTCO) enables the rapid construction of 18F-PET probes via tetrazine ligation. *Theranostics*. **2016**, *6*, 887–895.
(20) George, A.; Krishna Priya, G.; Ilamaran, M.; Kamini, N. R.; Ganesh, S.; Easwaramoorthi, S.; Ayyadurai, N. Accelerated Strain-Promoted and Oxidation-Controlled Cyclooctyne-Quinone Cycloaddition for Cell Labeling. *ChemistrySelect* **2017**, *2*, 7117–7122.
(21) George, A.; Indhu, M.; Ashokraj, S.; Shanmugam, G.; Ganesan, P.; Kamini, N. R.; Ayyadurai, N. Genetically encoded dihydroxyphenylalanine coupled with tyrosinase for strain promoted labeling. *Bioorg. Med. Chem.* **2021**, *50*, Article number 116460.
(22) Zhan, H.; De Jong, H.; Löwik, D. W. P. M. Comparison of Bioorthogonally Cross-Linked Hydrogels for *in Situ* Cell Encapsulation. *ACS Appl. Bio Mater.* **2019**, *2*, 2862–2871.
(23) The difference in reactivities and difference in the height of the activation barriers is in accordance with $\Delta\Delta G^{‡}$=-R·T·ln(k_{rel}).
(24) Sivakumar, K.; Xie, F.; Cash, B. M.; Long, S.; Barnhill, H. N.; Wang, Q. A fluorogenic 1,3-dipolar cycloaddition reaction of 3-azidocoumarins and acetylenes. *Org. Lett.* **2004**, *6*, 4603–4606.
(25) Dommerholt, J.; Van Rooijen, O.; Borrmann, A.; Guerra, C. F.; Bickelhaupt, F. M.; Van Delft, F. L. Highly accelerated inverse electron-demand cycloaddition of electron-deficient azides with aliphatic cyclooctynes. *Nat. Commun.* **2014**, *5*, 5378.
(26) Haase, J.; Krebs, A. Die Molekülstruktur des Cyclooctins C_8H_{12}. *Z. Naturforsch. A*. **1971**, *26*, 1190–1193.

(27) Smith, M. B.; March, J. March's Advanced Organic Chemistry: Reactions, Mechanisms, and Structure. Sixth Edition. Hoboken, New Jersey, United States of America: John Wiley & Sons, Inc.; **2007**.
(28) Antony-Mayer, C.; Meier, H. Bicyclo[6.1.0]nonine. *Chem. Ber.* **1988**, *121*, 2013–2018.
(29) Gordon, C. G.; MacKey, J. L.; Jewett, J. C.; Sletten, E. M.; Houk K.N.; Bertozzi, C. R. Reactivity of biarylazacyclooctynones in copper-free click chemistry. *J. Am. Chem. Soc*. **2012**, *134*, 9199−9208.
(30) Royzen, M.; Yap, G. P. A.; Fox, J. M. A photochemical synthesis of functionalized trans-cyclooctenes driven by metal complexation. *J. Am. Chem. Soc.* **2008**, *130*, 3760–3761.
(31) Dolomanov, O.V.; Bourhis, L.J.; Gildea, R.J.; Howard, J.A.K.; Puschmann, H. OLEX2: A complete structure solution, refinement and analysis program. *J. Appl. Cryst.* **2009**, *42*, 339–341.
(32) Eyring, H. The activated complex in chemical reactions. *J. Chem. Phys*. **1935**, *3*, 107–115.
(33) Evans M. G.; Polanyi M. Some applications of the transition state method to the calculation of reaction velocities, especially in solution. *Trans. Faraday Soc*. **1935**, *31*, 875–894.
(34) Wynne-Jones W. F. K.; Eyring, H. The Absolute Rate of Reactions in Condensed Phases. *J. Chem. Phys*. **1935**, *3*, 492–502.
(35) Laidler, K. J.; King, M. C. The development of transition-state theory. *J. Phys. Chem*. **1983**, *87*, 2657–2664.

Chapter 6

Synthesis of novel click-declick probes for cell surface chemokine release

J.A.M. Damen, Dr. B. Albada, Prof. Dr. F.L. van Delft

Abstract

A novel SDF-1α construct was developed to allow for two-stage targeted release in the tumor microenvironment based on orthogonal bio-orthogonal chemistries involving (a) covalent attachment of the SDF-1α construct to methylcyclopropene-enriched tumor glycocalyx via tetrazine-based click chemistry followed by (b) release of SDF-1 α via iminosydnone-DBCO-based declick chemistry. Detachment of the SDF-1α chemokine is anticipated to result in a chemogradient from the proliferating cells into the tumor environment, thereby inducing T-cell recruitment. Moreover, the declicking event of the iminosydnone-dansyl absorption quencher pair of the linker with a fluorescent DBCO probe is expected to lead to dual labelling of both glycocalyx and SDF-1α. This Chapter covers the linker design and synthesis thereof.

Manuscript in preparation

1. Introduction

In continuation of our metabolic cell surface labelling in **Chapters 2 and 3**, we envisioned attaching biologically active compounds onto the cellular surface. As pointed out in the previous chapters, the main ambition of investigation in this research is to understand and potentially modulate the mechanism of T cell evasion by hypertrophic tumor cells. These tumors are often undetected by the immune system as a consequence of the ticker cellular glycocalyx, which as a physical barrier suppresses the requisite cell-cell interactions for induction of tumor immunity. In **Chapters 2 and 3** we demonstrated specific labeling and targeting of hypertrophic tumor cells by metabolic incorporation of glycan-based click tags, which are incorporated as non-natural sialic acid residues in the more densely labeled glycocalyx. Besides application in imaging and visualization of tumor cells by fluorescent labeling, the click chemistry also opens up the possibility of attachment of biologically active compounds to the tagged glycocalyx exterior of the cell with the potential to evoke immune responses towards these tumors. Ideally such a bioactive molecule would be an interleukin or cytokine that elicits an immunological response from an array of leukocytes, such as cytotoxic T cells. Albeit conceptually appealing from the perspective of chemical biology, the immunological function of chemokines (subclass of cytokines) has proven otherwise: normally chemokines are released from cells during an immunological event, creating a chemogradient from the site of action towards local blood or lymph vessels to attract leukocytes. In order to recreate this “breadcrumb trail” scenario, we devised a strategy to trigger release of an initially covalently attached chemokine from the tumor cell surface, which would not only provide a powerful tools to image and study T cell immunotherapy, but eventually could constitute a novel approach for targeted cancer therapy.

The general strategy is depicted in **Figure 1** and consists of three steps: **A)** metabolic labelling of the (extracellular) glycocalyx with a monosaccharide that contains a bio-orthogonal functional handle. **B)** covalently surface attachment of an SDF-1α construct that bears both a terminal click handle and an internal declick handle. **C)** triggered release of SDF-1α from the chemokine-enriched cell surface (with concomitant fluorescent labelling of both surface and protein). The resulting chemogradient of SDF-1α should result in chemotaxis of T cells to the tumor cell.

2. Design

2.1 Choice of the chemokine

SDF-1α (or CXCL12) was chosen as the target chemokine, due to its known chemoattractant properties and effectiveness in recruiting and activating T cells.[1-4] It is a rather small protein that consists of 67 amino acids in the primary sequence. The secondary structure consists of an antiparallel three-stranded β-sheet and a C-terminal α-helix that fold together in a tertiary structure joined together by two disulfide bonds. The exposed N-terminus is conformationally flexible and is crucial for biological function. For example: truncation of the N-terminal lysine residue yields an unfunctional chemokine.[2,3] As the N-terminus was not suitable as conjugation site of the protein to the declickable linker, and C-terminal site-specific attachment is not readily achieved without genetic modification of the protein, we decided to chemically synthesize the protein and to introduce alkyne-functionalized lysine moiety at a defined position at the C-terminal end of the protein. In collaboration with

Leiden University, the 68 amino acid protein (peptide) was assembled by means of microwave-assisted SPPS. The linear peptide was then properly refolded to ensure the right secondary and tertiary structures and the correct disulfide bridges were obtained, as confirmed by circular dichroism (CD).[2]

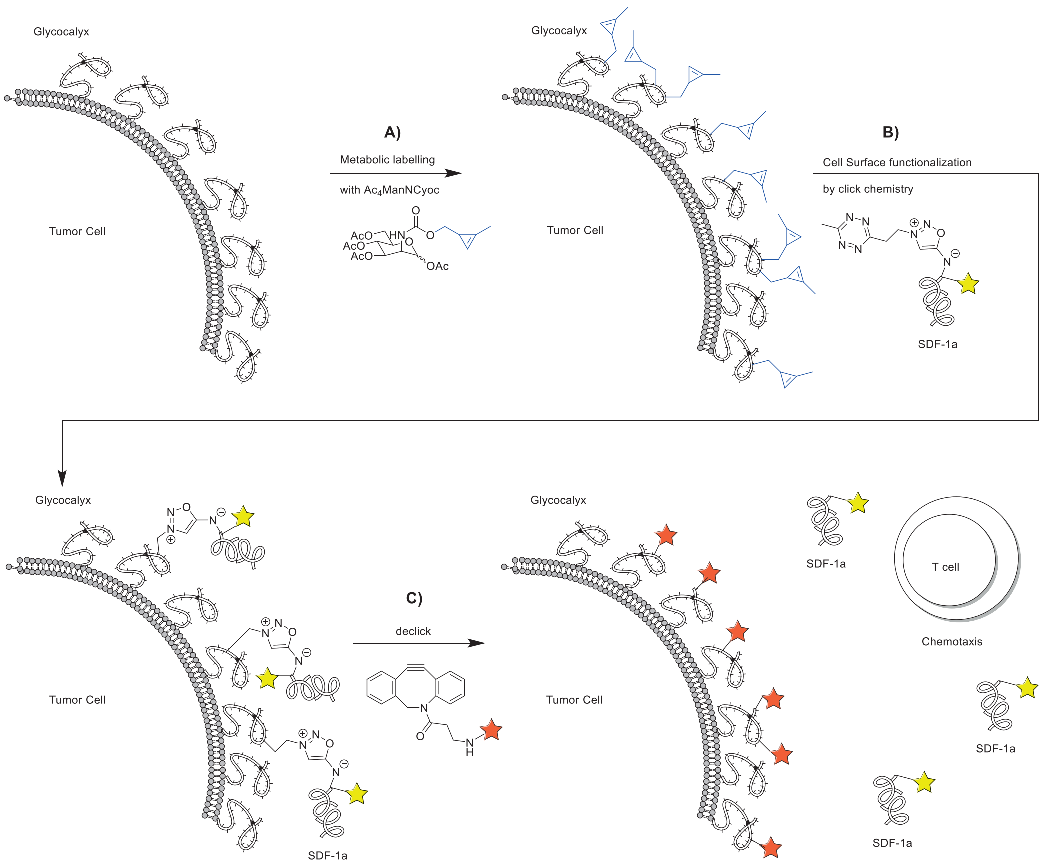
Glycocalyx
Tumor Cell
A)
Metabolic labelling
with Ac4ManNCyoc
AcO
AcO
AcO
HN
O
O
O
OAc
Glycocalyx
Tumor Cell
B)
Cell Surface functionalization
by click chemistry
SDF-1a
Glycocalyx
Tumor Cell
SDF-1a
C)
declick
N
O
N
H
Glycocalyx
Tumor Cell
SDF-1a
T cell
Chemotaxis
SDF-1a
SDF-1a

Figure 1: General metabolic labelling and declick strategy: **A)** Metabolic labelling with Ac$_4$ManNCyoc to introduce the cyclopropene tag onto the tumor glycocalyx. **B)** Covalent attachment of SDF-1α construct **1** to the cell surface by tetrazine-cyclopropene IEDDA. **C)** Iminosydnone declick with fluorescent DBCO-probes to release SDF-1α and concomitantly fluorescently label the cell surface and recruit T cells.

2.2 Choice of declick system

The proper design of a compatible declickable linker system that can be appended to the SDF-1α protein and is also suitable for metabolic labelling is crucial, not only to ensure that the declick chemistry is biocompatible with a complex cellular environment, but also to ensure that the combination of click handles in the probes are compatible with each other (preventing autoreactive structures), also known as orthogonal bio-orthogonal chemistry. Currently, three declick systems are available, each of which was considered for application in our study, see **Scheme 1**:

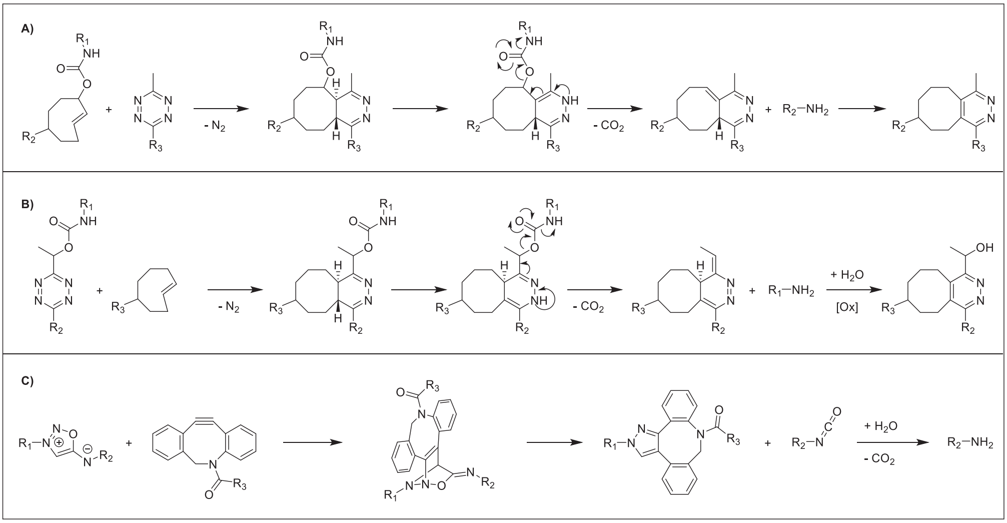

Scheme 1: The currently available three declick systems: **A)** and **B)** Robillard's IEDDA reactions of carbamate derivatives of TCO and tetrazines, eliminating the payload after a rearrangement reaction. **C)** Taran's iminosydnones showing reactivity with DBCO, releasing the payload after a (3+2) cycloaddition followed by a retro-Diels–Alder reaction.

2.2.1 TCO–tetrazine declick systems A and B

Two systems that are known to successfully declick are Robillard's IEDDA reactions of either TCO-3-carbamates with tetrazines **(A)** or reaction of tetrazine-carbamates with TCOs **(B)**, see **Scheme 1A,B**.[5-8] In both cases, the appending carbamate group collapses in an elimination step of the formed intermediate, releasing the amine payload. The pyridazine product is then formed by a subsequent rearrangement reaction in **(A)** or by a hydration and oxidation sequence in **(B)**. Both strategies are elegant and first of their kind, but the use of TCO is not preferred in our complex biological system due to the known sensitivity of TCO structures towards thiols in serum resulting in isomerization.[9,10]

2.2.2 Iminosydnone–cycloalkyne declick system C

It was anticipated that the most suitable declick system for our application would be based on Taran's iminosydnones, see **Scheme 1C**. It comprises of iminosydnones, which are mesoionic dipolar heterocycles that have a delocalized positive and negative charge, however through delocalization of charges these compounds behave like net neutral, rather than as zwitterionics.**[11-13]** Iminosydnones functionalized on two sides can be declicked by a (3+2) cycloaddition with a strained cycloalkyne (*e.g.* BCN, DBCO or THS), followed by a retro-Diels–Alder reaction to release the payload. After thorough investigation of the functionalization pattern of iminosydnones,**[14-20]** the most reactive structure was determined to be the ImSyd core structure, see **Scheme 2** highlighted in **(c)**, whilst still remaining a stable compound.**[14,15]** Halogenation with Br or Cl of the ImSyd itself can further increase reactivity, but at the cost of stability.**[14,21]** So it was decided not to use the halogenated form of the ImSyd core structure.

2.3 Design of metabolic labelling with a click-declick linker

As the ImSyd system declicks with strained alkynes, two other orthogonal click methodologies are required to covalently attach the two biological functionalities to the opposite ends of the linker. The applicability of SPAAC or SPOCQ click chemistries is therefore not possible (see **Chapters 3 – 5**), regarding their typical use of cycloalkynes for these click chemistries. For example: attempts to label an azide-enriched cellular surface with a DBCO-ImSyd-SDF1α construct would fail, as the DBCO-ImSyd-SDF1α construct would autoreact either intramolecularly, or in a bimolecular fashion.

The inability to use SPAAC chemistry for metabolic labelling therefore necessitated a different approach in installing a click handle and covalently attaching the payload to the cell's surface. Fortunately, Prescher *et al.* have shown that methylcyclopropene-functionalized monosaccharides are tolerated and incorporated by the sialic acid biosynthetic pathway.**[22,23]** Thus we are able to install methylcyclopropenes onto the cell surface glycocalyx, which then can be used for click reactions with tetrazines. It was already shown by their previous investigations that carbamate-linked Ac_4ManNCyoc, depicted in **Figure 1A**, is the preferred clicking partner as it has 100-fold increased reactivity as compared to its amide analogue Ac_4ManNCp. This is due to electronic factors as amide bonded cyclopropenes react in the IEDDA reactions with electron-poor tetrazines with a k_2 value of only 0.137 $M^{-1}s^{-1}$, whereas carbamate linked cyclopropenes can react at speeds of k_2 = 13 $M^{-1}s^{-1}$.**[22,24-26]** It also means that Ac_4ManNCyoc (processed to SiaNCyoc when incorporated in the glycocalyx) exhibits a reactivity in tetrazine IEDDA that surpasses the reactivity of THS-SPAAC. Earlier, we found that the labeling rates need to be sufficiently high for successful chemical modification of the cellular glycocalyx, see **Chapter 3**. So the tetrazine–methylcyclopropene click couple posed the perfect combination for cellular labelling in the sense of (i) metabolic tolerability of the cyclopropene moiety, (ii) orthogonality of cyclopropene towards (imino)sydnones,**[27]** (iii) the high reaction rate of the IEDDA click reaction, and (iv) the (photo)stability of each respective click partner. Therefore, our declickable probe was designed to feature on one side a *para*-(methyltetrazine)-benzylamine warhead, with enhanced reactivity over common tetrazine**[26]**, and on the other end with an azide that can be coupled to a terminal alkyne by means of CuAAC, see **Scheme 2**.

The probe was further functionalized with the small non-charged fluorophore dansyl to facilitate tracking of the declicked derivative in a cellular environment by fluorescence microscopy (*vide infra*). A lysine amino acid building block was therefore used on the right sidearm to allow for the triple functionality in this part of the molecule. Short PEG-linkers were then included into the design where possible to compensate for the apolar aromatic systems in providing enhanced solubility in water. Covalent attachment of the SDF-1α-alkyne protein by CuAAC click chemistry results in the structure of the declickable SDF-1α construct **1** depicted in **Scheme 2**, which corresponds with the cartoon structure used in **Figure 1**.

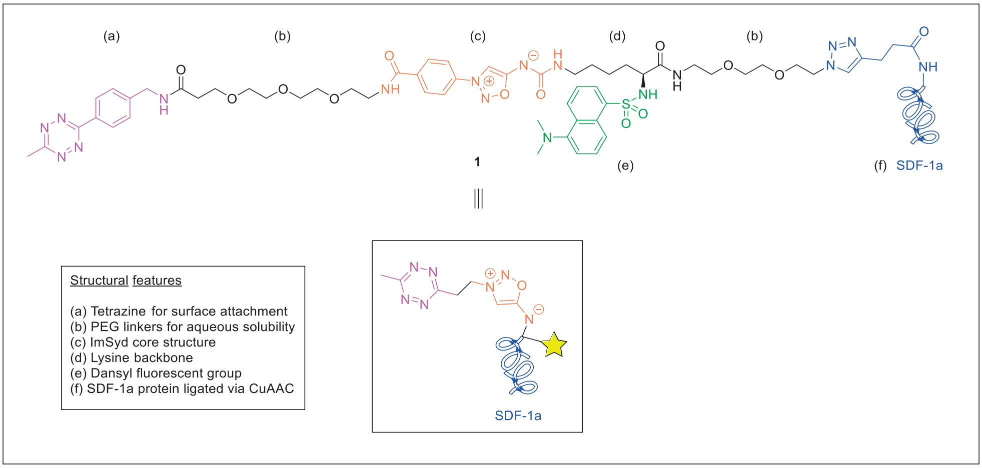
(a)
(b)
(c)
(d)
(b)
(e)
(f) SDF-1a
1
|||
Structural features
(a) Tetrazine for surface attachment
(b) PEG linkers for aqueous solubility
(c) ImSyd core structure
(d) Lysine backbone
(e) Dansyl fluorescent group
(f) SDF-1a protein ligated via CuAAC
SDF-1a

Scheme 2: Design of the declickable tetrazine-ImSyd-SDF1α construct **1**. The ImSyd core structure **(c)** is designed to bear a tetrazine functionality **(a)** for the final clicking onto a cell surface and on the other side the SDF1α-alkyne protein **(f)** which is attached via a triazole linkage bij means of CuAAC. The structure is also decorated with a dansyl group **(e)** for fluorescence spectroscopy via a lysine-based linker **(d)**. PEG linkers **(b)** were also included for increasing water solubility, resulting in structure **1**. Compound **1** is also represented by the cartoon depiction shown in **Figure 1**.

2.4 Declick concept

The declickable SDF-1α construct **1** can be covalently attached to methylcyclopropene-enriched tumor cell surface glycocalyx by means of an inverse electron-demand Diels–Alder (IEDDA) reaction to a proper tetrazine functionality installed on the declickable linker, see **Scheme 3**. With full temporal control, a cycloalkyne can next be administered to undergo a (3+2) cycloaddition with the iminosydnone core, after which the intermediate bicyclic structure collapses by means of a retro-Diels–Alder reaction. As a result, a pyrazole product and a urea-isocyanate are released, the latter of which in aqueous solution will hydrate and decompose to the urea product and carbon dioxide. The iminosydnone declick can be performed with either DBCO or BCN.**[14]** We found that THS is also reactive with ImSyds in qualitative experiments. The declick reaction is typically associated with the following second-order rate constants: $k_2 = 0.232 \pm 0.005\ M^{-1}s^{-1}$ and $k_2 = 2.799 \pm 0.390\ M^{-1}s^{-1}$ for BCN and DBCO, respectively, with this type of core ImSyd.**[14]** The declick thus exceeds the reaction rate requirement of click labelling at the cell surface ($0.8\ M^{-1}s^{-1}$, see **Chapter 3**) when DBCO is used, circumventing issues regarding the timescale of cellular biolabeling experiments. As such, it is feasible to use commercially available DBCO-fluorophore probes, which are nowadays available in a large range of the visible electromagnetic spectrum. When using DBCO-fluorophores, the fluorophore itself ends up on the glycocalyx after the declick reaction. This enables concomitant visualization of glycocalyx thickness, evaluating the cellular distribution of cyclopropene-functionalized sialic acid derivatives, and providing a measure of evaluating declick efficacy.

Another feature of interest for fluorescence microscopy of the declick probe is the built-in dansyl fluorescent group, to allow for the tracking of the detached part after declicking. In our case it means that the released SDF-1α is fluorescently labelled and its diffusion or intercellular localization can be tracked on a second channel in fluorescence microscopy. The choice of the dansyl group was not only based on the fact that it is a non-charged, relatively small fluorophore with easy synthetic handling, but also due to the fact that it typically absorbs violet light when excited (λ_{ex} = 350 nm; λ_{em} = 520 nm).**[28]** The iminosydnone core structures at hand also have a distinct absorption band in the 330–365 nm range of the UV-Vis spectrum (dependent on substitution pattern).**[12]** When incorporating both ImSyd and dansyl in a probe, absorption of ultraviolet light will be more dominant by the ImSyd due to the higher molar extinction coefficients,**[12]** with minimal photoexcitation and therefore no fluorescence arising from dansyl until the iminosydnone is cleaved in the declick step. Besides, the dansyl group was placed in close proximity to the ImSyd to form the absorption quencher pair, to ensure high quenching efficacy, as any type of fluorescence quenching is heavily proximity dependent (as like in FRET pairs).**[28,29]** This strategy thus allows cellular labelling with a non-fluorescent SDF-1α protein construct, which upon declick with a fluorescent DBCO-probe simultaneously generates a fluorescent glycocalyx and a fluorescently labelled protein. Both can be monitored simultaneously on two different channels in fluorescence microscopy. The absorption quencher pair theory was indeed shown when synthesizing the linker: any molecule bearing a dansyl group (compounds **7–8** and intermediates) fluoresced heavily when exited with 366 nm light. When the ImSyd was introduced in compound **9**, the target compound lost its fluorescent properties through the subsequent synthetic steps.

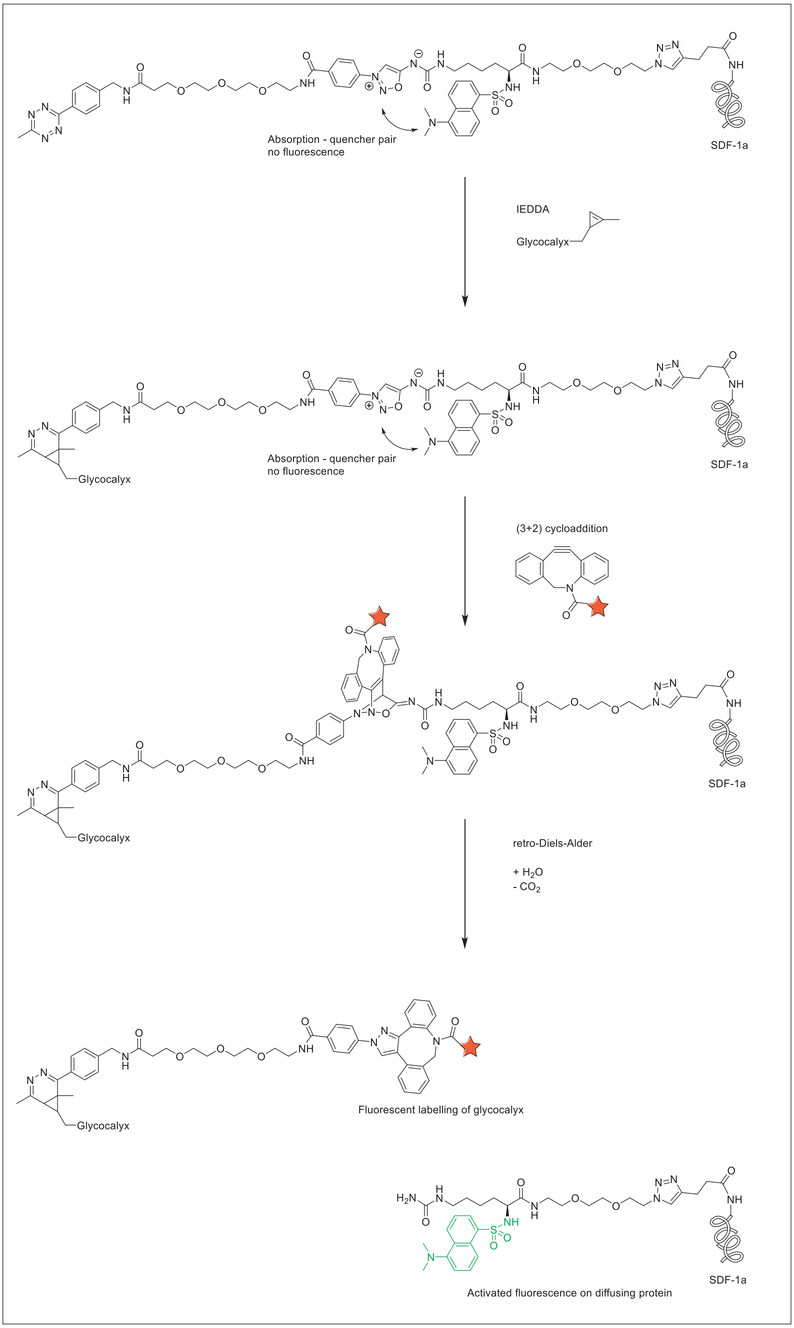
Absorption - quencher pair
no fluorescence
SDF-1a
IEDDA
Glycocalyx
Absorption - quencher pair
no fluorescence
Glycocalyx
SDF-1a
(3+2) cycloaddition
SDF-1a
Glycocalyx
retro-Diels-Alder
+ H2O
- CO2
Glycocalyx
Fluorescent labelling of glycocalyx
SDF-1a
Activated fluorescence on diffusing protein

Scheme 3: Concept of the declick reaction. SDF1α construct **1** is clicked onto the cyclopropene enriched cellular glycocalyx via tetrazine IEDDA. The ImSyd-dansyl fluorescence absorption-quencher pair accounts at this point for no fluorescent signal. The ImSyd is then cleaved via a (3+2) cycloaddition and retro-Diels–Alder reaction with a fluorescent DBCO probe. The DBCO probe fluorescently labels the glycocalyx and the dansyl fluorescence is activated on the diffusing SDF1α protein.

3. Results

3.1 Synthesis

The declickable linker construct with an azide on one end and a tetrazine on the other was prepared according to the synthesis route depicted in **Scheme 4**. First, the iminosydnone core had to be prepared. For this, ethyl 4-aminobenzoate **2** was alkylated with chloroacetonitrile in refluxing toluene using catalytic potassium iodide and an excess of triethylamine.[30] This yielded *N*-methylene cyanide compound **3** as sole product, which was separated from the starting material by flash chromatography, resulting in a yield of 78%. No di- or trialkylation was observed and this was attributed to the loss of nucleophilicity of the aniline's nitrogen atom due to the adjacent electron withdrawing nitrile group after monoalkylation. With compound **3** in hand, *N*-nitroso species **4** was cleanly formed by treatment with isoamyl nitrite in THF overnight.[31] The intermediate **4** was directly cyclized to the iminosydnone under acidic conditions, by bubbling HCl gas through the reaction mixture for 10 minutes. The reaction was instantaneous according to TLC and the iminosydnone·HCl salt crashed out of solution. Pure iminosydnone·HCl **5** was obtained after recrystallisation from hot absolute ethanol as white needle crystals in 20% yield over two steps. This is a very satisfactory result as this particular iminosydnone compound is notoriously hard to cyclize or isolate even at all, as reported by other groups.[15,30]

In order to couple iminosydnone **5** to the side chain of the lysine building block, the backbone amine of N_ε-Boc-L-lysine methyl ester hydrochloride **6** was first functionalized with a dansyl group by reacting it with dansyl-chloride and triethylamine in DCM . This yielded fluorescent compound **7** after purification in 92% yield. Saponification of the methyl ester with KOH in THF/H_2O and subsequent amide coupling reaction of azido-PEG$_2$-amine with HATU and DIPEA in DCM yielded fluorescent compound **8** in 82% yield over two steps. Compound **8** was then dissolved in DCM and was treated with 4M HCl in dioxane to remove the Boc protecting group. The amine side arm was transformed *in situ* into an isocyanate using Taran's optimized biphasic conditions with triphosgene and $NaHCO_3$ in DCM/H_2O at 0 °C. To this reaction mixture was added the iminosydnone·HCl salt **5**, which turns into a freebase, and then under mild conditions reacts with the strong electrophile isocyanate forming the urea bond. Upon coupling of the ImSyd and dansyl fragments, the product lost its fluorescent properties due to intramolecular fluorescence quenching, as predicted. Compound **9** was acquired in 46% yield over two steps. Saponification of the ImSyd ester **9** with KOH in THF/H_2O and subsequent neutralization with acidic resin yielded the completely water-soluble target carboxylic acid intermediate. This compound was then amide-coupled to commercially available methyltetrazine-PEG$_3$-amine with HATU and DIPEA in DCM. This yielded compound **10** after purification in 31% yield over two steps. Attachment of the linker system to the SDF-1α-alkyne protein **11** by CuAAC click chemistry to afford final compound **1** still has to be performed once the SDF-1α-alkyne **11** is made available by our collaborators.

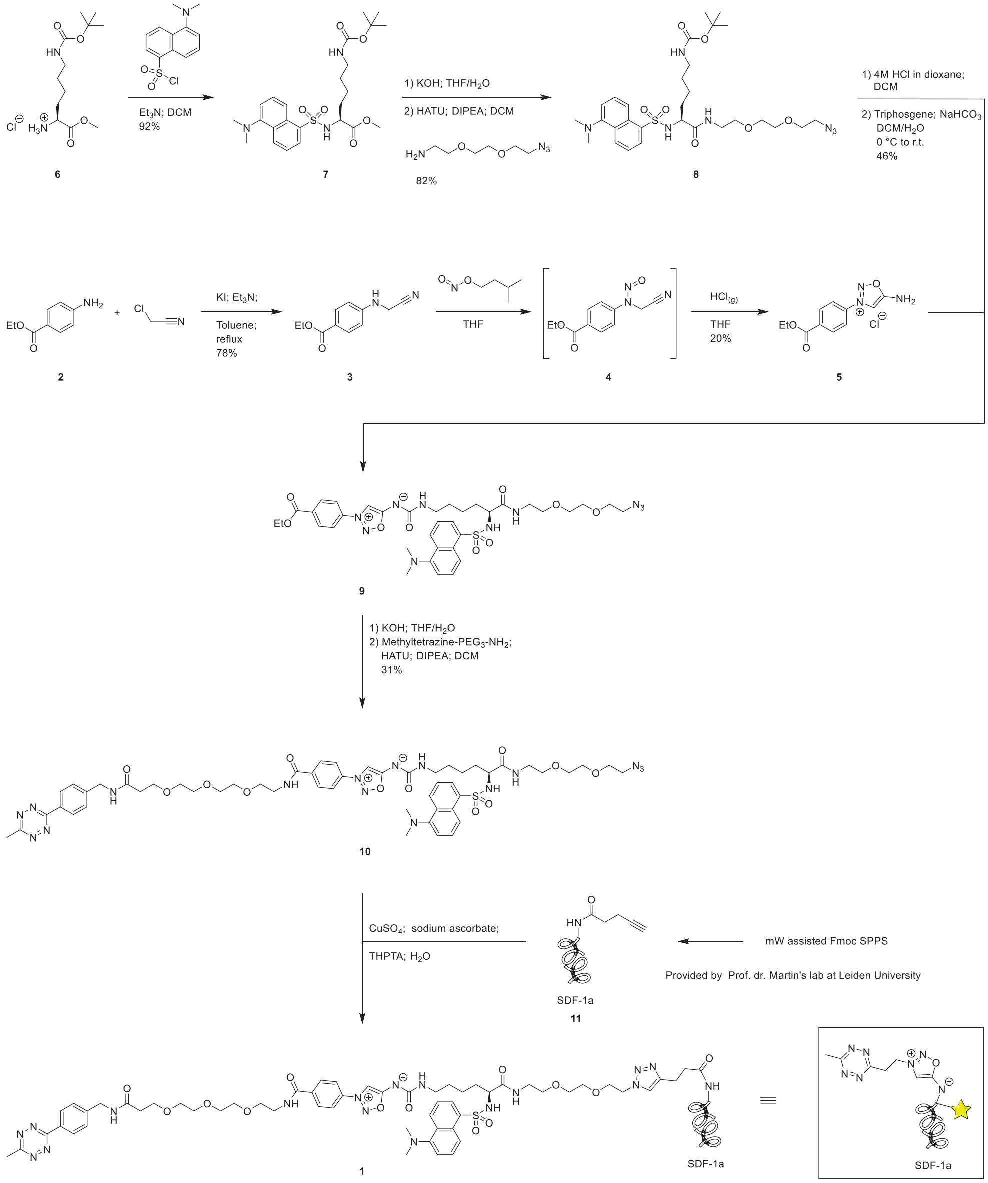
Et$_3$N; DCM
92%
6
7
1) KOH; THF/H$_2$O
2) HATU; DIPEA; DCM
82%
8
1) 4M HCl in dioxane; DCM
2) Triphosgene; NaHCO$_3$ DCM/H$_2$O 0 °C to r.t.
46%
KI; Et$_3$N;
Toluene; reflux
78%
2
3
THF
4
HCl$_{(g)}$
THF
20%
5
9
1) KOH; THF/H$_2$O
2) Methyltetrazine-PEG$_3$-NH$_2$; HATU; DIPEA; DCM
31%
10
CuSO$_4$; sodium ascorbate;
THPTA; H$_2$O
mW assisted Fmoc SPPS
Provided by Prof. dr. Martin's lab at Leiden University
SDF-1a
11
1
SDF-1a
SDF-1a

Scheme 4: General synthesis route to the declickable tetrazine-ImSyd-SDF1α construct **1**.

4. Conclusion and Discussion

In conclusion, we have described the design of a new metabolic cell labelling strategy to enable the immunological recruitment of T cells towards otherwise undetected hypertrophic tumor cells. The basis of this strategy lays in a click–declick approach in which a synthetically produced SDF-1α is released from the tumor cell surface to create a chemogradient intended to attract T cells. The fundamental underlying design of the clickable and declickable linker, along with its metabolic labelling, and mechanistic design of the release of a payload is discussed. The built-in absorption quencher pair allows for dual fluorescent labelling of both glycocalyx and of SDF-1α upon release. The synthesis of the linker system is discussed extensively. Future plans include the covalent attachment of SDF-1α-alkyne to the linker, after which cellular experiments can be conducted to test whether the proposed hypothesis works. The SDF-1α-alkyne synthesis is currently being upscaled by our collaborator at Leiden University. However, it still needs to be checked whether it is bioactive in cellular assays by our collaborators at RadboudUMC Nijmegen. This still needs to be evaluated before continuation of the project in order to make sure that the protein is functional.

4.2 Acknowledgements

The SDF-1α protein bearing a terminal alkyne was prepared by means of microwave-assisted solid phase peptide synthesis (SPPS) by our collaborators at the research group of Prof. dr. N.I. Martin at Leiden University. The details of the protein synthesis and purification are beyond the scope of this dissertation, but are included in the upcoming publication. Prof. dr. Martin and colleagues are gratefully acknowledged and thanked for their efforts in developing the synthesis of this protein.

5. Experimental

5.1. General information

5.1.1 Instruments

^{1}H-NMR (400 MHz) and ^{13}C-NMR spectra (101 MHz) were recorded on a Bruker 400 MHz AV400 NMR spectrometer and chemical shifts were reported in ppm referenced against the residual solvent peaks of the NMR solvent. Synthesized compounds were analyzed by reverse phase ultra-high performance liquid chromatography (RP-UHPLC) coupled to mass spectrometry (HESI-MS, measuring in switching positive/negative mode, calibrated with a Thermo Finnigan calibration mixture) using a Q Exactive Focus Agilent 1290 Infinity UHPLC-MS system. The UHPLC system is equipped with a diode array detector (DAD G4212A, at 215 nm and 254 nm for detection) and a Dr. Maisch ReproSil Gold 120 C18, 3 µm, 200 x 3 mm column containing a 10 mm guard with a flow rate of 0.4 mL/min. The eluent contained for buffer A: 10 mM triethylammonium acetate in Milli-Q; and for buffer B: acetonitrile. A gradient of 5→5→75→75→5→5%, percentage buffer B (0→5→25→28→29→35 min) was applied. ESI-HRMS spectra were recorded simultaneously on a Q Exactive Focus Mass Spectrometer (Thermo Scientific) and mass values were calculated with enviPat Web.[32] Lyophilization of samples was performed on a Labconco FreeZone lyophilizer (2.5 L; -84 °C) connected to a XDS35i Edwards Oil-Free Dry Scroll Pump. Deionized water was produced with a Milli-Q Integral 3 system (Millipore, Molsheim/France).

5.1.2 General chemicals:

N_{ε}-Boc-L-lysine methyl ester hydrochloride; 4.0 M HCl in dioxane; potassium hydroxide; hydrochloric acid (37%); chloroform-*d* (99.8 atom % D, contains 0.03 % (v/v) TMS); and Ion exchanger Dowex® 50W-X8 (H^+ form) were purchased from Sigma-Aldrich Merck. Triphosgene and dansyl chloride were purchased from TCI Europe. Ethyl 4-aminobenzoate; chloroacetonitrile; isopentyl nitrite (97%, stab. with 0.2% anhyd. sodium carbonate) and sodium sulfate were all purchased from Thermo Scientific™ / Fisher Scientific. *N*,*N*-diisopropylethylamine (Peptide Synthesis grade) was also purchased from Thermo Scientific™ / Fisher Scientific, but was distilled prior to use. Sodium bicarbonate; potassium iodide and triethylamine were purchased from Acros Organics. Triethylammonium acetate buffer (BioUltra, Volatile Buffer 1.0 M in H_2O, Fluka®, Honeywell Research Chemicals) and dimethyl sulfoxide-d_6 (99.8 atom % D) were purchased from VWR. HATU was purchased from Fluorochem (Hadfield, United Kingdom). Azido-PEG$_2$-amine (catalog number: BP-20692) and methyltetrazine-PEG$_3$-amine·TFA (catalog number: BP-26276) were purchased from BroadPharm® (San Diego, CA, United States). DMF (HPLC); toluene (HPLC) and THF (unstabilised; HPLC) were purchased from Biosolve. Diethyl ether (puriss. p.a.); dichloromethane (CHROMASOLV™, for HPLC); *n*-hexane(CHROMASOLV™, for HPLC); ethanol absolute (CHROMASOLV™ for HPLC) and acetonitrile (CHROMASOLV™, for HPLC) were purchased from Honeywell Riedel-de Haën™. Methanol (ChromAR® for HPLC) and ethyl acetate (ChromAR® for HPLC) were purchased from Macron Fine Chemicals. All of these chemicals were used as purchased unless otherwise stated. MilliQ deionized water was produced with a Milli-Q Integral 3 system (Millipore, Molsheim/France).

Ac$_4$ManNCyoc can be accessed according to the previously published synthetic methodologies by Prescher *et. al.*[22]

5.1.3 Chromatography:

Flash chromatography was performed on SiliaFlash® P60 40-63 µm (230-400 mesh) 60 Å Irregular Silica Gel (R12030B) (SiliCycle, Quebec City (Quebec), Canada). Thin Layer Chromatography was performed on TLC Silica gel 60 F_{254} on aluminium sheets (Merck, Darmstadt, Germany). After development, TLC plates were dip stained and heated with a heat gun for visualization of spots. $KMnO_4$ stain was used as a general stain and was prepared by dissolving 1.5 g $KMnO_4$, 10 g K_2CO_3 and 1.25 mL 10% NaOH in 200 mL water.

5.2. Chemical syntheses

Ethyl 4-((cyanomethyl)amino)benzoate **3** was synthesized according a literature procedure by Xu *et al.*[30] The synthesis of ImSydH$^+$Cl$^-$ **5** was based on adapting the general protocol of Beal and Turnbull.[31]

5.2.1** Synthesis of Ethyl 4-((cyanomethyl)amino)benzoate **3

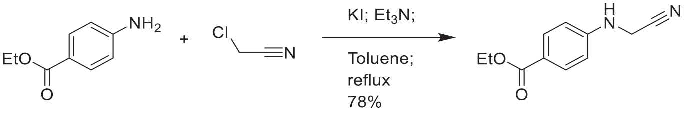

2 **3**

A 100 mL round-bottom flask was charged with ethyl 4-aminobenzoate **2** (4 g; 24.2 mmol; 1 eq), KI (450 mg; 2.7 mmol; 0.1 eq) and boiling stones. The solids were suspended in 50 mL toluene and Et_3N (13 mL; 93.8 mmol; 3.9 eq) and chloroacetonitrile (3.2 mL; 50.6 mmol; 2.1 eq) were added successfully. The mixture was refluxed for 20 hours. TLC analysis indicated formation of product **3** (R_f = 0.19 in 30% EtOAc/PE) as compared to starting material **2** (R_f = 0.41 in 30% EtOAc/PE). Solvent was removed *in vacuo*. The crude product was taken up in 100 mL EtOAc and was washed sequentially with 100 mL deionized water and with 100 mL brine. The organic phase was then separated from the aqueous phase, dried over Na_2SO_4, filtered, and the solvent was removed *in vacuo*. Target product **3** was purified by flash chromatography (dry packed on silica with DCM; eluent: 20% → 100% EtOAc/hexane). This afforded 3.87 g of ethyl 4-((cyanomethyl)amino)benzoate **3** as dark red oil that crystallized on standing. Yield 78%. The compound structure was confirmed by ^{1}H-NMR. All analytical data agrees with values presented in the literature.[30]

^{1}H NMR (400 MHz, $CDCl_3$) δ 7.96 (d, *J* = 8.8 Hz, 2H), 6.69 (d, *J* = 8.8 Hz, 2H), 4.34 (q, *J* = 7.1 Hz, 2H), 4.16 (s, 2H), 1.37 (t, *J* = 7.1 Hz, 3H).

5.2.2 *Synthesis of ImSydH$^+$Cl$^-$* ***5***

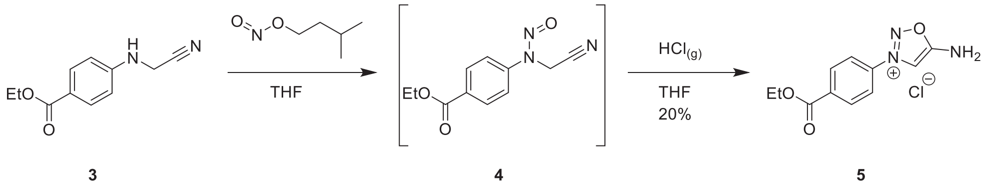

A 30 mL scintillation vial was charged with ethyl 4-((cyanomethyl)amino)benzoate **3** (1087 mg; 5.3 mmol; 1 eq) and was dissolved in 8 mL THF under magnetic stirring to form a homogeneous solution. Isopentyl nitrite (2 mL; 14.9 mmol; 2.8 eq) was added to the reaction mixture and was stirred for 24 hours. Formation of intermediate **4** was complete according to TLC (R_f = 0.54 in 30% EtOAc/PE). The reaction mixture was then bubbled through with HCl gas for 10 minutes **(note 1)** and left to stir for 1.5 hours during which it turned into a turbid orange suspension. The stirring bar was removed and the solids were left to settle. TLC analysis indicated complete consumption of intermediate **4** and formation of product **5** (R_f = baseline in 30% EtOAc/PE). The scintillation vial was centrifuged at 6000 rpm for 10 minutes, after which the supernatant was decanted off the powder bed. The solids were washed three times with 5 mL Et_2O and centrifuged. After drying, the solid material (300 mg) was recrystallized from 2 mL hot absolute EtOH to give white needle crystals. The crystals were collected and dried in an oven at 70 °C. This afforded 287 mg of ImSydH$^+$Cl$^-$ **5** as beige crystalline powder. Yield 20% over two steps. The compound structure was confirmed by ^{1}H-NMR. All analytical data agrees with values presented in the literature.**[30]**

^{1}H NMR (400 MHz, DMSO-d_6) δ 10.11 (s, 2H), 8.78 (s, 1H), 8.27 (d, J = 8.5 Hz, 2H), 8.22 (d, J = 8.6 Hz, 2H), 4.38 (q, J = 7.1 Hz, 2H), 1.36 (t, J = 7.1 Hz, 3H).

Notes:

1) The HCl was generated with a HCl-gas generator as described in Vogel's Textbook of Practical Organic Chemistry (5th ed.), page 438, Section 38. Method 1*.**[33]**

5.2.3 *Synthesis of Dansyl-L-Lys(Boc)-OMe* **7**

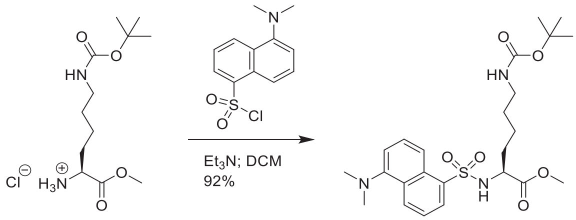

6 **7**

A 4 mL scintillation vial was charged with N_ε-Boc-L-lysine methyl ester hydrochloride **6** (103.1 mg; 0.347 mmol; 1 eq), 2 mL DCM and Et_3N (150 µL; 1.08 mmol; 3.1 eq) to form a homogeneous solution under magnetic stirring. Dansyl chloride (96 mg; 0.356 mmol; 1 eq) was added to the reaction mixture and was stirred for 21.5 hours. Formation of product **7** could be monitored with TLC analysis (R_f = 0.56 in 50% EtOAc/PE). The reaction mixture was diluted with 10 mL DCM and was washed sequentially with 10 mL 1M HCl and with 10 mL saturated $NaHCO_3$ solution. Combined organic phases were dried over Na_2SO_4, filtered, and the solvent was removed *in vacuo* to afford 158 mg of very pure dansyl-L-Lys(Boc)-OMe **7** as a yellow solid foam that fluoresces under 366 nm light. Yield 92%.

^{1}H NMR (400 MHz, $CDCl_3$) δ 8.54 (d, *J* = 8.5 Hz, 1H), 8.31 (d, *J* = 8.6 Hz, 1H), 8.23 (dd, *J* = 7.3, 1.3 Hz, 1H), 7.59 (dd, *J* = 8.7, 7.6 Hz, 1H), 7.51 (dd, *J* = 8.5, 7.3 Hz, 1H), 7.20 (dd, *J* = 7.6, 0.9 Hz, 1H), 5.39 (d, *J* = 8.9 Hz, 1H), 4.37 (s, 1H), 3.87 (ddd, *J* = 8.9, 7.0, 5.8 Hz, 1H), 3.28 (s, 3H), 2.88 (s, 8H), 1.62 – 1.53 (m, 2H), 1.44 (s, 9H), 1.32 – 1.10 (m, 4H).
^{13}C NMR (101 MHz, $CDCl_3$) δ 171.7, 155.9, 151.9, 134.5, 130.8, 129.8, 129.8, 129.7, 128.4, 123.2, 118.9, 115.3, 55.7, 52.2, 45.4, 40.0, 32.6, 29.2, 28.4, 22.0.

UHPLC: t_R = 23.2 min. HRMS (ESI) calc. for $C_{24}H_{34}N_3O_6S$ $[M-H]^-$ 492.2174; found 492.2176 .

5.2.4 *Synthesis of Dansyl-L-Lys(Boc)-NH-PEG$_2$-N$_3$* ***8***

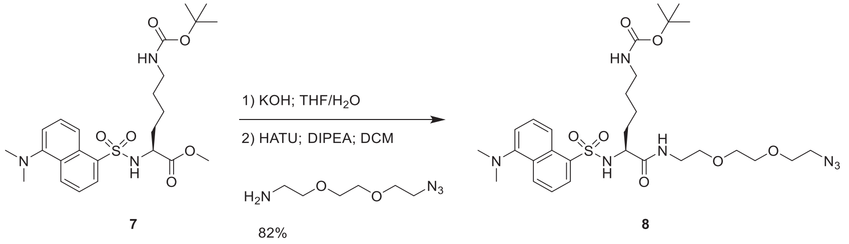

A 25 mL round-bottom flask was charged with dansyl-L-Lys(Boc)-OMe **7** (151.1 mg; 0.306 mmol; 1 eq) and was dissolved in 3 mL THF and under magnetic stirring 3 mL deionized water was added. To this mixture, 1M KOH (0.8 mL; 0.8 mmol; 2.6 eq) was added and was left to stir for 22 hours. TLC analysis indicated completion of reaction (carboxylic acid intermediate: R_f = baseline in 50% EtOAc/PE) **(note 2)**. THF was removed *in vacuo* and the aqueous layer was diluted with 15 mL deionized water. The aqueous phase was acidified by addition of 2 mL 1M HCl to pH 2 (pH paper) and was then extracted twice with 10 mL DCM. The combined organic phases were dried over Na_2SO_4; filtered; and the solvent was removed *in vacuo* to afford the carboxylic acid intermediate as a yellow foam in a 25 mL round-bottom flask. This compound was then dissolved in 3 mL DCM under magnetic stirring and HATU (182.1 mg; 0.479 mmol; 1.6 eq) and DIPEA (167 µL; 0.959 mmol; 3.1 eq) were added. The reaction mixture was left to preactivate for 3 minutes, after which a solution of azido-PEG$_2$-amine (109.6 mg; 0.629 mmol; 2.1 eq) in 2 mL DCM was added. The mixture was left to react for 2 hours, following the formation of compound **8** by TLC (R_f = 0.45 in EtOAc). The reaction mixture was then diluted with 10 mL DCM and was washed sequentially with 15 mL 1M HCl and with 15 mL saturated $NaHCO_3$ solution. The organic phase was dried over Na_2SO_4, filtered, and the solvent was removed *in vacuo.* Target product **8** was purified by flash chromatography (dry packed on silica with DCM; eluent: 50% → 100% EtOAc/*n*-hexane). This afforded 159.4 mg of dansyl-L-Lys(Boc)-NH-PEG$_2$-N$_3$ **8** as yellow oil that fluoresces under 366 nm light. Yield 82% over two steps.

^{1}H NMR (400 MHz, $CDCl_3$) δ 8.55 (d, *J* = 8.5 Hz, 1H), 8.33 (d, *J* = 8.6 Hz, 1H), 8.23 (dd, *J* = 7.4, 1.3 Hz, 1H), 7.60 (dd, *J* = 8.7, 7.6 Hz, 1H), 7.52 (dd, *J* = 8.5, 7.3 Hz, 1H), 7.20 (d, *J* = 7.5 Hz, 1H), 6.67 (s, 1H), 5.85 (d, *J* = 7.2 Hz, 1H), 4.41 (s, 1H), 3.76 – 3.68 (m, 2H), 3.68 – 3.62 (m, 2H), 3.62 – 3.55 (m, 3H), 3.46 – 3.37 (m, 4H), 3.34 – 3.20 (m, 2H), 2.89 (s, 6H), 2.82 – 2.68 (m, 2H), 1.91 (s, 1H), 1.57 – 1.46 (m, 1H), 1.45 (s, 9H), 1.23 – 1.11 (m, 1H), 1.08 – 0.95 (m, 2H), 0.94 – 0.77 (m, 1H).
^{13}C NMR (101 MHz, $CDCl_3$) δ 171.0, 156.1, 152.0, 134.2, 130.8, 130.1, 129.8, 129.6, 128.6, 123.2, 118.8, 115.4, 79.3, 70.4, 70.3, 70.0, 69.5, 56.9, 50.7, 45.4, 39.6, 39.2, 32.0, 29.2, 28.4, 21.7.

UHPLC: t_R = 22.3 min. HRMS (ESI) calc. for $C_{29}H_{44}N_7O_7S$ $[M-H]^-$ 634.3028; found 634.3034

Notes:

2) Dansyl bearing compounds fluoresce when exposed to 366 nm light. This simplifies identification on TLC plates and chromatographic purification.

5.2.5 *Synthesis of Dansyl-L-Lys(ImSyd-OEt)-NH-PEG$_2$-N$_3$* ***9***

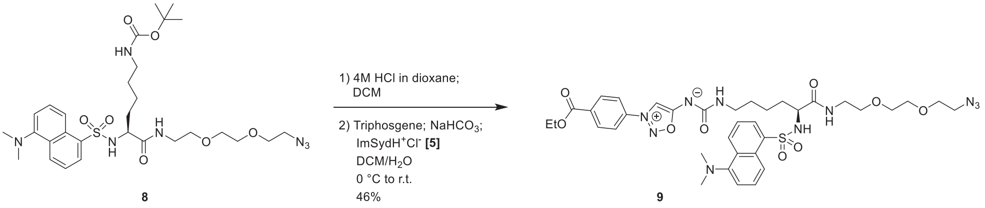

A 25 mL round-bottom flask was charged with dansyl-L-Lys(Boc)-NH-PEG$_2$-N$_3$ **8** (134.9 mg; 0.212 mmol; 1 eq) and was dissolved in 4 mL DCM. 4 mL 4M HCl in dioxane was added under magnetic stirring and immediately a precipitate was formed. TLC indicated completion of reaction. The precipitate was solubilized with 6 mL MeOH, after which all solvent was removed *in vacuo*. The residue was co-evaporated twice with DCM to afford 123.5 mg of the amino intermediate as HCl salt as a white foam that fluoresces under 366 nm light. Yield quant.

A solution of NaHCO$_3$ (91.9 mg; 1.09 mmol; 5.2 eq) in 4 mL deionized water was added to the round-bottom flask containing the intermediate under magnetic stirring to form a green solution, which was cooled to 0 °C. An at 0 °C precooled solution of triphosgene (20.0 mg; 0.067 mmol; 0.32 eq) in 4 mL DCM was added to the vigorously stirred reaction mixture at 0 °C and was left to stir for 1 hour to form the isocyanate. ImSydH$^+$Cl$^-$ **5** (63.9 mg; 0.237 mmol; 1.1 eq) was added to the reaction mixture and was left to vigorously stir for 3.5 hours warming up to room temperature (ice/water bath was removed after 15 minutes). The formation of target product was monitored by TLC (R_f = 0.11 in EtOAc; non-fluorescent yellow spot). The reaction mixture was diluted with 15 mL DCM and was washed with 15 mL brine. The aqueous phase was re-extracted with 5 mL DCM. The combined organic phases were dried over Na$_2$SO$_4$, filtered, and the solvent was removed *in vacuo.* Target product **9** was purified by flash chromatography (dry packed on silica with DCM; eluent: 0% → 5% MeOH/EtOAc). This afforded 77.9 mg of dansyl-L-Lys(ImSyd-OEt)-NH-PEG$_2$-N$_3$ **9** as a non-fluorescent orange/red foam. Yield 46% over two steps.

^{1}H NMR (400 MHz, CDCl$_3$) δ 8.91 (s, 1H), 8.53 (d, *J* = 8.3 Hz, 1H), 8.43 (d, *J* = 8.6 Hz, 1H), 8.24 (d, *J* = 8.7 Hz, 2H), 8.12 (d, *J* = 8.8 Hz, 2H), 7.91 (d, *J* = 3.7 Hz, 1H), 7.58 – 7.52 (m, 1H), 7.51 (dd, *J* = 7.5, 6.3 Hz, 1H), 7.15 (d, *J* = 7.5 Hz, 1H), 5.70 (s, 1H), 4.40 (q, *J* = 7.2 Hz, 2H), 3.74 – 3.59 (m, 6H), 3.59 – 3.46 (m, 2H), 3.46 – 3.34 (m, 3H), 3.31 (dt, *J* = 7.6, 3.3 Hz, 1H), 3.19 (q, *J* = 6.1 Hz, 2H), 2.87 (s, 6H), 2.80 (s, 1H), 1.81 – 1.52 (m, 6H), 1.40 (t, *J* = 7.1 Hz, 3H), 1.33 – 0.87 (m, 2H).
^{13}C NMR (101 MHz, CDCl$_3$) δ 173.1, 171.7, 164.6, 163.0, 152.0, 136.9, 134.4, 132.9, 131.6, 131.3, 130.8, 129.8, 129.7, 128.4, 123.2, 121.6, 118.7, 115.2, 103.2, 70.6, 70.4, 70.0, 69.8, 61.9, 57.3, 50.6, 45.4, 39.2, 37.3, 30.1, 30.1, 19.7, 14.2.

UHPLC: t_R = 21.9 min. HRMS (ESI) calc. for $C_{36}H_{45}N_{10}O_9S$ [M-H]$^-$ 793.3097; found 793.3108 .

5.2.6 *Synthesis of Dansyl-L-Lys(ImSyd-NH-PEG$_3$-methyltetrazine)-NH-PEG$_2$-N$_3$* **10**

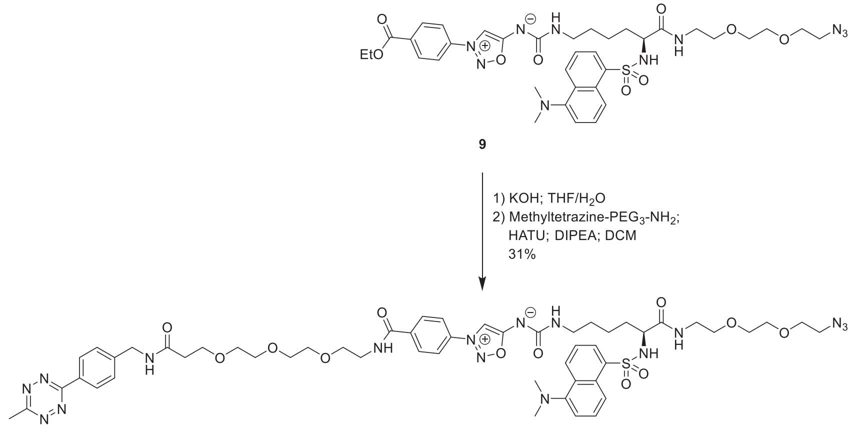

A 30 mL scintillation vial was charged with dansyl-L-Lys(ImSyd-OEt)-NH-PEG$_2$-N$_3$ **9** (199.2 mg; 0.251 mmol; 1 eq) and was dissolved in 4 mL THF and 3 mL deionized water under magnetic stirring to form a homogeneous solution. 1M KOH (1 mL; 1 mmol; 4 eq) was added to the reaction mixture and was left to stir for 1.5 hours. TLC indicated completion of reaction (carboxylic acid intermediate: R_f = baseline in 5% MeOH/DCM. R_f = 0.49 in 5% MeOH/DCM + 1% AcOH. Compound **9** R_f = 0.55 in 5% MeOH/DCM). 680 mg Dowex® 50W-X8 (H$^+$ form) was added to the reaction mixture to neutral pH and was stirred for 10 minutes, after which it was filtered. The filtrate was collected and solvent was removed *in vacuo*, including co-evaporating with toluene (6 mL twice); MeOH (10 mL); and DCM (10 mL). This afforded 133 mg of the carboxylic acid intermediate as a red solid.

The solid was then dissolved in 6 mL DCM under magnetic stirring and HATU (146 mg; 0.384 mmol; 1.5 eq) and DIPEA (134 µL; 0.769 mmol; 3.1 eq) were added. The reaction mixture was left to preactivate for 5 minutes, after which a solution of methyltetrazine-PEG$_3$-amine·TFA (203.8 mg; 0.393 mmol; 1.6 eq) and DIPEA (200 µL; 1.15 mmol; 4.6 eq) in 3 mL DCM was added. The mixture was left to react for 2 hours, following the formation of compound **10** by TLC (R_f = 0.31 in 5% MeOH/DCM; R_f = baseline in 2.5% MeOH/DCM; orange spot that stains immediately yellow with KMnO$_4$ stain). The reaction mixture was then diluted with 15 mL DCM and was washed sequentially with 20 mL 1M HCl and with 30 mL saturated NaHCO$_3$ solution. The organic phase was dried over Na$_2$SO$_4$, filtered, and the solvent was removed *in vacuo.* Target product **10** was purified by Flash Chromatography (dry packed on silica with DCM; eluent: 2% → 6% MeOH/DCM). This afforded 88.9 mg of dansyl-L-Lys(ImSyd-NH-PEG$_3$-methyltetrazine)-NH-PEG$_2$-N$_3$ **10** as a red solid glass. Yield 31% over two steps.

^{1}H NMR (400 MHz, CDCl$_3$) δ 8.85 (s, 1H), 8.52 (d, *J* = 8.4 Hz, 1H), 8.46 (d, *J* = 8.2 Hz, 2H), 8.42 (d, *J* = 8.7 Hz, 1H), 8.23 (dd, *J* = 7.4, 1.3 Hz, 1H), 8.05 (d, *J* = 8.6 Hz, 2H), 8.02 – 7.97 (m, 3H), 7.51 (ddd, *J* = 16.3, 8.7, 7.5 Hz, 2H), 7.42 (d, *J* = 8.2 Hz, 2H), 7.13 (d, *J* = 7.2 Hz, 2H), 6.93 (t, *J* = 6.0 Hz, 1H), 5.78 (t, *J* = 6.8 Hz, 1H), 4.48 (d, *J* = 6.0 Hz, 2H), 3.71 (t, *J* = 5.8 Hz, 2H), 3.67 – 3.45 (m, 21H), 3.44 – 3.33 (m, 4H), 3.32 – 3.26 (m, 1H), 3.19 (q, *J* = 6.0 Hz, 2H), 3.08 (s, 3H), 2.86

(s, 6H), 2.48 (t, *J* = 5.7 Hz, 2H), 1.81 – 1.72 (m, 1H), 1.64 – 1.54 (m, 1H), 1.36 – 1.13 (m, 7H), 1.01 – 0.79 (m, 3H).

^{13}C NMR (101 MHz, $CDCl_3$) δ 173.3, 171.8, 171.8, 167.4, 165.4, 163.9, 163.4, 152.1, 143.7, 138.5, 135.9, 133.0, 131.4, 131.0, 130.8, 129.9, 129.8, 129.4, 128.5, 128.2, 123.3, 121.7, 118.8, 115.4, 103.0, 70.6, 70.6, 70.4, 70.4, 70.3, 70.1, 69.9, 69.7, 67.3, 57.4, 50.8, 45.5, 43.1, 40.2, 39.3, 37.3, 37.0, 30.3, 30.2, 29.8, 21.3, 19.8.

HRMS (ESI) calc. for for $C_{53}H_{67}N_{16}O_{12}S$ $[M-H]^-$ 1151.4851; found 1151.4866

The supporting information and appendices are made available via the QR-code below.

6. References

(1) Clark-Lewis, I.; Moser, B.; Walz, A.; Baggiolini, M.; Scott, G. J.; Aebersold, R. Chemical Synthesis, Purification, and Characterization of Two Inflammatory Proteins, Neutrophil Activating Peptide 1 (Interleukin-8) and Neutrophil Activating Peptide 2. *Biochemistry* **1991**, *30*, 3128–3135.
(2) Veldkamp, C. T.; Koplinski, C. A.; Jensen, D. R.; Peterson, F. C.; Smits, K. M.; Smith, B. L.; Johnson, S. K.; Lettieri, C.; Buchholz, W. G.; Solheim, J. C.; Volkman, B. F. Production of Recombinant Chemokines and Validation of Refolding. *Methods Enzymol.* **2016**, *570*, 539–565.
(3) Crump, M. P.; Gong, J.-H.; Loetscher, P.; Rajarathnam, K.; Amara, A.; Arenzana-Seisdedos, F.; Virelizier, J.-L.; Baggiolini, M.; Sykes, B. D.; Clark-Lewis, I. *EMBO J.* **1997,** *16*, 6996–7007.
(4) Dealwis, C.; Fernandez, E. J.; Thompson, D. A.; Simon, R. J.; Siani, M. A.; Lolis, E. Crystal structure of chemically synthesized [N33A] stromal cell-derived factor 1*α*, a potent ligand for the HIV-1 "fusin" coreceptor. *Proc. Natl. Acad. Sci. USA* **1998**, *95*, 6941–6946.
(5) Versteegen, R. M.; Rossin, R.; ten Hoeve, W.; Janssen, H. M.; Robillard, M. S. Click to release: Instantaneous doxorubicin elimination upon tetrazine ligation. *Angew. Chem. Int. Ed.* **2013**, *52*, 14112–14116.
(6) Versteegen, R. M.; ten Hoeve, W.; Rossin, R.; de Geus, M. A. R.; Janssen, H. M.; Robillard, M. S. Click-to-Release from trans-Cyclooctenes: Mechanistic Insights and Expansion of Scope from Established Carbamate to Remarkable Ether Cleavage. *Angew. Chem. Int. Ed.* **2018**, *57*, 10494–10499.

(7) Liu, B.; ten Hoeve, W.; Versteegen, R. M.; Rossin, R.; Kleijn, L. H. J.; Robillard, M. S. A Concise Synthetic Approach to Highly Reactive Click-to-Release *Trans*-Cyclooctene Linkers**. *Chem. Eur. J.* **2023**, *29*, e202300755.
(8) Van Onzen, A. H. A. M.; Versteegen, R. M.; Hoeben, F. J. M.; Filot, I. A. W.; Rossin, R.; Zhu, T.; Wu, J.; Hudson, P. J.; Janssen, H. M.; ten Hoeve, W.; Robillard, M. S. Bioorthogonal Tetrazine Carbamate Cleavage by Highly Reactive *trans*-Cyclooctene. *J. Am. Chem. Soc.* **2020**, *142*, 10955–10963.
(9) Taylor, M. T.; Blackman, M. L.; Dmitrenko, O.; Fox, J. M. Design and synthesis of highly reactive dienophiles for the tetrazine-*trans*-cyclooctene ligation. *J. Am. Chem. Soc.* **2011**, *133*, 9646–9649.
(10) Rossin, R.; van den Bosch, S. M.; ten Hoeve, W.; Carvelli, M.; Versteegen, R. M.; Lub, J.; Robillard, M. S. Highly Reactive *trans*-Cyclooctene Tags with Improved Stability for Diels–Alder Chemistry in Living Systems. *Bioconjugate Chem.* **2013**, *24*, 1210–1217.
(11) Daeniker H. U.; Druey J. Heilmittelchemische Studien In Der Heterocyclischen Reihe 35. Mitteilung. Über Sydnonimine. I. Herstellung und Eigenschaften von Sydnonimin-Salzen. *Helv. Chim. Acta* **1962**, *45*, 2426–2441.
(12) Daeniker H. U.; Druey J. Heilmittelchemische Studien In Der Heterocyclischen Reihe 36. Mitteilung. Über Sydnonimine. II. Herstellung und Eigenschaften von Sydnoniminen mit Acyl-, Carbamoyl- und Thiocarbamoyl-Substituenten am exocyclischen Stickstoffatom. *Helv. Chim. Acta* **1962**, *45*, 2441–2462.
(13) Daeniker H. U.; Druey J. Heilmittelchemische Studien In Der Heterocyclischen Reihe 37. Mitteilung. Ü Syndnonimine. III. N-Sulfanilyl-sydnonimine. *Helv. Chim. Acta* **1962**, *45*, 2462–2465.
(14) Riomet, M.; Decuypere, E.; Porte, K.; Bernard, S.; Plougastel, L.; Kolodych, S.; Audisio, D.; Taran, F. Design and Synthesis of Iminosydnones for Fast Click and Release Reactions with Cycloalkynes. *Chem. Eur. J.* **2018**, *24*, 8535–8541.
(15) Bernard, S.; Audisio, D.; Riomet, M.; Bregant, S.; Sallustrau, A.; Plougastel, L.; Decuypere, E.; Gabillet, S.; Kumar, R. A.; Elyian, J.; Trinh, M. N.; Koniev, O.; Wagner, A.; Kolodych, S.; Taran, F. Bioorthogonal Click and Release Reaction of Iminosydnones with Cycloalkynes. *Angew. Chem. Int. Ed.* **2017**, *56*, 15612–15616.
(16) Ribéraud, M.; Porte, K.; Chevalier, A.; Madegard, L.; Rachet, A.; Delaunay-Moisan, A.; Vinchon, F.; Thuéry, P.; Chiappetta, G.; Champagne, P. A.; Pieters, G.; Audisio, D.; Taran, F. Fast and Bioorthogonal Release of Isocyanates in Living Cells from Iminosydnones and Cycloalkynes. *J. Am. Chem. Soc.* **2023**, *145*, 2219–2229.
(17) Porte, K.; Riomet, M.; Figliola, C.; Audisio, D.; Taran, F. Click and Bio-Orthogonal Reactions with Mesoionic Compounds. *Chem. Rev.* **2021**, *121*, 6718–6743.
(18) Riomet, M.; Porte, K.; Madegard, L.; Thuéry, P.; Audisio, D.; Taran, F. Access to N-Carbonyl Derivatives of Iminosydnones by Carbonylimidazolium Activation. *Org. Lett.* **2020**, *22*, 2403–2408.
(19) Decuypère, E.; Plougastel, L.; Audisio, D.; Taran, F. Sydnone-alkyne cycloaddition: Applications in synthesis and bioconjugation. *Chem. Commun.* **2017**, *53*, 11515–11527.
(20) Dovgan, I.; Hentz, A.; Koniev, O.; Ehkirch, A.; Hessmann, S.; Ursuegui, S.; Delacroix, S.; Riomet, M.; Taran, F.; Cianférani, S.; Kolodych, S.; Wagner, A. Automated linkage of proteins and payloads producing monodisperse conjugates. *Chem. Sci.* **2020**, *11*, 1210–1215.
(21) Feng, M.; Madegard, L.; Riomet, M.; Louis, M.; Champagne, P. A.; Pieters, G.; Audisio, D.; Taran, F. Selective chlorination of iminosydnones for fast release of amide, sulfonamide and urea-containing drugs. *Chem. Commun.* **2022**, *58*, 8500–8503.

(22) Patterson, D. M.; Jones, K. A.; Prescher, J. A. Improved cyclopropene reporters for probing protein glycosylation. *Mol. BioSyst.* **2014**, *10*, 1693–1697.
(23) Parle, D. R.; Bulat, F.; Fouad, S.; Zecchini, H.; Brindle, K. M.; Neves, A. A.; Leeper, F. J. Metabolic Glycan Labeling of Cancer Cells Using Variably Acetylated Monosaccharides. *Bioconjugate Chem.* **2022**, *33*, 1467–1473.
(24) Yang, J.; Šečkute, J.; Cole, C. M.; Devaraj, N. K. Live-cell imaging of cyclopropene tags with fluorogenic tetrazine cycloadditions. *Angew. Chem. Int. Ed.* **2012**, *51*, 7476–7479.
(25) Patterson, D. M.; Nazarova, L. A.; Xie, B.; Kamber, D. N.; Prescher, J. A. *J. Am. Chem. Soc.* **2012**, *134*, 18638–18643.
(26) Oliveira B. L.; Guo Z.; Bernardes G. J. L. Inverse electron demand Diels-Alder reactions in chemical biology. *Chem. Soc. Rev.* **2017**, *46*, 4895–4950.
(27) Bristiel, A.; Cadinot, M.; Pizzonero, M.; Taran, F.; Urban, D.; Guignard, R.; Guianvarc'h, D. 2′-Modified Thymidines with Bioorthogonal Cyclopropene or Sydnone as Building Blocks for Copper-Free Postsynthetic Functionalization of Chemically Synthesized Oligonucleotides. *Bioconjugate Chem.* **2023**, *34*, 1613–1621.
(28) Lakowicz J. R. Principles of Fluorescence Spectroscopy. 2nd ed. New York, NY, United States: Kluwer Academic / Plenum Publishers; **1999**. *Specifically: Chapter 3.2.A. Protein-Labeling Reagents, pages 67–69.*
(29) Riomet, M.; Porte, K.; Wijkhuisen, A.; Audisio, D.; Taran, F. Fluorogenic iminosydnones: Bioorthogonal tools for double turn-on click-and-release reactions. *Chem. Commun.* **2020**, *56*, 7183–7186.
(30) Xu, W.; Shao, Z.; Tang, C.; Zhang, C.; Chen, Y.; Liang, Y. Fluorogenic sydnonimine probes for orthogonal labeling. *Org. Biomol. Chem.* **2022**, *20*, 5953–5957.
(31) Beal, E. N.; Turnbull, K. An Efficient, One-Pot Synthesis of 3-Alkyl or Aryl Sydnoneimines. *Synth. Commun.* **1992**, *22*, 673–676.
(32) Loos, M., Gerber, C., Corona, F., Hollender, J., Singer, H. Accelerated isotope fine structure calculation using pruned transition trees, *Anal. Chem.* **2015**, *87*, 5738–5744.
(33) Furniss, B. S.; Hannaford, A. J.; Smith, P. W. G.; Tatchell, A. R. Vogel's textbook of practical organic chemistry. 5th ed. Harlow, Essex, England: Longman Scientific & Technical. Copublished in New York, NY, United States: John Wiley & Sons, Inc.; **1989**. *Specifically: Chapter 4.2.38 Hydrogen Chloride, Method 1*, page 438.*

Chapter 7

General Discussion

J.A.M. Damen

1. Introduction

The work described in this dissertation presents an overview of the reactivity and rates of click chemistries in bioconjugations (**Chapter 1**), followed by research into: the development of new strained cycloalkyne click reagents (**Chapters 2 and 3**), a deepened understanding into the reactivity and kinetics of the inverse electron-demand Diels–Alder cycloaddition between *ortho*-quinones and strained alkenes or alkynes (SPOCQ, **Chapters 4 and 5**) and finally the development of declick approaches for tumor cell label-to-release of cytokines (**Chapter 6**). This final **Chapter 7** covers the outlook and further potentials of the methodologies that were investigated in this dissertation.

2. Considering cyclooctyne design

Chapter 2 addressed the necessity for faster cyclooctyne reagents to enable rapid SPAAC-mediated labeling of the tumor glycocalyx using azide-enriched tumor cell surfaces. A higher efficacy and faster rate was required to label the glycocalyx sufficiently to accurately determine its thickness and distribution, role in cell-cell interactions and, moreover, in tumor cell evasion. Investigating the role of the glycocalyx when it comes to the ability of tumor cells to suppress recognition by lymphocytes, by functioning as “wearing a thick fur coat”, was initially the main topic of this research. Unfortunately, endocytosis of azide-enriched glycocalyx occurs on the same timescale as with which SPAAC would occur with DBCO-fluorophores, resulting in diminished labelling of the cell surface. This thus requires a cycloalkyne reagent that would react faster in SPAAC than any of the currently available reagents. Besides, the cycloalkyne should remain compatible with biological conditions, sufficiently water-soluble to enable labelling in the aqueous glycocalyx domain and relatively non-lipophilic to avoid accumulation in lipophilic domains, *e.g.* lipid bilayers or hydrophobic protein-protein interfaces.

Therefore, we initiated the development of a novel click reagent by taking a cyclooctyne skeleton based on COMBO. Incorporating heteroatoms tethered to the propargylic positions would result in substantial rate enhancement in SPAAC (see structures **1** and **2** in **Scheme 1**), as was predicted by computational studies.[1] Many synthetic attempts to make these cyclooctynes failed, which lead to the conclusion that we were unable to access the envisioned structures **1** and **2**. Structurally related cyclooctynes were also reported as unobtainable by other groups during the course of our research.[2] By structural comparison, this lead us to conclude that our approach suffered from similar flaws in structural design and not from poor choices made in synthetic methodology. The instability of our designed structure was attributed to a decomposition pathway of the cycloalkyne via a 1,4-*tele*-elimination,[3] which also explains why both our designed compounds and reported structurally related compounds are highly unstable, whereas the all-carbon compound COMBO is stable.[4]

A way to mitigate the postulated 1,4-*tele*-elimination decomposition pathway would be to shift the position of the heteroatoms within the ring (see structures **3** and **4** in **Scheme 1**). Such structures would unfortunately not be applicable as a click reagents due to expected instability. Oxygen or nitrogen bearing acetylenes such as 1-alkynyl ethers or yneamines are uncommon due to their (extreme) reactivity. Linear bis(dialkylamino)acetylenes $R_2NC{\equiv}CNR_2$ (ynediamines) and yneamines $HC{\equiv}CNR_2$ are described as extremely water-sensitive.[5-7]. As such, strained variants of these compounds (if synthetically accessible) would bear no applicability in bioorthogonal click chemistry. Employing a different cyclooctyne scaffold, such as a BCN-type skeleton (see structures **5** and **6** in **Scheme 1**), would likely also be associated with instability issues as described above for a COMBO-type design, and therefore does not seem a feasible alternative. It was therefore decided to reevaluate the thiacycloheptyne class of reagents in **Chapter 3**.

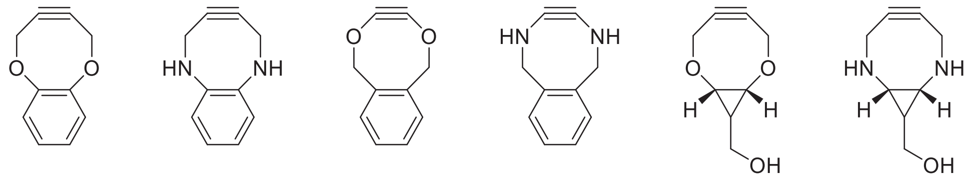

1 **2** **3** **4** **5** **6**

Scheme 1: Scope of synthetically unfeasible cyclooctyne candidates as concluded from the findings in this dissertation.

3. The potential of thiacycloheptynes and -heptenes in click chemistry

Thiacycloheptynes were reevaluated as a reagent class, and THS (originally reported as TMTH-SI,[8] but here referred to as THS for convenience) proved to be a highly versatile new click reagent for application in both SPAAC (**Chapter 3**) and SPOCQ (**Chapters 3 and 4**). We described the improved and reproducible synthesis of THS itself, as well as of THS-derived fluorescent probes, which was problematic in previous works.[8,9] Our crystallographic determinations of the structures of THS, BCN and DBCO (see also **Chapter 5**) showed that THS is the current recordholder in alkyne bending whilst remaining a stable reagent. XRD also finally gave structural insights into the solid state structures of the two most employed cycloalkyne click reagents BCN and DBCO. The solid state structures are representative for the conformation of the species in solution, as supported by NMR, and are not subject to fluxional behavior at room temperature (*e.g.*, ring flipping). Comparison of alkyne bending of cycloheptyne THS (151.0° and 151.4°) with cyclooctynes DBCO (152.3° and 154.2°) and BCN (154.2° and 154.5°) reveals that the higher extent of alkyne bond bending of the reagent linearly correlates to the higher reactivity trend observed in SPAAC. Also, comparison of the alkyne bending of THS (151.0° and 151.4°) to that of the unstable thioether compound TMTH (145.8°),[10] allows the conclusion that the C-C≡C alkyne bending-stability maximum at room temperature lies in between these angular values, which is a useful consideration when designing new cycloalkynes using geometry optimizations with DFT as input for screening potential candidate structures.

Inspired by THS, one may envisage a ***t****rans*-**t**hiacyclo**h**eptene (**TTH**) based probe for which a 4-step synthesis route is proposed in **Scheme 2**. The synthetic route consists of dialkylation of sodium sulfide with 3-chloro-2,2-dimethylpropanal, which is then cyclized via a McMurry reaction and is followed by a sulfoximidation reaction to yield the *cis*-precursor for **TTH**. Finally, photoisomerization should lead to the formation of **TTH**.[11-13] The reactivity of a **TTH** reagent would be interesting to evaluate as it is expected to be very reactive in various (de)clicking methodologies, except for azides and (imino)sydnones, analogous to TCO. This might be the basis for similar orthogonality as witnessed for TCO (compared to, *e.g.*, BCN), whilst retaining the high reactivity of a THS-based scaffold, along with its other structural benefits as size and aqueous solubility. As such, one can think of THS-linker-TTH constructs as the next generation of BCN-linker-TCO constructs.

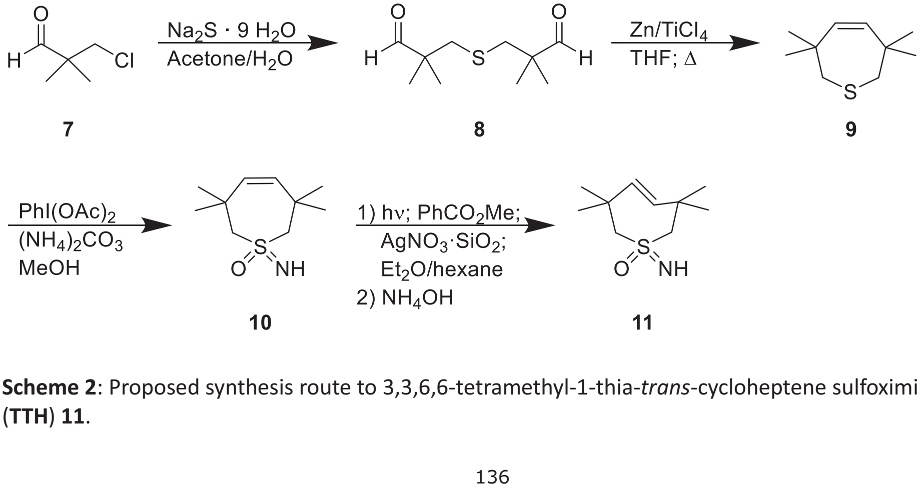

Scheme 2: Proposed synthesis route to 3,3,6,6-tetramethyl-1-thia-*trans*-cycloheptene sulfoximine (**TTH**) **11**.

4. Future prospects of SPOCQ kinetics studies

This dissertation is comprised of a number of kinetics studies into SPOCQ (see **Chapters 4 and 5**), which provided new fundamental insights into a click methodology which has only been investigated to limited extent in the past. Our findings mainly reveal that the cycloaddition of both strained cycloalkynes and cycloalkenes with *ortho*-quinone is dominated by entropic factors and that only minimal enthalpies are involved. Therefore, the extent of conformational preorganization of a strained reagent towards a SPOCQ transition state will impact the rate of the reaction likely much more than, for example, putting more strain on such a reagent. Also, diastereomeric effects on distal parts of a strained reagent (*e.g.*, *endo/exo*) do not affect the general reactivity so much, at least less than was presented to be the case for SPAAC.[14,15] In fact, we determined that this was not only the case for SPOCQ, but were also unable to confirm the claimed differences between *endo*-BCN and *exo*-BCN in SPAAC using an aromatic fluorogenic azide. Finally, the involvement of secondary orbital interactions (SOIs) in SPOCQ as a significant rate-determining factor between cycloalkynes and cycloalkenes[16,17] was excluded. These are important considerations in the rational design of future reagents specific for SPOCQ.

However, some other points have to be addressed for future improvements for these kinetics studies to further our understanding of SPOCQ. As *ortho*-quinones are very reactive species that readily undergo polymerization reactions or nucleophilic additions, kinetic investigations into these *ortho*-quinones as reactive intermediates are not straightforward. The 4-*tert*-butyl-*ortho*-quinone that we employed is one of the few stable isolable *ortho*-quinones known. The use of the bulky *tert*-butyl group on our model *ortho*-quinone obviously perturbs the assay as it differs from *ortho*-quinones used in conjugation chemistry. With the minimal enthalpies of activation experimentally found for both cycloalkyne and cycloalkene cycloaddition with 4-*tert*-butyl-*ortho*-quinone, and the main heights of the transition state barriers being defined by the entropies of activation, we expect that the main perturbation of the *tert*-butyl group is reflected in the latter ($\Delta S^{\ddagger}$) on the basis of both theoretical understanding (the enhanced required organization of a reagent around the bulky *tert*-butyl group) and on experimental values ($\Delta H^{\ddagger} << |T\Delta S^{\ddagger}|$). The perturbation of the *tert*-butyl group in the assay will therefore have increased the magnitude of the $\Delta S^{\ddagger}$ values. Theoretically, the reaction of a less bulky decorated *ortho*-quinone will result in smaller $\Delta S^{\ddagger}$ values, resulting in higher reaction kinetics (*i.e.*, higher k_2-values). The assumption in this case is that the enthalpies of activation remain equally low in both scenarios.

The smallest substituted *ortho*-quinone model compound would be 4-methyl-*ortho*-quinone, resembling a truncated version of a quinone formed from a tyrosine, which are used as click handles in bioconjugation approaches (see **Chapters 1 and 3**).[18-23] Conventional chemical oxidation of 4-methylcatechol and isolation of the *ortho*-quinone is complicated by concomitant quinone methide formation and accompanying polymerizations,[24,25] see **Scheme 3**.

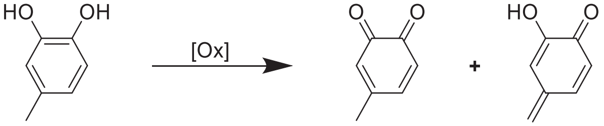

12 **C** **13** **OQ** **14** **QM**

Scheme 3: Oxidation of substituted catechol such as 4-methylcatechol may lead to the formation of either an *ortho*-quinone or a *para*-quinone methide or both.

As 4-methylcatechol can also undergo electrochemical oxidization, which has been studied with cyclic voltammetry,[26] I propose such a method of forming the required 4-methyl-*ortho*-quinone species *in situ*. Specifically, the *ortho*-quinone can be electrochemically generated and subsequently identified by combining cyclic voltammetry (CV) with infrared (IR) or ultraviolet-visible (UV-Vis) spectroscopy in an optically transparent thin-layer electrochemical (OTTLE) cell.[27-29] The apparatus consist of a liquid sample IR spectroscopy cell in which three electrodes (working, counter and reference) are placed for CV measurements, for the design see **Figure 1**. The cell can be placed into a spectrophotometer and attached to a potentiostat. Upon electrochemical generation of a species of interest, the spectral beam passes only through the working electrode minigrid where the species was generated[29], allowing for collection of IR or UV-Vis spectral data of the analyte. CV can then be used for screening at which voltage the *ortho*-quinone of interest is formed selectively by using concomitant IR spectroscopy for structural identification (*e.g.*, by counting the number of carbonyl absorption frequencies). By repeating the experiment with CV-UV-Vis, specific absorption bands in the UV-Vis spectrum can be assigned to the *ortho*-quinone (or even to other species generated at different voltages, such as a quinone methide). In this manner one indirectly couples IR spectroscopy to UV-Vis spectroscopy of an electrochemically generated intermediate species. Once the optimal electrochemical conditions for generating the *ortho*-quinone are found by OTTLE cell screening, the experiment can be repeated under (macro)electrolysis at a set potential, in a different electrolysis setup. When performed under high dilution, polymerization can be limited and the formed solution of 4-methyl-*ortho*-quinone can be used for kinetics studies by stopped-flow spectrophotometric analysis. This can reveal the kinetics values of SPOCQ of a substrate that shows closer resemblance to structures used in more complex molecules, *e.g.*, the tyrosine side chain in peptides and proteins.

An alternative OTTLE cell – stopped-flow UV-vis setup would also be possible, the design of which is depicted in **Figure 2**. This has to be constructed specifically if the *ortho*-quinone analyte is short-lived and needs to be measured fast after generation, or if macroelectrolysis towards the analyte is not an option, see **Figure 2**. Lastly, a specific chemical oxidizing agent might be identified by UV-Vis that selectively forms the *ortho*-quinone from 4-methylcatechol, by comparison to the reference spectra from the CV-UV-Vis experiments. The 4-methyl-*ortho*-quinone analyte can then be formed chemically *in situ* under high dilution and can be subjected to normal stopped-flow UV-Vis spectroscopy in the setup we used for the studies described in **Chapter 4 and 5**.

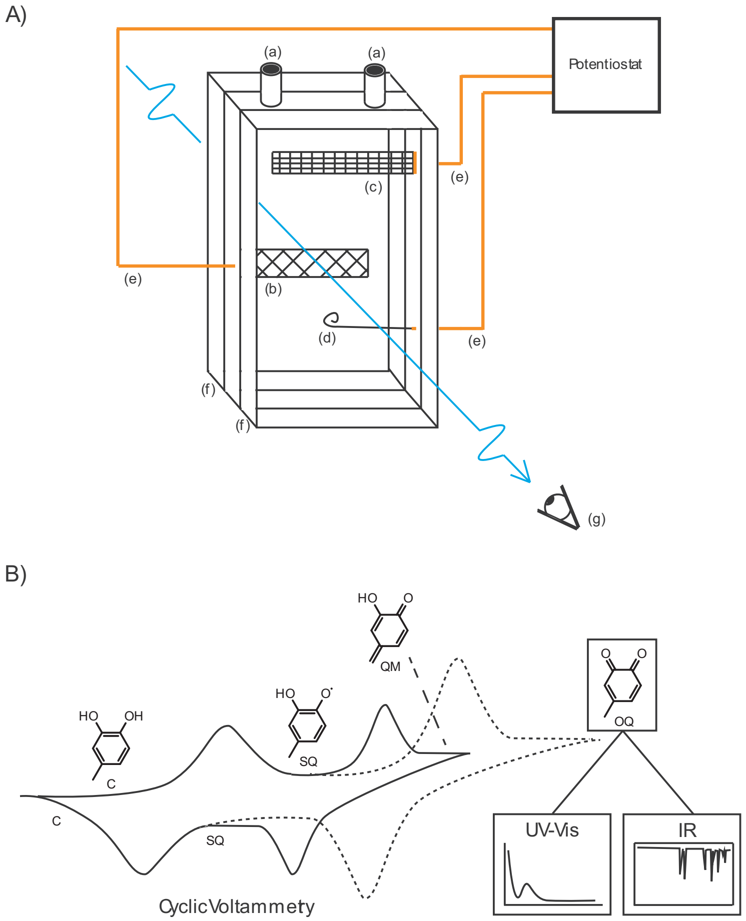

Figure 1: **A)** OTTLE cell design based on an IR liquid cell as described by Krejčik[29]: (a) Luer-lock fittings for liquid sample loading via syringe; (b) Au minigrid working electrode; (c) Pt mesh counter electrode; (d) Ag wire pseudoreference electrode; (e) electronic attachment of the electrodes to a potentiostat for CV measurements; (f) the setup is mounted between two KBr windows or quartz glass windows. UV-Vis or IR spectra can be recorded of electrochemically generated analytes at the working electrode mesh interface / diffusion layer through which the photon beam is passed, reaching the detector (g). **B)** The OTTLE cell experiment allows for the concomitant recording of UV-Vis or IR spectra of electrochemically generated species, which are formed at a set voltage determined from the CV sweep in prior experiments. The hypothetical scenario in which a 4-methyl-catechol (C) is oxidized via a semiquinone radical (SQ) to either a quinone methide (QM; solid line) at a lower electrochemical potential or to an *ortho*-quinone (OQ; dotted line) at a higher potential, is depicted in a simplified voltammogram in the middle. One can vary the experimental parameters by sweeping the potential in the voltammogram to different extents or directions to determine the electrochemical behavior. The experiment can then be repeated at a set potential to generate the species of interest and record spectral features in IR or UV-Vis.

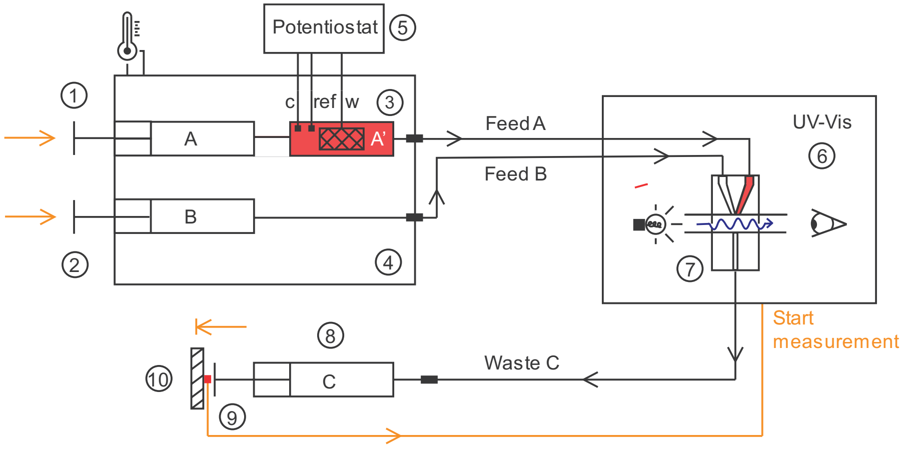

Figure 2: Design of a custom electrolysis-stopped-flow UV-Vis setup. The design is similar to a general stopped-flow UV-Vis setup as described in **Chapter 4**. However, a (macro)electrolysis cell is placed in between one of the driving syringes (which is of equal volume as the cell) and the mixing chamber. The cell contains a three-dimensional Au mesh working electrode; counter electrode and reference electrode, all attached to a potentiostat. One of the precursor solutions can be freshly electrolyzed to form the reagent of interest in a homogeneous fashion on the 3D working electrode mesh (with only minimal diffusion from this mesh[29]). When electrolysis is complete, the driving syringes can be flown simultaneously into a cuvette with observing window equipped with a turbulent flow mixer until abruptly stopping the flow and recording the data. Reagent solution **B** is fed directly into the cuvette, whereas the flow of precursor solution **A** pushes the electrolyzed reagent solution **A'** into the cuvette in one go. This design prevents damaging of the fragile electrodes and the speed of the operation prevents mixing of solutions **A** and **A'** by completely emptying the contents of the driving syringes when performing the measurement.

5. Future applications of declick chemistry

Regarding future applications of declick chemistry, one might employ triggered release of a chemokine in a different manner as the one that is described in **Chapter 6**. Once the chemoattractant properties of SDF-1α are established in the biological assays, we can repurpose the declick method of chemokines such as SDF-1α by attaching them onto a tumor-binding mAb. Custom built antibody-conjugates can be prepared by subjecting a mAb of choice (independent of IgG isotype) to glycan remodeling of the conserved glycan on the heavy chain.[30] It has been shown that azide moieties can be built in specifically on these glycans by means of a glycan remodeling approach.[30,31] I hereby propose that a small methylcyclopropene moiety may be installed in a similar way by employing UDP-GalNCyoc with a galactosyltransferase, for which the synthesis and substrate tolerability[32] by the enzyme needs to be evaluated in future research. As such, a mAb(methylcyclopropene)$_2$ ADC-precursor can be accessed in principle, see **Scheme 4**. The declickable cytokine payload, such as SDF-1α, can be made by installing an iminosydnone on a water soluble tetrazine and covalently attaching this to an *in situ* formed (thio)isocyanate generated on a lysine residue of recombinant SDF-1α. When this ligation would occur on the surface exposed N-terminal lysine that is known to be crucial for its biological activity, its biologically activity is simultaneously suppressed (see **Chapter 6**). This inactive SDF-1α construct can then be clicked onto the mAb via the tetrazine-methylcyclopropene click couple, forming a mAb(ImSyd-SDF-1α)$_2$ antibody-cytokine conjugate at a set ratio of 2:1, as shown in **Scheme 4**.

When a particular mAb that does not undergo cellular uptake is used for constructing the antibody-cytokine conjugate, it can then be employed for *in vitro* or *in vivo* studies as depicted in **Figure 3**. After accumulation of the antibody-cytokine conjugate onto the target tissue and opsonizing the tumor cell surface, a small DBCO construct bearing a secondary payload can be administered to the patient intravenously. The DBCO construct will then declick the ImSyds moieties, potentially attaching a secondary payload to the mAb, whilst releasing the activated SDF-1α for T cell recruitment toward the tumor microdomain, see **Figure 3**. The DBCO secondary payload can for instance be a PET tracer for localizing the tumor in the body; a (fluorescent) dye for assisting surgeons in removing tumor tissue; or a radionuclide/radioligand for radiotherapy treatment of the patient. The small size of the DBCO payload construct should allow facile renal clearance of excess probe that is administered to the patient, limiting exposure time to the patient, except for in the target tumor tissue. Importantly, adequate wash-out of mAb(ImSyd-SDF-1α)$_2$ from the patients circulation, prior to DBCO administration, is required to prevent premature declicking of SDF-1α chemokines of still circulating antibody-conjugates. To counter prolonged circulation, one might consider the use of shorter circulating nanobodies (with employing a different ligation method due to the absence of a glycan handle).[33,34]

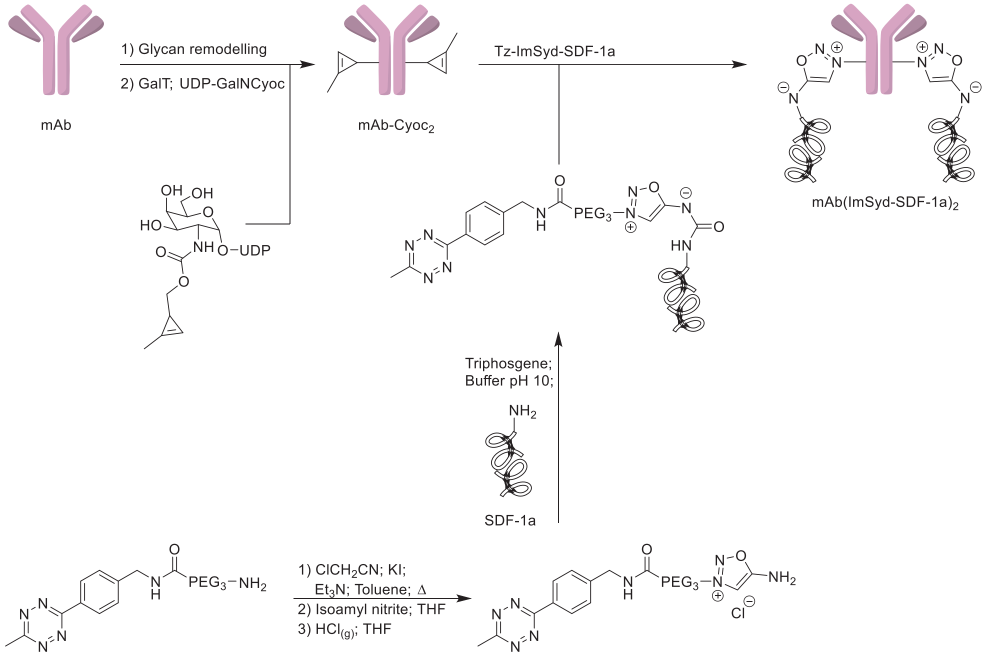
mAb
1) Glycan remodelling
2) GalT; UDP-GalNCyoc
mAb-Cyoc2
Tz-ImSyd-SDF-1a
mAb(ImSyd-SDF-1a)2
O-UDP
PEG3
Triphosgene;
Buffer pH 10;
NH2
SDF-1a
PEG3-NH2
1) ClCH2CN; KI;
Et3N; Toluene; Δ
2) Isoamyl nitrite; THF
3) HCl(g); THF
Cl

Scheme 4: Proposed synthesis route to a mAb(ImSyd-SDF-1α)₂ antibody-cytokine conjugate: First an opsonizing IgG mAb is subjected to glycan remodeling and is then treated with a GalNAc-transferase (GalNAc-T) and UDP-GalNCyoc to afford mAb(Cyoc)₂. An iminosydnone functionality is then installed on a water soluble tetrazine and then attached onto a recombinant SDF-1α. Then both mAb(Cyoc)₂ and Tz- ImSyd-SDF-1α are ligated together via tetrazine-methylcyclopropene click chemistry to afford the mAb(ImSyd-SDF-1α)₂ antibody-cytokine conjugate.

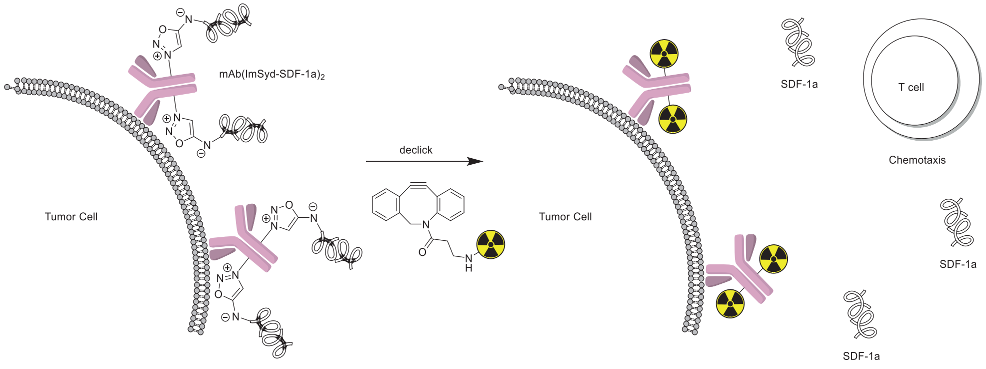
mAb(ImSyd-SDF-1a)2
Tumor Cell
declick
Tumor Cell
SDF-1a
T cell
Chemotaxis
SDF-1a
SDF-1a

Figure 3: A two-stage antibody treatment strategy based on declick chemistry: First, the tumor cell surface is opsonized by mAb(ImSyd-SDF-1α)₂ antibody-cytokine conjugate *(left)*. Upon administration of a DBCO-radioligand construct, a secondary payload is attached to the mAb-opsonized surface whilst releasing and activating the SDF-1α chemokine, effecting concomitant T cell recruitment *(right)*.For the general declick mechanism, one is referred to **Scheme 3** in **Chapter 6**. However, in this current approach no fluorescence absorption-quencher pair is used.

6. Final remarks

This dissertation presents a variety of developments in the field of bioorthogonal click chemistry, ranging from the development of new strained cycloalkynes, whilst pushing the boundaries of alkyne bending, to deepening our fundamental understanding of *ortho*-quinone click chemistry and finally exploring declick methodologies. Our studies revealed that model compounds not only provide valuable information for real-life applications, we also discovered that ring-strain –as derived from bond angles of involved strained alkynes– is a dominant factor in SPAAC, but less in SPOCQ. As such, the work described in this dissertation shows that the research area of click chemistry still offers sufficient room for improvement, regarding kinetics studies and reagent design. These advancements may not only lead to better applications in areas where click chemistry already has shown its values, but even in novel areas where click chemistry has not yet been applied to its full potential.

7. References

(1) Gold, B.; Dudley, G. B.; Alabugin, I. V. Moderating strain without sacrificing reactivity: Design of fast and tunable noncatalyzed alkyne-azide cycloadditions via stereoelectronically controlled transition state stabilization. *J. Am. Chem. Soc.* **2013**, *135*, 1558–1569.
(2) Danilkina, N. A.; Govdi, A. I.; Khlebnikov, A. F.; Tikhomirov, A. O.; Sharoyko, V. V.; Shtyrov, A. A.; Ryazantsev, M. N.; Bräse, S.; Balova, I. A. Heterocycloalkynes Fused to a Heterocyclic Core: Searching for an Island with Optimal Stability-Reactivity Balance. *J. Am. Chem. Soc.* **2021**, *143*, 16519–16537.
(3) Verboom, W.; Everhardus, R. H.; Bos, H. J. T.; Brandsma, L. A simple synthesis of *N,N*-dialkyl-3-alken-1-yn-1-amines. *Recl. Trav. Chim., Pays-Bas* **1979**, *98*, 508–511.
(4) Varga, B. R.; Kállay, M.; Hegyi, K.; Béni, S.; Kele, P. A non-fluorinated monobenzocyclooctyne for rapid copper-free click reactions. *Chem. Eur. J.* **2012**, *18*, 822–828.
(5) Brandsma, L. Studies in Organic Chemistry 34: Preparative Acetylenic Chemistry. Second edition. Amsterdam, The Netherlands: Elsevier Science Publishers B.V.; **1988**. Chapter IX: 2.19 Bis(diaIkylamino)acetyIenes from 1-Chloro-bis(dialkylamino)ethenes, 185–186.
(6) Brandsma, L. Synthesis of Acetylenes, Allenes and Cumulenes: Methods and Techniques. First edition. Oxford, UK: Elsevier Ltd.; **2004**. Chapter 10: 10.2.11 N^1,N^1,N^2,N^2-Tetraalkyl-1-acetylenediamines from 2-chloro-*N*,*N*,N^1,N^1-tetraalkyl-1,1-ethylenediamines and potassium amide, 218–219.
(7) Brandsma, L. Studies in Organic Chemistry 34: Preparative Acetylenic Chemistry. Second edition. Amsterdam, The Netherlands: Elsevier Science Publishers B.V.; **1988**. Chapter IX: 2.21 Dimethylaminoacetylene, 187–189.
(8) Weterings, J.; Rijcken, C. J. F.; Veldhuis, H.; Meulemans, T.; Hadavi, D.; Timmers, M.; Honing, M.; Ippel, H.; Liskamp, R. M. J. TMTHSI, a superior 7-membered ring alkyne containing reagent for strain-promoted azide–alkyne cycloaddition reactions. *Chem. Sci*. **2020**, *11*, 9011–9016.
(9) Personal communication with prof. dr. R.M.J. Liskamp of University of Glasgow.
(10) Haase, J.; Krebs, A. Die Molekülstruktur des 3.3.6.6-Tetramethyl-1-thiacycloheptins ($C_{10}H_{16}S$). *Z. Naturforsch. A*. **1972**, *27*, 624–627.
(11) Royzen, M.; Yap, G. P. A.; Fox, J. M. A photochemical synthesis of functionalized *trans*-cyclooctenes driven by metal complexation. *J. Am. Chem. Soc.* **2008**, *130*, 3760–3761.

(12) Fang, Y.; Zhang, H.; Huang, Z.; Scinto, S. L.; Yang, J. C.; Am Ende, C. W.; Dmitrenko, O.; Johnson, D. S.; Fox, J. M. Photochemical syntheses, transformations, and bioorthogonal chemistry of: Trans-cycloheptene and sila *trans*-cycloheptene Ag(I) complexes. *Chem. Sci.* **2018**, *9*, 1953–1963.
(13) Sondag, D.; Maartense, L.; de Jong, H.; de Kleijne, F. F. J.; Bonger, K. M.; Löwik, D. W. P. M.; Boltje, T. J.; Dommerholt, J.; White, P. B.; Blanco-Ania, D.; Rutjes, F. P. J. T. Readily Accessible Strained Difunctionalized *trans*-Cyclooctenes with Fast Click and Release Capabilities**. *Chem. Eur. J.* **2023**, *29*, e202203375.
(14) Dommerholt, J.; Schmidt, S.; Temming, R.; Hendriks, L. J. A.; Rutjes, F. P. J. T.; Van Hest, J. C. M.; Lefeber, D. J.; Friedl, P.; Van Delft, F. L. Readily accessible bicyclononynes for bioorthogonal labeling and three-dimensional imaging of living cells. *Angew. Chem. Int. Ed*. **2010**, *49*, 9422–9425.
(15) Dommerholt, J.; Van Rooijen, O.; Borrmann, A.; Guerra, C. F.; Bickelhaupt, F. M.; Van Delft, F. L. Highly accelerated inverse electron-demand cycloaddition of electron-deficient azides with aliphatic cyclooctynes. *Nat. Commun.* **2014**, *5*, 5378.
(16) Levandowski, B. J.; Svatunek, D.; Sohr, B.; Mikula, H.; Houk, K. N. Secondary Orbital Interactions Enhance the Reactivity of Alkynes in Diels-Alder Cycloadditions. *J. Am. Chem. Soc*. **2019**, *141*, 2224−2227.
(17) Levandowski, B. J.; Svatunek, D.; Sohr, B.; Mikula, H.; Houk K. N. Correction to "Secondary Orbital Interactions Enhance the Reactivity of Alkynes in Diels–Alder Cycloadditions". *J. Am. Chem. Soc*. **2019**, *141*, 18641.
(18) Bruins, J. J.; Westphal, A. H.; Albada, B.; Wagner, K.; Bartels, L.; Spits, H.; Van Berkel, W. J. H.; Van Delft, F. L. Inducible, Site-Specific Protein Labeling by Tyrosine Oxidation-Strain-Promoted (4 + 2) Cycloaddition. *Bioconjugate Chem.* **2017**, *28*, 1189−1193.
(19) Bruins, J. J.; Blanco-Ania, D.; Van Der Doef, V.; Van Delft, F. L.; Albada, B. Orthogonal, dual protein labelling by tandem cycloaddition of strained alkenes and alkynes to: *Ortho*-quinones and azides. *Chem. Commun.* **2018**, *54*, 7338–7341.
(20) Bruins, J. J.; Van de Wouw, C.; Keijzer, J. F.; Albada, B.; Van Delft, F. L. Inducible, Selective Labeling of Proteins via Enzymatic Oxidation of Tyrosine. In *Enzyme-Mediated Ligation Methods*, Nuijens, T.; Schmidt, M., Eds.; Springer New York: New York, NY, **2019**; pp 357–368.
(21) Bruins, J. J.; Van de Wouw, C.; Wagner, K.; Bartels, L.; Albada, B.; Van Delft, F. L. Highly Efficient Mono-Functionalization of Knob-in-Hole Antibodies with Strain-Promoted Click Chemistry. *ACS Omega*. **2019**, *4*, 11801−11807.
(22) Bruins, J. J.; Damen, J. A. M.; Wijdeven, M. A.; Lelieveldt, L. P. W. M.; Van Delft, F. L.; Albada, B. Non-Genetic Generation of Antibody Conjugates Based on Chemoenzymatic Tyrosine Click Chemistry. *Bioconjugate Chem*. **2021**, *32*, 2167−2172.
(23) Shajan I.; Rochet L. N. C.; Tracey S. R.; Jackowska B.; Benazza R.; Hernandez-Alba O.; Cianférani S.; Scott C. J.; Van Delft F. L.; Chudasama V.; Albada B. Rapid Access to Potent Bispecific T Cell Engagers Using Biogenic Tyrosine Click Chemistry. *Bioconjugate Chem.* **2023**, *34*, 2215–2220.
(24) Sugumaran, M. Reactivities of quinone methides versus *o*-Quinones in catecholamine metabolism and eumelanin biosynthesis. *Int. J. Mol. Sci.* **2016**, *17*, 1576.
(25) Bruins, J. J.; Albada, B.; Van Delft, F. *ortho*-Quinones and Analogues Thereof: Highly Reactive Intermediates for Fast and Selective Biofunctionalization. *Chem. Eur. J.* **2018**, *24*, 4749–4756.

(26) Nematollahi D.; Golabi S.M. Electrochemical study of catechol and 4-methylcatechol in methanol. Application to the electro-organic synthesis of 4,5-dimethoxy- and 4-methoxy-5-methyl-o-benzoquinone. *J. Electroanal. Chem.* **1996**, *405*, 133–140.
(27) Gamage, R. S. K. A.; Umapathy, S.; McQuillan, A. J. OTTLE cell study of the UV-visible and FTIR spectroelectrochemistry of the radical anion and dianion of 1,4-benzoquinone in DMSO solutions. *J. Electroanal. Chem.* **1990**, *284*, 229–235.
(28) Finklea, H. O.; Boggess, R. K.; Trogdon, J. W.; Schultz, F. A. Thin-Layer Spectroelectrochemistry Cell with Demountable Gold or Mercury-Gold Minigrid Electrodes. *Anal. Chem.* **1983**, *55*, 1177–1179.
(29) Krejčik M.; Daněk M.; Hartl F. Simple construction of an infrared optically transparent thin-layer electrochemical cell. Applications to the redox reactions of ferrocene, $Mn_2(CO)_{10}$ and $Mn(CO)_3$(3,5-di-t-butyl-catecholate)$^-$. *J. Electroanal. Chem.* **1991**, *317*, 179–187.
(30) van Geel, R.; Wijdeven, M. A.; Heesbeen, R.; Verkade, J. M. M.; Wasiel, A. A.; van Berkel, S. S.; van Delft, F. L. Chemoenzymatic Conjugation of Toxic Payloads to the Globally Conserved N-Glycan of Native mAbs Provides Homogeneous and Highly Efficacious Antibody-Drug Conjugates. *Bioconjugate Chem.* **2015**, *26*, 2233–2242.
(31) de Bever, L.; Popal, S.; van Schaik, J.; Rubahamya, B.; van Delft, F. L.; Thurber, G. M.; van Berkel, S. S. Generation of DAR1 Antibody-Drug Conjugates for Ultrapotent Payloads Using Tailored GlycoConnect Technology. *Bioconjugate Chem.* **2023**, *34*, 538–548.
(32) Liu, F.; Chen, H.-M.; Armstrong, Z.; Withers, S. G. Azido Groups Hamper Glycan Acceptance by Carbohydrate Processing Enzymes. *ACS Cent. Sci.* **2022**, *8*, 656–662.
(33) Muyldermans, S. Nanobodies: Natural single-domain antibodies. *Annu. Rev. Biochem.* **2013**, *82*, 775–797.
(34) Oliveira, S.; Heukers, R.; Sornkom, J.; Kok, R. J.; van Bergen En Henegouwen, P. M. P. Targeting tumors with nanobodies for cancer imaging and therapy. *J. Control. Release* **2013**, *172*, 607–617.

Summary

Summary

Click chemistry is one of the few synthetic methodologies that allows for the construction of stable covalent bonds between two reagents in an aqueous solution. This is a unique feature over conventional synthetic organic chemistry, where water often hampers reactions. The advent of click chemistry therefore allows to perform synthetic chemistry on large proteins or even on live cells. Click chemistry makes use of highly selective reactions between specific sets of reagents (so called *orthogonality*), that do not cross-react with the biological environment (so called *bio-orthogonality*). The reagents used are designed with great care and their creation often involves the delicate synthesis of highly reactive “spring-loaded” molecules.

The applications for which we develop new types of click chemistries in this dissertation are for attaching chemical payloads onto biomolecules (a *bioconjugation* reaction). This discipline of bioconjugation technology falls within the field of *chemical biology,* in which we use chemical tools to alter, modulate and study biological processes. Tumor-cell labelling with fluorescent dyes and subsequent observation in microscopy allows scientists to study the behavior of tumor cells towards cells of the immune system (*study*). Another example is the construction of antibody-drug conjugates (ADCs) (*modulate*) to use the specific ability of an antibody to binds to foreign or unwanted antigens (viruses, bacteria, tumors) and deliver a bioactive payload. An example of this is attaching a very potent cytotoxic drug onto an tumor-binding antibody, which then delivers with great precision the drug to the tumor.

The research done in this dissertation focusses primarily on developing the fundamental chemistry that allows us to attach or even detach molecules of interest (dyes, drugs) onto a biological system (peptides/proteins; antibodies; whole cells), with an emphasis on click chemistry methods.

Chapter 1 gives the definition of click chemistry and presents an overview of what kind of cycloaddition reactions are used and how fast they react in bioconjugations. It also formulates the boundaries of existing knowledge and identifies knowledge gaps that require further investigation.

In **Chapters 2 and 3** we describe the investigation on what role the glycocalyx-dynamics plays in cell-cell interactions. The glycocalyx is the extracellular matrix consisting of large carbohydrate polymers covering the cellular membrane. Some hypertrophic tumor cells have a thicker than normal glycocalyx layer effectively wearing a thick “fur-coat” and thus do not get recognized by the immune system, leading to metastasis. We envisioned that “feeding” these tumor cells with small carbohydrates that bear a click handle (an azide) results in uptake and subsequent metabolism-assisted delivery on the glycocalyx surface. The azide handle on the cell surface can specifically react with a reactive cycloalkyne probe that is attached to a fluorescent dye (a SPAAC click reaction). This fluorescently labels the glycocalyx of tumor cells and allows us to study their distribution and dynamics. **Chapters 2 and 3** focus on the chemical synthesis of novel fluorescently labeled, highly strained seven- and eight-membered cycloalkyne rings that are required for highly-resolved tumor glycocalyx imaging.

Chapters 4 and 5 comprise of a number of detailed kinetics studies into SPOCQ click chemistry, which is a click methodology that has been used for protein modification, hydrogel synthesis, and for the generation of antibody-drug conjugates (ADCs). However, it has only been investigated to a limited extent in the past, especially as the reaction rates and the thermodynamic reaction parameters that underly the unusually high reaction kinetics were not yet established. We now extensively studied SPOCQ reactions by means of spectroscopy and physical chemistry to obtain fundamental understanding of this click reaction. With this deepened understanding we can now design even better reagents for this particular type of click chemistry.

In **Chapter 6** we designed and prepared a new linker construct that can be applied in a declick methodology. Benefiting from our developments described in **Chapter 3**, we aimed for a novel approach to locally activate T cells in order to initiate tumor clearance. For this, we wanted to attach a chemokine onto the cell surface using metabolic labeling and click chemistry. Upon subsequent addition of a DBCO-dye, the cytokine will be released from the glycocalyx of the tumor cell, and generate a chemical gradient that recruits immune cells towards the tumor cell, ideally restoring recognition and phagocytosis. We developed the entire click–declick methodology for this application by means of rational design and chemical synthesis.

Lastly, **Chapter 7** gives a future outlook on the developments described in this dissertation.

Samenvatting

Klikchemie is één van de weinige synthetische methoden waarmee in een waterige oplossing stabiele covalente bindingen tussen twee reagentia kunnen worden gemaakt. Dit is een unieke eigenschap ten opzichte van conventionele synthetische organische chemie, waar water reacties vaak belemmert. De opkomst van klikchemie maakt het daarom mogelijk om synthetische chemie uit te voeren op grote eiwitten of zelfs op levende cellen. Klikchemie maakt gebruik van zeer selectieve reacties tussen specifieke sets van reagentia (zogenaamde *orthogonaliteit*), die geen kruisreactiviteit heeft met de biologische omgeving (zogenaamde *bio-orthogonaliteit*). Deze reagentia worden met grote zorg ontworpen en verworven door middel van de delicate synthese van deze zeer reactieve "opgespannen" moleculen.

In dit proefschrift ontwikkelen we nieuwe soorten klikchemie voor toepassing op het hechten van chemische payloads aan biomoleculen (een *bioconjugatiereactie*). Deze discipline van bioconjugatie-technologie valt binnen het gebied van de *chemische biologie*, waarin we chemische hulpmiddelen gebruiken om biologische processen te veranderen, te moduleren en te bestuderen. Het labelen van tumorcellen met fluorescente kleurstoffen en de daaropvolgende observatie met microscopie stelt wetenschappers in staat om het gedrag van tumorcellen ten opzichte van cellen van het immuunsysteem te bestuderen (*bestuderen*). Een ander voorbeeld is de constructie van antilichaam-drug conjugaten (ADC's) (*moduleren*), waarin het specifieke vermogen van een antilichaam om te binden aan vreemde of ongewenste antigenen (virussen, bacteriën, tumoren) wordt benut om een bioactieve verbinding als lading doeltreffend af te leveren. Een voorbeeld hiervan is het binden van een zeer krachtig cytotoxisch geneesmiddel aan een tumorbindend antilichaam, welke vervolgens met grote precisie het geneesmiddel aflevert bij alleen de tumor.

Het onderzoek in dit proefschrift richt zich voornamelijk op het ontwikkelen van de fundamentele chemie die ons in staat stelt om moleculen naar keuze (kleurstoffen, medicijnen) aan een biologisch systeem (peptiden/eiwitten; antilichamen; gehele cellen) te koppelen, of zelfs los te koppelen, middels klikchemie-methoden.

Hoofdstuk 1 geeft de definitie van klikchemie en geeft een overzicht van wat voor soort cycloadditie reacties gebruikt worden en hoe snel ze reageren in bioconjugaties. Het expliciteert ook de grenzen van de bestaande kennis en identificeert daarin hiaten die verder onderzoek vereisen.

In **Hoofdstukken 2 en 3** beschrijven we het onderzoek naar welke rol glycocalyx-dynamica speelt in cel-cel interacties. De glycocalyx is de extracellulaire matrix die bestaat uit grote koolhydraatpolymeren die de celmembraan bedekken. Sommige hypertrofische tumorcellen hebben een dikkere glycocalyxlaag dan normaal, waardoor ze effectief een dikke "bontjas" dragen en dus niet herkend worden door het immuunsysteem, hetgeen weer leidt tot metastasering. Door deze tumorcellen te "voeden" met kleine koolhydraten waaraan een klikhandvat (een azide) hangt, resulteert het in de opname en daaropvolgende metabole incorporatie en expressie van deze “tag” op het glycocalyxoppervlak. De azide-tag op het celoppervlak kan vervolgens specifiek reageren met een reactieve cycloalkyn sonde waaraan een fluorescente kleurstof is gekoppeld (een zogenoemde SPAAC klikreactie). Hierdoor wordt de glycocalyx van tumorcellen fluorescent gelabeld en kunnen we de glycocalyx distributie en dynamiek bestuderen. **Hoofdstukken 2 en 3** richten zich op de chemische synthese van nieuwe fluorescent gelabelde, sterk gespannen zeven- en achtring cycloalkynen die gebruikt worden in hoge-resolutie tumorglycocalyx imaging.

De **Hoofdstukken 4 en 5** beschrijven gedetailleerde kinetiek studies naar SPOCQ klikchemie, welke een klikmethodologie is die gebruikt wordt voor eiwitmodificatie, hydrogelsynthese en voor het genereren van antilichaam-drug conjugaten (ADC's). De exacte oorsprong van de ongebruikelijk hoge snelheden is in het verleden slechts in beperkte mate onderzocht en de correlatie tussen de reactiesnelheden en de thermodynamische reactieparameters waren nog niet bepaald. We hebben nu SPOCQ-reacties uitgebreid bestudeerd met behulp van spectroscopie en fysische chemie om fundamentele inzichten in deze klikreactie te verkrijgen. Met dit nieuw verkregen begrip kunnen we nu nog betere reagentia ontwerpen voor dit specifieke soort klikchemie.

In **Hoofdstuk 6** hebben we een nieuw linker construct ontworpen en gesynthetiseerd, welke kan worden toegepast in een ontklik methodologie. Gebaseerd op de ontwikkelingen van **Hoofdstuk 3**, streefden we naar een nieuwe aanpak om T-cellen lokaal te activeren, welke vervolgens de tumorcellen moeten opruimen. Hiervoor plakken we een chemokine aan het celoppervlak van de tumor met behulp van metabole labeling en klikchemie. Na toevoeging van een DBCO-kleurstof sonde zal het cytokine vrijkomen uit de glycocalyx van de tumorcel en een chemisch gradiënt creëren, die immuun cellen naar de tumorcel lokt, waardoor idealiter herkenning van de tumorcel door de immuun cellen wordt hersteld en fagocytose optreedt. We hebben de gehele klik-ontklik methodologie ontwikkeld voor deze toepassing door middel van het rationeel ontwerp en vervolgens door chemisch synthese van de linker.

Tot slot geeft **Hoofdstuk 7** een toekomstige blik op de toepassingen van de ontwikkelingen die in dit proefschrift zijn beschreven.

Acknowledgements

Acknowledgements

Promotors & thesis committee

First and foremost, I would like to thank my promotor **Prof. dr. Floris van Delft** for giving me the opportunity to conduct my doctoral study at Wageningen University & Research, resulting in this dissertation. It was an honor and privilege to have been able to discuss my research with my promotor on a weekly basis. I found our discussions invigorating as it often required quickly shifting gears due the nature of the project, which I personally like. The high level of synthetic chemistry and the ease with which it was discussed also provided many lessons. You also always listened to my suggestions, which is an admirable characteristic. We often agreed on matters. The few occasions where we did not resulted in fierce discussions, in which you were a good sparring partner and a mentor. This is the best example of how science in the field should be conducted. Floris, I want to thank you for all the lessons that you taught me. In the end, I have matured on both a personal level and as a scientist, under your guidance.

Secondly, I want to thank my co-promotor **Dr. ing. Bauke Albada**, the person who actually reeled me in as a PhD candidate. I want to thank you for guiding the overall project into a focused direction, whereas the profs and me could get lost in details. Also, the discussions about the tactical choices when considering collaborations were of great value. Next to that, I want to thank you for all the help regarding the writing and for teaching me to be more patient with people. The trust you put in your PhD candidates results in a very pleasant working environment which I experienced over the course of my time at the WUR. I greatly appreciated the open and informal way of communicating and discussing science.

Thirdly, I want to thank my second promotor **Prof. dr. Han Zuilhof** for his help and insights into the physical organic chemistry part of my dissertation. You have always shown great interest in my work in stopped-flow kinetics studies and provided crucial insights into the interpretation of the thermodynamic data. I also appreciate the outside perspective that you provided, being my second promotor, which helped to steer the projects that now comprise my dissertation.

I want to thank the members of the thesis committee: **Prof. dr. ir. Frans Leermakers**, **Prof. dr. Eelco Ruijter**, **Prof. dr. ir. Ingrid Dijkgraaf** and **Prof. dr. Sander van Kasteren** for reading, evaluating and allowing me to defend my dissertation.

Paranymphs

I want to express my gratitude to my paranymph **Jasper van de Sande** for assisting me during the defense. I consider it as a return for that one time I had to dismantle a cold trap where you managed to distill a more than considerable amount of a mysterious blue fluid into. Regardless, you are an esteemed lab mate of mine in the sense of both chemistry and biology. I want to express my gratitude to my paranymph **Dr. Dieuwertje Streefkerk** for assisting me during the defense. I also want to thank you for the always enthusiastic discussions regarding organic synthesis and your judicious advises, which were of great value to me.

Collaborators

I want to thank our collaborators that made this interdisciplinary research possible. First of all, **Daan Smits** and **Prof. dr. Peter Friedl** (Radboud University Medical Center). Although the cell biological research has been cumbersome over the last years, we can be very proud of the results that were achieved regarding the unprecedented quality of glycocalyx labelling, resulting in the submission to *Nat. Chem. Biol.* Secondly, I want to thank **Dr. Jorge Escorihuela** (Universitat de València) for his computational investigations that helped us to understand the nature of SPOCQ reactions. I also want to thank **Dr. Gabriele Kociok-Köhn** (University of Bath) for resolving the single crystal X-ray structures of our cycloalkynes. Lastly, I want to thank **Prof. dr. Nathaniel Martin** (Leiden University) and colleagues for their efforts in developing the synthesis of the SDF-1α-alkyne protein. It would have been a too long peptide for us to synthesize in house, so your expertise in this field is greatly appreciated. I am looking forward to see the upcoming results emerge from our collaboration with the group at RadboudUMC.

Colleagues

I would generally like to thank past and current members of ORC as a whole, but some deserve special mentioning.

Dr. Fedor Miloserdov and **Dr. Maurice Franssen** are acknowledged with great gratitude for their conversations and advises in both synthetic chemistry and the ways of research and science in general.

Dr. Jorick Bruins is gratefully acknowledged for introducing me into the bioconjugation field in my first few weeks in the lab. I want to thank **Dr. Jordi Keijzer** and **Dr. Ian de Bus** for the critical exchange of ideas concerning science on a daily basis and for the everlasting humor in the office. I also want to thank my current colleagues from office 8038 **Irene Shajan**, **Zhen Yang** and **Ids Lemmink** for the good atmosphere.

I particularly want to thank ORC's current and former members with whom I have had valuable conversations and necessary laughs: **Dr. Andriy Kuzmyn**, **Dr. Alice Guarneri**, **Dr. Lucas Teunissen**, **Dr. Jayaruwan Gamaethiralalage**, **Si Huang**, **Yifei Zhou**, **Julian Engelhardt**, along with our postdoctoral researchers **Dr. Dong-Dong Liang**, **Dr. Muthusamy Subramaniam** and **Dr. Hamit Eren**.

Regarding the technical support I would like to express my gratitude to **Frank Claassen**, **Barend van Lagen†** and **Dr. Sidhu Pujari**.

I would very much like to thank the secretariat consisting of **Elly Geurtsen**, **Aleida Ruisch** and **Eveline van Dijk** for providing much essential support behind the scenes. I would also like to thank **Henny Li** for ordering and maintaining a steady supply of chemicals to the laboratory.

Last but not least, I would like to mention my students **Jorren Steenbergen**, **Sigrid Bolder**, **Twan Tjoa** and **Arthur Bleumers**. I wish you all the best in your own (academic) futures!

To conclude the academic contributions, I want to thank all my teachers from the past and all those who gave me a chance to become the scientist that I am today.

Friends and family

I personally also would like to thank all my old friends and new friends made during this journey, along with the clientèle of De Rooie Haen, for providing the necessary relief of an often so troubled academics' mind.

I want to thank my family for their support during my academic career. For the support from abroad I want to thank **Susie**, **Kevin** and **Brandon** from across the pond. I also want to thank **Pa** and **Astrid** up in the mountains. Finally I am very grateful for the support from **Ma** and **Pip** to whom I owe a lot.

Lastly, I want to thank my wife **Amanda** for all her loving support. For without you, I could never have done this.

About the author

Curriculum vitae

Yuri Damen was born on the 3rd of December 1992 in ‘s-Hertogenbosch. At a young age he sparked an interest in natural sciences during his lower education (‘t Heibosch, Veghel) and this was further deepened whilst attending Gymnasium Bernrode, Heeswijk-Dinther. He graduated from the latter with a double profile Natuur & Techniek and Natuur & Gezondheid in 2012.

His academic career started with attending a Bachelors study in Pharmacy at Utrecht University. Early enrollment in the Honours Programme Pharmaceutical Sciences allowed him to conduct his BSc thesis, in the field of pharmaceutical colloidal chemistry, during the second year of the study. This resulted in the choice to pursue a future in research. As such, the rest of the courses were conducted at the Department of Chemistry, specializing in organic chemistry. He formally graduated with a BSc in Pharmacy in 2016.

He then conducted his Masters in Chemical Sciences (programme Drug Innovation) at Utrecht University and became a synthetic chemist with specializations in complex glycan total synthesis and organometallic chemistry, from which he graduated in 2019.

After acquiring his MSc degree, he was employed as a PhD candidate at Wageningen University & Research from November 2019 to January 2024. He conducted his PhD research under the supervision of Prof. dr. Floris van Delft, dr. Bauke Albada and Prof. dr. Han Zuilhof on synthesizing and studying highly strained cycloalkyne rings for (de)click chemistry in bioconjugations. Parts of the research conducted are described in this book.

After completing his PhD, he returned to his original ambition to chase a career in the pharmaceutical industry. He currently holds a position as Scientist at BioChem Oss.

List of publications

J.A.M. Damen, J. Escorihuela, H. Zuilhof, and B. Albada. Temperature-Dependent Reaction Rates of Quinone-Alkene Cycloaddition Reveal that Only Entropy Determines the Rate of SPOCQ Reactions. *Under review at Chem. Sci.* **2024**.

D. Smits *, **J.A.M. Damen***, F.L. van Delft, B. Albada and P. Friedl. Glycocalyx micro- and nanodomains in cell-cell and cell matrix interactions revealed by ultra-sensitive click chemistry. *Under review at Nat. Chem. Biol.* **2024**.

*Shared first author

J. A. M. Damen, J. Escorihuela, H. Zuilhof, F. L. van Delft and B. Albada. High Rates of Quinone-Alkyne Cycloaddition Reactions are Dictated by Entropic Factors. *Chem. Eur. J.* **2023**, *29*, e202300231.

J. J. Bruins, **J. A. M. Damen**, M. A. Wijdeven, L. P. W. M. Lelieveldt, F. L. van Delft and B. Albada. Non-Genetic Generation of Antibody Conjugates Based on Chemoenzymatic Tyrosine Click Chemistry. *Bioconjugate Chem.* **2021**, *32*, 2167−2172.

S. Tretiakov, **J. A. M. Damen**, M. Lutz and M.-E. Moret. A dianionic C3-symmetric scorpionate: synthesis and coordination chemistry. *Dalton Trans.* **2020**, *49*, 13549–13556.

Overview of completed training activities

Discipline specific activities	Organizing institute	Year
Advanced Organic chemistry course from VLAG	VLAG	2020-2023
WUR 102nd Dies Natalis	WUR	2020
CHAINS 2020	KNCV	2020
ICI PhD Day 2021	ICI	2021
ICI 2021 Chemical Immunology Conference	ICI	2021
Holland Research School of Molecular Chemistry. Summer School Organic Synthesis 2021	HRSMC	2021
CHAINS 2021	KNCV	2021
ICI 2022 Chemical Immunology Conference – poster presentation	ICI	2022
ICI PhD Day 2022	ICI	2022
EPS workshop “Plant Hormones”	EPS	2023
KNCV SOC MCCB Lunteren symposium 2023	KNCV	2023
105th Dies Natalis of Wageningen University & Research	WUR	2023
ICI PhD-Day 2023	ICI	2023
ICI 2023 Chemical Immunology Conference – poster presentation	ICI	2023
IUPAC CHAINS – poster presentation	KNCV	2023
ESOR2023 – oral presentation	Vrije Universiteit Amsterdam	2023

General courses	Organizing institute	Year
VLAG 46th PhD week	VLAG	2020
ICI PhD programma module 1 "Personal effectiveness: time and project management"	ICI	2021
ICI PhD programme Module 2 “Communication in science“	ICI	2021
ICI PhD programme Module 3 “From Student to Professional”	ICI	2022
ICI PhD programme Module 4 "From Student to Professional – A PhD, what next?"	ICI	2023
Career perspectives	WGS	2023
Scientific Integrity	WGS	2023

Assisting in teaching and supervision activities	Organizing institute	Year
Supervision of BSc students	ORC	2020-2023
Development of MSc course organometallic chemistry BNT 52306	WUR	2022

Other activities	Organizing institute	Year
Preparation of research proposal	ORC	2019-2022
Weekly colloquium / seminars	ORC	2019-2023
Monthly BORC meetings	ORC	2019-2023
Interview on PhD topic, Published in ICI bulletin no. 11.	ICI	2021

The research described in this thesis was financially supported by the NWO Gravity Program Institute for Chemical Immunology (ICI), project number ICI00027.

Financial support from Wageningen University for printing this thesis is gratefully acknowledged.

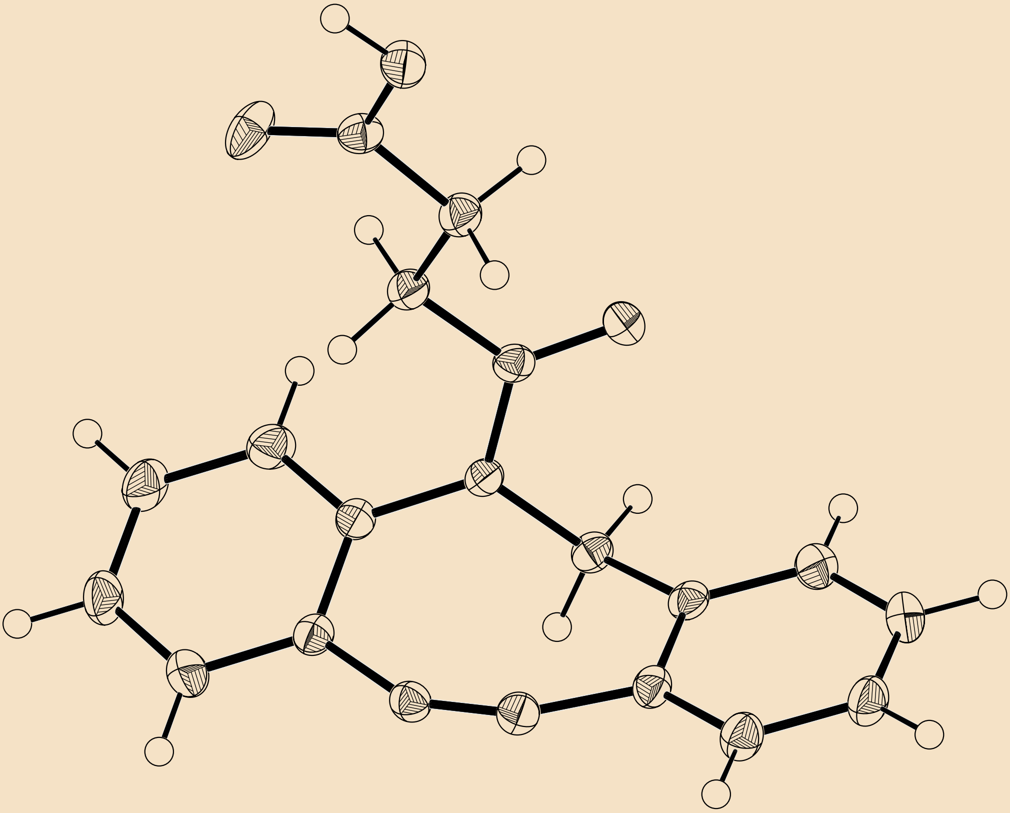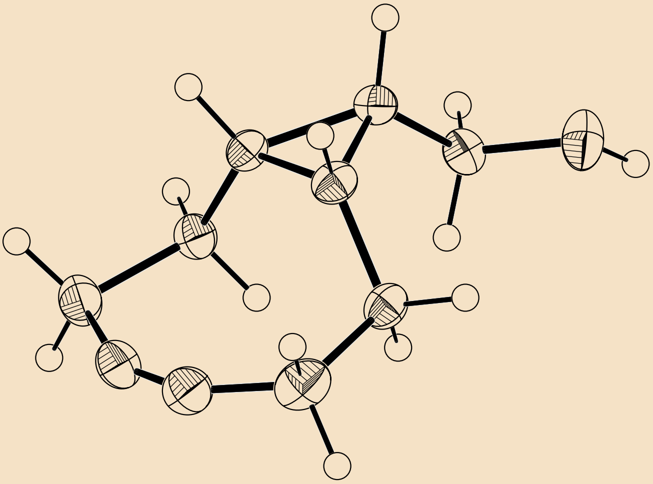Cover design by J.A.M. Damen
Printed by Ipskamp Printing